LBL-9565

Lawrence Berkeley Laboratory
UNIVERSITY OF CALIFORNIA

Materials & Molecular
Research Division

FLOW-THROUGH POROUS ELECTRODES

James Arthur Trainham, III
(Ph.D. thesis)

August 1979

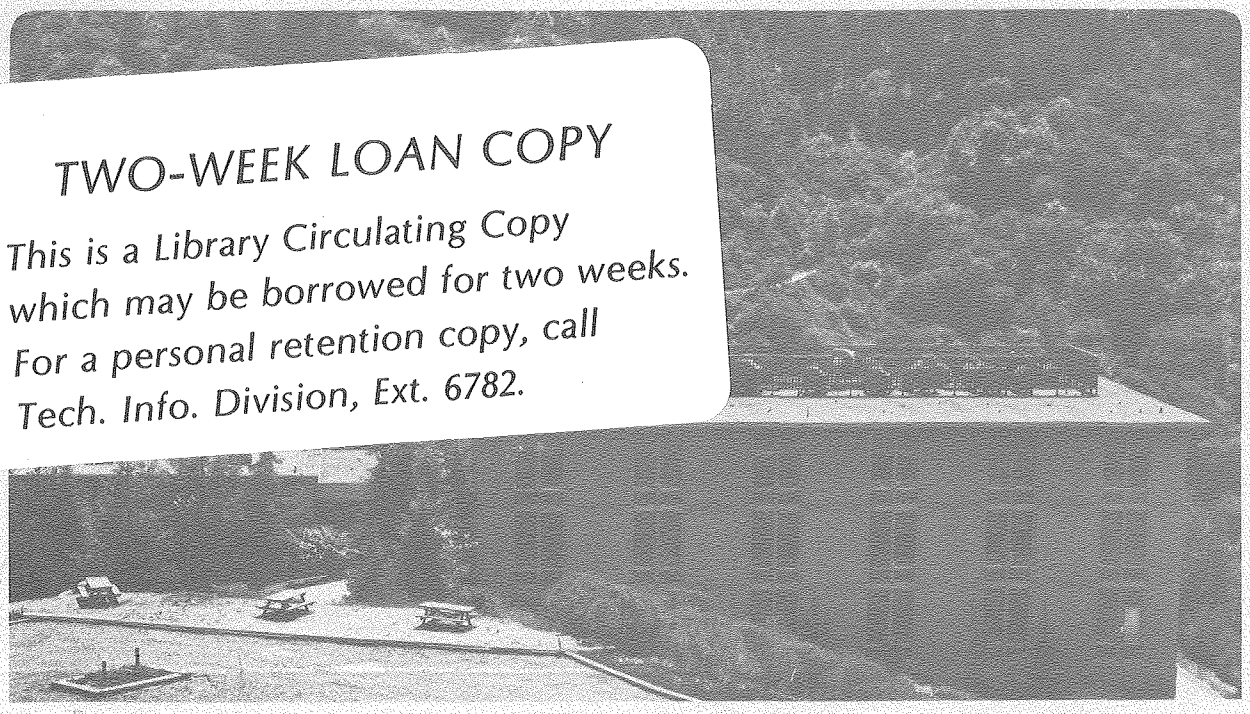

Prepared for the U.S. Department of Energy under Contract W-7405-ENG-48

DISCLAIMER

LBL-9565

FLOW-THROUGH POROUS ELECTRODES

James Arthur Trainham, III
(Ph.D. Thesis)

August 1979

Prepared for the U.S. Department of Energy
under Contract No. W-7405-Eng-48

Flow-Through Porous Electrodes

James Arthur Trainham, III

Materials and Molecular Research Division, Lawrence Berkeley Laboratory
and Department of Chemical Engineering, University of California,
Berkeley, California 94720

June 1979

Abstract

The analysis and the behavior of flow-through porous electrodes operating above and below the limiting current are the subjects of this dissertation.

Firstly, the minimum concentration attainable in a flow-through porous electrode is estimated by applying the thermodynamics of electrochemical cells with a knowledge of the maximum operating potential. This predicted concentration is the equilibrium wall concentration at the back of the reactor and is qualitatively compared to the experimentally measured minimum average bulk values observed by various authors for the deposition of copper, silver, lead and mercury, and the oxidation of ferrous ions. It is suggested that a knowledge of the current versus reactor operating potential will elucidate the lower limits observed for any metal system.

Secondly, a one-dimensional model for flow-through porous electrodes operating above and below the limiting current of a metal deposition reaction is developed. The model assumes that there is one primary reactant species in an excess of supporting electrolyte and that a simultaneous side reaction may occur. The model predicts non-uniform reaction rates due to ohmic, mass-transfer, and heterogeneous kinetic limitations; the effects of axial diffusion and dispersion are

included. Results are compared with the experimental data observed by various authors on two different chemical systems: (i) the removal of copper from sulfate solutions and (ii) the removal of silver from thiosulfate solutions. Satisfactory agreement between model predictions and experimental data on over-all reactor performance and deposit distributions has been accomplished. The model is then used to predict the effluent concentration as a function of matrix conductivity and electrode length for upstream and downstream placement of the counterelectrode and current collector relative to the fluid inlet of the working electrode. For an infinite matrix conductivity, the lowest effluent concentration is achieved when the counterelectrode is placed upstream to the fluid inlet of the working electrode. When the matrix conductivity is small, the lowest effluent concentration is still achieved for upstream placement of the counterelectrode; however, the optimum placement of the current collector depends on the chemical system and the value of the matrix conductivity that can be achieved in practice. Calculations show that for downstream placement of the counterelectrode a limiting current distribution cannot be achieved (for electrode lengths of interest here). Distribution of potential, reaction rate, and electric driving force are presented for four different configurations.

Thirdly, preliminary data on mercury removal from a sodium chloride brine using a flow-through porous carbon electrode show that this process has great potential. The mercury concentration was reduced from approximately 600 mg/l in the feed to less than 0.1 mg/l in the dilute product stream.

In the last portion of this dissertation, an economic comparison is made between two electrode configurations for flow redox battery applications: (i) the flow-through configuration (current parallel to the fluid flow) and (ii) the flow-by configuration (current perpendicular to the fluid flow). Steady-state computer models are developed for each electrode system. These models are used to predict current density, cell voltage, and power density over a complete cycle (charge and discharge). The economic comparison is made by optimizing each configuration with respect to an objective function appropriate for this application. In this case, only the variable costs are considered. The results of the optimization show that the flow-by configuration is superior. The flow-through configuration not only yields a lower return on investment, but it is impractical due to a requirement of extremely low flow rates ($Re < 0.001$). Its failure is due to current flow (and ohmic potential drop) in the same direction as the fluid flow.

Dedication

To my parents

Flow-Through Porous Electrodes

Contents

I. Introduction

1.1. Perspective

This dissertation discusses some aspects of electrochemical reactor analysis. In particular, the behavior of flow-through porous electrodes is examined in applications to metal-ion removal from dilute streams and to flow-redox batteries. Because electrochemical reactor analysis is not a common subject, even to chemical engineers, a brief description of a flow-through porous electrode is in order. This is done most simply by analogy. A flow-through porous electrode can be thought of as the electrochemical analogue of a packed bed catalytic reactor. The packing material in this case is electrically conducting and continous. Also, the catalytic properties of the packing can be just as important as in chemical reactors. This latter characteristic is especially true in battery applications.

Flow-through porous electrodes have potential not only for metal-ion recovery and for the storage of energy, but also for the synthesis of chemicals. This is because of their high specific interfacial areas and the intimate contact provided between the electrolytic solution and the conducting matrix.

The theme of this dissertation is the prediction and interpretation of physicochemical phenomena which can occur in flow-through porous electrodes. This is accomplished through modeling. Since the purpose of modeling is ultimately linked to design, a useful model will only include those features which emphasize the limiting factors of the system. Therefore, let us consider some of these limitations:

a. Mass transfer. For metal-ion removal applications, the porous electrode must operate at an appreciable fraction of the

limiting current (the concentration of the limiting reactant approaches zero at the electrode surface; therefore, this current corresponds to the maximum rate at which mass-transfer can occur) if a large percentage of metal ions are to be removed from solution. To describe the rate of mass transfer from the solution phase to the matrix phase, the concept of a mass-transfer coefficient must be used, since we cannot adequately describe the fluid flow in the random porous geometry. The effects of axial diffusion and dispersion are included in the model for completeness. However, only in battery applications are these phenomena important because convection dominates in the metal recovery systems.

b. Ohmic potential drop. Because the capital investment of these reactors may determine whether they can compete successfully with other processes, it will be advantageous to operate the reactor at the highest possible flow rate while maintaining the desired product conversion. However, this optimum flow rate may not be achieved in practice, because the ohmic potential drop within the reactor may become unacceptably large. This can lead to low current efficiencies due to excessive side reactions, and a decrease in cell voltage on discharge in battery applications. Thus, the ohmic potential drop limits the flow rate.

c. Heterogeneous reaction kinetics. If a porous electrode is operating under conditions other than the limiting current (battery applications in particular), a polarization or kinetic equation is needed to describe the dependence of the local reaction rate on concentration and the potential jump at the matrix-solution interface. Because electrode kinetics do not follow fundamental laws, one has to assume an expression for the polarization equation. Here a form of the

Butler-Volmer equation was used.

d. Side reactions. In these times of energy consciousness, any cost optimization must include conversion and current efficiency in relationship to energy consumption. To account for this, the possibility of a simultaneous side reaction must be included in the analysis. It will be shown later how the presence of a side reaction places limitations on attaining a high conversion or achieving a very low effluent concentration of the limiting reactant.

The analysis of flow-through porous electrodes above and below the limiting current is intrinsically complicated by the intimate contact that exists between the flowing solution and the electrode matrix. Both the ohmic potential drop and the mass-transfer rate are in series and in parallel with the processes that occur at the electrode surface (i.e., heterogeneous reaction kinetics and double layer charging) and cannot be separated to yield simple analytic solutions. However, certain limiting cases are tractable and can provide insight into the more complete models presented here (see Bennion and Newman (1972) and Newman and Tiedemann (1978)).

1.2 Scope

At the time this dissertation was written, chapters 2 through 4 had been already published. The titles of these chapters remain the same as the published form; however, some changes have been incorporated to add continuity between the chapters. In addition, the reference format has been changed to alphabetical by first author. A review of the literature is included with each chapter; however, it is very specific since Newman and Tiedemann (1975 and 1978) have extensively reviewed the porous electrode literature.

Chapter 2 (J. Appl. Electrochem., 7, 287 (1977)) is concerned with estimating the minimum concentration attainable in a flow-through porous electrode. This is done by applying the thermodynamics of electrochemical cells with an experimentally determined value of the maximum operating potential (the potential of the working electrode relative to a reference electrode placed in the dilute product stream). This chapter grew out of a paper by Kuhn and Houghton (1974) which considered antimony removal. The purpose was to explain their data using fundamental thermodynamic principles.

In Chapter 3 (J. Electrochem. Soc., 124, 1528 (1977)), a theoretical model for flow-through porous electrodes is developed for the removal of metal ions from dilute streams. The model predicts non-uniform reaction rates due to ohmic, mass-transfer, and heterogeneous kinetic limitations in the presence of side reaction. Results are presented for upstream placement of the counterelectrode (relative to the fluid inlet of the working electrode) and for a matrix conductivity much greater than the solution conductivity.

In Chapter 4 (J. Electrochem. Soc., 125, 58 (1978)), the model developed in Chapter 3 is used to predict the performance of a flow-through porous electrode for variations of electrode current density and length, matrix conductivity, flow rate, chemical system, and configuration.

Chapter 5 presents some preliminary data on mercury removal from a sodium chloride brine using a flow-through porous carbon electrode. The results show that this process is extremely effective for mercury recovery. The discussion includes suggestions for obtaining data suitable for design purposes.

In Chapter 6, two different electrode systems are compared on an economic basis for redox battery applications. This is done by developing an electrode model for each system and optimizing these systems with respect to an objective function appropriate for the redox battery application. The first model presented is for the flow-through configuration (current parallel to the fluid flow). This model is essentially the same as that developed in Chapter 3 for metal-ion removal, except that provision is made for a redox reaction. The second model developed is for the flow-by configuration (current perpendicular to the fluid flow). This model is not as sophisticated as the previous models presented, since it would require a two-dimensional analysis. However, it is sufficient for the economic comparison considered here. This comparison is based solely on the variable costs. Results show that the flow-by configuration is superior.

2. A thermodynamic estimate of the minimum concentration attainable in a flow-through porous electrode

2.1 Introduction

The removal of heavy metals from industrial wastes by flow-through porous electrode reactors is promising, though not yet proved to be technologically and economically feasible. Encouraging results have been obtained in studies by Bennion and Newman (1972), Posey (1973), Chu, Fleischmann and Hills (1974), Williams and Keating (1975), Wenger and Bennion (1976), and Van Zee and Newman (1977) on the removal of various metals and in comparisons to other electrochemical reactors (Kuhn and Houghton (1974a), and Kreysa, Pionteck and Heitz (1975)).

On the other hand, there are results which are less encouraging. In the removal of lead ions Trainham and Newman (1974) have had difficulty in reducing the effluent concentration below 0.5 mg/ℓ. In the work of Kuhn and Houghton (1974b), the concentration of antimony was reduced from 100 mg/ℓ in the feed to a dilute product concentration not lower than 5 mg/ℓ. This apparent limit was explained as being the equilibrium concentration at which deposition and dissolution of antimony occurs at the same rate.

The purpose of this chapter is to suggest a criterion by which one may estimate the minimum attainable dilute product concentration given the maximum operating potential, or given a desired dilute product concentration the minimum value of the operating potential at which this dilute product concentration can be achieved, thus providing a basis for design and operation.

In the design of electrochemical reactors, it is desirable to avoid side reactions. Such reactions occur if the potential variation in the solution exceeds a certain limit. Since a characteristic of flow-through porous electrodes is the non-uniform ohmic potential drop, the operating potential may not be set arbitrarily high. The maximum operating potential is that potential which may be maintained in the electrode at which an appreciable side reaction does not occur. This can be determined experimentally by measuring the current versus the potential of the working electrode current collector relative to a given reference electrode placed in the effluent stream (VOP, shown schematically in Figure 1). VOP as shown in Figure 1 is the potential difference $\Phi_{met} - \Phi_{soln}$, where Φ_{met} is the electrostatic potential of the constant potential current collector and Φ_{soln} is the quasi-electrostatic potential (see, for example, Newman (1973), chapters 2 and 3) of the solution leaving the reactor.

Various authors (Bennion and Newman (1972), Trainham and Newman (1974), Van Zee and Newman (1977), and Adams, Hollandsworth and Bennion (1975)) have used the configuration shown in Figure 1 to obtain the current-potential behavior of these reactors. Inspection of the resulting current-potential curve yields a value of the maximum operating potential VOP_{max}. If it is assumed that the reactant species leaving the reactor is in equilibrium with the working electrode current collector at the potential VOP_{max}, a value of the lower limit of removal of the reactant species may be calculated.

To attain a low effluent concentration, we envision placement of the counterelectrode upstream of the working electrode in Figure 1.

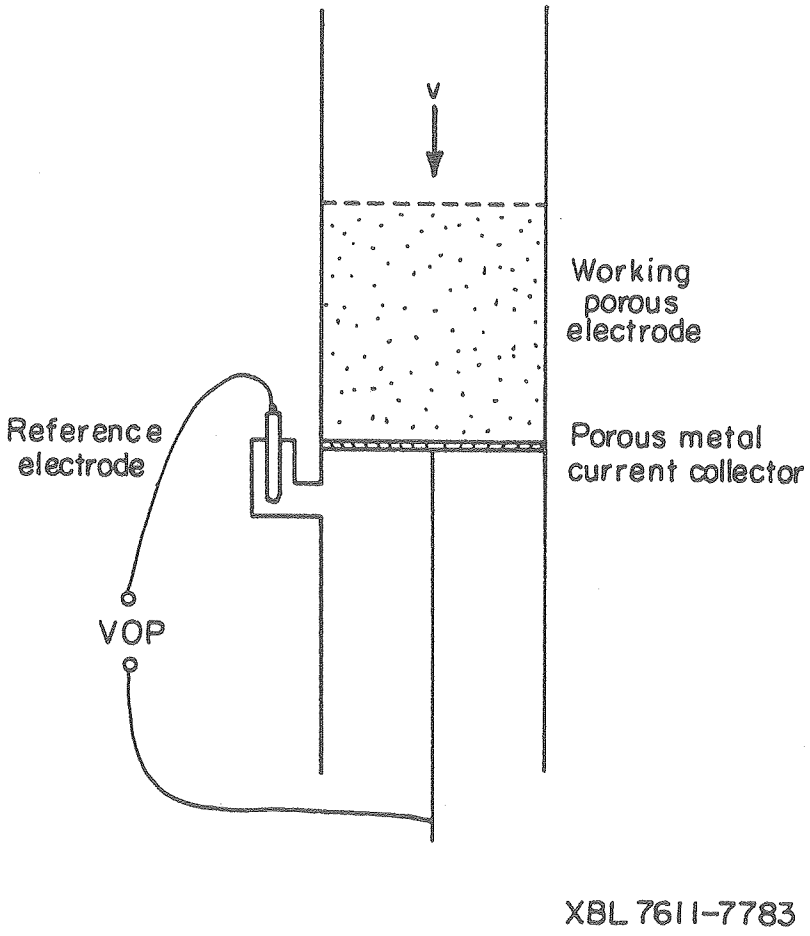

Figure 2-1. Measurement of VOP in a flow-through porous electrode.

This results in the potential distribution shown in Figure 2 (see chapters 3 and 4, also Trainham and Newman (1977b) for details). The current flowing in the solution drops to zero at the back of the electrode and, because the reaction rate is also low in this region, the potential variation in the solution may also be small over a considerable portion of the thickness of the electrode. In this region, the potential difference between the matrix and the solution will be approximately equal to VOP ($-\Phi_{2L}$ in Figure 2), and thus there may be some substantial distance over which the bulk concentration can be approaching the wall concentration.

An alternative electrode configuration used by (Roe (1964), and Alkire and Ng (1974, 1977)) involves placement of the counterelectrode adjacent to the working electrode, so that the fluid flow is parallel to the separation between the electrodes. (A similar configuration has been used by Backhurst, Coulson, Goodridge, Plimley and Fleischmann (1969) where the electrodes are fluidized beds rather than packed beds.) To attain a low effluent concentration, the electrodes are then made long in the direction of flow. Since the reaction rate decreases in the downstream region, there will again be a substantial distance where the potential difference between the matrix and the solution will be approximately equal to VOP.

An undesirable configuration, from the point of view of attaining a low effluent concentration, is where the counterelectrode is placed downstream and the current collector upstream in Figure 1. The corresponding potential distribution in the solution is also shown in Figure 2 as a dashed curve and is drawn for the same total current as

Figure 2-2. Calculated (see chapter 4 for details) solution-phase and solid-matrix-phase potential distributions for the deposition of copper and simultaneous formation of dissolved hydrogen for the following cases: 1) downstream placement of the counterelectrode with an upstream current collector and 2) upstream placement of the counter-electrode with a downstream current collector, where the matrix conductivity σ is considerably greater than the solution conductivity κ. Φ_2 is the potential measured with a copper reference electrode with $c_{Cu^{2+}} = c_f$ in the reference electrode compartment. The calculations in both cases were done for $v = 3.328\times10^{-3}$ cm/sec, $c_f = 1.05\times10^{-5}$ mole/cm^3, $a = 25$ cm^{-1}, $i = -0.007$ A/cm^2, and $L = 6$ cm.

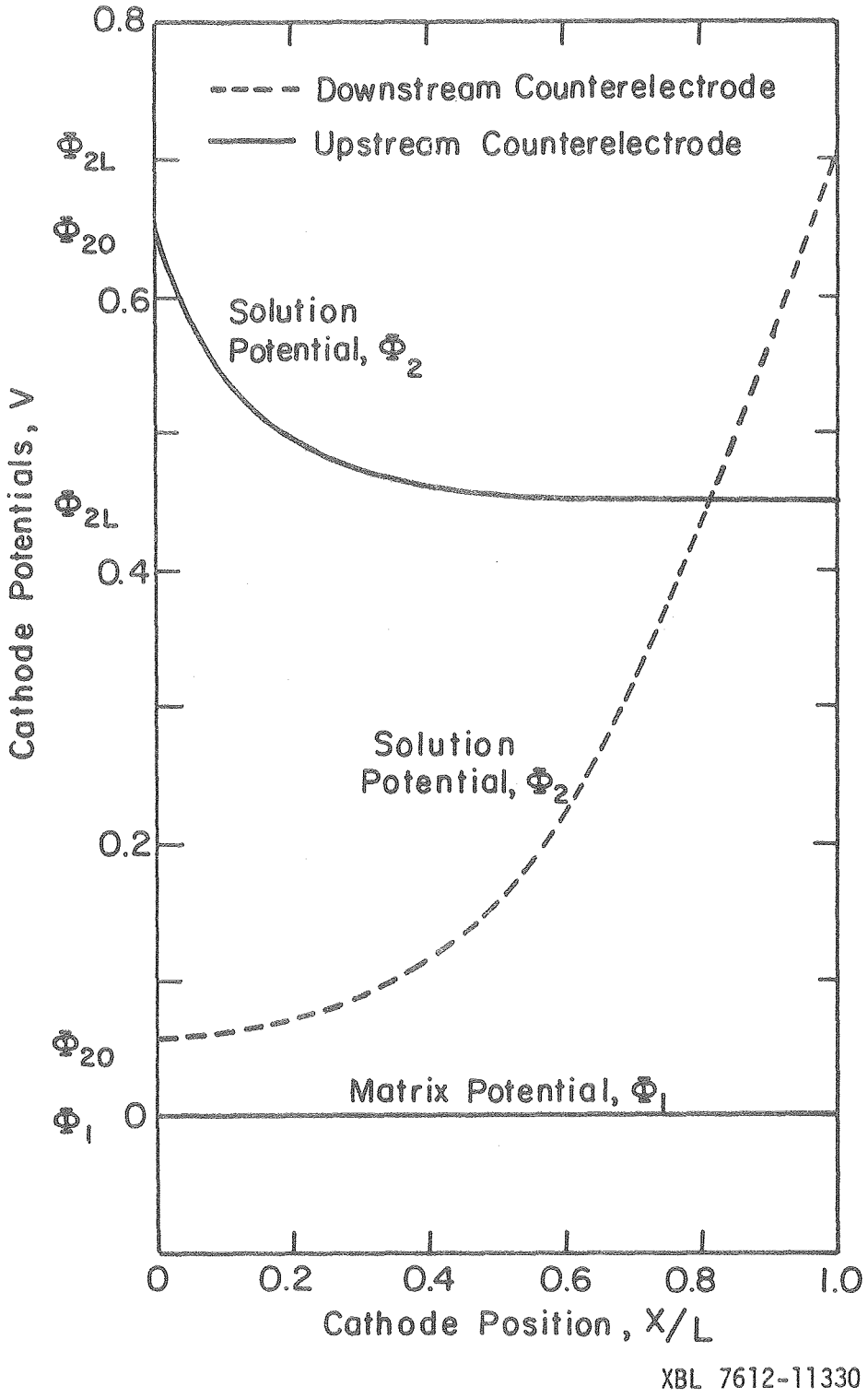

Figure 2-2. See next page for figure caption.

the curve for the upstream counterelectrode (for these calculated potential distributions the effluent concentration is less by a factor of 61 for the upstream placement of the counterelectrode than for the downstream placement of the counterelectrode). In contrast to the two configurations discussed above, the solution potential varies substantially in the downstream region, because the current here is the total current flowing to the counterelectrode, and an increase of the electrode dimension in the direction of fluid flow will not necessarily have a beneficial effect on the removal or recovery of the solute. The maximum electric driving force $(\Phi_1 - \Phi_2)$ occurs at the downstream end of the electrode, but this does not prevail over a substantial distance. If this maximum electric driving force is restricted so that undesirable side reactions are maintained at a tolerable level, then only a greatly diminished electric driving force will be available over much of the electrode thickness, and the effluent concentration cannot be expected to drop to the thermodynamic value corresponding to the measured value of VOP ($-\Phi_{2L}$ in Figure 2).

In the applications of this work, we think in terms of the first two configurations, where the potential difference between the matrix and the solution can be made approximately equal to VOP over a considerable distance. Also in a recycle system (Kuhn and Houghton (1974b)) or a system with several reactors in series, it is possible to allow adequate opportunity for the effluent concentration to approach the thermodynamic value corresponding to a given value of VOP.

2.2 Analysis

In order to calculate the minimum attainable concentration in a flow-through porous electrode reactor, using the values of VOP_{max}, one can construct mentally an electrochemical cell which consists of the working electrode and the given reference electrode. An expression for the open-circuit cell potential U may then be derived using thermodynamics if the following assumptions are made:

1) The reactor has been run sufficiently long that metal deposition of the reactant has occurred.

2) Equilibrium exists between the reacting species and the deposited metal.

3) The molecular and ionic forms of the reacting species are known.

The value of VOP_{max} is then substituted for U, and the equilibrium wall concentration for a particular reacting species is obtained. The total equilibrium wall concentration is simply the sum of all the reacting species which are in equilibrium with the deposited metal. This calculated value will be lower than the actual effluent concentration because of a lack of equilibrium at the downstream end of the reactor due to a nonzero reaction rate and electrode kinetic and mass-transfer limitations.

The following examples will help to clarify the method.

Example 1. Copper deposition from sulfate solutions

Bennion and Newman (1972) have obtained the current-potential behavior of a porous carbon reactor used in the removal of copper from sulfate solutions. From their data, a value of VOP_{max} equal to

-0.25 V may be chosen. A schematic representation of this cell is as follows:

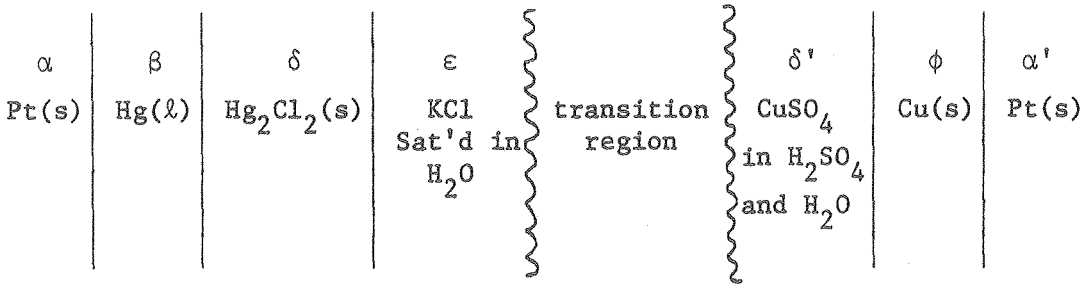

where the reaction at the left electrode is

$$2Hg + 2Cl^- \rightleftarrows Hg_2Cl_2 + 2e^- , \qquad (2\text{-}1)$$

and one possible reaction at the right electrode is

$$Cu^{2+} + 2e^- \rightleftarrows Cu . \qquad (2\text{-}2)$$

An expression for the open-circuit cell potential U may be derived using the thermodynamics of electrochemical cells (for example, see Newman, 1973, chapters 2 and 3). For this cell, the open-circuit cell potential was found to be

$$FU = FU^{\theta} + \frac{1}{2} RT \ln \frac{c_{Cu^{2+}} c^2_{Cl^-,sat}}{\rho_o^3} + \frac{1}{2} RT \ln f_{Cu^{2+},Cl^-}$$

$$+ F(\Phi^{\varepsilon} - \Phi^{\delta'}) , \qquad (2\text{-}3)$$

where

$$FU^{\theta} = \mu^o_{Hg} - \frac{1}{2} \mu^o_{Cu} - \frac{1}{2} \mu^o_{Hg_2Cl_2} + \frac{1}{2} RT \ln \lambda^{\theta}_{Cu^{2+},Cl^-} . \qquad (2\text{-}4)$$

Thus, the value of the standard cell potential for this cell at 25°C is

$$U^{\theta} = 0.337 \text{ V} - 0.2676 \text{ V} = 0.0694 \text{ V} .$$

Omission of the activity coefficient and liquid-junction potential terms (the fourth and fifth terms) in equation 3 will result in a satisfactory estimate of the equilibrium copper concentration. With these considerations equation 3 may be re-arranged to yield an expression for the equilibrium cupric concentration as follows:

$$c_{Cu^{2+}} = \frac{\rho_o^3}{c^2_{Cl^-,sat}} \exp\left(\frac{2F}{RT}\Delta V_k\right) = 9.07\times10^{-13} \text{ mole}/\ell \qquad (2\text{-}5)$$

where U has been set equal to VOP_{max}, $\Delta V_k = VOP_{max} - U^{\theta}$, and $c_{Cl^-,sat} = 4.17$ moles/ℓ .

As was mentioned previously, the deposition of copper from cupric ions is not the only equilibrium electrode process. Cuprous ions are also in equilibrium with both the deposited copper and the cupric ions. The equilibrium cuprous concentration can be calculated as was done earlier for the cupric ions. However, cuprous ions disproportionate according to

$$2\ Cu^{+} \rightleftarrows Cu + Cu^{2+} . \qquad (2\text{-}6)$$

The equilibrium constant for this reaction is given by Newman (1973), p. 57 as

$$\frac{c_{Cu^+}^2 f_{Cu^+}^2}{c_{Cu^{2+}} f_{Cu^{2+}} \rho_o} = \frac{1}{1.67\times10^6} \frac{\text{mole}}{\text{Kg}} . \qquad (2\text{-}7)$$

With neglect of activity coefficients the equilibrium cuprous concentration is found to be:

$$c_{Cu^+} = \left(c_{Cu^{2+}} \rho_o / 1.67\times10^6 \frac{\text{Kg}}{\text{mole}} \right)^{1/2}$$

$$= 7.359\times10^{-10} \frac{\text{moles}}{\ell} . \qquad (2\text{-}8)$$

Therefore the total equilibrium copper concentration

$$(c_{Cu})_{total} = c_{Cu^{2+}} + c_{Cu^+} = 7.37\times10^{-10} \text{ moles}/\ell$$

or 4.68×10^{-5} mg/ℓ .

Example 2. Silver deposition from photographic fixing solutions

Van Zee and Newman (1977) have obtained the current-potential behavior (see also chapter 4) of a porous carbon reactor used for removing silver from photographic fixing solutions. From their data, a value of $VOP_{max} = -0.46$ V was chosen due to appreciable side reaction, thought to be

$$S_2O_3^{2-} + 8e^- + 8H^+ \rightarrow 2HS^- + 3H_2O , \qquad (2\text{-}9)$$

which occurs at a significant rate for more extreme values of VOP. Silver ions in solutions containing thiosulfate form a very stable complex (Trotman and Dickerson (1973)):

$$Ag^{+} + 2S_2O_3^{2-} \rightleftarrows Ag(S_2O_3)_2^{3-} , \qquad (2\text{-}10)$$

which has a value of the stability constant β_2 of approximately:

$$\beta_2 = \frac{{}^{f}_{Ag(S_2O_3)_2^{3-}} \; {}^{c}_{Ag(S_2O_3)_2^{3-}} \; \rho_o^2}{{}^{f}_{Ag^{+}} \; {}^{c}_{Ag^{+}} \left({}^{f}_{S_2O_3^{2-}} \; {}^{c}_{S_2O_3^{2-}} \right)^2}$$

$$= \frac{{}^{\lambda^{\theta}}_{Ag^{+}} \left({}^{\lambda^{\theta}}_{S_2O_3^{2-}} \right)^2}{{}^{\lambda^{\theta}}_{Ag(S_2O_3)_2^{3-}}} = 1.7 \times 10^{13} \left(\frac{Kg}{mole} \right)^2 . \qquad (2\text{-}11)$$

Therefore, it will be necessary to consider the deposition of silver from the silver-thiosulfate complex:

$$Ag + 2S_2O_3^{2-} \rightleftarrows Ag(S_2O_3)_2^{3-} + e^{-} , \qquad (2\text{-}12)$$

which has an expression for the standard electrode potential

$$FU^{\theta}_{Ag/Ag(S_2O_3)_2^{3-}} = \frac{1}{2} \mu^{*}_{H_2} - \mu^{o}_{Ag} - 2 \, RT \, \ell n \, {}^{\theta}_{S_2O_3^{2-}} + RT \, \ell n \, {}^{\theta}_{Ag(S_2O_3)_2^{3-}} / {}^{\theta}_{H^{+}} . \qquad (2\text{-}13)$$

The value for $U^{\theta}_{Ag/Ag(S_2O_3)_2^{3-}}$ may be calculated from the value of the stability constant of the species $Ag(S_2O_3)_2^{3-}$ and the standard electrode potential of the non-complexed silver deposition reaction:

$$Ag \rightleftarrows Ag^{+} + e^{-} . \qquad (2\text{-}14)$$

The expression for the standard electrode potential is

$$FU^{\theta}_{Ag/Ag^{+}} = \frac{1}{2}\mu^{*}_{H_2} - \mu^{o}_{Ag} + RT\ \ell n\ \lambda^{\theta}_{Ag^{+}}/\lambda^{\theta}_{H^{+}} \qquad (2\text{-}15)$$

where $U^{\theta}_{Ag/Ag^{+}} = 0.7991$ V . Equations 13 and 15 lead to

$$U^{\theta}_{Ag/Ag(S_2O_3)_2^{3-}} = U^{\theta}_{Ag/Ag^{+}} - \frac{RT}{F}\ \ell n\ \beta_2$$

$$= 0.0164 \text{ V} , \qquad (2\text{-}16)$$

which indicates that silver will be much more difficult to plate in the presence of thiosulfate ions due to hydrogen evolution.

A schematic of the electrochemical cell which consists of a silver-silver thiosulfate electrode and the calomel reference electrode is as follows:

α	β	δ	ε		δ'	ϕ	α'
Pt(s)	Hg(ℓ)	Hg_2Cl_2(s)	KCl Sat'd in H_2O	tran-sition region	$Ag(S_2O_3)_2^{3-}$ in $Na_2S_2O_3 \cdot 5H_2O$, $NaHSO_3$, NaBr	Ag(s)	Pt(s)

An expression for the equilibrium $Ag(S_2O_3)_2^{3-}$ concentration as a function of VOP may be derived as was done previously for the copper system. This expression with neglect of activity coefficients and the liquid-junction potential is

$$c_{Ag(S_2O_3)_2^{3-}} = \frac{c^2_{S_2O_3^{2-}}}{c_{Cl^-,sat}} \exp\left(\frac{F}{RT}\Delta V_k\right) , \qquad (2\text{-}17)$$

where $\Delta V_k = VOP - U^{\theta}_{Ag/Ag(S_2O_3)_2^{3-}} + U^{\theta}_{cal}$. For $c_{S_2O_3^{2-}} = 1.737$ moles/ℓ and $VOP_{max} = -0.46$ V , the value of the equilibrium silver concentration is 2.14×10^{-4} moles/ℓ or 23 mg/ℓ of silver.

Example 3. Mercury removal from brine solutions

This example combines aspects of the previous two examples, i.e., multiple electrode reaction equilibria and complexing. Mercuric ions Hg^{2+} form very stable chloride complexes with stability constants of the form

$$\beta_\varepsilon = \frac{f_{HgCl_\varepsilon^{2-\varepsilon}} c_{HgCl_\varepsilon^{2-\varepsilon}}}{f_{Hg^{2+}} c_{Hg^{2+}} \left(f_{Cl^-} c_{Cl^-}\right)^\varepsilon} = \frac{a^{\theta}_{Hg^{2+}} \left(a^{\theta}_{Cl^-}\right)^\varepsilon}{a^{\theta}_{HgCl_\varepsilon^{2-\varepsilon}}} \qquad (2\text{-}18)$$

which have values: $\ell n\ \beta_1 = 12.2$, $\ell n\ \beta_2 = 29.4$, $\ell n\ \beta_3 = 32.0$, and $\ell n\ \beta_4 = 34.3$ (see Meites (1962)). Baes and Mesmer (1976) report that the mercurous dimer Hg_2^{++} does not complex appreciably in chloride solutions.

Table 1 lists the expressions and values for the standard electrode potentials of mercury. The standard electrode potentials involving the complexed species were calculated using the above stability constant data. For example, entries 6 and 8 were calculated from entries 2 and 1, respectively, using the value of β_4 as follows:

Table 2-1. Standard electrode potentials of mercury referred to the hydrogen electrode. Aqueous solutions at 25°C.

	Reaction	FU^{θ}	U^{θ}, volt
1)	$Hg_2^{++} \rightarrow 2Hg^{2+} + 2e^-$	$\frac{1}{2}\mu^*_{H_2} - \frac{1}{2}RT \ln \lambda^{\theta}_{Hg_2^{++}} + RT \ln \lambda^{\theta}_{Hg^{2+}}/\lambda^{\theta}_{H^+}$	0.920
2)	$Hg \rightarrow Hg^{2+} + 2e^-$	$\frac{1}{2}\mu^*_{H_2} - \frac{1}{2}\mu^o_{Hg} + \frac{1}{2}RT \ln \lambda^{\theta}_{Hg^{2+}}/\left(\lambda^{\theta}_{H^+}\right)^2$	0.8545
3)	$2Hg \rightarrow Hg_2^{++} + 2e^-$	$\frac{1}{2}\mu^*_{H_2} - \mu^o_{Hg} + \frac{1}{2}RT \ln \lambda^{\theta}_{Hg_2^{++}}/\left(\lambda^{\theta}_{H^+}\right)^2$	0.789
4)	$Hg + 2Cl^- \rightarrow HgCl_2 + 2e^-$	$\frac{1}{2}\mu^*_{H_2} - \frac{1}{2}\mu^o_{Hg} - RT \ln \lambda^{\theta}_{Cl^-} + \frac{1}{2}RT \ln \lambda^{\theta}_{HgCl_2}/\left(\lambda^{\theta}_{H^+}\right)^2$	0.4768
5)	$Hg + 3Cl^- \rightarrow HgCl_3^- + 2e^-$	$\frac{1}{2}\mu^*_{H_2} - \frac{1}{2}\mu^o_{Hg} - \frac{3}{2}RT \ln \lambda^{\theta}_{Cl^-} + \frac{1}{2}RT \ln \lambda^{\theta}_{HgCl_3^{2-}}/\left(\lambda^{\theta}_{H^+}\right)^2$	0.4434
6)	$Hg + 4Cl^- \rightarrow HgCl_4^{2-} + 2e^-$	$\frac{1}{2}\mu^*_{H_2} - \frac{1}{2}\mu^o_{Hg} - 2RT \ln \lambda^{\theta}_{Cl^-} + \frac{1}{2}RT \ln \lambda^{\theta}_{HgCl_4^{2-}}/\left(\lambda^{\theta}_{H^+}\right)^2$	0.4138
7)	$Hg_2^{2+} + 6Cl^- \rightarrow 2HgCl_3^- + 2e^-$	$\frac{1}{2}\mu^*_{H_2} - \frac{1}{2}RT \ln \lambda^{\theta}_{Hg_2^{++}}\left(\lambda^{\theta}_{H^+}\right)^2 - RT \ln \left(\lambda^{\theta}_{Cl^-}\right)^3/\lambda^{\theta}_{HgCl_3^-}$	0.09787
8)	$Hg_2^{++} + 8Cl^- \rightarrow 2HgCl_4^{2-} + 2e^-$	$\frac{1}{2}\mu^*_{H_2} - \frac{1}{2}RT \ln \lambda^{\theta}_{Hg_2^{++}}\left(\lambda^{\theta}_{H^+}\right)^2 - RT \ln \left(\lambda^{\theta}_{Cl^-}\right)^4/\lambda^{\theta}_{HgCl_4^{2-}}$	0.03852

$$U^{\theta}_{Hg/HgCl_4^{2-}} = U^{\theta}_{Hg/Hg^{2+}} - \frac{RT}{2F} \ln \beta_4 \ . \qquad (2\text{-}19)$$

$$U^{\theta}_{Hg_2^{++}/HgCl_4^{2-}} = U^{\theta}_{Hg_2^{++}/Hg^{2+}} - \frac{RT}{F} \ln \beta_4 \ . \qquad (2\text{-}20)$$

Expressions for the equilibrium mercuric chloride complex concentration as a function of VOP may be derived as was done in previous examples:

$$c_{HgCl_2} = \frac{c^2_{Cl^-} \rho_o}{c^2_{Cl^-,sat}} \exp\left(\frac{2F}{RT} \Delta V_k\right) , \qquad (2\text{-}21)$$

$$c_{HgCl_3^-} = \frac{c^3_{Cl^-}}{c^2_{Cl^-,sat}} \exp\left(\frac{2F}{RT} \Delta V_k\right) , \qquad (2\text{-}22)$$

$$c_{HgCl_4^{2-}} = \frac{c^4_{Cl^-}}{\rho_o c^2_{Cl^-,sat}} \exp\left(\frac{2F}{RT} \Delta V_k\right) , \qquad (2\text{-}23)$$

where ΔV_k refers to the electrode reaction involving the appropriate mercuric complex (activity coefficient corrections and the liquid-junction potential were neglected). The expression for the species $HgCl^+$ and Hg^{2+} are not given since their contribution to the equilibrium mercury concentration is negligible in comparison with the highly complexed species. The equilibrium concentration of the mercurous dimer may be related to the mercuric chloride complex concentrations by the appropriate disproportionation reaction. For example, consider the reaction

$$Hg_2^{++} + 3Cl^- \rightleftarrows Hg + HgCl_3^- , \qquad (2\text{-}24)$$

with the result

$$c_{Hg_2^{++}} = \frac{\rho_o^3 c_{HgCl_2^-}}{c_{Cl^-}^3} \exp\left[\frac{2F}{RT}\left(U^\theta_{Hg_2^{++}/HgCl_3^-} - U^\theta_{Hg/HgCl_3^-}\right)\right] . \qquad (2\text{-}25)$$

From entries 5 and 7 of Table 1,

$$c_{Hg_2^{++}} = \frac{\rho_o^3 c_{HgCl_3^-}}{c_{Cl^-}^3} (2.08\times10^{-12}) \text{ mole}/\ell , \qquad (2\text{-}26)$$

and may therefore be neglected from further consideration. Preliminary data on this system have been obtained by Trainham and Newman (1975) in a porous carbon reactor. For a feed concentration of 4.12 mg/ℓ of mercury, a value of $VOP_{max} = -0.46$ V was found, with $c_{Cl^-} = 4.35$ moles/ℓ in the brine. Substituting these values into equations 21 through 23 yields a total mercuric concentration of 1.36×10^{-14} mg/ℓ, the complex $HgCl_4^{2-}$ predominating. Under these conditions equation 25 or 26 yields the estimate of the mercurous dimer as 1.52×10^{-27} mg/ℓ.

Example 4. Lead removal from lead-sulfate solutions

A preliminary study has been made on this system by Trainham and Newman (1974). An expression for the equilibrium lead ion concentration may be obtained by considering the working electrode reaction to be

$$Pb^{2+} + 2e^{-} \rightarrow Pb \quad , \quad U^{\theta}_{Pb/Pb^{2+}} = -0.126 \text{ V} \quad , \tag{2-27}$$

with the result

$$c_{Pb^{2+}} = \frac{\rho_o^3}{c^2_{Cl^-,sat}} \exp\left(\frac{2F}{RT} \Delta V_k\right) \quad . \tag{2-28}$$

For a feed concentration of lead of 4.32 mg/ℓ a maximum operating potential VOP_{max} was found to be -0.56 V . Substituting this value into equation 28 yields an equilibrium lead ion concentration of $c_{Pb^{2+}} = 1.35 \times 10^{-7}$ mole/ℓ or 0.028 mg/ℓ of lead.

Example 5. Oxidation of ferrous ion

Adams, Hollandsworth, and Bennion (1975) have studied ferrous oxidation on a porous carbon electrode from a dilute stream containing 1.43 g/ℓ of H_2SO_4 . On an inert carbon electrode, only the following redox reaction need be considered:

$$Fe^{++} \rightarrow Fe^{+++} + e^{-} \quad , \quad U^{\theta} = 0.771 \text{ V} \quad , \tag{2-29}$$

where the equilibrium ferrous composition may be estimated from

$$c_{Fe^{++}} = \frac{c_{Fe^{+++}} c_{Cl^-,sat}}{\rho_o} \exp\left(\frac{-F}{RT} \Delta V_k\right) \tag{2-30}$$

if the ferric composition is known. If the reactor is long enough, the reaction (equation 29) will have gone to complete conversion except for the equilibrium composition exiting at a particular value of the

operating potential. Thus, for a feed composition of 705 mg/ℓ ferrous ion and a maximum value of the operating potential of $VOP_{max} = 0.7$ V, the equilibrium ferrous concentration may be estimated to be $c_{Fe^{++}} = 1.4$ mg/ℓ .

2.3 Experimental minimum concentration

The minimum wall concentration calculated in the above examples must be compared with the minimum bulk average concentration leaving the reactor because the equilibrium wall concentration is not easily measured. Table 2 lists the measured minimum bulk concentration obtained by various authors in flow-through porous electrode reactors. Also shown are the predicted minimum wall concentrations for these systems which were calculated in examples 1 through 5 for the experimental values listed in the table.

The experimental bulk concentration will approach the predicted wall concentration values if the reaction is carried to a greater degree of completion. This may be achieved by reducing the flowrate, while holding VOP constant, making the electrode thicker (upstream counterelectrode only), or adding additional reactors operating with equal values of VOP.

The discrepancies which exist between the predicted minimum wall concentration and the experimental bulk values may be explained as follows. For copper removal, the reactor was designed to operate with a mass-transfer limitation to remove copper from 667 mg/ℓ to 1 mg/ℓ , and not to remove all the copper. For mercury removal, the experimental minimum bulk concentration of less than 5×10^{-3} mg/ℓ

Table 2-2. Experimental minimum bulk concentration and predicted minimum wall concentration for various systems.

System	Feed Concentration mg/ℓ	Observed Effluent Concentration mg/ℓ	Electrode Potential V	Calculated Wall Concentration mg/ℓ
copper	667	0.06	-0.25	4.7×10^{-5}
silver	1000	42	-0.46	23
lead	4.32	0.55	-0.56	0.028
mercury	4.12	<0.005	-0.46	1.36×10^{-14}
antimony	100	5	-0.3828*	1.62×10^{-13}
ferrous oxidation	705	1	0.7	1.4

*Potential at which the calculated antimony wall concentration exhibits a minimum (see Figure 3).

reported in Table 2 is due to the limitations of the analytical technique used for detecting mercury. For the operating potential reported, samples obtained from the dilute product stream of the reactor contained no detectable mercury. For ferrous oxidation only, the predicted minimum wall concentration is greater than the observed bulk value. Adams et al. (1975) report that the current measured for this system is greater than that based on the feed composition ($i = nF\ v\ c_f$) at current efficiencies approaching 100 percent. One explanation presented by these authors is the oxidation of ferrous species by oxygen, a reaction which is catalyzed on a graphite surface. For silver, the agreement is good; it should be noted that effluent values as low as 0.8 mg/ℓ were achieved at VOP values as extreme as -0.55 V , but with a considerable loss of current efficiency due to side reactions.

2.4 The removal of antimony

As mentioned earlier, Kuhn and Houghton (1974b) have reported an apparent limit in the removal of antimony from aqueous solutions using a flow-through porous electrode reactor. Application of the criterion suggested in previous sections using the data of Kuhn and Houghton (1974b) is not possible since their study was one of transient response and no steady-state current-potential data were provided. However, qualitative information about their experiments allows a thermodynamic analysis to be undertaken which indicates that a minimum exists in the antimony concentration as a function of VOP.

2.5 Analysis of antimony removal

The chemistry of antimony in aqueous solutions is quite complex, and many molecular and ionic species are possible. Kuhn and Houghton (1974b) report that in their experiments the oxidation state of the dissolved antimony species was plus three. Table 3 lists the standard electrode potentials of various antimony species which are known to exist in the plus three oxidation state (values of which have been calculated from thermodynamic data (Wagman, Evans, Parker, Halow, Bailey and Schumm (1968)) or found tabulated in the literature (Weast (1971)). Stability data indicate that $Sb(OH)_3$, and SbO^+ are the most probable species and that Sb^{+++} rarely exists except under extremely acidic conditions (Baes and Mesmer (1976)). Expressions for the equilibrium wall concentration as a function of VOP for each of the antimony species may be derived as before and are also given in Table 3.

2.6 Results for antimony removal

Figure 3 depicts the dependence on VOP of the equilibrium wall concentration of the various antimony species found in Table 3, where the concentration of hydrogen ion has been set to 1 mole/ℓ. The solid line represents the total equilibrium antimony concentration if all of these species are present in solution.

The minimum exhibited by the total antimony concentration is due to the evolution of stibine (SbH_3) in a minus three valence state at high cathodic potentials (negative values of VOP). This supposition is supported qualitatively by the data of Kuhn and Houghton (1974b), who report stibine evolution and low current efficiencies. The low current efficiencies are due to cell operation at too high cathodic

Table 2-3. Standard electrode potentials of antimony referred to the hydrogen electrode. Aqueous solutions at 25°C. Equilibrium wall concentration of antimony as a function of VOP.

	Reaction	U^{θ}, volt	Concentration, mole/ℓ
1)	$SbH_3 \rightarrow Sb + 3H^+ + 3e^-$	-0.5104	$c_{SbH_3} = \frac{\left(c_{H^+} c_{Cl^-,sat}\right)^3}{\rho_o^5} \exp\left(-\frac{3F}{RT}\Delta V_k\right)$
2)	$2Sb + 3H_2O \rightarrow Sb_2O_3 + 6H^+ + 3e^-$	0.1445	$c_{Sb_2O_3} = \frac{\rho_o^{13}}{\left(c_{H^+} c_{Cl^-,sat}\right)^3} \exp\left(\frac{6F}{RT}\Delta V_k\right)$
3)	$Sb + H_2O \rightarrow SbO^+ + 2H^+ + 3e^-$	0.2075	$c_{SbO^+} = \frac{\rho_o^6}{c_{H^+}^2 c_{Cl^-,sat}^3} \exp\left(\frac{3F}{RT}\Delta V_k\right)$
4)	$Sb + 3H_2O \rightarrow Sb(OH)_3 + 3H^+ + 3e^-$	0.2307	$c_{Sb(OH)_3} = \frac{\rho_o^7}{\left(c_{H^+} c_{Cl^-,sat}\right)^3} \exp\left(\frac{3F}{RT}\Delta V_k\right)$
5)	$Sb + 2H_2O \rightarrow HSbO_2 + 3H^+ + 3e^-$	0.2309	$c_{HSbO_2} = \frac{\rho_o^7}{\left(c_{H^+} c_{Cl^-,sat}\right)^3} \exp\left(\frac{3F}{RT}\Delta V_k\right)$
6)	$Sb + 2H_2O \rightarrow SbO_2^- + 4H^+ + 3e^-$	0.4633	$c_{SbO_2^-} = \frac{\rho_o^8}{c_{H^+}^4 c_{Cl^-,sat}^3} \exp\left(\frac{3F}{RT}\Delta V_k\right)$

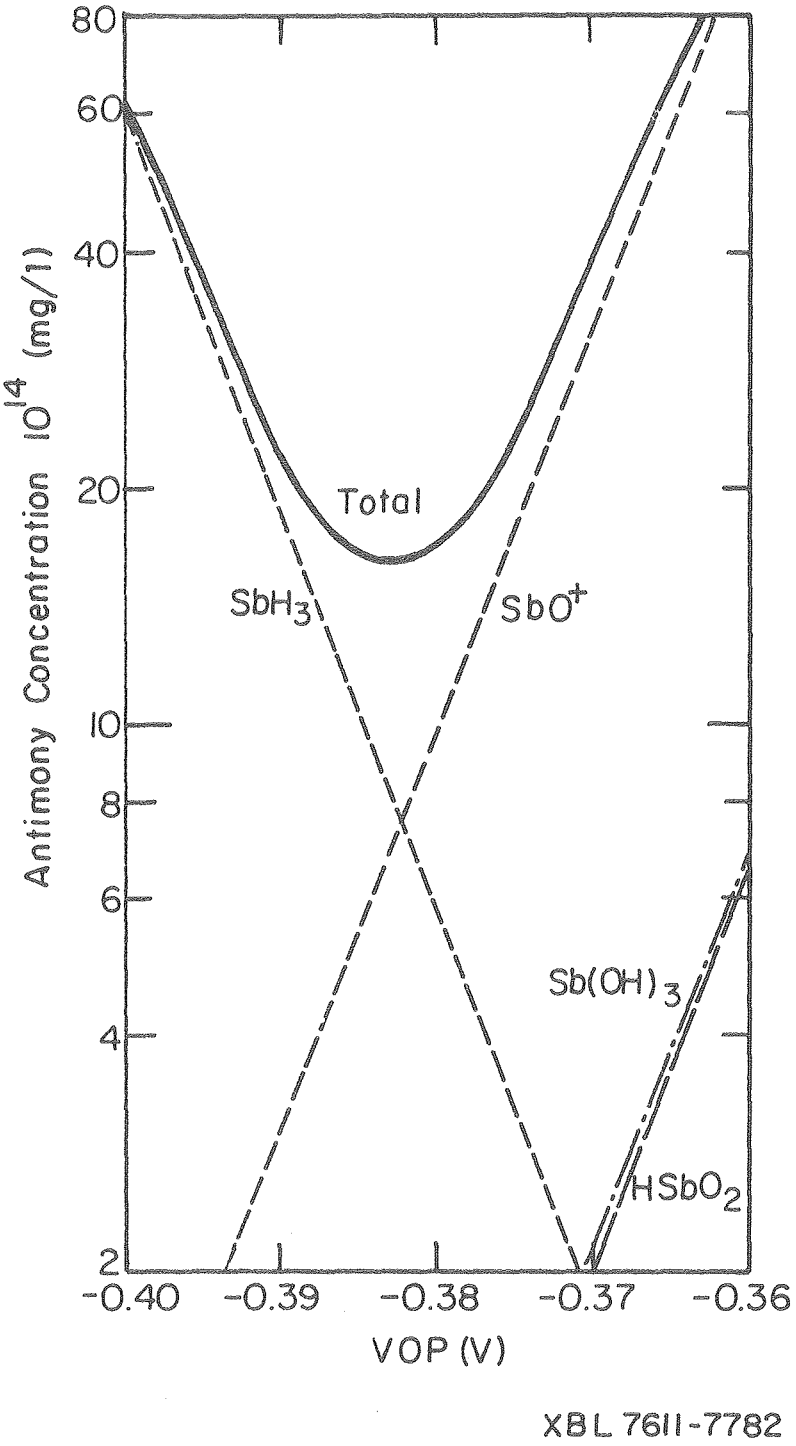

Figure 2-3. Equilibrium antimony concentration as a function of electrode potential relative to a saturated calomel electrode.

potentials where both the evolution of stibine and hydrogen are appreciable. However, quantitatively the estimated equilibrium wall concentration (shown in Figure 3) lies thirteen orders of magnitude below the reported bulk value. As discussed earlier, the bulk value will exceed the equilibrium value somewhat because of electrode-kinetic and mass-transfer limitations; however, a large discrepancy does exist. This may be explained by considering the range of potential at which the predicted equilibrium wall concentration is less than or equal to the measured bulk value (5 mg/ℓ). Calculations (using the expressions found in Table 3) indicate that this range of potential is $-0.655 \leq \text{VOP} \leq -0.130$ V . Since Kuhn and Houghton (1974b) operated their cell galvanostatically, their cell potential could vary over a wide range. To resolve the question of the practical lower limit attainable for antimony removal, careful, controlled-potential, steady-state experiments will be required.

2.7 General considerations

As discussed earlier, the bulk concentration of the reactant species will approach the equilibrium wall concentration predicted by thermodynamics if the reactor is made thicker (upstream counterelectrode only) or additional reactors are placed in series. This may be seen quantitatively by considering the analysis presented by Bennion and Newman (1972) for a reactor operating at the limiting current with an upstream counterelectrode (see Newman and Tiedemann (1976) for the analysis of a downstream counterelectrode).

For reactions carried to a high degree of completion, the allowable potential variation across a reactor can be estimated approximately as

$$\Delta\Phi_2' \sim - \frac{nF\ v^2 c_f}{s_R a\ k_m \kappa} \ . \qquad (2\text{-}31)$$

This equation shows that the ohmic potential drop across a reactor is directly proportional to the feed concentration. In the copper recovery process of Bennion and Newman (1972) a value of the operating potential VOP may be chosen to be -0.25 V (the potential at the fluid outlet). If their reactor were operating at the design specification, $\Delta\Phi_2' = 0.2$ V , the driving force at the front of the reactor would be -0.45 V . The data indicate that the magnitude of this value does not produce appreciable side reactions -- thus if this driving force could be maintained throughout the depth of the reactor the effluent concentration will utlimately be reduced. With this in mind, the ultimate value of VOP is then -0.45 V . Equations 5 and 8 then yield an estimate of the lowest attainable equilibrium wall concentration for copper of 1.94×10^{-8} mg/ℓ .

In order to achieve this in practice, consider reactors placed in series: if for example the concentration in the first reactor has been reduced by 99 percent, then the total current density in the second reactor ($i = nF\ v\ c_f$) will be smaller resulting in a reduction in the ohmic potential drop (see equation 31), and the electrode potential can be maintained closer to -0.45 V throughout the second reactor.

This also applies to short reactors where the reaction rate is non-zero at the back of the reactor resulting in an appreciable surface overpotential, thereby producing a wall concentration higher than the equilibrium value. Increasing the reactor thickness will also decrease the wall concentration toward the equilibrium value if the

counterelectrode and current collector are placed upstream (or if the matrix couductivity is increased, see, for example Newman and Tiedemann (1976) and Trainham and Newman (1977c)).

2.8 Conclusions

A criterion has been suggested for determining the minimum concentration attainable in a flow-through porous electrode reactor. This may be done by measuring the cell current as a function of the potential of the working electrode current collector relative to a reference electrode of a given kind placed in the effluent stream (see Figure 1). Thermodynamics may then be applied by assuming that this measured potential can be set equal to an expression for the open-circuit cell potential between these electrodes, thereby yielding a value of the equilibrium wall concentration of the reactant species. It should be emphasized that the value of the minimum concentration obtained is a lower limit.

Comparison of this concentration with the experimentally observed effluent concentration suggests that the procedure is essentially correct, although the effluent concentration will be higher than that calculated if the reactor thickness is small and mass-transfer and electrode-kinetic limitations still exist at the fluid outlet. If either mass-transfer limitations or kinetic factors appear to be dominant, the reactor may well have been designed so that the effluent concentration can be predicted on the basis of these governing factors -- and an estimation based on thermodynamic considerations would not be necessary.

Measurement of the reactor operating potential as described above should help to clarify lower limits observed in flow-through electrochemical reactors. It should also aid in the design of reactor systems, since information on the allowable ohmic potential variation within the solution from the inlet to the outlet of the reactor is provided.

3. A flow-through porous electrode model: application to metal-ion removal from dilute streams

3.1 Introduction

This chapter develops a theoretical model which describes the macroscopic behavior of flow-through porous electrodes. In the macroscopic treatment of flow-through porous electrodes, the geometric detail of the porous structure is disregarded. The solid-matrix phase and the electrolyte phase filling the pores are described mathematically as a superposition of two continua (see Newman and Tiedemann (1975) for details). (Also, see Appendix B or Dunning (1971) for the definition of the averaged quantities used in this description and a detailed derivation of the equation of continuity for a species i .) The model described here will be applied throughout the remainder of this thesis.

In previous work (Bennion and Newman (1972), Newman and Tiedemann (1975), Alkire and Gracon (1975), Newman and Tiedemann (1976), and Sioda (1975)), a flow-through porous electrode operating at the limiting current was treated. Sioda (1972) gave an analysis for a flow-through porous electrode operating below the limiting current for a reversible reaction described by the Nernst equation, which also includes treatment of the interfacial mass-transfer resistance. Alkire and Gracon (1975) included a very general analysis of a single electrode reaction below the limiting current, including the effects of axial diffusion; results are given for an upstream counterelectrode. Recently, Alkire and Gould (1976) have extended this work to multiple reaction sequences, which includes: deposition of several metals, deposition of a metal in the presence of a re-dox system, and an ECE sequence applicable

to electro-organic synthesis; results are given for a downstream counter-electrode. Ateya and Austin (1977) give an analysis similar to Sioda (1972) for a single electrode reaction described by the Nernst equation and study the effects of axial diffusion and dispersion under conditions when the interfacial mass-transfer resistance appears to be negligible.

The present analysis complements previous work by predicting nonuniform reaction rates due to ohmic, mass-transfer, and heterogeneous kinetic limitations in the presence of a side reaction. Also included are the effects of axial diffusion and dispersion without simplification of the Danckwerts (1953), Werner-Wilhelm (1956) boundary conditions as was done in previous work (Alkire and Gracon (1975) and Alkire and Gould (1976)). Simplifications made possible in the treatment of the side reaction due to the small reactant concentration and the desire to operate at high current efficiencies should make this analysis attractive for design purposes.

3.2 Model

The case of metal-ion removal from dilute streams using a flow-through porous electrode with parallel current and fluid flow can be modeled with the following restrictions:

1) The model is one-dimensional.

2) The porous cathode is of length L and has an isotropic porosity ε and specific surface area a which remain constant in time.

3) The hydrodynamics are characterized by the superficial velocity v and an average mass-transfer coefficient k_m, where axial diffusion and dispersion account for deviations from plug-flow.

4) There is one reactant species in excess supporting electrolyte.

5) A simultaneous side reaction may occur, which is characterized by its rate at the half-wave potential of the primary reaction. Also, if the side reaction involves generation of a gas, it is assumed that the gas will remain in solution so that the velocity profile will not be disturbed.

6) The conductivity of both the matrix and pore solution phases is uniform.

Assumptions 1 through 3 simplify the calculational procedure and are necessary due to the lack of a better description of the complex porous geometry. The validity of assumptions 4 through 6 rests on the small reactant concentration. As a consequence of assumptions 4 and 5, the current efficiency should be high, which further simplifies the model by removing the need to follow any reactant species concentration which participates in the side reaction. This approach emphasizes the salient features of the interaction between the unwanted side reaction and the metal deposition reaction.

3.3 Analysis

The equations which describe the behavior of porous electrodes have been reviewed recently by Newman and Tiedemann (1975).

Only one material balance is required -- that for the metal-ion reactant. At steady-state, this may be expressed as

$$\frac{dN_R}{dx} = a\, j_{Rn} \,, \qquad (3\text{-}1)$$

where in the absence of migration effects the superficial flux N_R of the metal-ion reactant in the direction of the fluid flow is given by

$$N_R = -\varepsilon(D_R + D_a)\frac{dc_R}{dx} + c_R v \ , \qquad (3\text{-}2)$$

and the local pore-wall flux to the flowing solution is related to the average mass-transfer coefficient k_m (corrected for axial diffusion and dispersion, see Newman and Tiedemann (1976)) by

$$j_{Rn} = k_m(c_{Rw} - c_R) \ . \qquad (3\text{-}3)$$

The quantities c_{Rw} and c_R are the wall concentration and the pore-solution concentration of the metal-ion reactant averaged over the volume of the pores. In equation 2, D_R is the effective diffusion coefficient of the metal-ion reactant within the pore solution and represents a correction to the molecular diffusion coefficient D_o for tortuosity ($D_R = D_o/\tau^2$, where τ is the tortuosity factor). D_a is the axial dispersion coefficient taken to be (Newman and Tiedemann (1976))

$$D_a = \frac{3v}{a\varepsilon}(1 - \varepsilon) \ , \qquad (3\text{-}4)$$

which is a fit of a large number of data correlated by Sherwood et al. (1975) (see also, Newman and Tiedemann (1975)).

In the matrix phase, the transport of electrons is governed by Ohm's law

$$i_1 = -\sigma d\Phi_1/dx \ . \qquad (3\text{-}5)$$

Since it has been assumed that the concentration of the limiting reactant is small compared to the supporting electrolyte concentration, the diffusion potential is neglected; consequently, the current density i_2 in the solution phase is also governed by Ohm's law

$$i_2 = -\kappa \, d\Phi_2/dx \ , \tag{3-6}$$

where κ is the effective conductivity of the solution within the pores, related to the bulk conductivity κ_o as follows (Rue and Tobias (1959))

$$\kappa = \kappa_o \varepsilon^{1.5} \ . \tag{3-7}$$

A consequence of electroneutrality is that charge is conserved between the matrix and pore-solution phases. Mathematically this means the divergence of the total current is zero

$$\frac{di_1}{dx} + \frac{di_2}{dx} = 0 \ . \tag{3-8}$$

The transfer current is due to the sum of the individual electrode reactions:

$$\frac{di_2}{dx} = \sum_j a \, i_{nj} \ , \tag{3-9}$$

where i_{nj} is the average transfer current density (from the matrix phase to the pore solution phase) due to reaction j in an electrode reaction of the form

$$\sum_i s_{ij} M_i^{z_i} \rightarrow n_j e^- \quad . \tag{3-10}$$

With the assumption that the principal reactant R participates only in the primary reaction, we can write

$$i_{nR} = -\frac{nF}{s_R} j_{Rn} = \frac{nF}{s_R} k_m (c_R - c_{Rw}) \quad . \tag{3-11}$$

For the case under consideration, the mass-transfer resistance is unimportant for the side reaction, and substitution of equation 11 into equation 9 yields

$$\frac{di_2}{dx} = -\frac{anF}{s_R} j_{Rn} + a\, i_{nS} \quad , \tag{3-12}$$

where the subscript S refers to the side reaction.

In general, the average transfer current density due to reaction j may be approximated by the Butler-Volmer equation

$$i_{nj} = i_{oj} \left[\exp\left(\frac{\alpha_{aj} F}{RT} \eta_{sj} \right) - \exp\left(-\frac{\alpha_{cj} F}{RT} \eta_{sj} \right) \right] \quad , \tag{3-13}$$

where i_{oj} is the exchange current density which is assumed to have a composition dependence of the form

$$i_{oj} = i_{oj,ref} \prod_i \left(\frac{c_{iw}}{c_{i,ref}} \right)^{\gamma_{ij}} \quad , \tag{3-14}$$

where $i_{oj,ref}$ is the value of the exchange current density for reaction j at a reference composition $c_{i,ref}$. It was further assumed that

the transfer coefficients α_{aj} and α_{cj} sum to n_j (a positive number, see equation 10) and that the exponents γ_{ij} have the form

$$\gamma_{ij} = q_{ij} + \frac{\alpha_{cj}}{n_j} s_{ij} , \qquad (3\text{-}15)$$

such that $q_{ij} = -s_{ij}$ for a cathodic reactant and zero otherwise.

In equation 13, the surface overpotential for reaction j is given by

$$\eta_{sj} = \Phi_1 - \Phi_2 - U_{jw} , \qquad (3\text{-}16)$$

where

$$U_{jw} = U_j^{\theta} - U_r^{\theta} - \frac{RT}{n_j F} \sum_i s_{ij} \ln \frac{c_{iw}}{\rho_o} + \frac{RT}{n_r F} \sum_i s_{ir} \ln \frac{c_{ir}}{\rho_o} , \qquad (3\text{-}17)$$

which is the theoretical open-circuit potential for reaction j at the local wall composition relative to a reference electrode of a given kind, where the subscript r refers to the reference electrode compartment. (The pure-solvent density ρ_o should be expressed in kg/cm^3 if the concentrations are given in $mole/cm^3$.)

For the case of metal-ion removal from dilute streams, equations 13 through 17 can be simplified greatly. Let the reference electrode be of the same kind as the metal deposition reaction, where the concentration of the primary reactant in the reference electrode compartment c_{Rr} and the reference concentration in equation 14 $c_{R,ref}$ are set equal to c_{Rf} (the upstream feed concentration of the metal-ion reactant). Also assume that the stoichiometric coefficient $s_R = -1$. Then equation 13 for a metal deposition reaction reduces to

$$i_{nR} = i_{ok,ref}\left\{\exp\left[\frac{\alpha_{aR}F}{RT}(\Phi_1 - \Phi_2)\right] - \frac{c_{Rw}}{c_{Rf}}\exp\left[-\frac{\alpha_{cR}F}{RT}(\Phi_1 - \Phi_2)\right]\right\} . \quad (3\text{-}18)$$

For a simultaneous side reaction, such as the decomposition of the solvent, equation 13 reduces to an even simpler form

$$i_{nS} = i_{oS,ref}\left\{\exp\left[\frac{\alpha_{aS}F}{RT}(\Phi_1 - \Phi_2 - \Delta U)\right] - \exp\left[-\frac{\alpha_{cS}F}{RT}(\Phi_1 - \Phi_2 - \Delta U)\right]\right\}, \quad (3\text{-}19)$$

where ΔU is the difference in the theoretical open-circuit potentials of the side reaction and the primary reaction ($\Delta U = U_S - U_R$) at the reference concentration, which in this case are at the upstream feed composition. Note that any explicit dependence of the rate of the side reaction on the composition has been ignored. This assumption is justified if the current efficiency is high and the ratio of the metal-ion reactant to the reactant species involved in the side reaction (e.g., the hydrogen ion) is small.

Let $\eta = \Phi_1 - \Phi_2$ be defined as the local overpotential, and combine equations 5 and 6:

$$d\eta/dx = d(\Phi_1 - \Phi_2)/dx = -i_1/\sigma + i_2/\kappa . \quad (3\text{-}20)$$

The elimination of c_{Rw} between equations 3 and 18 yields

$$j_{Rn} = -\frac{\frac{c_R}{c_{Rf}} - \exp\left[(\alpha_{aR} + \alpha_{cR})F\eta/RT\right]}{\frac{1}{c_{Rf}k_m} - \frac{nF}{s_R i_{oR,ref}}\exp\left[\alpha_{cR}F\eta/RT\right]} . \quad (3\text{-}21)$$

Next combine equations 1, 2, and 21 to eliminate N_R and j_{Rn}, which results in a material balance equation for the limiting reactant with unknowns c_R and η :

$$v \frac{dc_R}{dx} = \varepsilon(D_R + D_a) \frac{d^2 c_R}{dx^2} - a \frac{\frac{c_R}{c_{Rf}} - \exp\left[(\alpha_{aR} + \alpha_{cR})F\eta/RT\right]}{\frac{1}{c_{Rf} k_m} - \frac{nF}{s_R i_{oR,ref}} \exp\left[\alpha_{cR} F\eta/RT\right]} . \quad (3\text{-}22)$$

An equation for the potential distribution results from elimination of i_1, i_2, and i_{nS}, between equations 8, 12, 19, 20, and 21 by differentiating equation 20:

$$\frac{d^2\eta}{dx^2} = \left(\frac{1}{\kappa} + \frac{1}{\sigma}\right) a \left\{ i_{oS,ref} \left[\exp\left(\frac{\alpha_{aS} F}{RT}(\eta - \Delta U)\right) - \exp\left(-\frac{\alpha_{cS} F}{RT}(\eta - \Delta U)\right)\right] \right.$$

$$\left. - \left(-\frac{nF}{s_R}\right) \frac{\frac{c_R}{c_{Rf}} - \exp\left[(\alpha_{aR} + \alpha_{cR})F\eta/RT\right]}{\frac{1}{c_{Rf} k_m} - \frac{nF}{s_R i_{oR,ref}} \exp\left[\alpha_{cR} F\eta/RT\right]} \right\} . \quad (3\text{-}23)$$

Before equations 22 and 23 can be solved simultaneously for c_R and η, four boundary conditions are required. For c_R the following conditions were used

$$c_{Rf} v = c_R v - \varepsilon(D_R + D_a) \frac{dc_R}{dx} \quad \text{at} \quad x = 0 \quad (3\text{-}24)$$

where c_{Rf} is the upstream feed concentration, and

$$\frac{dc_R}{dx} = 0 \quad \text{at} \quad x = L \quad (3\text{-}25)$$

-- the Danckwerts (1953), Wehner-Wilhelm (1956) conditions when axial diffusion and dispersion are included. The conditions on η depend on the placement of the counterelectrode. For an upstream counterelectrode, the current density is zero in the matrix phase at the cathode inlet and equal to $-i$ (the total current density to the electrode) in the pore solution phase; the opposite is true at the cathode outlet. Application of these conditions to equation 20 yields appropriate conditions on η :

$$\frac{d\eta}{dx} = -\frac{i}{\kappa} \quad \text{at} \quad x = 0 \ , \tag{3-26}$$

and

$$\frac{d\eta}{dx} = \frac{i}{\sigma} \quad \text{at} \quad x = L \ . \tag{3-27}$$

To reduce the large number of parameters, equations 22 through 27 may be expressed in dimensionless form:

Material balance

$$\frac{d\theta}{dy} = D' \frac{d^2\theta}{dy^2} - \frac{\theta - P_1 \exp\left[(\alpha_{aR}/\alpha_{cR} + 1)\eta'\right]}{1 + \exp(\eta')} \ . \tag{3-28}$$

Potential distribution

$$\frac{d^2\eta'}{dy^2} = P_2 \left\{ P_3 \exp(-\alpha_{cS}\eta'/\alpha_{cR}) \left[1 - P_4 \exp\left(\frac{\alpha_{aS} + \alpha_{cS}}{\alpha_{cR}} \eta' \right) \right] + \frac{\theta - P_1 \exp\left[(\alpha_{aR}/\alpha_{cR} + 1)\eta'\right]}{1 + \exp(\eta')} \right\} . \tag{3-29}$$

Boundary conditions

$$\theta - D' \frac{d\theta}{dy} = 1 \quad \text{and} \quad \frac{d\eta'}{dy} = P_5 I^* \quad \text{at} \quad y = 0 \ , \tag{3-30}$$

and

$$\frac{d\theta}{dy} = 0 \quad \text{and} \quad \frac{d\eta'}{dy} = -P_6 I^* \quad \text{at} \quad y = \alpha L \ , \tag{3-31}$$

where θ is the reactant concentration divided by its value upstream in the feed. Here the distance and the overpotential were made dimensionless in such a manner as to emphasize the pertinent physical phenomena. The dimensionless coordinate y, as suggested by the limiting current analysis of Bennion and Newman (1972), is the physical distance x divided by the quantity $1/\alpha = v/a\ k_m$, representing the effective depth of penetration of the reaction into the electrode at the limiting current. In this way, the parameter

$$D' = (D_R + D_a) a\ k_m / v^2 \tag{3-32}$$

relates to the effect of axial diffusion and dispersion. For flow-through reactors, effects of convection, reaction, and mass-transfer to the wall are dominant, while axial diffusion and dispersion are secondary. Thus, it is appropriate to have these latter effects included in only one parameter, D', and to have the dimensionless coordinate y determined by the dominant effects. However, at low Péclet numbers, $v/a\ D_o < 100$, axial diffusion and dispersion effects are not small (Newman and Tiedemann (1976)), and the inclusion of the corresponding terms in equation 28 and in the boundary condition (equation 30) is necessary.

The local overpotential η was made dimensionless by the relation

$$\exp(\eta') = -\frac{nFk_m c_{Rf}}{s_R i_{oR,ref}} \exp(\alpha_{cR} F\eta/RT) , \qquad (3\text{-}33)$$

which also shifts the overpotential by an additive amount based on the exchange current density $i_{oR,ref}$ of the main reaction and the feed concentration c_{Rf} of the reactant. This shift is in recognition of the fact that the electrode will be run with a relatively high electric driving force so that the main reaction can be carried to a high degree of completion. The backward term of the main reaction is then characterized by the parameter

$$P_1 = \left(-\frac{s_R i_{oR,ref}}{nFk_m c_{Rf}}\right)^{1+\alpha_{aR}/\alpha_{cR}} , \qquad (3\text{-}34)$$

which will be insignificant when the reaction exhibits Tafel behavior.

Under these conditions, the relative importance of the ohmic potential drop within the porous electrode is characterized by the parameter

$$P_2 = \frac{\alpha_{cR} nF^2 v^2 c_{Rf}}{s_R a\, k_m RT}\left(\frac{1}{\kappa} + \frac{1}{\sigma}\right) , \qquad (3\text{-}35)$$

and the side reaction is characterized by

$$P_3 = -\frac{s_R i_{oS,ref}}{nFk_m c_{Rf}} e^{\alpha_{cS} F\Delta U/RT}\left(-\frac{nFk_m c_{Rf}}{s_R i_{oR,ref}}\right)^{\alpha_{cS}/\alpha_{cR}} \qquad (3\text{-}36)$$

at the half-wave potential of the main reaction. The half-wave potential may be calculated from equation 33 by setting η' equal to zero. This is seen from the second term on the right side of equation 28, which represents the dimensionless transfer current of the primary reaction -- setting η' equal to zero yields a value in the denominator of two. The backward term of the side reaction is characterized by the magnitude of the parameter

$$P_4 = \left(- \frac{s_R i_{oR,ref}}{nFk_m c_{Rf}} \right)^{\frac{\alpha_{aS}+\alpha_{cS}}{\alpha_{cR}}} \exp\ [-F(\alpha_{aS} + \alpha_{cS})\Delta U/RT] \ . \qquad (3\text{-}37)$$

The parameters P_5 and P_6 represent the relative importance of the ohmic potential drop in the pore solution phase and the matrix phase, respectively, and are related to the parameter P_2 :

$$P_5 = - \frac{\sigma P_2}{\sigma + \kappa} \ , \qquad (3\text{-}38)$$

and

$$P_6 = - \frac{\kappa P_2}{\sigma + \kappa} \ , \qquad (3\text{-}39)$$

so that

$$-P_2 = P_5 + P_6 \ . \qquad (3\text{-}40)$$

The total current density i to the reactor was made dimensionless with the limiting current density that would exist if all the reactant in the feed were completely reacted:

$$I^* = \frac{s_R i}{nFvc_{Rf}} \quad . \tag{3-41}$$

3.4 Numerical solution

The governing equations 28 and 29 were first linearized about a trial solution and then, along with the boundary conditions (equations 30 and 31), cast in finite-difference form accurate to order h^2, where h is the dimensionless distance between the mesh points, and solved by a numerical technique developed by Newman (1973, Appendix C).

Unfortunately, it was found that the standard central-difference approximations of the derivatives were not sufficiently accurate to approach the limiting-current result, which can be calculated analytically. This anomalous behavior was primarily due to the high degree of non-uniformity in the current and concentration distributions near the front of the electrode. Therefore, to obtain accurate results, new finite-difference approximations to the derivatives were developed (see Appendix A).

3.5 Results

Comparisons between model predictions and experiments. For the calculations to be presented, the counterelectrode is upstream, the primary reaction is the deposition of copper, and the side reaction is the generation of dissolved hydrogen. Two types of data on copper removal (Bennion and Newman (1972) and Alkire and Gracon (1975)) are utilized to demonstrate the effectiveness of the model. In the first data set (Bennion and Newman (1972)), predictions of the overall reactor performance are tested -- this includes predicting the current-potential

behavior of the porous cathode and the effluent concentration of the reactant species. The remaining data set (Alkire and Gracon (1975)) is used to test model calculations of the current distribution within the porous cathode.

Figure 1 displays the model fit to the data of Bennion and Newman (1972) for copper removal using a porous carbon electrode. The quantities I and VOP are the total current to the reactor and the potential of the cathode current collector relative to a saturated calomel reference electrode placed in the effluent stream, respectively. The experimental effluent copper concentrations (in mg/ℓ) are shown as the numbers below each curve corresponding to the open triangles Δ, squares □ , and circles O. The numbers above each curve correspond to the solid circles ● and are the calculated values of the effluent copper concentration. Values of the parameters used to fit the data shown in Figure 1 are given in Table 1.

Five parameters were adjusted to obtain agreement between the calculated and experimental values in Figure 1: one value of the exchange current density for copper deposition was determined by fitting the data at the left side of the top curve; one value of the exchange current density for hydrogen evolution attempts to fit the rise in the current due to the observed onset of hydrogen evolution at the right side of the top curve; and three values of the mass-transfer coefficient k_m corresponding to the three different flow rates were determined mainly by the effluent concentration at the right side of each experimental curve.

In Figure 2, the fitted values of k_m (shown by the open triangles Δ) have been plotted in terms of the dimensionless Sherwood number

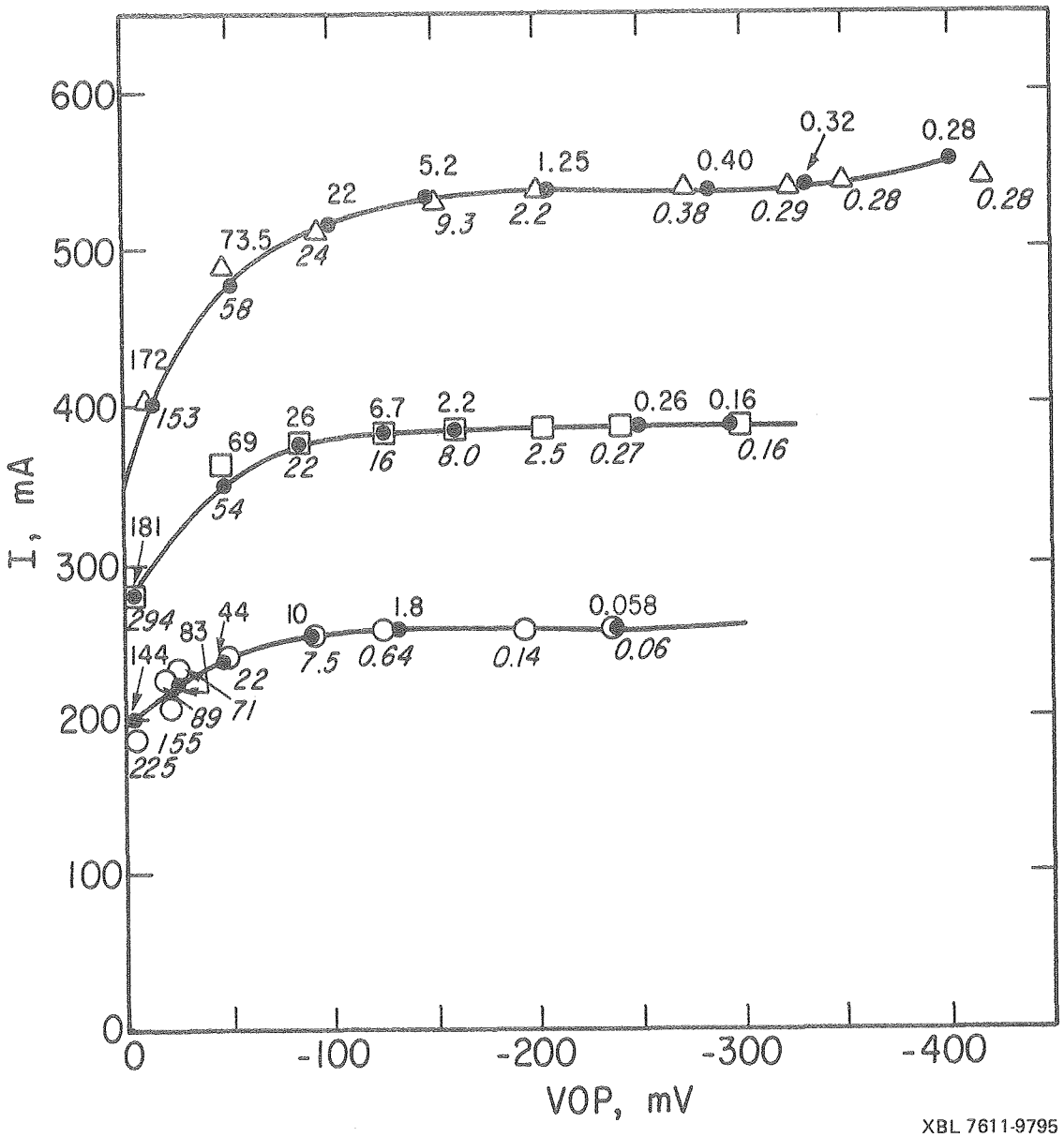

Figure 3-1. Current-potential curves for an electrode 10.1 cm in diameter and 6 cm deep, packed with porous carbon flakes and chips. Open symbols are experimental data points; closed symbols are calculated. Calculated effluent concentrations (in mg/ℓ) are indicated above the corresponding points in upright type; experimental values are given in *italic* type below the corresponding data points. The flow rate was 8 cm^3/min for the circles, 12 cm^3/min for the squares, and 16 cm^3/min for the triangles.

Table 3-1. Values of the parameters used in fitting the data in Figure 1 and in generating the curves in Figures 5 through 11.

$a = 25\ cm^{-1}$	$\varepsilon = 0.3$	$D_o = 6\times10^{-6}\ cm^2/s$
$\kappa_o = 0.17$ mho/cm	$\sigma = 10^4$ mho/cm	$s_R = -1$
$n = 2$	$T = 298.15$ K	$\alpha_{aR} = 1.5$
$\alpha_{cR} = 0.5$	$\gamma = 0.75$	$\alpha_{aS} = 0.5$
$\alpha_{cS} = 0.5$	$U_S - U_R = 0.281$ V	$L = 6$ cm

$k_m\times10^4$, cm/s	$v\times10^3$, cm/s
1.922	3.328
1.620	2.496
1.315	1.664

$i_{oR} = 3.8\times10^{-5}\ A/cm^2$ at $c_R = 0.1$ mole/ℓ

$i_{oS} = 7\times10^{-6}\ A/cm^2$ at $c_S = 1$ mole/ℓ, $p_S = 1$ atm

$i_{oS,ref} = 3.717\times10^{-12}\ A/cm^2$

dimensionless parameters as a function of c_{Rf} and v

$c_{Rf}\times10^5$, moles/cm^3	1.050	1.050	1.050	1.011	1.003	0.1003	0.01003
$v\times10^3$, cm/s	9.984	6.656	3.328	2.496	1.664	1.664	1.664
$P_1\times10^9$	9.461	22.99	104.9	215.9	501.3	5013.	50130.
P_2	-16.05	-8.905	-3.254	-2.091	-1.136	-0.1136	-0.01136
$P_3\times10^5$	1.247	1.247	1.247	1.295	1.305	13.05	130.5
$P_4\times10^9$	1.761	2.745	5.863	8.253	12.53	12.53	12.53
P_5	16.05	8.905	3.254	2.091	1.136	0.1136	0.01136
$P_6\times10^6$	44.83	24.87	9.089	5.842	3.173	0.3173	0.03173
$D'\times10^2$	7.385	8.877	12.17	13.68	16.70	16.70	16.70

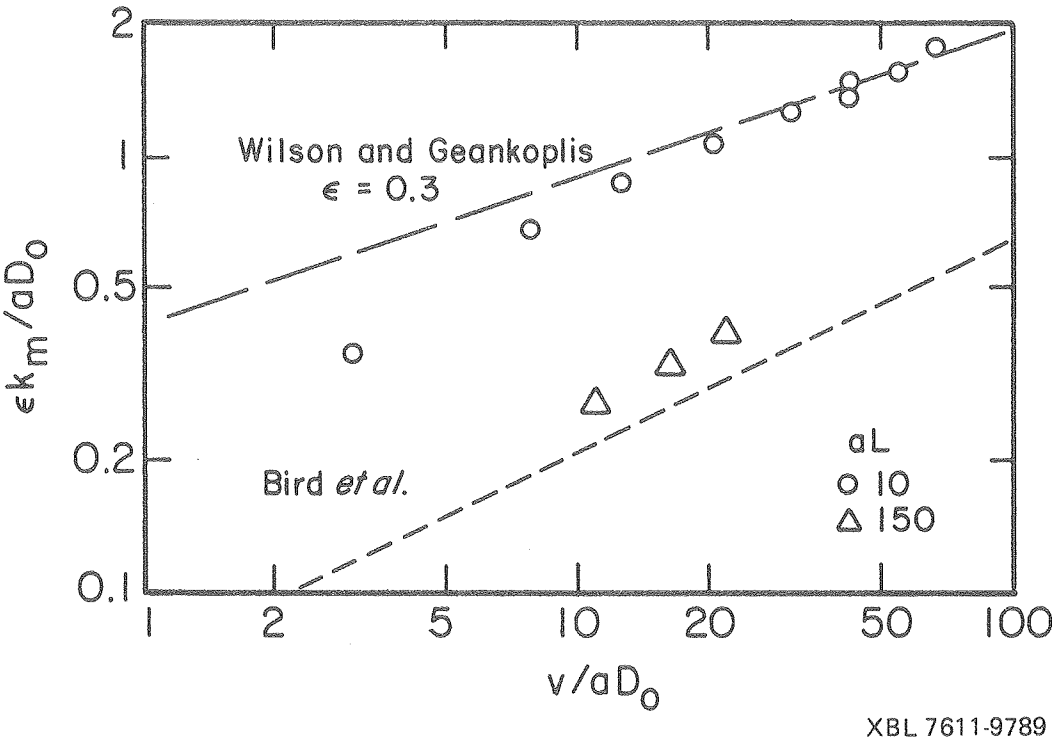

Figure 3-2. Correlation of the Sherwood number as a function of Péclet number and dimensionless electrode thickness aL. Open triangles come from a fit of the data of figure 1; open circles are the results of Appel and Newman. Two correlations from the literature are also shown.

$\varepsilon k_m/aD_o$ as a function of the dimensionless Péclet number v/aD_o. The upper dashed line is the Wilson and Geankoplis (1966) correlation

$$\frac{\varepsilon k_m}{aD_o} = \frac{1.09}{[6(1-\varepsilon)]^{2/3}} \left(\frac{v}{aD_o}\right)^{1/3}, \qquad (3\text{-}42)$$

and the lower dashed line is a correlation suggested by Bird et al. (1960)

$$\frac{\varepsilon k_m}{aD_o} = 0.91\ \varepsilon \left(\frac{v}{a\nu\psi}\right)^{0.49} \psi^2 \left(\frac{\nu}{D_o}\right)^{1/3}, \qquad (3\text{-}43)$$

where a value of $\varepsilon = 0.3$ has been used in calculating each line. Also shown in Figure 2 by means of the open circles O are the data of Appel and Newman (1976), where $\varepsilon = 0.372$. It should be noted that it has been assumed that the dimensionless correlations for k_m (given by equation 42 and 43) have been corrected for dispersion; Appel's results have not, and therefore k_m in this case is fundamentally a different quantity (see Newman and Tiedemann (1976) for this correction and a discussion of different definitions of k_m).

The model fit of the limiting current-distribution data of Alkire and Gracon (1975) for copper deposition on platinum screen electrodes is shown in Figure 3. The transfer current density for the main reaction di_{2R}/dx has been normalized by the total current density i_R due to the primary reaction and the electrode length L. A uniform current distribution would correspond to a horizontal line at an ordinate value of 1. Values of the parameters used to fit these data are given in Table 2.

The data for the smallest flowrate (v = 0.1067 cm/s) were fitted first by using literature values of the exchange current densities

Table 3-2. Values of the parameters used in fitting the data in Figure 3.

$a = 260\ cm^{-1}$	$\varepsilon = 0.64$	$D_o = 7.6\times10^{-6}\ cm^2/s$
$\kappa_o = 0.55\ mho/cm$	$\sigma = 10^4\ mho/cm$	$s_R = -1$
$n = 2$	$T = 298.15\ K$	$\alpha_{aR} = 1.5$
$\alpha_{cR} = 0.5$	$\gamma = 0.75$	$\alpha_{aS} = 0.5$
$\alpha_{cS} = 0.5$	$U_S - U_R = 0.481\ V$	$L = 0.4\ cm$

$i_{oR} = 10^{-3}\ A/cm^2$ at $c_R = 0.1$ mole/ℓ

$i_{oS} = 10^{-7}\ A/cm^2$ at $c_S = 1$ mole/ℓ, $p_S = 1$ atm

$i_{oS,ref} = 1.732\ 10^{-12}\ A/cm^2$

dimensionless parameters

as a function of v

($c_{Rf} = 2\times10^{-6}$ mole/cm^3)

v, cm/s	0.1067	0.2750	0.4133
$P_1\times10^9$	290.3	82.17	47.73
P_2	-0.1968	-0.9532	-1.880
$P_3\times10^5$	3.779	3.779	3.779
$P_4\times10^{12}$	4.001	2.128	1.622
P_5	0.1967	0.9532	1.880
$P_6\times10^6$	5.540	26.84	52.93
$D'\ 10^2$	6.040	3.203	2.439

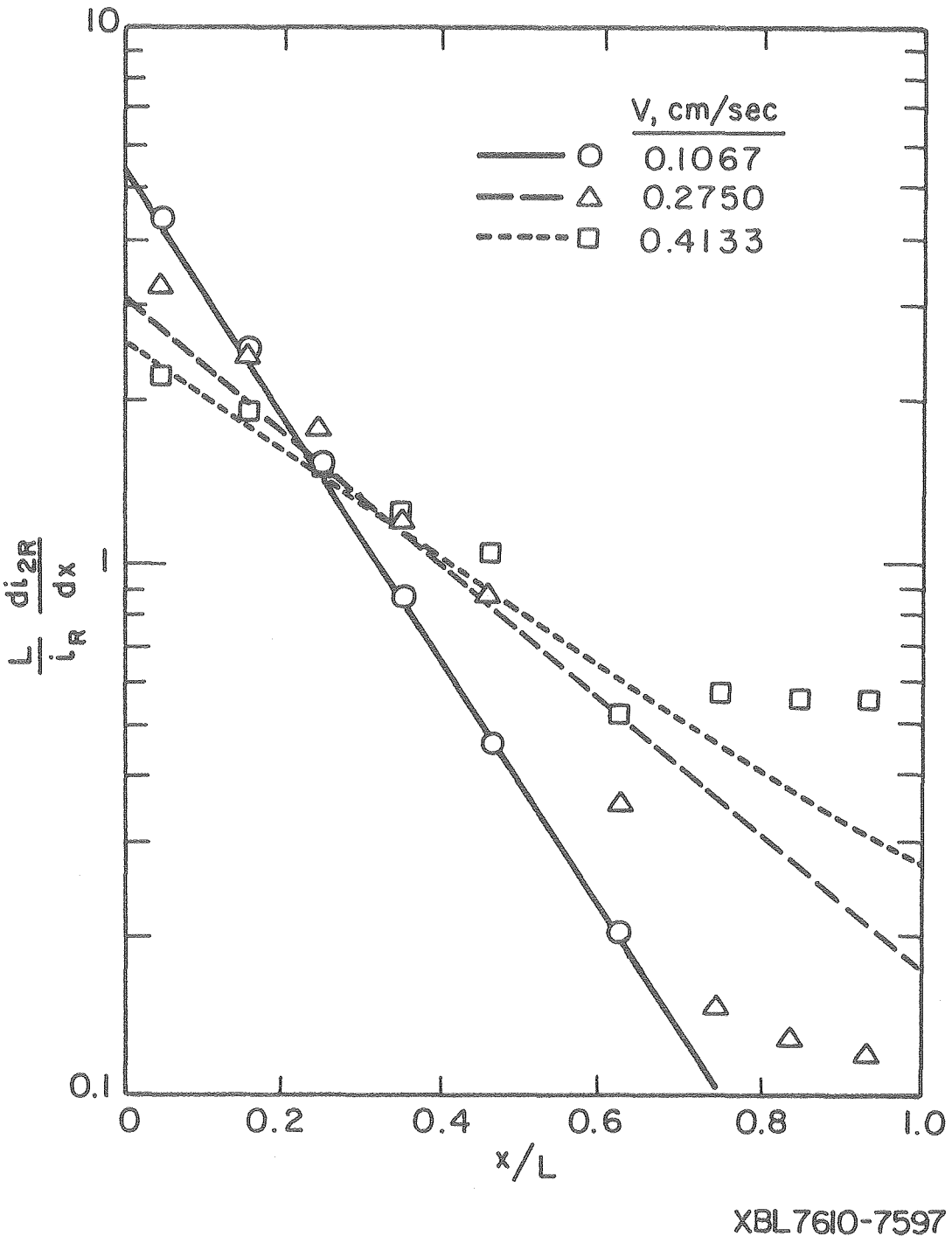

Figure 3-3. Normalized distribution of copper deposition. Experimental data and calculations are for deposition from a 2 mM cupric solution onto a bed 0.4 cm thick with a porosity of 0.64 and a specific surface area of 260 cm^{-1}, constructed of layers of Pt screens.

in Figure 3.

Theoretical predictions. -- Again the results presented are divided into two categories, microscopic distributions and overall reactor performance. For the calculations which follow, the counter-electrode is upstream, the primary reaction is again the deposition of copper, and the side reaction is the generation of dissolved hydrogen.

Figure 4 shows the reaction rate distributions for the primary electrode reaction only, at and below the limiting current, for the physical parameters and dimensionless parameters (corresponding to $v = 3.328\times10^{-3}$ cm/s) in Table 1, but with P_3 and P_4 equal to zero (i.e., a single electrode reaction). The limiting current distribution includes the effect of axial diffusion and dispersion and was determined from the analysis of Newman and Tiedemann (1976):

$$\frac{di_2^*}{dy} = \frac{Be^{-y/B} + (B - 1)e^{By/D'} \exp\left[-\alpha L\left(\frac{1}{B} + \frac{B}{D'}\right)\right]}{B^2 - \frac{D'}{B}(B - 1) \exp\left[-\alpha L\left(\frac{1}{B} + \frac{B}{D'}\right)\right]} \qquad (3\text{-}45)$$

where

$$i_2^* = \frac{s_R i_2}{nFvc_{Rf}}, \qquad (3\text{-}46)$$

and

$$B = \frac{1 + \sqrt{1 + 4D'}}{2}. \qquad (3\text{-}47)$$

for copper deposition and hydrogen evolution on copper (see for example, Newman (1973), p. 177, and Erdey-Gruz (1972), p. 165; note almost any i_o values would work, except, too large a value of i_o for the side reaction which would not allow a limiting current to be maintained throughout the electrode, because the data of Alkire and Gracon (1975) were obtained at the limiting current) and adjusting the value of the mass-transfer coefficient k_m to obtain reasonable agreement between the calculated and experimental values. This value for the mass-transfer coefficient was then used to change the coefficient in the Wilson-Geankoplis (1966) correlation (given by equation 42) to 0.85:

$$\frac{\varepsilon k_m}{aD_o} = \frac{0.85}{[6(1-\varepsilon)]^{2/3}} \left(\frac{v}{aD_o}\right)^{1/3} . \qquad (3\text{-}44)$$

The remaining lines in Figure 3 for the higher flowrates were then calculated using this expression for the mass-transfer coefficient and no additional adjustment of parameters.

It may be noted that Alkire and Gracon (1975) proposed that the estimated specific interfacial area be reduced by a multiplier of 0.81 to yield an adjusted value. When used in the Wilson-Geankoplis (1966) correlation, this effectively reduces the coefficient to 0.947 if one continues to use the estimated value. In this case, the value of ak_m (which is the quantity which enters into the model equations) is reduced by a multiplier of 0.704 from the value which would be predicted by the Wilson-Geankoplis (1966) correlation and the estimated area. By our reducing the coefficient from 1.09 to 0.85, we have effectively reduced the value of ak_m by a multiplier of 0.78. Alkire and Gracon's choice of the multiplier of 0.81 was evidently based on the values of the total limiting current, not on a fit of the distribution data as

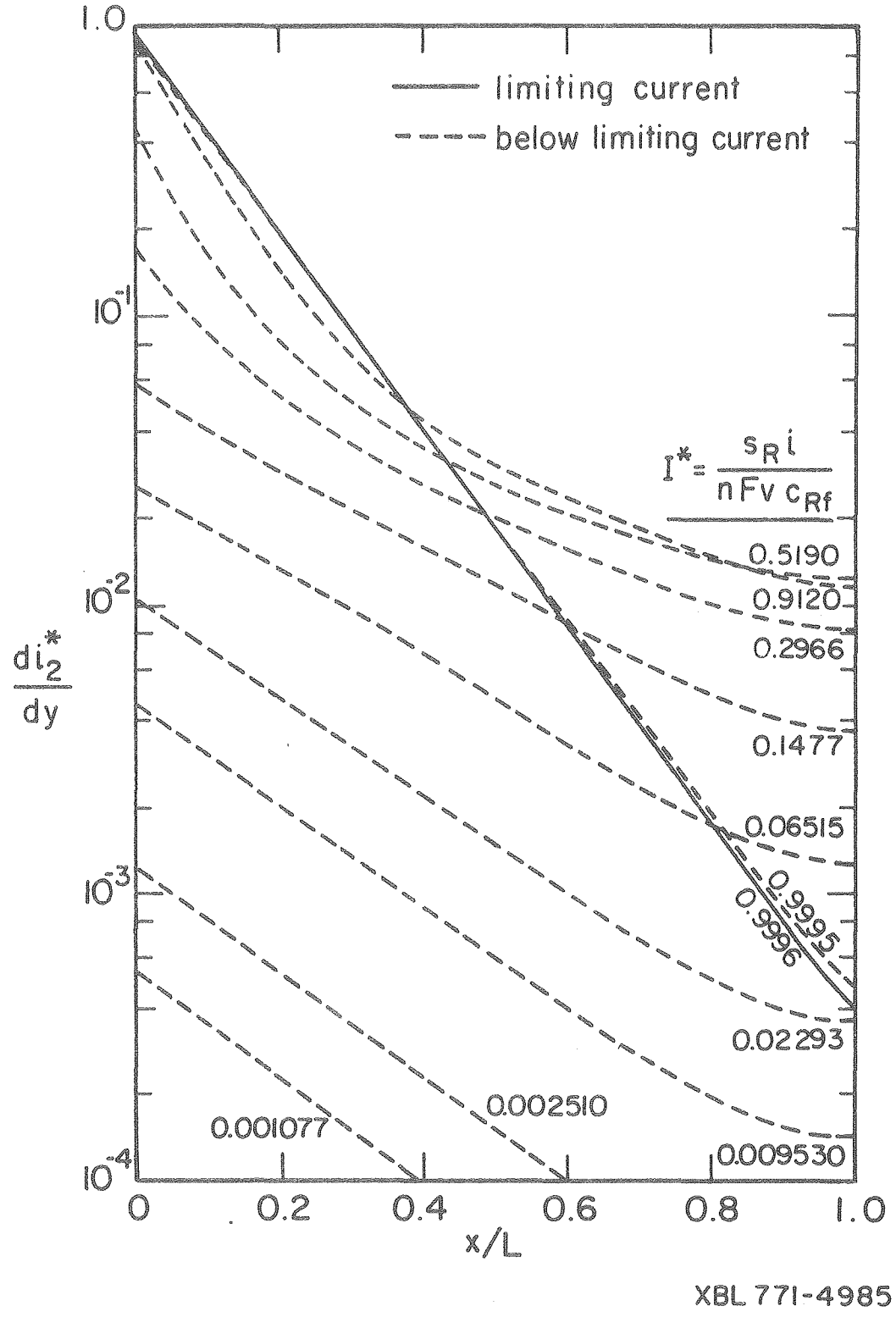

Figure 3-4. Reaction distribution for copper deposition in the absence of a side reaction, calculated for $\alpha L = 8.663$, $D' = 0.1217$, and $P_2 = -3.254$.

Integration of equation 45 from $y = 0$ to $y = \alpha L$ yields an expression for the total dimensionless limiting current density to the electrode:

$$-i_2(0) = I^* = \frac{1 - e^{-\alpha L/B} + \frac{D'(B-1)}{B^3} \exp\left[-\alpha L \frac{1}{B} + \frac{B}{D'}\right](e^{B\alpha L/D'} - 1)}{1 - \frac{D'}{B^3}(B - 1) \exp\left[-\alpha L \frac{1}{B} + \frac{B}{D'}\right]} . \quad (3\text{-}48)$$

Figures 5 through 8 show current, potential, current efficiency, and concentration distributions within a reactor operating at conditions which correspond to the point on the upper curve of Figure 1 where VOP = -403 mV and the outlet concentration is 0.28 mg/ℓ .

In Figure 9 the solution-phase ohmic potential drop $\Delta\Phi_2$ across a reactor has been plotted as a function of the electrical driving force at the back of the reactor $(\Phi_1 - \Phi_2)_{\alpha L}$ for two cases: 1) the primary reaction only and 2) when the side reaction is included, for values of the physical parameters and dimensionless parameters (corresponding to $v = 3.328\times10^{-3}$ cm/s) in Table 1. The ohmic potential drop has been made dimensionless with the quantity

$$\Delta\Phi_2' = \frac{nFvc_{Rf}}{s_R\kappa} \frac{v}{ak_m} , \quad (3\text{-}49)$$

which is an estimate of the ohmic potential drop across a reactor operating at the limiting current (Bennion and Newman (1972)) when the effluent concentration is zero and the effects of axial diffusion and dispersion are negligible. The potential $(\Phi_1 - \Phi_2)_{\alpha L}$ is the potential of the cathode current collector relative to a copper reference electrode (with a concentration of c_{Rf} in the reference electrode compartment) placed at the back of the reactor.

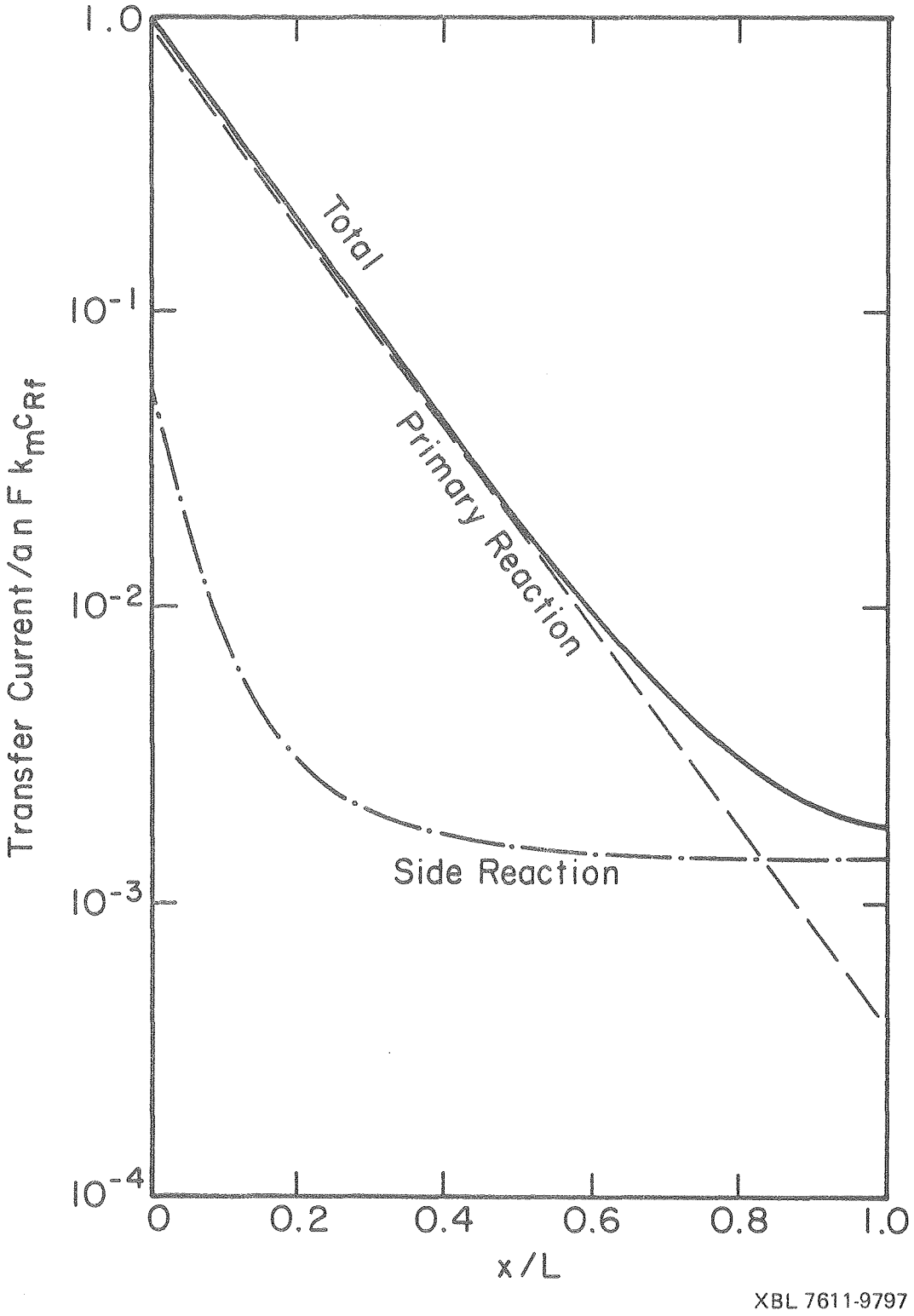

Figure 3-5. Current distributions for deposition of copper and generation of dissolved hydrogen within a porous electrode with fluid flow from left to right, calculated for v = 0.003328 cm/sec, $a = 25\ cm^{-1}$, $\varepsilon = 0.3$, L = 6 cm, $c_{Rf} = 0.0105$ mole/ℓ, and VOP = -0.403 V relative to a calomel reference electrode in the dilute-product stream.

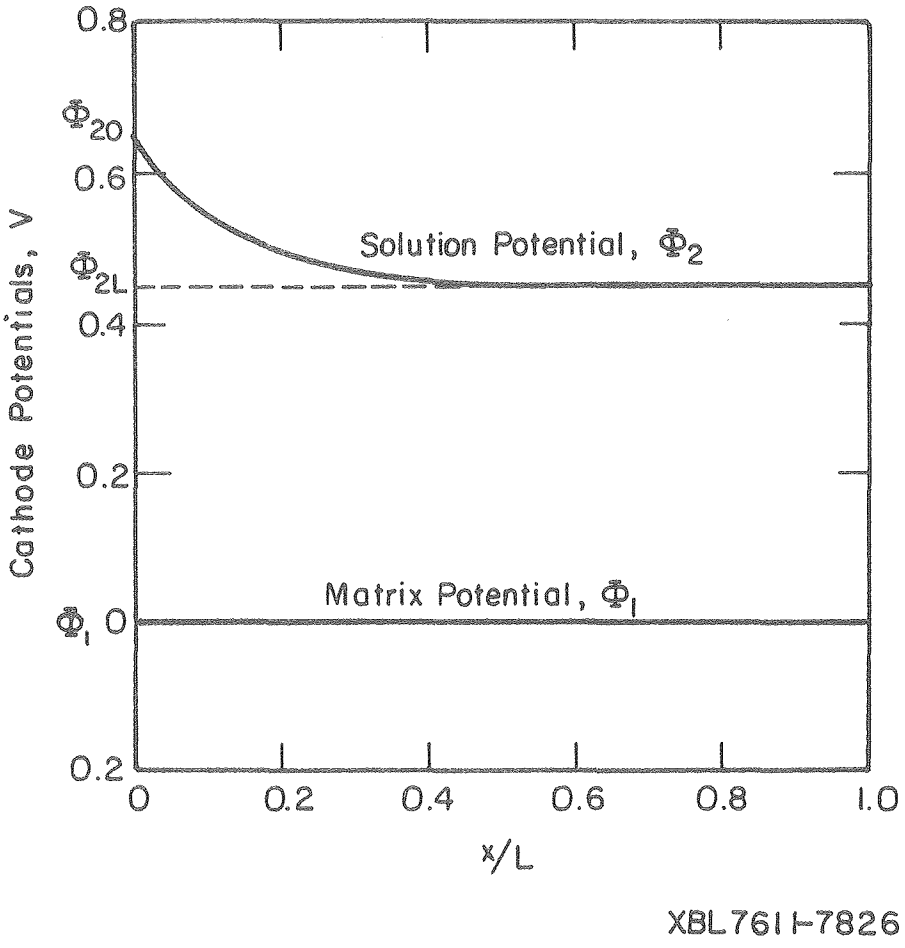

Figure 3-6. Solution-phase and solid-matrix-phase potentials, as functions of cathode position, for the conditions of Figure 5.

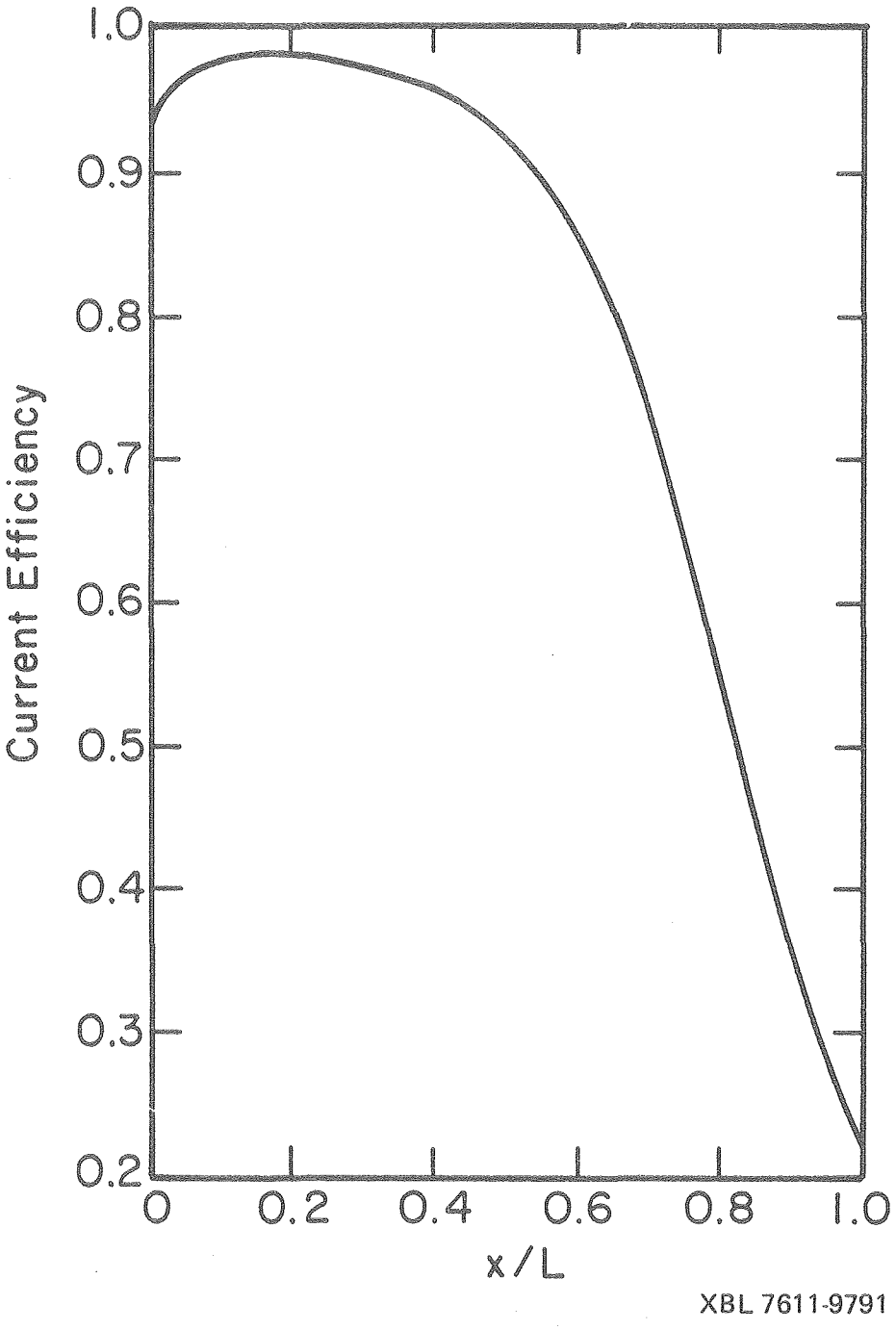

Figure 3-7. Local current efficiency as a function of cathode position, for the conditions of Figure 5. The overall current efficiency is 0.962.

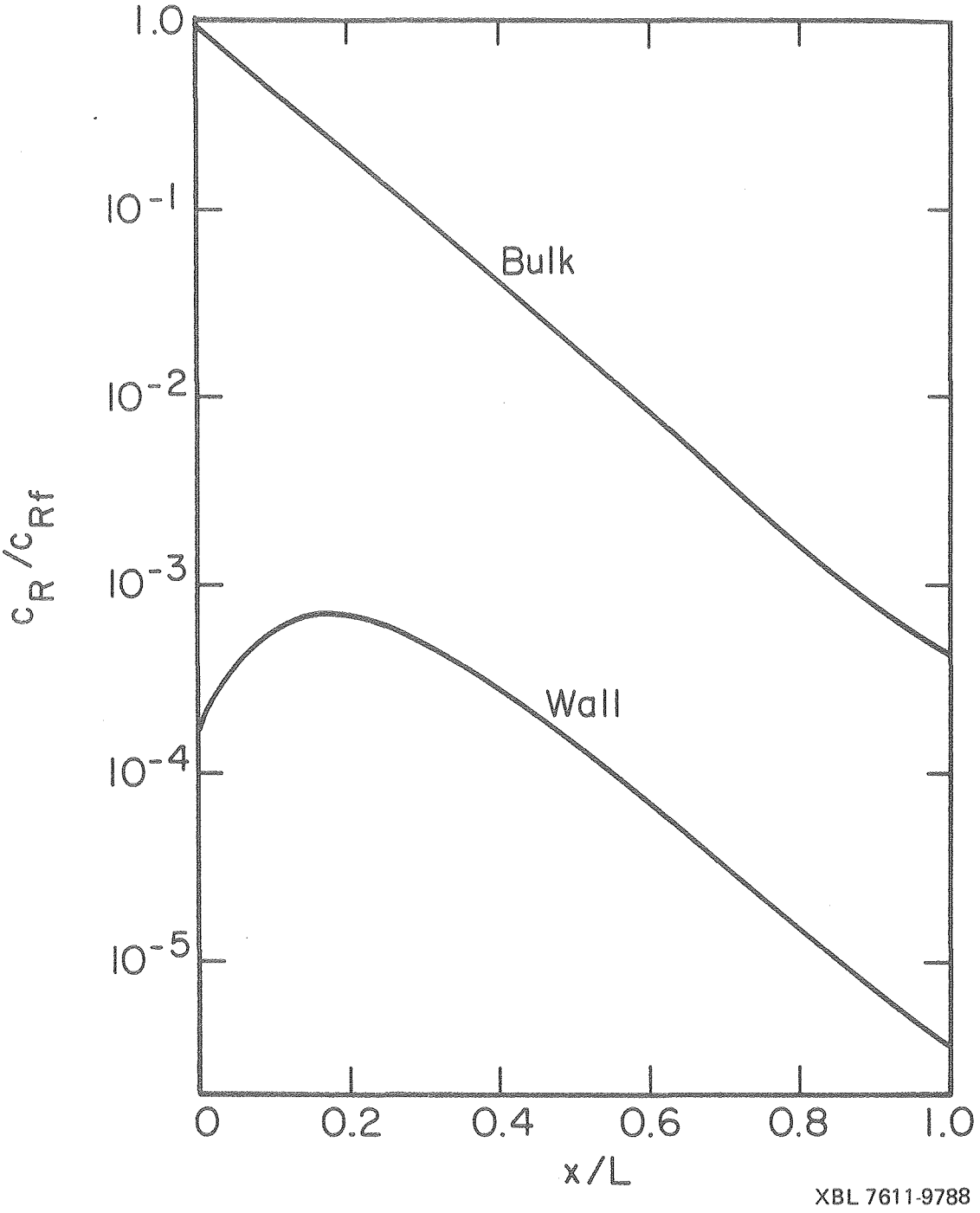

Figure 3-8. Distribution of copper concentration in the flowing stream and along the pore wall, for the conditions of Figure 5.

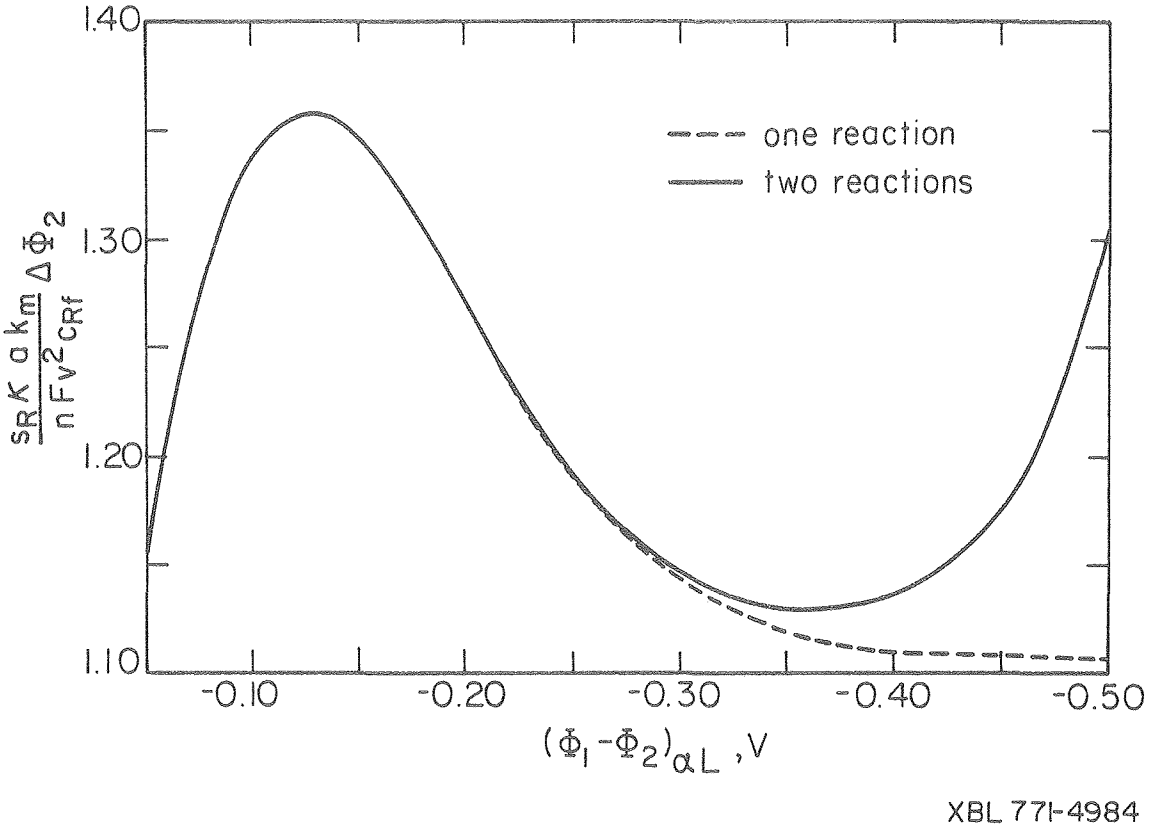

Figure 3-9. Ohmic potential drop across the solution within the porous electrode -- under the conditions of Figure 4 and also with simultaneous generation of dissolved hydrogen.

At large negative values of $(\Phi_1 - \Phi_2)_{\alpha L}$ when only the primary reaction is considered, the ordinate approaches the value predicted by the limiting-current analysis of Newman and Tiedemann (1976):

$$\frac{\Delta\Phi_2}{\Delta\Phi_2'} = \frac{\left(1 + \frac{D'}{B^2}\right)\left[B^2 - (\alpha L + 1 + D')e^{-\alpha L/B}\right]}{B + \frac{D'}{B^2}(1 - B)\exp\left[-\alpha L\left(\frac{1}{B} + \frac{B}{D'}\right)\right]} - \frac{D'}{B}, \qquad (3\text{-}50)$$

and has a value of 1.1057 in this case.

Figures 10 and 11 show the effect on the current-potential curve if the fluid velocity is increased or the feed concentration decreased. The curve labeled with a v in Figure 10 corresponds to the upper curve in Figure 1, and the curve labeled 10^{-2}M in Figure 11 corresponds to the lower curve in Figure 1. (See also Table 1.)

3.6 Discussion

Agreement between model calculations and the experimental data of Bennion and Newman (1972) shown in Figure 1 should be considered satisfactory. However, the values of the parameters found by fitting the data need some clarification.

The fitted values of the exchange current densities for copper deposition and hydrogen evolution on carbon (see Table 1) are 0.035 and 70 times the reported literature values ($i_{o,Cu} = 10^{-3}$ A/cm^2 (Newman (1973), p. 177) and $i_{o,H_2} = 10^{-7}$ A/cm^2 (Erdey-Gruz (1972), p. 165)) for these reactions on copper, respectively. However, it should not be interpreted that there is anything fundamental about these fitted values since the data are insufficient at the extreme values of the current to provide for their accurate evaluation. We also wish

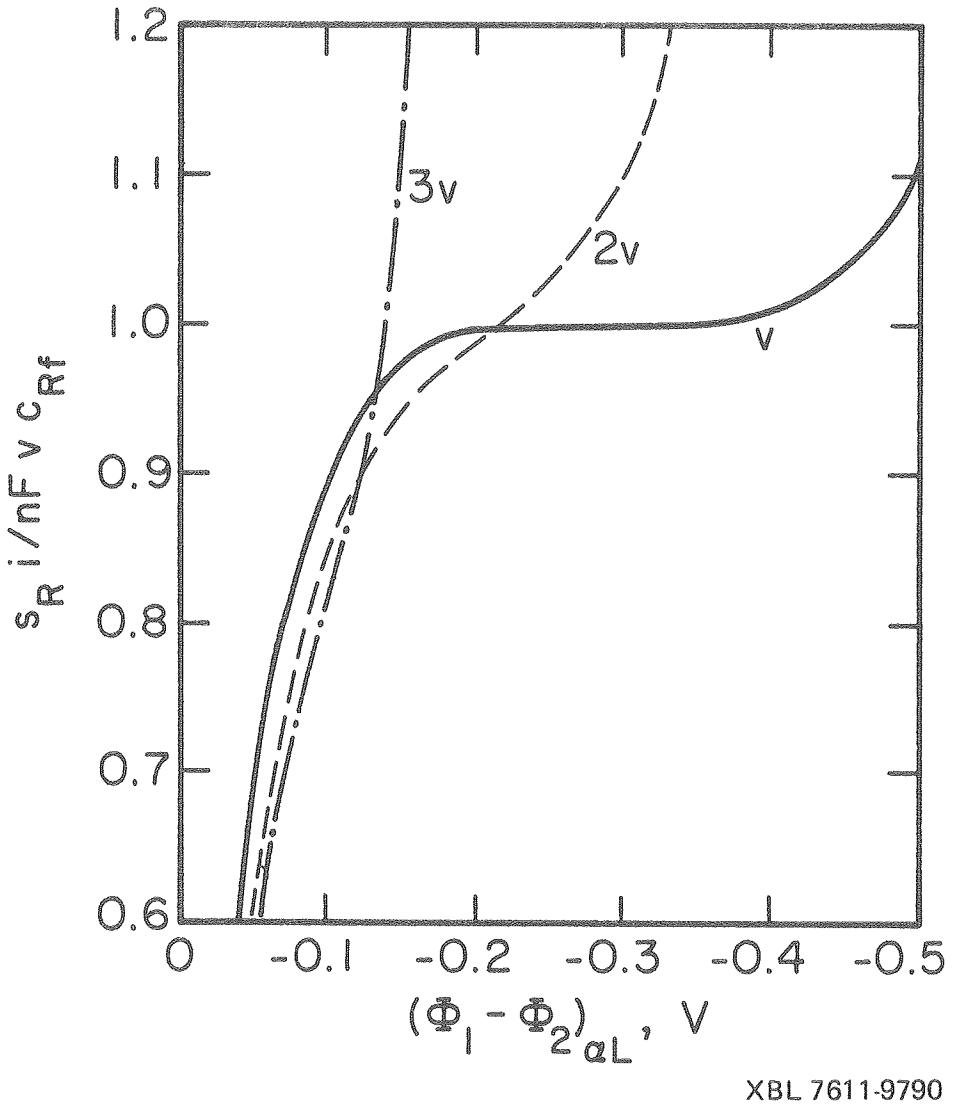

Figure 3-10. Effect of flow rate on the current-potential curve. Operation at flow rates substantially above the design value (Bennion and Newman (1972), here v = 0.003328 cm/s obscures the limiting-current plateau because of the high ohmic potential drop in the solution phase. For parameter values, see Table 1.

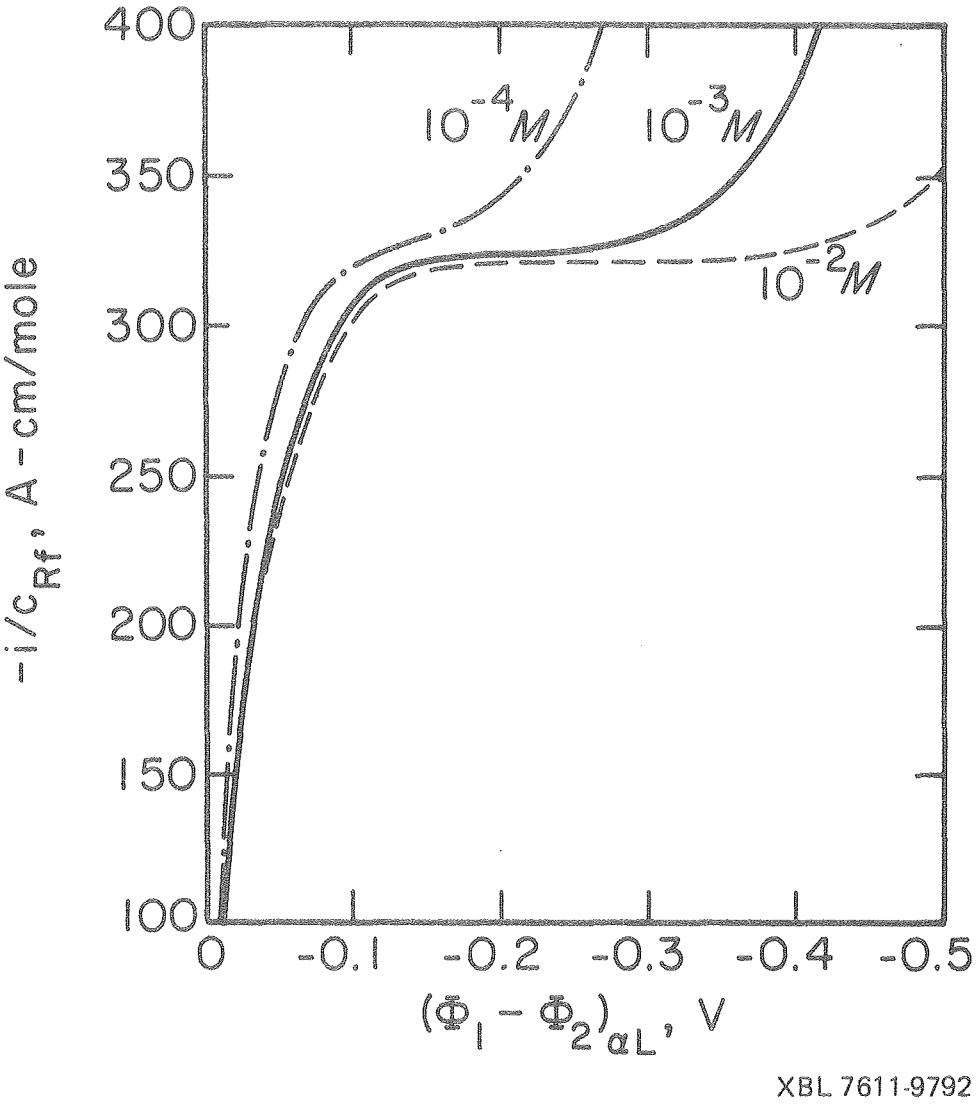

Figure 3-11. Effect of feed concentration on the current-potential curve. Low concentrations correspond to low currents for the primary reaction, and these are easily obscured by the side reaction even in the absence of a significant ohmic potential drop within the reactor. For parameter values, see Table 1.

to emphasize that we do not suggest this as a method for determining fundamental kinetic parameters, since the bed is operating with a highly nonuniform current density and mass-transport limitations dominate the data in certain regions.

The fitted values of k_m (given in Table 1), determined mainly by the effluent concentration at the right on the experimental curves of Figure 1 and plotted in Figure 2, show a clear dependence on the velocity as follows

$$\frac{\varepsilon k_m}{aD_o} = 0.07054 \left(\frac{v}{aD_o}\right)^{0.5454} . \qquad (3\text{-}51)$$

Data obtained in this manner yields fundamental information about k_m (e.g. Appel and Newman (1976)). Unfortunately, the value used for the specific interfacial area a of $25\ cm^{-1}$ is an effective value and may be low by a factor of 4 to 12 (Bennion (1976)). If larger values of a are used, the value of k_m will decrease, and the triangles plotted in Figure 2 would move down and to the left toward lower values of the Sherwood and Péclet numbers.

The purpose of Figure 2 is to call attention to the fact that the behavior of k_m is not well established in this flow region. Newman and Tiedemann (1976) have suggested, for a restricted range of flow rates: $1 \leq Pe < 10^4$ and $Re < 10$, where Pe is the Péclet number v/aD_o and Re is the Reynolds number $v/a\nu$, there should exist an entry region such that the local mass-transfer coefficient is larger than the asymptotic value for deep bed electrodes and that the average value of the mass-transfer coefficient will be dependent of the quantity aL.

Since most measurements for k_m involve short electrodes, small aL (e.g. equation 42 of Wilson and Geankoplis (1966), where $1.8 \leq aL \leq 27$), the entire electrode may be within the entry region and will therefore predict too large a value for k_m when aL is large (deep beds) as is the case for the data of Bennion and Newman (1972).

Also in Figure 2, a correlation found in Bird et al. (1960, equation 43) has been extrapolated by at least an order of magnitude in Reynolds number below the range for which the correlation has been tested. However, this equation appears to give a conservative estimate for k_m and may be useful for design purposes until better correlations are developed for this region of flow.

In Figure 3 agreement between model calculations and the experimental data of Alkire and Gracon (1975) for the smallest flow rate (0.1067 cm/s) is good. The almost linear behavior on the semi-log plot for the predicted limiting current distribution is expected based on the analysis of Bennion and Newman (1972) for the special case of mass-transfer control. As expected, the value of k_m which best fits the data (given by equation 44) is less than that predicted by equation 42 of Wilson and Geankoplis (1966) due to the large value of $aL = 104$. The reason for using equation 44 at the two higher flow rates is to have some basis for changing k_m with the velocity since no data on the effluent concentration are given in reference 13 to enable an estimation of k_m as was done with the data of Bennion and Newman (1972) in Figure 1. (A graph of the total limiting current is presented by Alkire and Gracon (1975), from which one could infer the effluent concentration if side reactions are negligible. However, values from this graph cannot be obtained with great precision, and,

as pointed out by Appel and Newman (1976) the total current is an inherently inaccurate method of measuring the mass-transfer coefficient when the overall conversion is close to 100 percent.)

In Figure 3, at least two reasons are responsible for the discrepancies between the model calculations and the experimental data at the higher flow rates. First the data are a re-plot of data taken from an arithmetic plot and are subject to error. Second k_m may not be a constant throughout the electrode as assumed in the model. However, the discrepancies in Figure 3 are considerably less than those between Alkire and Gracon's Figures 6 and 9, where the lack of explanation has already been noted in the literature (Ateya and Austin (1977)). One may speculate as to why the agreement between the model of Alkire and Gracon and their data is poor. This is perhaps due to the inadequate representation of the derivatives in the governing equations at the limiting current by standard central-difference approximations. New finite-difference approximations to the derivatives (developed in Appendix A) are required as discussed earlier.

The reaction rate distribution when only the metal deposition reaction is considered is plotted in Figure 4 for various fractions of the limiting current. The effect of axial diffusion and dispersion is apparent in the limiting current distributions as di_2^*/dy is less than one at x/L equal to zero. The fact that I^* is not equal to one for the limiting current distribution is because mass-transfer limitations exist within the electrode and therefore a small fraction of the feed concentration will escape unreacted.

For an appreciable fraction of the limiting current $(I^* > 0.9)$, the reaction rate near the front of the electrode is high and decreases

almost exponentially, similar to the behavior of the limiting current distribution (see equation 45). Near the back of the electrode, the rate of reaction for the limiting current distribution is small because most of the copper is removed near the front of the electrode. Therefore, the reaction rates below the limiting current are greater at the back of the electrode (for values of $I^* > 0.03$) and are more uniform than the limiting current distribution. Actually, the reaction rate at the back of the electrode $\left(di_2^*/dy|_{y=\alpha L}\right)$ increases as the value of I^* decreases from 0.9996 to 0.7273, passes through a maximum at $I^* = 0.7273$, and then decreases monotonically with I^*. Thus the effective depth of penetration of the reaction into the electrode also has a maximum near $I^* = 0.7273$.

For small values of the current $(I^* < 0.03)$, the reaction rate distributions take on the same shape and can be described by a model with linear electrode kinetics and no concentration variations (see Euler and Nonenmacher (1960) and Newman and Tobias (1962)).

Figure 5 shows the relative rates of reaction for the primary reaction and the side reaction as they are distributed throughout the porous electrode. The total current density to the electrode was chosen close to the limiting current $(I^* = 1.038)$ for the deposition of copper. Consequently, the reaction rate for the primary reaction decreases almost exponentially with distance (see equation 45), as the solution is depleted with copper while flowing through the electrode. The side reaction, generation of dissolved hydrogen, responds mainly to the electric driving force between the solid matrix and the electrolytic solution. Its rate is high near the entrance to the porous electrode and drops to a nearly constant value near the rear.

The reason for this can be seen in Figure 6, which represents the variation in the solution-phase potential Φ_2 for a counterelectrode placed upstream of the working electrode. The matrix conductivity is high, and therefore its potential Φ_1 is nearly a constant. The solution potential Φ_2 varies little near the rear because the current carried in the solution is small in this region. Because the driving force $(\Phi_1 - \Phi_2)$ is essentially uniform for some distance at the back of the electrode, measurement of $(\Phi_1 - \Phi_2)_{\alpha L}$ can lead to a lower bound thermodynamic estimate of the minimum concentration attainable in a flow-through porous electrode (see chapter 2 or Trainham and Newman (1977a) for details).

In Figure 7, the local current efficiency actually goes through a slight maximum near $x/L = 0.18$. The current efficiency is low at the entrance because the high electric driving force lead to a relatively high rate for the side reaction. For somewhat larger values of x, the rate of the side reaction decreases more rapidly than the primary reaction, and the local current efficiency rises. However, the primary reaction rate continues to decrease with distance because of the depletion of copper ions, and consequently the local current efficiency eventually drops to about 23 percent at the rear of the electrode. One might well ask, "Why not eliminate the last 40 percent of the thickness of the electrode?"

Figure 8 shows the concentration of copper ions through the thickness of the electrode. The high electric driving force at the entrance results in a very low wall concentration there. As the electric driving force decreases with x, the wall concentration rises toward the bulk value. With the diminishing reaction rate through the

next part of the electrode, the wall concentration is able to decrease also, despite the smaller electric driving force in this region. We can also see from this figure that the bulk concentration is depleted by an additional factor of 20 in the last 40 percent of the electrode, despite the lowered current efficiency in this region. This additional metal ion removal can be achieved with relatively little additional expense for the added electrode thickness and virtually no added cost due to added ohmic potential drop.

In Figure 9, the ohmic potential drop across the solution within the reactor exhibits a maximum and then a minimum as the driving force increases at the back of the reactor. The maximum occurs at $I^* = 0.95$ and is due to a combination of effects: 1) the driving force is high, and the current is only increasing slowly, 2) the reaction rate at the back of the electrode goes through a maximum at a value of $I^* = 0.7273$ as discussed previously in Figure 4, and 3) the driving force, though high, is not large enough for the side reaction to contribute substantially to the ohmic potential drop. For larger values of $(\Phi_1 - \Phi_2)_{\alpha L}$, the ohmic potential drop decreases due to a decreasing rate of reaction at the back of the electrode. Thus, the depth of penetration of the reaction is decreasing at $I^* = 0.95$. This was shown clearly in Figure 4 as the primary reaction approaches the limiting current distribution.

The minimum in the ohmic potential occurs simultaneously with the minimum in the total reaction rate at the back of the electrode $\left(di_2^*/dy\right)|_{\alpha L}$. At this point the rate of the side reaction becomes significant, and the ohmic drop increases accordingly.

We wish to emphasize that the existence of a local maximum and a local minimum is dependent on the physical parameters and operating conditions. For example, if the exchange current density for the side reaction were significantly larger relative to the primary reaction, the driving force required to make the side reaction occur to a significant extent would be much less. Thus instead of the ohmic potential drop exhibiting a local maximum due mainly to the effects of the primary reaction (or lack of effect of the side reaction), the side reaction becomes the controlling factor and $\Delta\Phi_2$ increases monotonically with increasing $(\Phi_1 - \Phi_2)_{\alpha L}$.

Another way to achieve a similar result (using the same physical parameters) is to increase the ohmic potential drop by increasing the superficial velocity as shown in Figure 10. The reactor cannot be operated at even twice the superficial velocity without loss of the limiting current-plateau and a lack of a local maximum and a local minimum in the ohmic potential drop, which is due to extensive interference by the side reaction. In harmony with the quantitative design principles of Bennion and Newman (1972), these calculations show that an increase in the superficial velocity increases the ohmic potential drop in the solution so that there is either excessive side reaction at the entrance to the porous electrode or a failure to maintain the limiting-current condition near the exit. A decrease in the feed concentration as shown in Figure 11 will also increase the side reaction relative to the primary reaction and cause the limiting-current plateau to become less distinct. The ability to calculate the current distributions below the limiting current and in the presence

of a side reaction permits one to determine the economically optimum operating conditions and even permissible operating conditions when the side reaction accounts for a substantial fraction of the total current, and there is a penalty for making the electrode thicker because the side reaction does not necessarily decrease with increasing distance through the electrode.

3.7 Conclusion and summary

A theoretical model for flow-through porous electrodes has been described for the specific application to metal-ion removal from dilute streams. A new set of dimensionless parameters has been suggested from the analysis, which characterize the relative importance of the following physical phenomena within a flow-through porous electrode: axial diffusion and dispersion (D'), backward rate of the primary reaction (P_1), ohmic potential drop (P_2), forward (P_3) and backward (P_4) rates of the side reaction.

Satisfactory agreement between model predictions and experimental data on overall reactor performance and deposition distributions has been achieved.

The knowledge of distributions of current, potential, and concentration in the presence of a side reaction above and below the limiting-current of the primary reaction makes it possible to design and optimize an electrode system for the most economical removal of metal ions. But this design may only be accomplished if there are sufficient expermental data. Most important are values for the specific interfacial area a, the mass-transfer coefficient k_m, and the exchange current densities for the primary reaction and the side reaction.

4. The effect of electrode placement and finite matrix conductivity on the performance of flow-through porous electrodes

4.1 Introduction

The model used in calculating the effects of counterelectrode placement and current collector placement (when the matrix conductivity is moderate) on the performance of flow-through porous electrodes was developed in chapter 3 (also, see Trainham and Newman (1977b)); however, results were presented only for the effective matrix conductivity σ much greater than the effective solution conductivity κ.

To date, previous models for flow-through porous electrodes (Sioda (1972), Alkire and Gracon (1975), Alkire and Gould (1976), Ateya and Austin (1977), and Paulin, Hutin and Coeuret (1977)) have considered only an infinite matrix conductivity, and no comparisons have been made on the performance of these electrochemical reactors as a function of counterelectrode placement.

The purpose of this chapter is to suggest the optimum electrode configuration for two cases: 1) when $\sigma >> \kappa$ we are concerned only with the upstream and downstream placement of the counterelectrode and 2) when $\sigma \approx \kappa$, placement of not only the counterelectrode is important but also the current collector placement must be considered. At least four geometric configurations are possible: 1) upstream counterelectrode, downstream current collector (UD), 2) downstream counterelectrode, upstream current collector (DU), 3) upstream counterelectrode, upstream current collector (UU) and 4) downstream counterelectrode, downstream current collector (DD), and are shown schematically in Figure 1. It should be noted that the direction of fluid flow through the counterelectrode is unimportant to the analysis

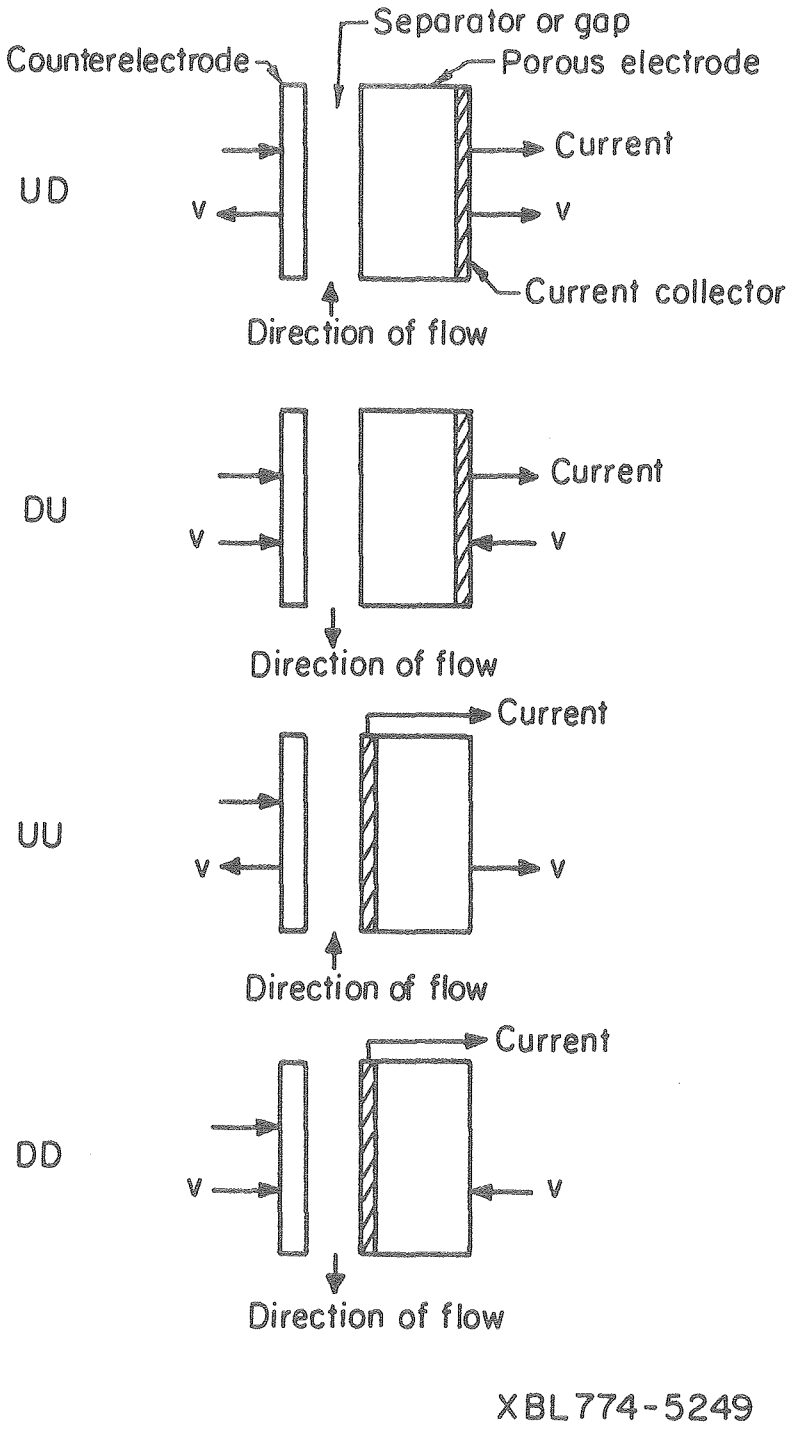

Figure 4-1. Various configurations of counterelectrode placement and current collector placement relative to the direction of the fluid flow.

to be considered as long as the products don't enter the electrode of interest.

4.2 Analysis

As mentioned earlier, calculations presented here are a direct application of a model for flow-through porous electrodes developed in chapter 3, and therefore, the governing equations will not be presented here.

For the removal of metal ions from dilute streams, the behavior of a flow-through porous electrode with parallel current and fluid flow as shown in Figure 1 can be described by two ordinary differential equations: one equation which describes the conservation of the metal-ion reactant and one charge balance equation given by equations 3-28 and 3-29, respectively.

Boundary conditions. Before equations 3-28 and 3-29 can be solved simultaneously for θ and η', four boundary conditions are required for each electrode configuration shown in Figure 1. For θ the following conditions were used

$$\theta - D' \frac{d\theta}{dy} = 1 \quad \text{at} \quad y = 0 \ ,$$

and

$$\frac{d\theta}{dy} = 0 \quad \text{at} \quad y = \alpha L \ , \tag{4-1}$$

which are the same conditions used in chapter 3 and are the Danckwerts (1953), Wehner-Wilhelm (1956) conditions when axial diffusion and dispersion are included. The conditions on η' depend on electrode configuration and may be determined from Ohm's law

$$\frac{d\eta}{dx} = \frac{d(\Phi_1 - \Phi_2)}{dx} = -\frac{i_1}{\sigma} + \frac{i_2}{\kappa} , \qquad (4\text{-}2)$$

and are tabulated in Table 1. The dimensionless parameters P_5 and P_6 which arise in the analysis are the same as defined in equations 3-38 to 3-40. The dimensionless current density I^* to the reactor was defined in equation 3-41.

Now that all the boundary conditions for each electrode configuration have been specified, equations 3-28 and 3-29 can be solved simultaneously for θ and η' using Newman's method (Newman (1973), Appendix C).

The potential distribution in each phase $\Phi_1(x)$ and $\Phi_2(x)$ can then be obtained by solving equation 3-33 for η using the known distribution for η' , along with the conservation of charge condition

$$\frac{di_1}{dx} = -\frac{di_2}{dx} . \qquad (4\text{-}3)$$

and substituting this condition into the derivative of equation 2

$$\frac{d^2\eta}{dx^2} = -\left(\frac{\kappa + \sigma}{\kappa\sigma}\right) \frac{di_1}{dx} , \qquad (4\text{-}4)$$

then finally substituting the derivative of Ohm's law for the matrix phase into equation 4 to yield

$$\frac{d^2\eta}{dx^2} = \frac{\kappa + \sigma}{\kappa} \frac{d^2\Phi_1}{dx^2} . \qquad (4\text{-}5)$$

Equation 5 may be integrated twice to yield an expression for Φ_1 :

$$\Phi_1 = \frac{\kappa}{\kappa + \sigma} (\eta + C_1 x + C_2) . \qquad (4\text{-}6)$$

Table 4-1. Current and potential boundary conditions for various electrode configurations.

Electrode Configuration	$i_1(0)$	$i_1(L)$	$i_2(0)$	$i_2(L)$	$d\eta/dx\|_{x=0}$	$d\eta/dx\|_{x=L}$	$d\eta'/dy\|_{y=0}$	$d\eta'/dy\|_{y=\alpha L}$
UD	0	$-i$	$-i$	0	$-i/\kappa$	i/σ	$P_5 I^*$	$-P_6 I^*$
DU	i	0	0	i	$-i/\sigma$	i/κ	$P_6 I^*$	$-P_5 I^*$
UU	i	0	$-i$	0	$-i\left(\frac{1}{\sigma}+\frac{1}{\kappa}\right)$	0	$-P_2 I^*$	0
DD	0	$-i$	0	i	0	$i\left(\frac{1}{\sigma}+\frac{1}{\kappa}\right)$	0	$P_2 I^*$

The value of C_1 for the various configurations is obtained from the derivative of equation 6 using the values of i_1 and $d\eta/dx$ at the boundaries found in Table 1. The value of C_2 is then obtained by specifying $\Phi_1 = 0$ at the current collector and using a known value of η at the appropriate boundary. Table 2 summarizes the results for $\Phi_1(x)$ for the various configuration; $\Phi_2(x)$ is simply obtained by subtracting $\eta(x)$ from $\Phi_1(x)$.

4.3 Chemical systems

For the calculations to be presented, two different chemical systems (copper removal from sulfate solutions, Bennion and Newman (1972), and silver removal from thiosulfate solutions, Van Zee and Newman (1977)) are used to illustrate the effects of counterelectrode placement and current collector placement (when the matrix conductivity is finite) on electrode performance. The purpose of presenting results for two different chemical systems is to obtain reasonable values for the model parameters so that a valid comparison of electrode performance can be made when the side reaction is substantial (as for silver removal from thiosulfate solutions, Van Zee and Newman (1977)) and when it is small (as for the copper recovery process, Bennion and Newman (1972)).

Figure 2 compares model calculations to the data of Van Zee and Newman (1977) for silver removal from thiosulfate solutions using a porous carbon electrode. The quantities I and VOP are the total current to the reactor and the potential of the cathode current collector relative to a saturated calomel reference electrode placed in the effluent stream, respectively. The experimental effluent silver concentration (in mg/ℓ) are shown as the numbers below each curve corresponding

Table 4-2. Matrix potential distribution for various electrode configurations.

Electrode Configuration	Matrix Potential Distribution $\Phi_1(x)/\left(\frac{\kappa}{\kappa+\sigma}\right)$
UD	$\eta(x) - \eta(L) + \frac{i}{\kappa} L(x/L - 1)$
DU	$\eta(x) - \eta(0) - \frac{i}{\kappa} x$
UU	$\eta(x) - \eta(0)$
DD	$\eta(x) - \eta(L)$

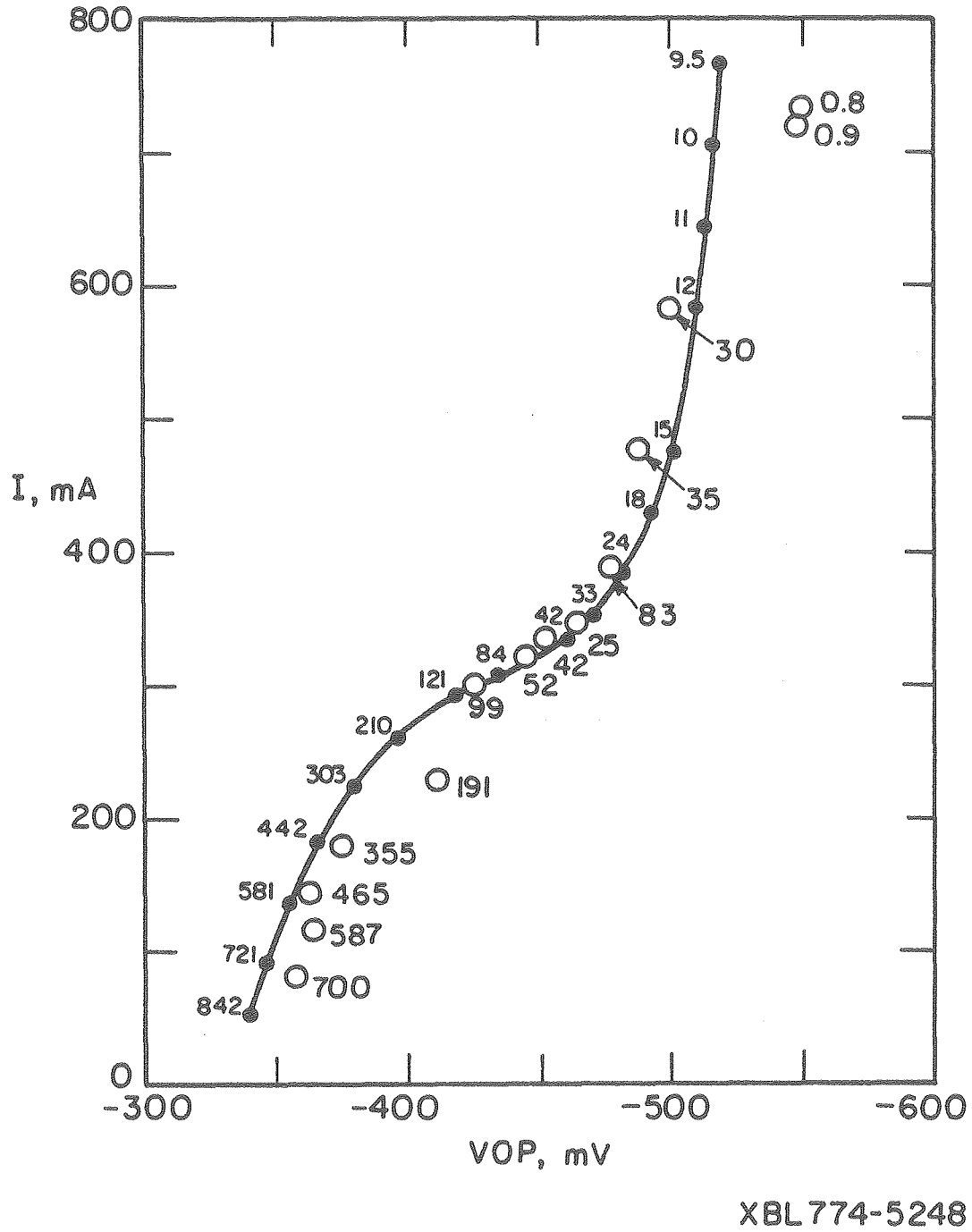

Figure 4-2. Current-potential curve for an electrode 5.5 cm deep and superficial electrode area of 61 cm^2, packed with carbon flakes and chips. Flow rate = 22 cm^3/min and the feed concentration = 1000 mg Ag/ℓ. Numbers below curve corresponding to the open circles O are experimental effluent concentrations (in mg/ℓ). The small numbers above the curve correspond to the solid dots • are calculated effluent concentrations (in mg/ℓ). VOP is the potential of the current collector with respect to a saturated calomel reference electrode placed in the dilute product stream.

to the open circles 0. The numbers above each curve correspond to the solid dots • and are the calculated values of the effluent silver concentration (in mg/ℓ).

A similar model fit to the data of Bennion and Newman (1972) for copper removal was given in chapter 3. Values of the parameters used to fit the data in chapter 3 and in Figure 2 are given in Table 3.

Four parameters were adjusted to obtain agreement between calculated and experimental values in Figure 1: one value of the exchange current density for the main reaction (silver deposition from thiosulfate solutions), assumed to be the electrode reaction (see, chapter 2 equation 2-12, or Trainham and Newman (1977a))

$$Ag(S_2O_3)_2^{3-} + e^- \rightarrow Ag + 2S_2O_3^{2-} \quad , \tag{4-7}$$

and has a standard electrode potential $U^{\theta}_{Ag/Ag(S_2O_3)_2^{3-}} = 0.0164$ V ;

one value of the exchange current density for the side reaction (the reduction of thiosulfate), which was assumed to be the following reaction (Van Zee and Newman (1977))

$$S_2O_3^{2-} + 8e^- + 8H^+ \rightarrow 2HS^- + 3H_2O \quad , \tag{4-8}$$

where the standard electrode potential can be calculated (Wagman et al. (1968), p. 47, and Dean (1973), pp. 6-14) to be $U^{\theta}_{HS^-/S_2O_3^{2-}} = 0.221$ V ;

one value each for the transfer coefficients for the side reaction α_{aS} and α_{cS}, which were assumed to sum to four. The freedom to assign arbitrary values to α_{aS} and αc_S is allowed in the model since the composition dependence of the polarization equation for the

Table 4-3.Values of the parameters used in fitting the data in Figure 2 and in generating Figures 3 through 17.

Copper deposition with simultaneous generation of dissolved hydrogen

$a = 25cm^{-1}$ $\varepsilon = 0.3$ $D_o = 6\times10^{-6}cm^2/s$ $\kappa_o = 0.17mho/cm$ $s_R = -1$

$n = 2$ $T = 298.15\ K$ $\alpha_{aR} = 1.5$ $\alpha_{cR} = 0.5$ $\alpha_{aS} = 0.5$

$\alpha_{cS} = 0.5$ $U_S-U_R = 0.281\ V$ $L = 6cm$ $k_m = 0.1922\times10^{-3}cm/s$ $v = 3.328\times10^{-3}cm/s$

$i_{oR,ref} = 7.009\times10^{-6}A/cm^2$ $i_{oS,ref} = 3.717\times10^{-13}A/cm^2$ $c_{Rf} = 1.05\times10^{-5}mole/cm^3$

$c_{Sf} = 10^{-3}mole/cm^3$

Silver reduction with simultaneous reduction of thiosulfate

$a = 25cm^{-1}$ $\varepsilon = 0.3$ $D_o = 1\times10^{-5}cm/s$ $\kappa_o = 0.123mho/cm$ $s_R = -1$

$n = 1$ $T = 298.15\ K$ $\alpha_{aR} = 0.5$ $\alpha_{cR} = 0.5$ $\alpha_{aS} = 2.75$

$\alpha_{cS} = 1.25$ $U_S-U_R = 0.489\ V$ $L = 5.5cm$ $k_m = 3.330\times10^{-3}cm/s$ $v = 6.011\times10^{-3}cm/s$

$i_{oR,ref} = 9.134\times10^{-5}A/cm^2$ $i_{oS,ref} = 1.20\times10^{-22}A/cm^2$ $c_{Rf} = 9.27\times10^{-6}mole/cm^3$

$c_{Sf} = 0.951\times10^{-3}mole/cm^3$

Table 4-3. (continued)

Dimensionless parameters

	Copper	Silver
P_1	1.050×10^{-7}	9.404×10^{-4}
P_2	-3.254 to -6.508	-3.738 to -7.476
P_3	1.247×10^{-4}	5.364×10^{-4}
P_4	5.863×10^{-8}	6.341×10^{-46}
P_5	3.254	3.738
P_6	9.089×10^{-11} to 3.254	3.777×10^{-15} to 3.738
D'	0.1217	0.1168

side reaction is neglected.

The value of the mass transfer coefficient k_m used in fitting the data was that obtained in fitting the data of Bennion and Newman (1972), and is given by equation 3-51.

In obtaining the fit to the silver removal data in Figure 2, it should not be interpreted that there is anything fundamental about the values of the fitted dimensional parameters found in Table 3, because not only are the data insufficient, but also the electrode is operating with a highly non-uniform current density and mass-transport limitations dominate in certain regions.

The model predictions of the current-potential behavior in Figure 2 are in satisfactory agreement with experimental data between 50 mA and 500 mA total current. However, at higher currents (above 500 mA), the data indicate the beginning of an additional limiting-current plateau, and agreement of the model calculations cannot be expected for the following reasons: 1) the side reaction postulated by Van Zee and Newman (1977) (equation 8) for the reduction of thiosulfate could be incorrect and there appears to be no fundamental kinetic information on this reaction and 2) if the limiting reactant species for the higher plateau were known, the model used here would not be sufficient since the concentration dependence for the side reaction was neglected and a more general model such as the one proposed by Alkire and Gould (1976) would be more appropriate.

Agreement between model predictions for the silver effluent concentration and the experimental values shown in Figure 2 are satisfactory near the limiting current. This is because the model parameters were chosen so as to fit the data in this region. However,

agreement should not be expected over the entire current-potential range because the data exhibit unexplained anomalies (Van Zee and Newman (1977)): 1) current efficiencies above 100 percent and 2) a minimum in the silver effluent concentration with increasing values of VOP.

A comparison of the dimensionless parameters in Table 3 between the two chemical systems suggests that the parameters P_1 and P_3 account primarily for the difference in behavior of these systems. The parameters P_1 and P_3 represent the relative importance of the backward rate of the main reaction and the forward rate of the side reaction and are 10^4 and 4.3 times greater, respectively, for the silver system than for the copper system. As will be observed later a low effluent concentration cannot be achieved for silver system and this is due to the combined effect of the parameters P_1 and P_3.

The magnitude of the side reaction is substantial for the silver system and this shields the back of the electrode (in the case of an upstream counterelectrode) from having a large electric driving force which results in a very small rate for the deposition of silver in this region. This is accentuated by the fact that P_1 is large, which causes the backward rate of the deposition reaction to be of the same order on the forward rate and the reactor can become thermodynamically limited.

4.4 Results and discussion

As a unifying concept here, let us consider how we can achieve a very high conversion or, equivalently, a very low effluent concentration of the limiting reactant while, at the same time, operating the reactor

at as high a flow rate as possible. Towards these ends, we can consider variations of electrode current density and length, flow rate, configuration, and matrix conductivity. By means of the computer program, we have the means to investigate in detail how the presence of a side reaction places limitations on the attainment of these goals.

Effect of electrode length. For the case of a very high matrix conductivity, Figure 3 shows the effect of electrode length and current density on the effluent concentration for the copper system. We see, first of all, that we must operate at or above the limiting current in order to reach a really low effluent concentration. If we operate at $I^* = 0.9501$, we cannot expect to remove more than 95 percent of the copper even if we have very high current efficiencies and substantial electrode lengths.

The curve on Figure 3 for an upstream counterelectrode and $I^* = 1.038$ shows essentially a limiting-current condition -- the effluent concentration decreases almost exponentially with electrode length. (See, for example, the analysis of Bennion and Newman (1972) and that of Newman and Tiedemann (1976) when axial diffusion and dispersion are included.) However, for downstream placement of the counterelectrode, a limiting-current distribution cannot be maintained except for electrode lengths less than 2 cm, and a truly low effluent concentration cannot be attained at all with this electrode configuration (at this flow rate). The current efficiency must necessarily be somewhat lower, and the extent of the side reaction somewhat higher, with the downstream counterelectrode.

Figures 4 and 5 introduce the effect of a finite matrix conductivity σ. Now, according to Figure 1, four different configurations are

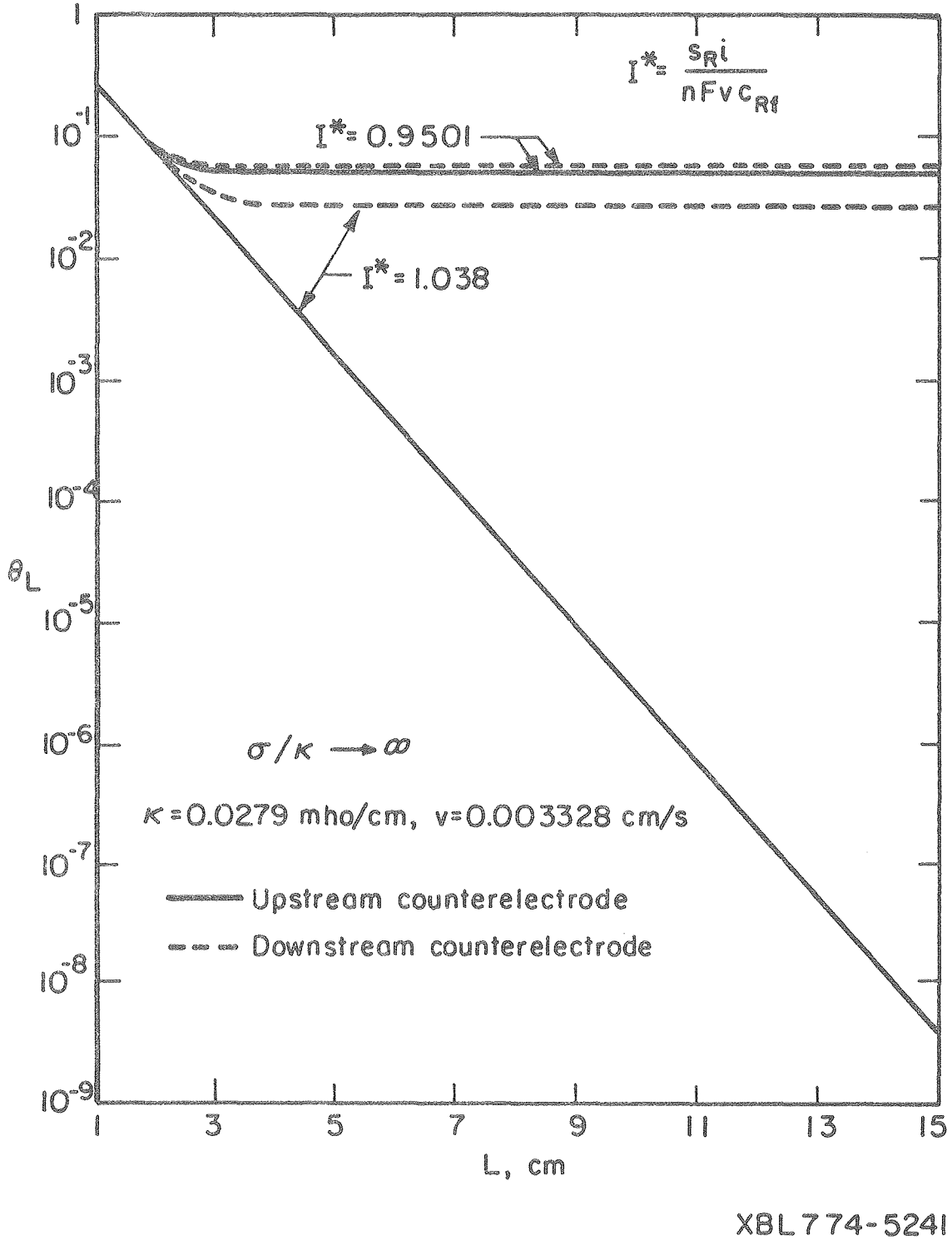

Figure 4-3. Effluent copper concentration as a function of electrode length for $c_{Rf} = 0.0105$ M .

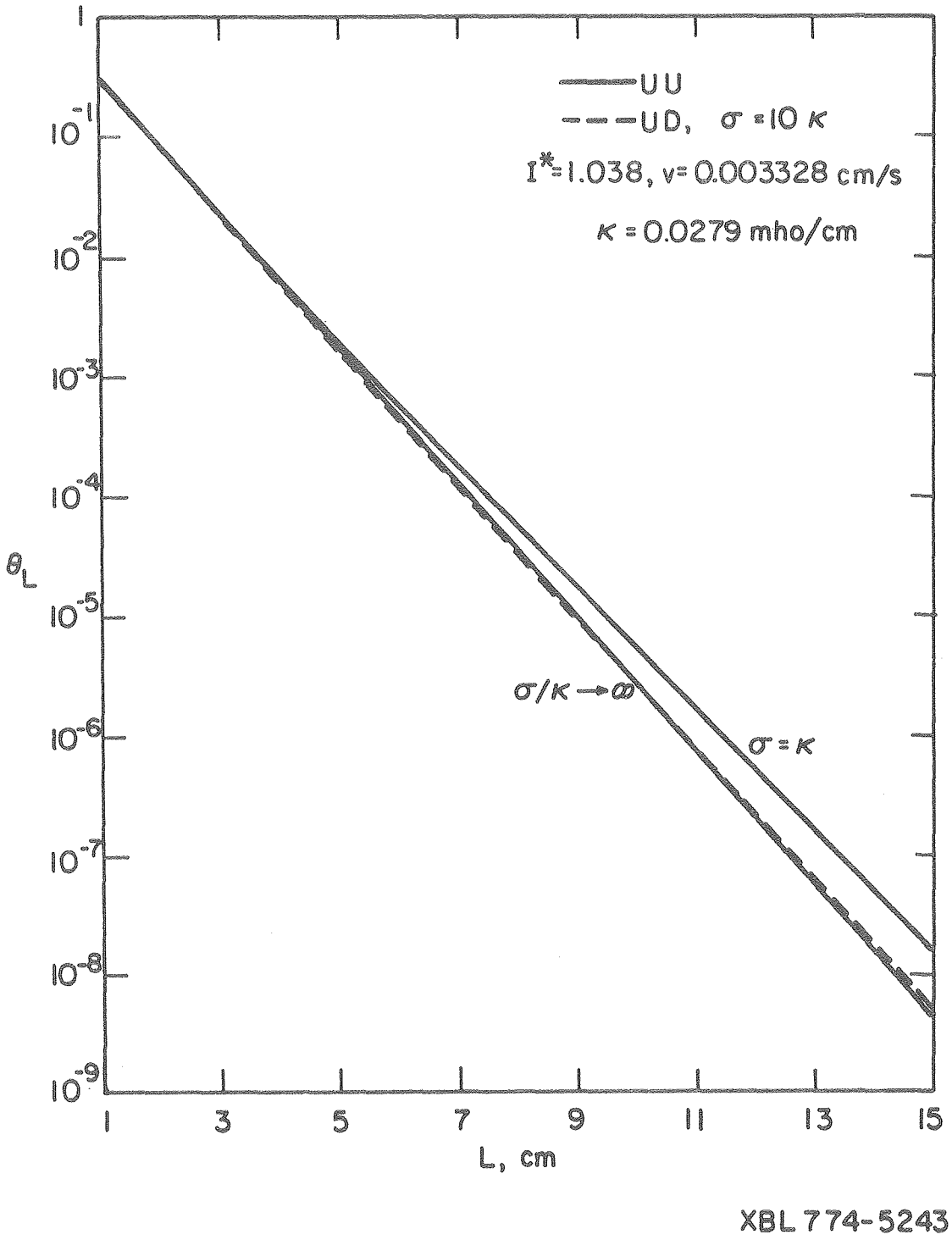

Figure 4-4. Effluent copper concentration as a function of electrode length.

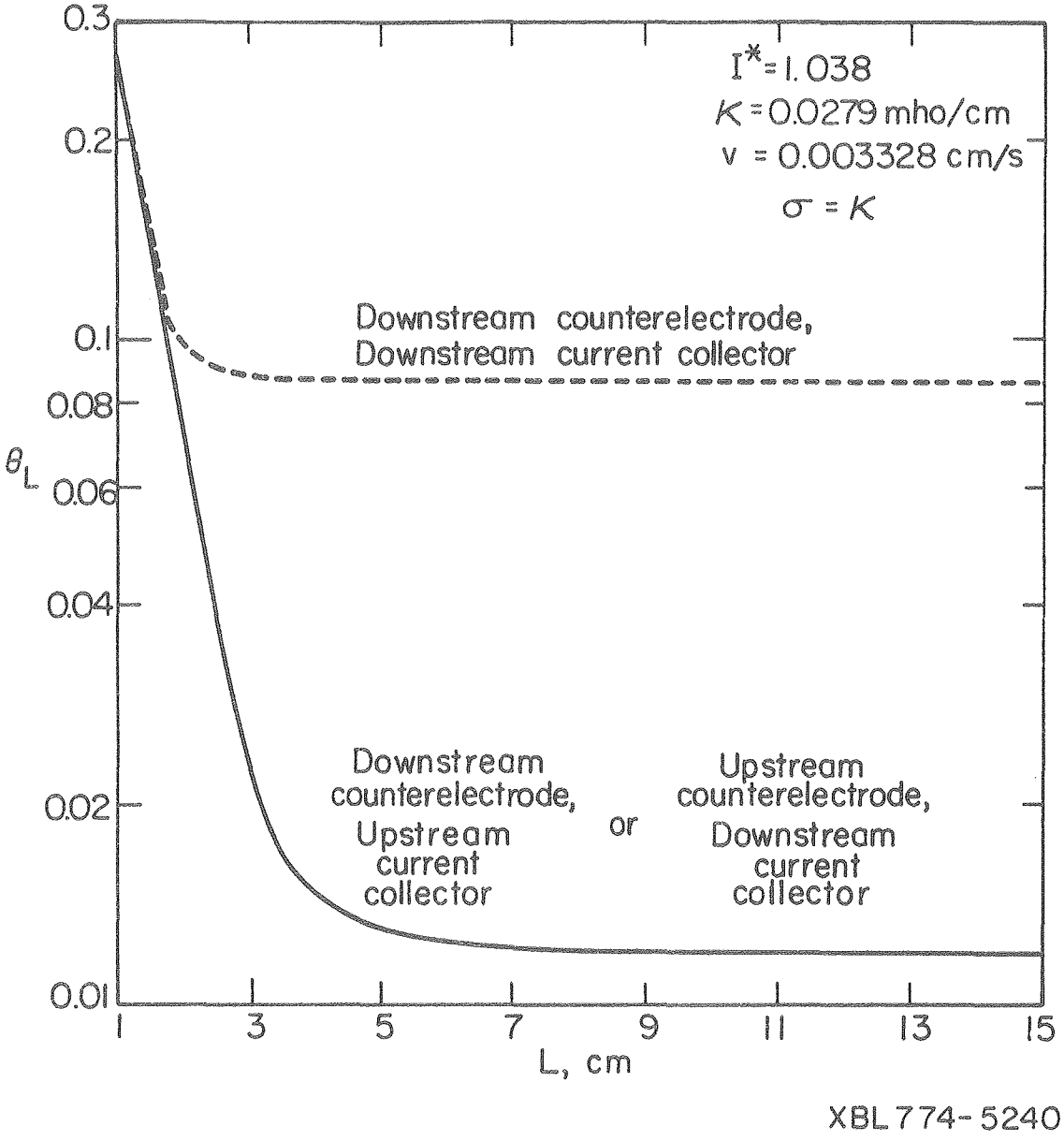

Figure 4-5. Effluent copper concentration as a function of electrode length.

relevant since the placement of the current collector must also be considered. Figure 4 shows that the UU configuration retains the exponential decrease of θ_L with L, although performance is slightly degraded by the additional ohmic potential drop compared to the case of the infinite matrix conductivity. (The curve for $\sigma = 10\,\kappa$ will be discussed later in connection with the optimum matrix conductivity.) Figure 5 shows the relatively poor performance achievable with the other configurations. In these cases, the ohmic potential drop in the matrix and solution phases prevents the entire reactor from being operated at a limiting-current condition, as we shall discuss in more detail later.

Figure 6 displays the silver effluent concentration as a function of electrode length for the various electrode configurations for cases where $\sigma >> \kappa$ and $\sigma = \kappa$. The results show that none of the electrode configurations yields an exponential decrease in θ_L with electrode length; thus a limiting-current distribution cannot be achieved in any of the geometries due to extensive interference by the side reaction.

Effect of matrix conductivity. Figures 7 and 8 show the dependence of the effluent copper concentration on the matrix resistivity $(1/\sigma)$. Figure 9 shows similar results for the silver system. Calculations for a DD placement are not presented here since this configuration does not allow a low effluent concentration, in comparison to the other configurations when the matrix conductivity is small.

In Figures 7 and 9, we observe that the UD configuration exhibits a minimum with matrix resistivity and therefore has an optimum value for σ (about equal to $0.1\,\kappa$ for the copper system). On the other

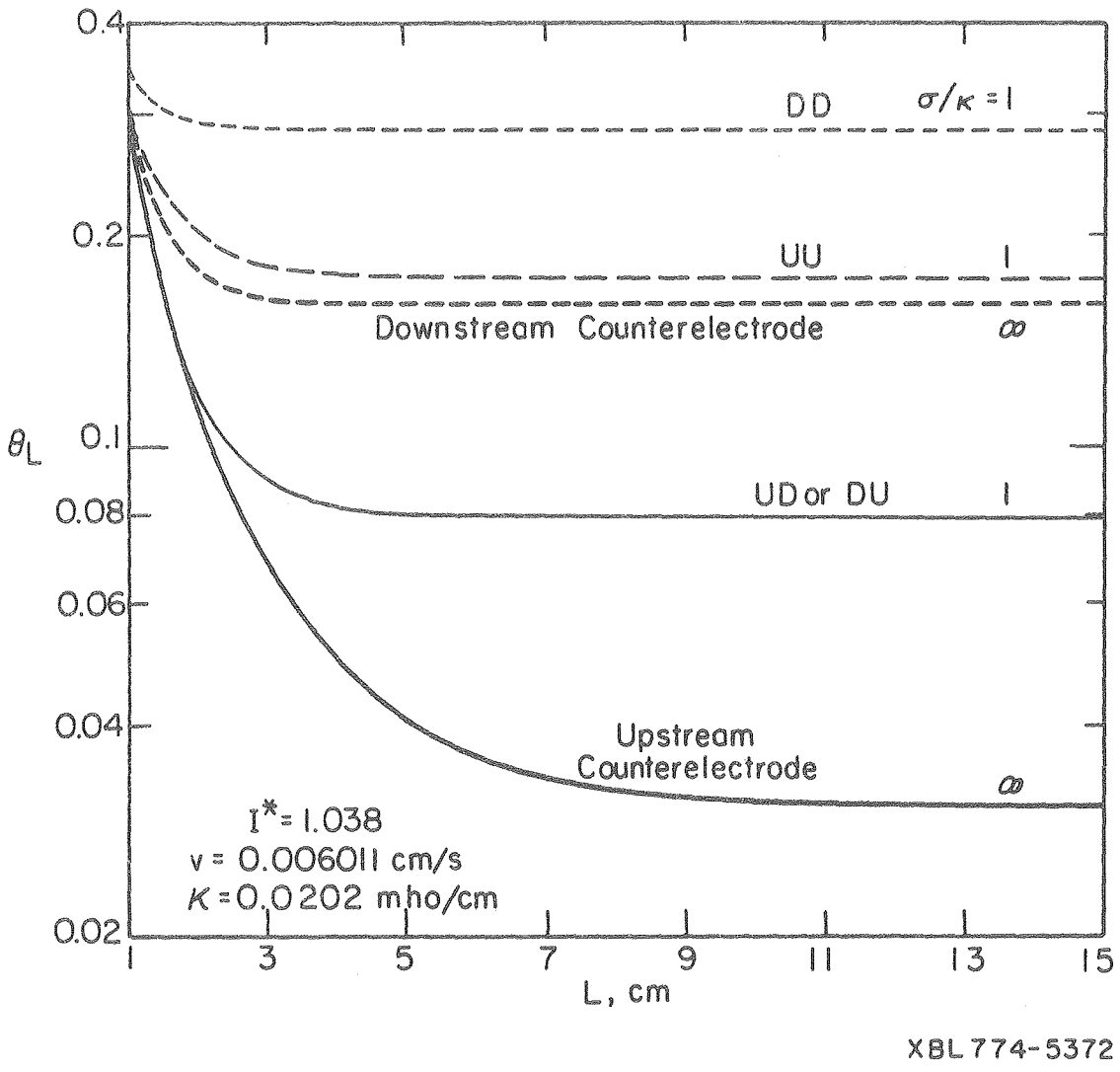

Figure 4-6. Effluent silver concentration as a function of electrode length for $c_{Rf} = 0.00927$ M .

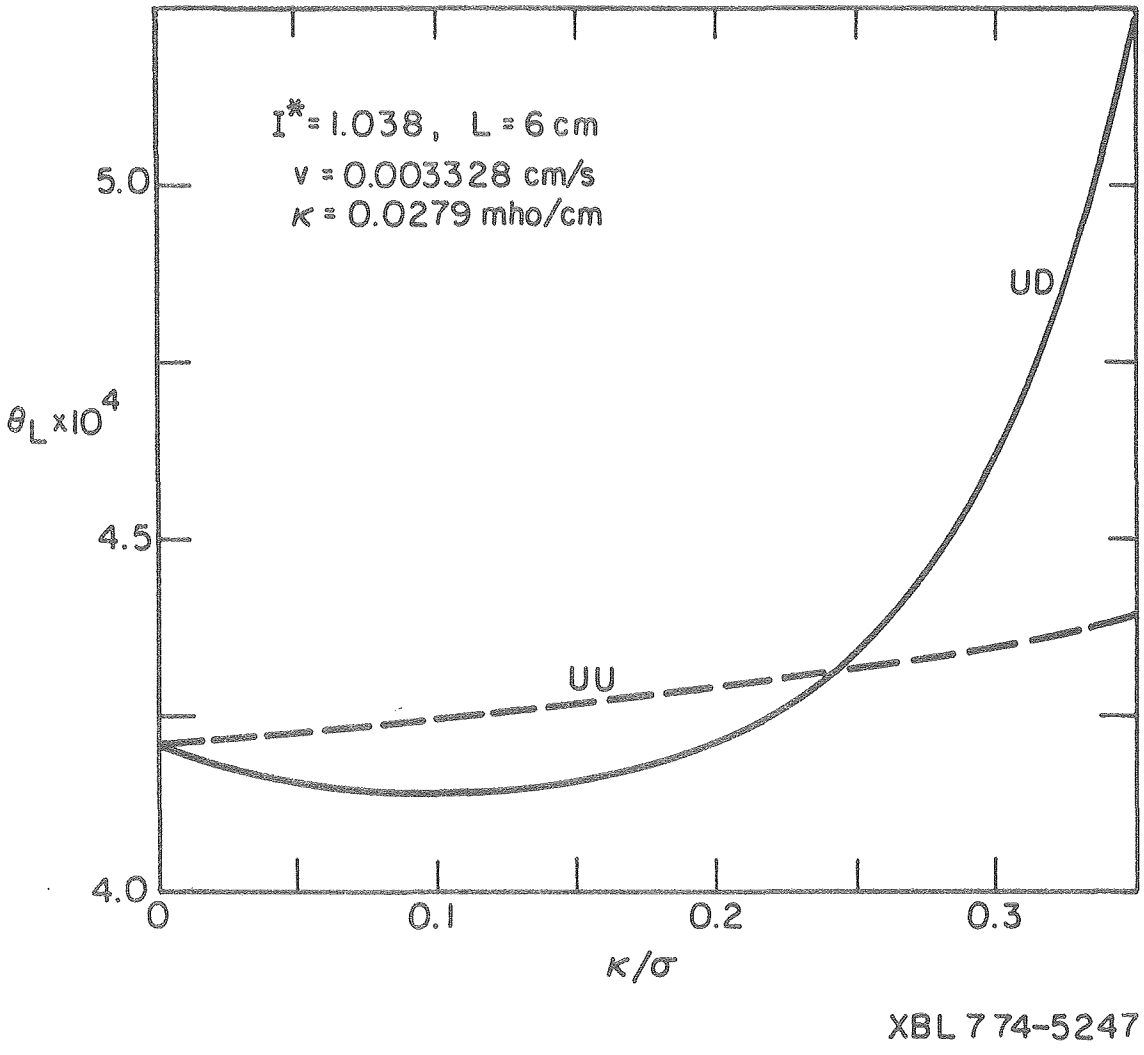

Figure 4-7. Dependence of the copper effluent concentration on the matrix resistivity.

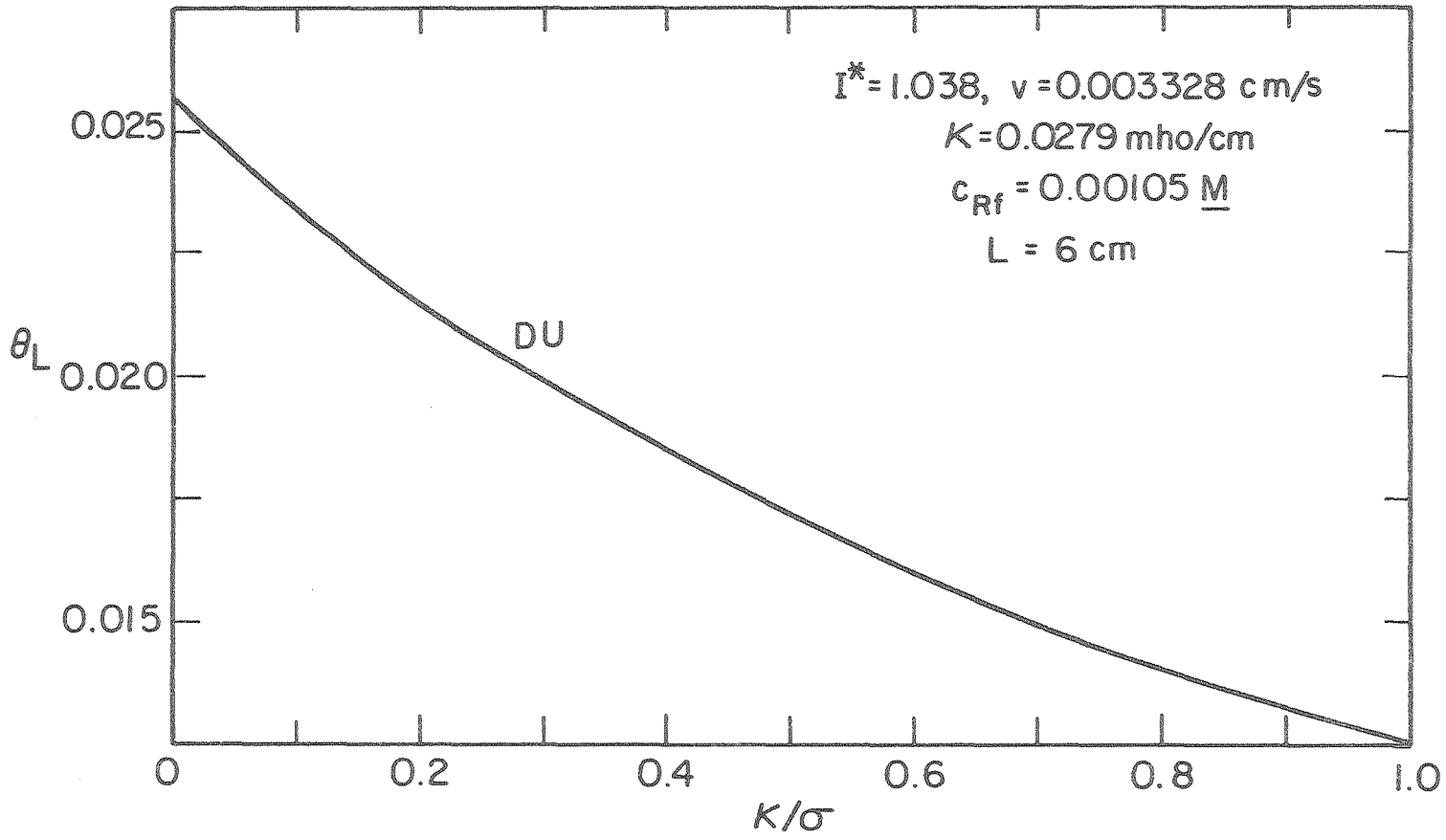

XBL 774-5246

Figure 4-8. Dependence of the copper effluent concentration on the matrix resistivity.

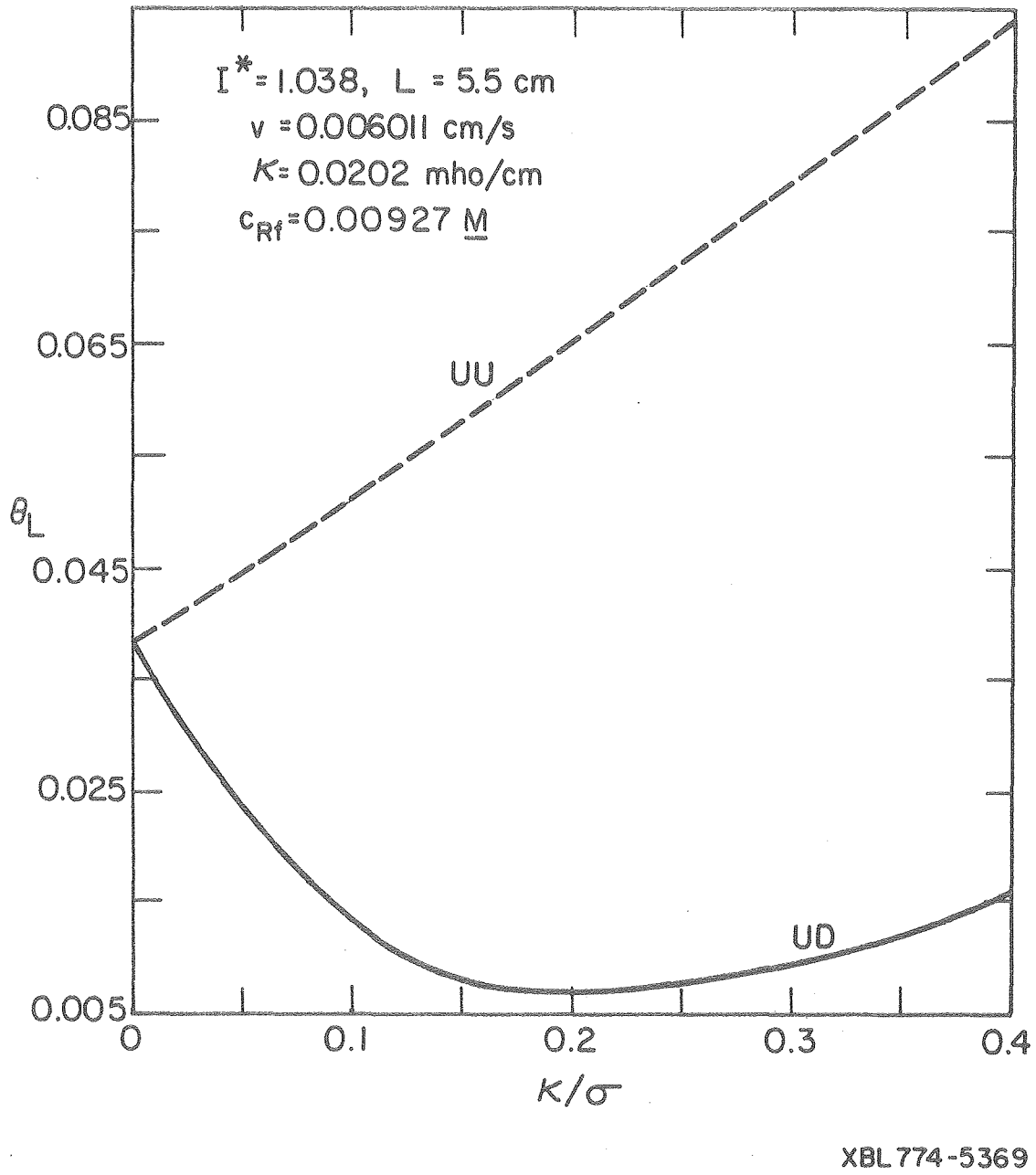

Figure 4-9. Dependence of the silver effluent concentration on the matrix resistivity.

hand, for the UU configuration, θ_L increases monotonically with increasing matrix resistivity. The DU configuration on Figure 8 would also show a minimum at values of κ/σ substantially greater than unity. This is of less interest than the minima for the UD configuration because matrix resistivities are usually much less than solution-phase resistivities and because the effluent concentrations are inherently large with the DU configuration. For example, the DU and UD configurations give the same effluent concentration when $\sigma = \kappa$ (see Figure 5) but at this point, the value of θ_L has risen to 0.0125 from a minimum of 4.14×10^{-4} on Figure 7. At $\sigma = \kappa$, the UU configuration is still able to attain a value of θ_L of 6.08×10^{-4} (see Figure 4). [Note, however, that the DU configuration performs better than the UU configuration for $\sigma = \kappa$ in the silver system, as displayed on Figure 6.]

Return for a moment to the dashed curve on Figure 4. For this curve, $\sigma = 10\ \kappa$, which corresponds to the minimum for the UD configuration shown in Figure 7, and an exponential dependence of θ_L on L can evidently be maintained. The performance is superior to the high-matrix-conductivity case for L less than about 10 cm, after which it becomes somewhat inferior. The optimum ratio of κ/σ depends on electrode length, for example, for an electrode 4 cm in length the optimum ratio is approximately 0.17, for an electrode 8 cm long the optimum ratio is approximately 0.07. Note that we get a markedly different view of the effect of configuration and matrix resistivity if we confine our attention to the cases $\sigma >> \kappa$ and $\sigma = \kappa$ on Figures 3, 4, and 5 from what we get if we include the variation of σ and the optimum value of σ. The UD configuration is totally unsatisfactory at $\sigma = \kappa$ but excellent at $\sigma = 10\ \kappa$.

For the silver system, other calculations show that, even at the optimum ratio of $\kappa/\sigma = 0.2$ shown on Figure 9 for the UD configuration, a limiting-current distribution and an exponential dependence of θ_L on L cannot be achieved. Similar results for the copper system can be obtained by increasing the flow rate to somewhat less than three times the value used in calculating Figures 3, 4, and 5.

Bennion and Newman (1972) have formulated design considerations for achieving a low effluent concentration while operating at as high a flow rate as possible. First, the electric driving force within the electrode must be maintained high enough to attain a limiting-current condition throughout the reactor. The electric driving force must also be maintained low enough to avoid excessive side reactions. These two conditions thus define a limited range of potentials allowable within the reactor. Since the electrode must be of substantial length in order to achieve a given effluent concentration, there is an upper limit on the flow rate above which these constraints cannot be satisfied simultaneously.

The effect of the side reaction is not one which can be compensated for by using a longer electrode or a higher current, even if one is willing to pay the price of a lower current efficiency and a higher cell potential. It is a characteristic of porous electrodes, leading to their inherently nonuniform reaction rate distributions, that substantial current densities flowing over substantial distances in either the matrix or solution phases make it impossible to maintain a uniform electric driving force (for the reactions) throughout the electrode.

On the basis of these considerations, an important quantity is the difference between the minimum electric driving force η_{min} and the maximum electric driving force η_{max} that prevail within the reactor. Figure 10 displays this quantity as a function of the conductivity ratio for the copper system and corresponds directly with the conditions of Figure 7. The ordinate, made dimensionless with $nFv^2c_{Rf}/s_R\kappa ak_m$, will have a magnitude on the order of unity if the current density is distributed like that for the limiting current for the main reaction (Bennion and Newman (1972), and Newman and Tiedemann (1976)). A graph similar to Figure 10 is given by Newman and Tiedemann (1976) for the case where the current densities are calculated according to the limiting-current distribution for the main reaction. The computer program used here permits analysis above and below the limiting current and in the presence of a side reaction.

The fact that the ordinate values on Figure 10 are of order unity illustrates how the constraints on the flow-through porous electrode can better be satisfied by operation at lower flow rates.

There is a correspondence between the shapes of the curves on Figures 7 and 10. Conditions which lead to an inherently smaller value of $|\eta_{max} - \eta_{min}|$ make it possible to achieve a limiting-current condition through a larger portion of the reactor, without extensive side reaction. For the UD configuration, the maximum electric driving force occurs at the fluid inlet for $\kappa/\sigma < 0.175$. The position of the maximum electric driving force then shifts to the fluid outlet for $\kappa/\sigma > 0.175$. This leads to the sharp minimum for the UD configuration in Figure 10.

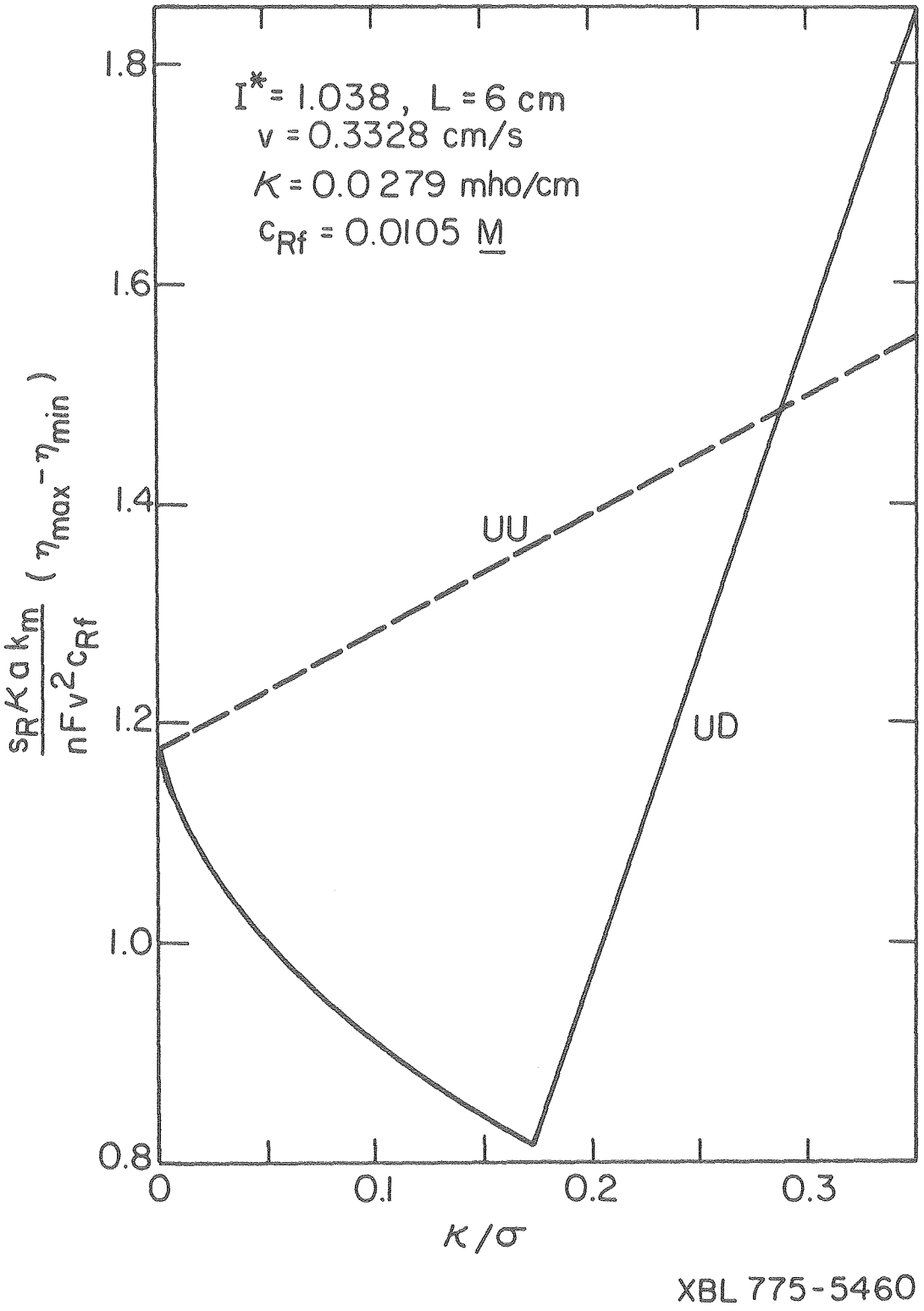

Figure 4-10. Variation in the difference between the maximum and minimum driving force for copper deposition with the matrix resistivity.

Detailed distributions. The behavior of these systems can be understood better by consideration of the calculated current, potential, and electric-driving-force distributions within the electrode. These are illustrated for the copper system with an electrode 6 cm long and by a 5.5 cm electrode for the silver system.

For the copper system with an infinite matrix conductivity, Figure 11 shows the relative rates of reaction for both the main and side reactions for both upstream and downstream placement of the counterelectrode. Figure 12 shows the corresponding distributions of potential in the matrix and pore solution. The total current density to the electrode was chosen close to the limiting current ($I^* = 1.038$) for the deposition of copper. For upstream placement of the counter-electrode, the main reaction rate decreases almost exponentially with distance through the electrode (as predicted by the limiting-current analyses of Bennion and Newman (1972), and Newman and Tiedemann (1976)). At the same time, the side reaction follows the electric driving force (see Figure 12), which is high at the fluid inlet and decreases toward a uniform value near the fluid outlet.

On the other hand, for the downstream placement of the counter-electrode, the main reaction rate does not show an exponential depen-dence on distance. Figure 12 shows that the electric driving force is very large at the outlet but too low at the inlet. Consequently, a limiting-current condition is not maintained near the front. At about 65 percent of the distance through the electrode, the electric driving force has become large enough to assure a limiting-current condition, and subsequently an exponential dependence on distance is exhibited. However, failure to utilize effectively the front part of the electrode

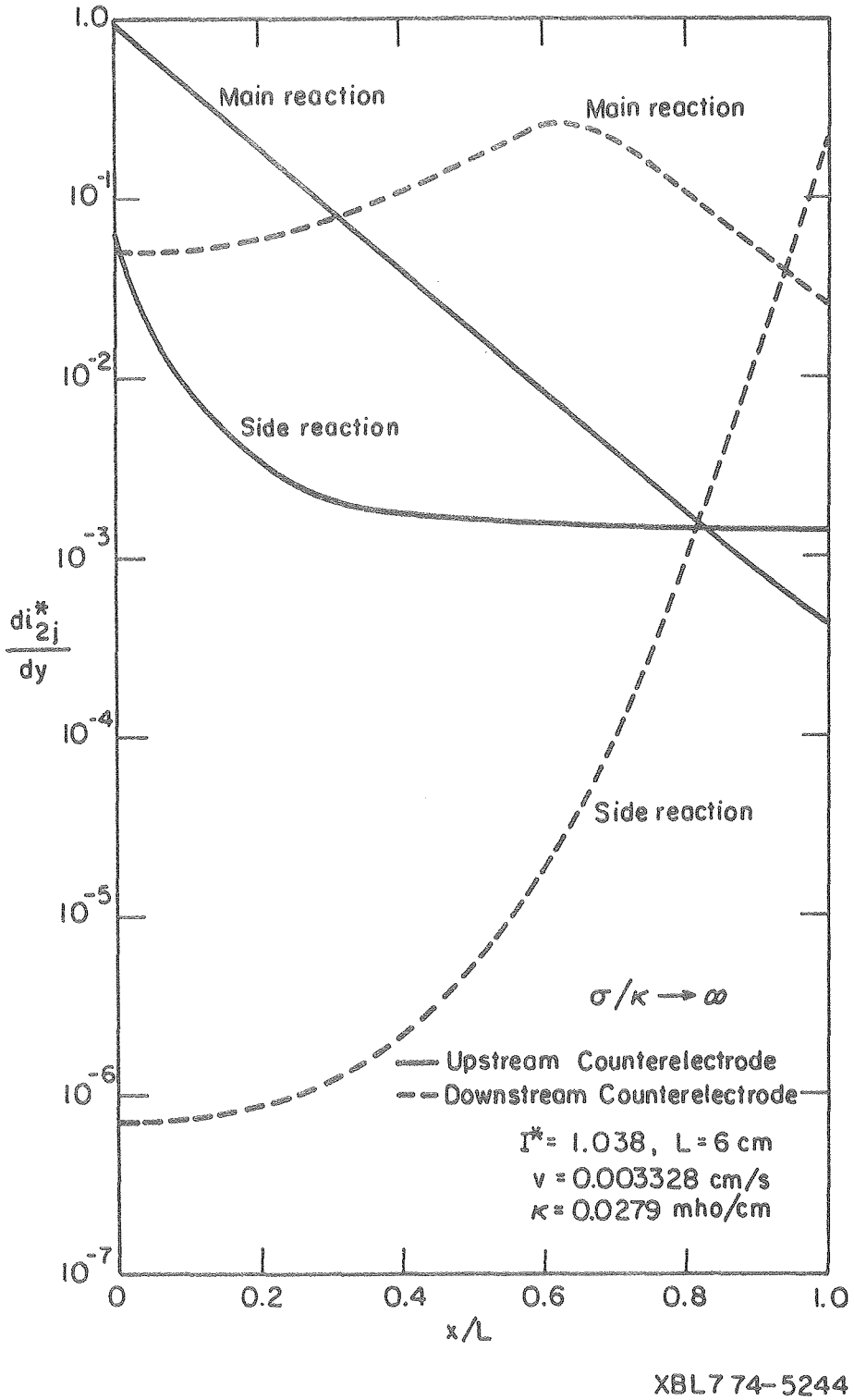

Figure 4-11. Current distributions for deposition of copper and generation of dissolved hydrogen within a porous electrode. Calculated for $c_{Rf} = 0.0105$ M .

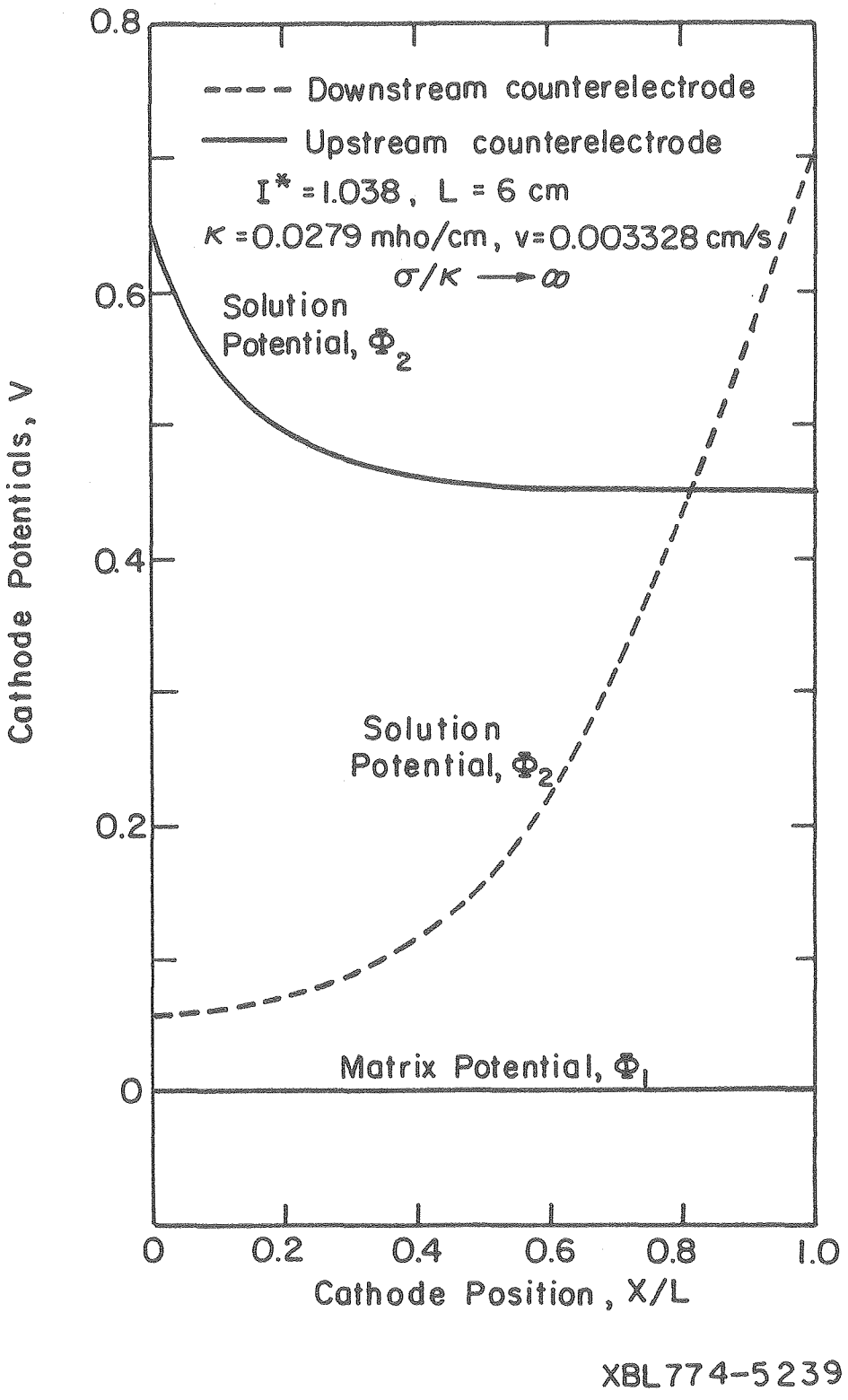

Figure 4-12. Calculated solution phase and solid matrix phase potential distributions for the deposition of copper and simultaneous formation of dissolved hydrogen.

makes it impossible to achieve a truly low effluent concentration, and increasing the electrode length would not help (see Figure 3). The resulting reaction-rate distribution now has a maximum; as the electric driving force increases toward the back of the electrode, the reaction rate goes up, and copper is depleted from the solution to the extent that the mass-transfer driving force becomes small. The reaction rate exhibits a maximum and then decreases with distance. (Similar reaction-rate distributions have been reported by Alkire and Gould (1976). These are examples of a general phenomenon (Newman (1966), Parrish and Newman (1969, 1970), and Hsueh and Newman (1970)) resulting from the competition of electric and mass-transfer driving forces.) The side reaction has a distribution in Figure 11 that again follows that of the electric driving force in Figure 12. Because of the somewhat lower rate of the main reaction, in comparison to the upstream placement of the counterelectrode, the side reaction now occurs at a somewhat higher rate on the average. For these comparisons at a constant total current ($I^* = 1.038$), an increase in the effluent concentration from one electrode to another is accompanied by a corresponding decrease in the current efficiency.

As in porous electrodes in general, the reaction rate distributions and ohmic potential drop shield the more remote parts of the reactor from having an adequate electric driving force. In this particular situation, the contrast between the cases of upstream and downstream placement of the counterelectrode arises in the following way. In order for there to be a high conversion, there must be a high reaction rate -- generating high current densities in the solution -- near the fluid inlet. Since the solution-phase conductivity κ is not high,

potential variations in the solution phase can be minimized if the current flows out of the electrode at the nearest possible point, namely, to a counterelectrode placed upstream. If the counterelectrode is placed downstream, the large currents which should be generated near the fluid inlet must flow in the solution through most of the thickness of the electrode, and this necessarily leads to large variations of potential. A similar explanation applied in the more complex cases to follow, where the matrix conductivity is also finite.

Figure 13 shows the reaction-rate distributions for the main and side reactions for the copper system where $\sigma = \kappa$. The corresponding potential distributions are shown in Figure 14. Because of the complexity of Figure 14, the distributions of electric driving force are also shown in Figure 15.

The reaction-rate and electric-driving-force distributions for the UD and DU configurations happen to be identical when $\sigma = \kappa$ since the boundary conditions given in Table 3 are then identical. However, the potential distributions in each phase will be different, as seen in Figure 14. In these configurations, the counterelectrode and the current collector are not at the same end of the reactor. Consequently, the current flows in the same direction in the matrix as in the solution, and to a certain extent the potential drop in the matrix can match that in the solution (see Figure 14). This makes it possible, in some cases, to reduce the variation of the electric-driving-force within the reactor (see Figure 10). It also means that the extreme values of the electric driving force occur at the ends of the reactor, with the minimum value occurring somewhere between (see Figure 15), and the side reaction follows this distribution (see Figure 13).

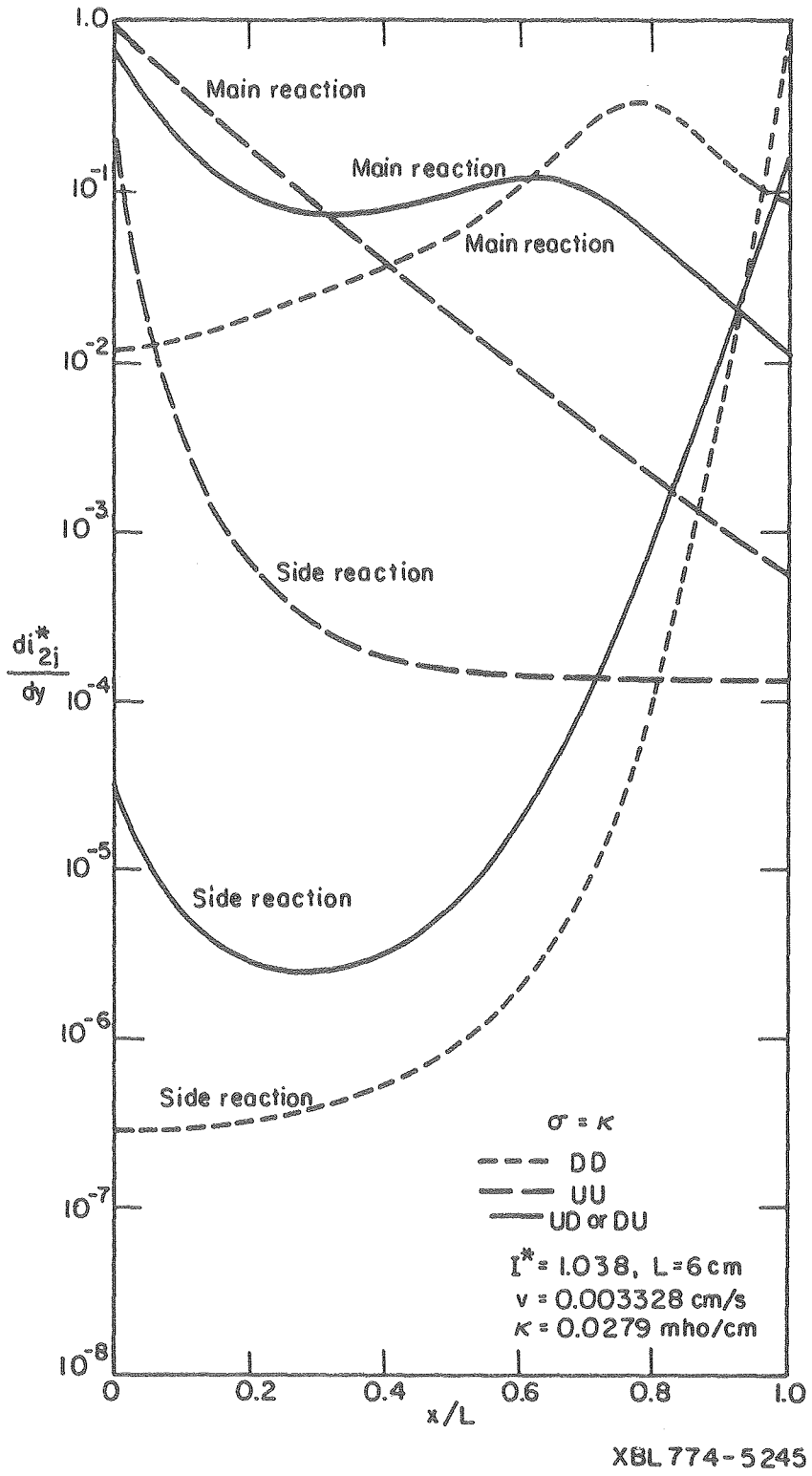

Figure 4-13. Current distributions for deposition of copper and generation of dissolved hydrogen within a porous electrode. Calculated for $c_{Rf} = 0.0105$ M .

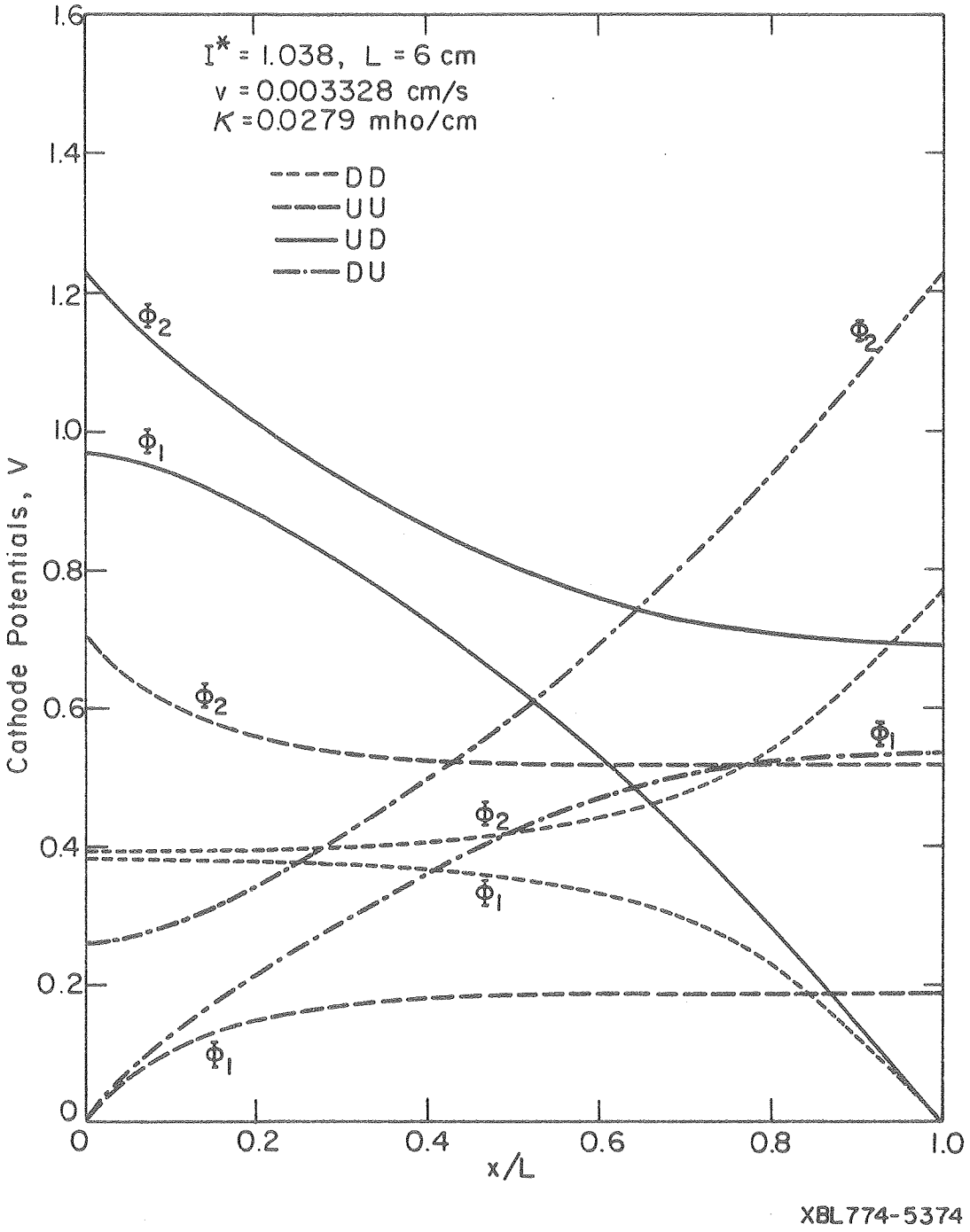

Figure 4-14. Calculated solution phase and solid matrix pnase potential distributions when $\sigma = \kappa$ for the depositions of copper and simultaneous formation of dissolved hydrogen.

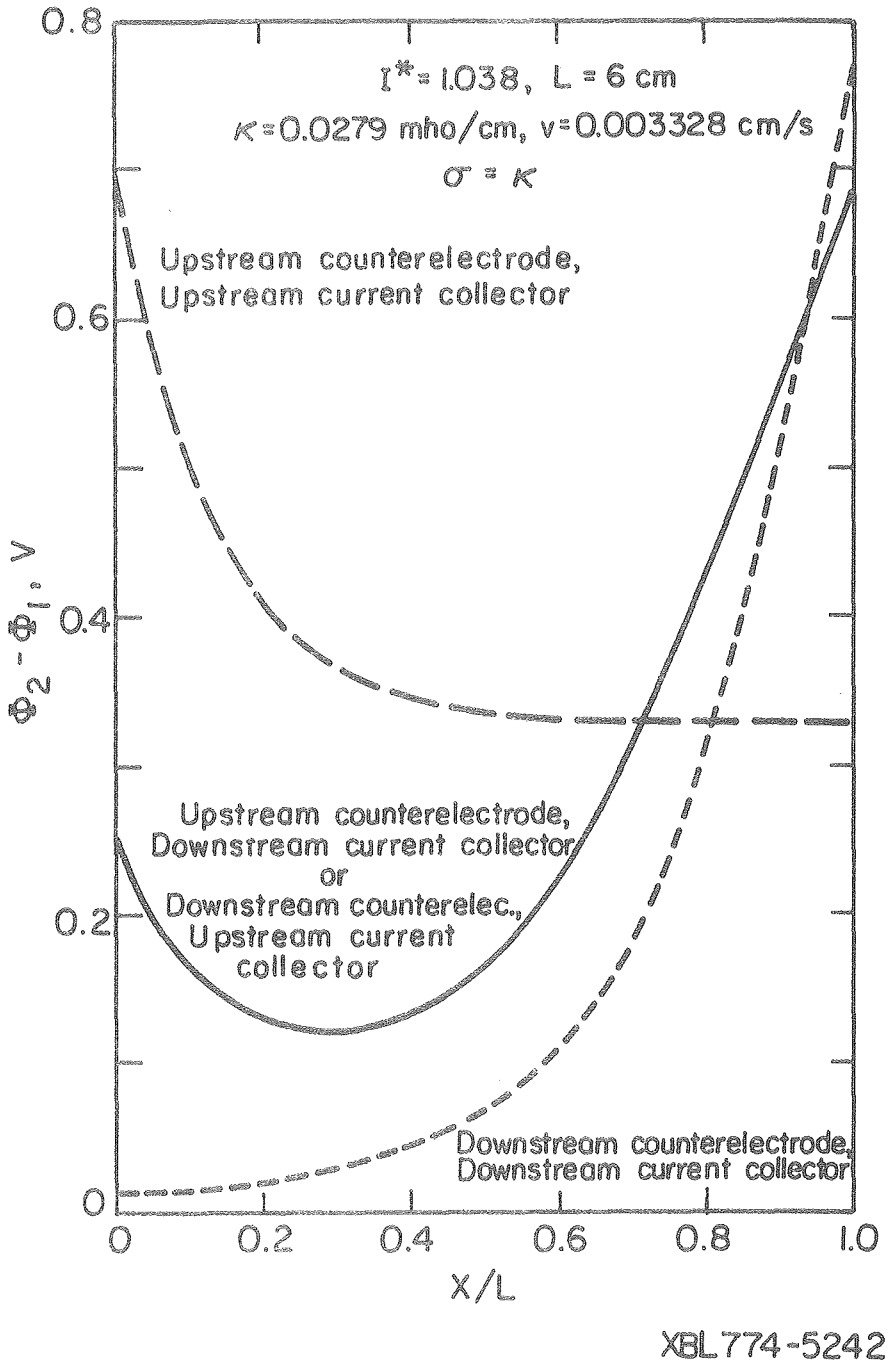

Figure 4-15. Electrical driving force distributions for the potential distributions shown in Figure 14.

For the UU configuration, the maximum electric driving force occurs at the inlet, and the minimum at the outlet, and conversely for the DD configuration. For the main reaction, only the UU configuration shows an exponential dependence of rate on distance (see Figure 13). For the other configurations, the main reaction is below the limiting current for a substantial (DD) or moderate (UD or DU) region near the inlet, and consequently the effluent concentration cannot be reduced to a truly low value. Only in the UU configuration are the current densities in both the solution and matrix phases small near the back of the electrode. In this region the electric driving force varies little (as is the case also for the upstream counterelectrode case in Figure 12, where $\sigma >> \kappa$), and measurement of $\Phi_1 - \Phi_2$ at $x = L$ can lead to a lower-bound thermodynamic estimate of the minimum attainable concentration in a flow-through porous electrode (see chapter 2).

Figures 16 and 17 show the reaction-rate and electric-driving-force distributions for the silver system. A limiting-current distribution is not achieved for any electrode configuration, due to extensive interference by the side reaction, as indeed, it is not, even for an infinite matrix conductivity (see Figure 6). As for the copper system, the electric driving force for the DD configuration is small at the front of the electrode, and for the UD and DU configurations it is small in the middle and only moderately large at the front. Under these conditions, the front and middle regions of the reactor are not effectively utilized, and a low effluent concentration cannot be achieved even though a limiting-current condition is maintained near the rear. However, for the UU configuration, the lowest electric driving force occurs at the rear of the reactor, and the rate of the

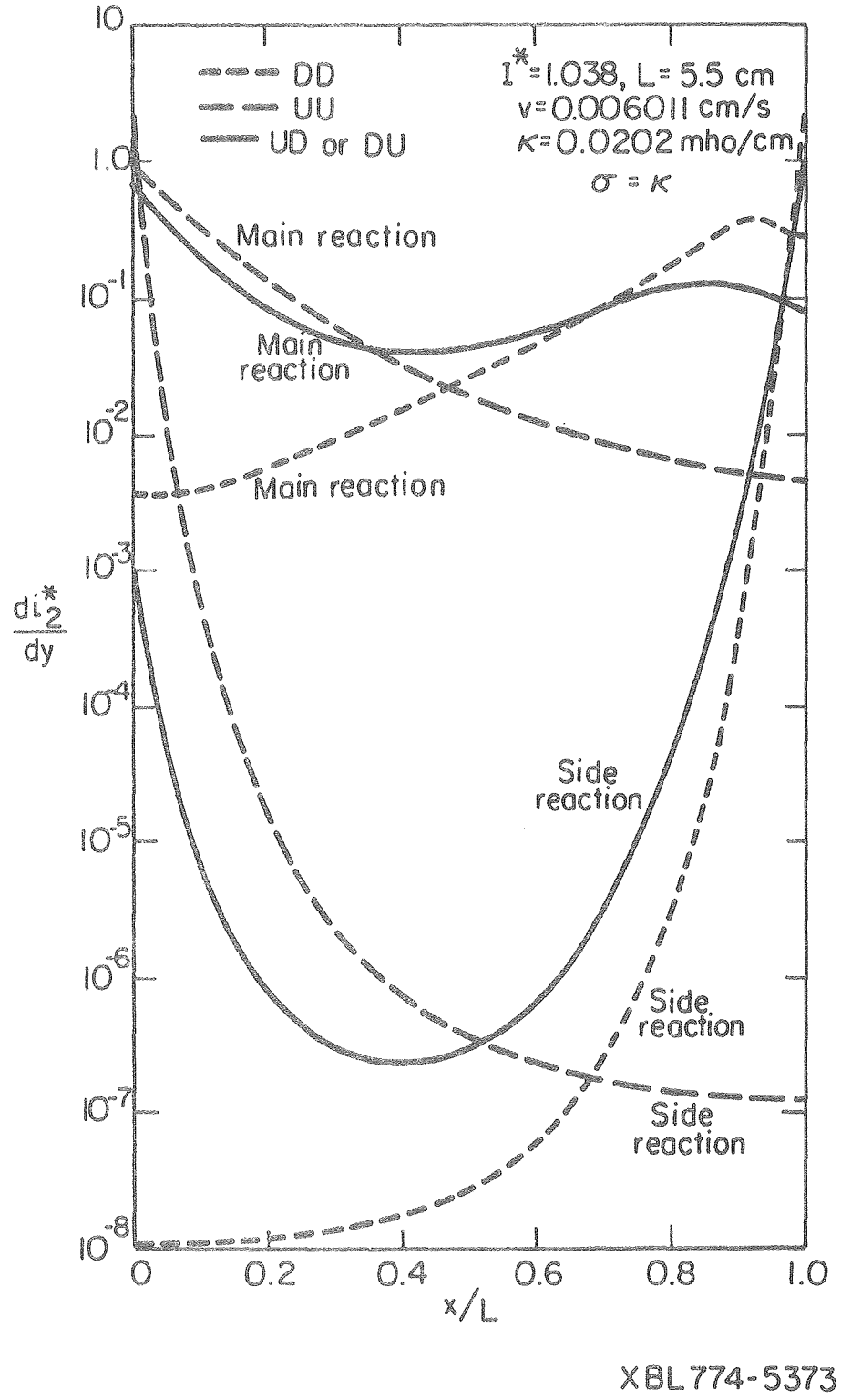

Figure 4-16. Current distributions for silver deposition and reduction of thiosulfate within a porous electrode. Calculated for c_{Rf} = 0.00927 M , and L = 5.5 cm.

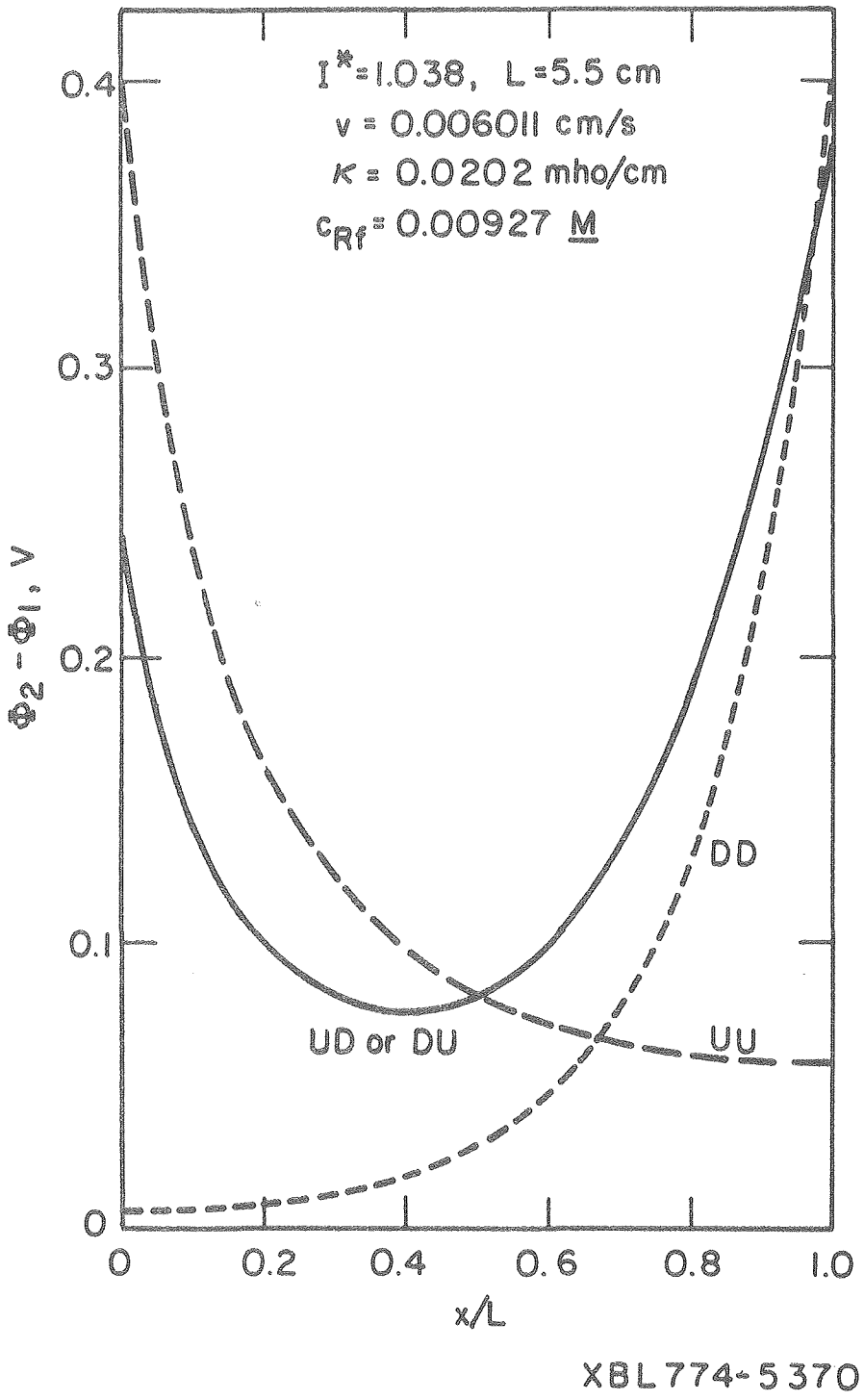

Figure 4-17. Electrical driving force distributions for the deposition of silver from thiosulfate solutions.

main reaction does not decrease exponentially with distance. In fact, with the higher value of P_1 for the silver system, the effluent concentration is very close to the thermodynamic limit determined by the electric driving force prevailing at the fluid outlet (see chapter 2).

Effect of configuration. The preceding discussion has permitted a comparison of several configurations under a variety of operating conditions. It is important to recognize that the lowest effluent concentration is achieved for upstream placement of the counterelectrode (see Figures 3 through 6). For downstream placement of the counter-electrode, a limiting-current distribution cannot be obtained (see Figures 11 and 13), principally because the current in the solution must flow through most of the length of the electrode, and this leads to a large ohmic potential drop.

For the DU configuration shown in Figure 8, θ_L decreases with increasing values of matrix resistivity. For a downstream counter-electrode, a situation is created where the ohmic potential drop in the solution is working against the favorable mass-transfer condition near the fluid inlet. Increasing the matrix resistivity increases the electric driving force near the fluid inlet because the matrix current must leave through the current collector placed there. This causes the rate of the main reaction at the front of the electrode to increase from about 0.05 when $1/\sigma \to 0$ (in Figure 11) to 0.67 when $\sigma = \kappa$ (In Figure 13).

As mentioned earlier, the DD configuration is the least efficient of the configurations shown in Figure 1. If the matrix resistivity is increased from zero, the electric driving force is further reduced near the fluid inlet, while it increases somewhat near the fluid outlet (compare Figures 14 and 15 with Figure 12). This causes the rate of the

4.5 Conclusions and summary

The theoretical model for flow-through porous electrodes developed in chapter 3 has been used to evaluate the effects of electrode placement relative to the fluid inlet and finite matrix conductivity on the performance of flow-through porous electrodes. If a low effluent concentration is desired, the electrode must be operated at a superficial current density sufficiently high so that the main reaction may achieve a limiting-current distribution. Calculations show that a limiting-current distribution can only be achieved for upstream placement of the counterelectrode and not for a downstream counterelectrode. However, if interference by the side reaction is substantial, as is the case for silver removal from thiosulfate solutions or for the copper system if the superficial velocity is too high, a limiting-current distribution cannot be achieved for any electrode configuration at any matrix conductivity.

For an upstream counterelectrode when the matrix conductivity is not large, the choice between upstream or downstream placement of the current collector depends on the chemical system and what matrix conductivity can be achieved in practice.

Below the limiting current, the performance is only slightly better for an upstream counterelectrode than for downstream placement of the counterelectrode.

Calculations for a small matrix conductivity show that the DD configuration should probably never be built.

It is evident from the results that simple limiting-current calculations are inadequate for describing the behavior of flow-through porous electrodes. Thus, the ability to calculate distributions of

main reaction near the front to decrease from about 0.05 when $1/\sigma \to 0$ to 0.012 when $\sigma = \kappa$ (see Figures 11 and 13). Since the rear of the electrode was already at a limiting current, the increase in the electric driving force in this region is of little benefit; the rate of the main reaction is higher than with $1/\sigma \to 0$ because the flowing stream was not depleted as much in the upsteam region, not because the electric driving force is larger. The integrated reaction rate is 6.3 percent lower when $\sigma = \kappa$, and the rest of the current goes into the side reaction, driven by the higher electric driving force near the rear.

For upstream placement of the counterelectrode, conditions are already more favorable when the matrix resistivity is small. For the UU configuration, increase of $1/\sigma$ decreases the electric driving force in the rear region and causes the current locally to drop below the limiting value. Consequently, θ_L increases, as shown in Figures 7 and 9. For the UD configuration, the electric driving force decreases near the inlet and increases near the outlet as $1/\sigma$ increases. This is favorable until the reaction rate drops below the limiting value near the inlet, and this leads to the minimum in the curve of θ_L versus κ/σ. The choice between the UD and UU configurations is dependent on the chemical system and the matrix conductivity. However, the UD configuration will display a minimum in the effluent concentration as a function of κ/σ and is therefore the best configuration if this electrode could be built in practice.

current, potential, and concentration in the presence of side reaction above and below the limiting current makes it possible to choose the optimum electrode configuration so as to design and optimize an electrode system for the most economical removal of metal-ions.

5. The removal of mercuric ions from a sodium chloride brine

5.1. Introduction

The use of mercury cells in the production of chlorine increased steadily from a low of 5% in 1945 to a high of 30% in 1968 (Beck (1977)). After this time, their use has decreased due to strict environmental standards on mercury effluents. In fact, most of the large producers of chlorine are committed to replacing all mercury cells with diaphragm or membrane cells. However, a major problem associated with replacing the mercury cells is that the brine feed stocks have become contaminated with mercury. Mercury concentrations in the brine vary from approximately 0.1 ppm to 8 ppm. Membrane separators are extremely sensitive even to this level of mercury, and their performance degrades quickly. In addition, the recovery of mercury can be financially viable as this amounts to one kilogram per tonne of chlorine. The present industrial method for mercury recovery is precipitation with H_2S.

In this chapter, some preliminary experiments were performed to demonstrate the use of flow-through porous electrodes for the removal of dilute concentrations of mercuric ions (approximately 0.6 mg/l) from a 4.2 M sodium chloride brine. The results presented are rather crude and, therefore, are not suitable for design purposes; however, the data do demonstrate that a flow-through porous electrode is a very effective system for removing mercury ions from brine.

5.2 Electrochemical system

At the cathode, mercuric ions Hg^{2+} are electrodeposited on a carbon bed from a variety of stable chloride complexes of the form $HgCl_{\varepsilon}^{2-\varepsilon}$ $(0 \leq \varepsilon \leq 4)$ as discussed in Chapter 2 (see Table 2-1 for the

standard electrode potentials of mercury). The competing side reaction is hydrogen evolution. The anodic reactions on platinum-rhodium screen are simultaneous evolution of chlorine gas and oxygen gas.

Cell design. The cell constructed for this study followed closely the design of Bennion and Newman (1972), Yip (1973), and Appel and Newman (1976).

The porous cathode with a downstream current collector made of tantalum (drilled with holes) was placed under the anode and packed with irregularly shaped carbon particles (Union Carbide granules plus particles, GP-22) between 0.1 and 0.001 cm characteristic dimension. The anode was made of two layers of 80 mesh platinum-10% rhodium screen and spot welded to a perforated tantalum current collector. The current collector in the anode and the cathode were each attached to a 0.635 cm diameter tantalum rod. The anode and the cathode were separated by a perforated Kel-F plate backed with Whatman 40 Filter paper and approximately 8 layers of 0.3 cm diameter glass beads. The cell housing was made of two sections of 7.62 cm I.D. glass pipe and attached to a lucite-feed ring by means of a standard glass pipe fitting.

In more recent work completed by Fedkiw (1978), substantial improvements in the cell design have been made so that very fine control of the flow rate is possible. It is therefore suggested, that all such improvements be incorporated when taking data on metal-ion removal systems.

Fluid and electrical circuits. Similar fluid flow and electrical systems as described by Fedkiw (1978) were used. Two modes of operation for applying current to the cell were employed. The first mode of

operation was galvanostatic control using a Princeton Applied Research (PAR) model 371 potentiostat/galvanostat. The electrical circuit for this mode can be found in Fedkiw (1978, Figure 7.6) without the 2 μF capacitor between the calomel reference electrode and the counter-electrode. The difference is that Fedkiw used potentiostatic control rather than galvanostatic control as was done here. In the second mode of operation, the cell voltage was set with a model 6101A Hewlett-Packard power supply. The electrical circuit for this mode of operation is the same as that given by Fedkiw (1978, Figure 7.5).

Feed solution. The 4.2 M NaCl brine contained 556 mg/l to 576 mg/l of mercuric ion and was prepared from AR grade NaCl and HgO and distilled water, which was first run through a deionizing column. The variation in the mercuric ion concentration is due to evaporation over the course of the experiments. No significant changes in the Cl^- concentration could be detected. A feed sample was taken before and after each run, and the composition was checked using atomic absorption spectroscopy (AA). A run is defined as the measurement of a polarization curve at a specific flow rate.

The concentration of mercury in the feed is significantly higher than that encountered in industrial brine feed stocks. It was chosen because of the limitations of the analytical technique (resolution $\leq$ 0.1 mg-Hg/l). Thus, a reduction in the feed composition by a factor of 1/6000 could be detected. However, it will be shown that the dilute product concentration was consistently below the limits of detectability.

5.3 Results and Discussion

Figures 1 and 2 show the total cell current (in mA) versus VOP (the potential of the cathode current collector relative to a saturated

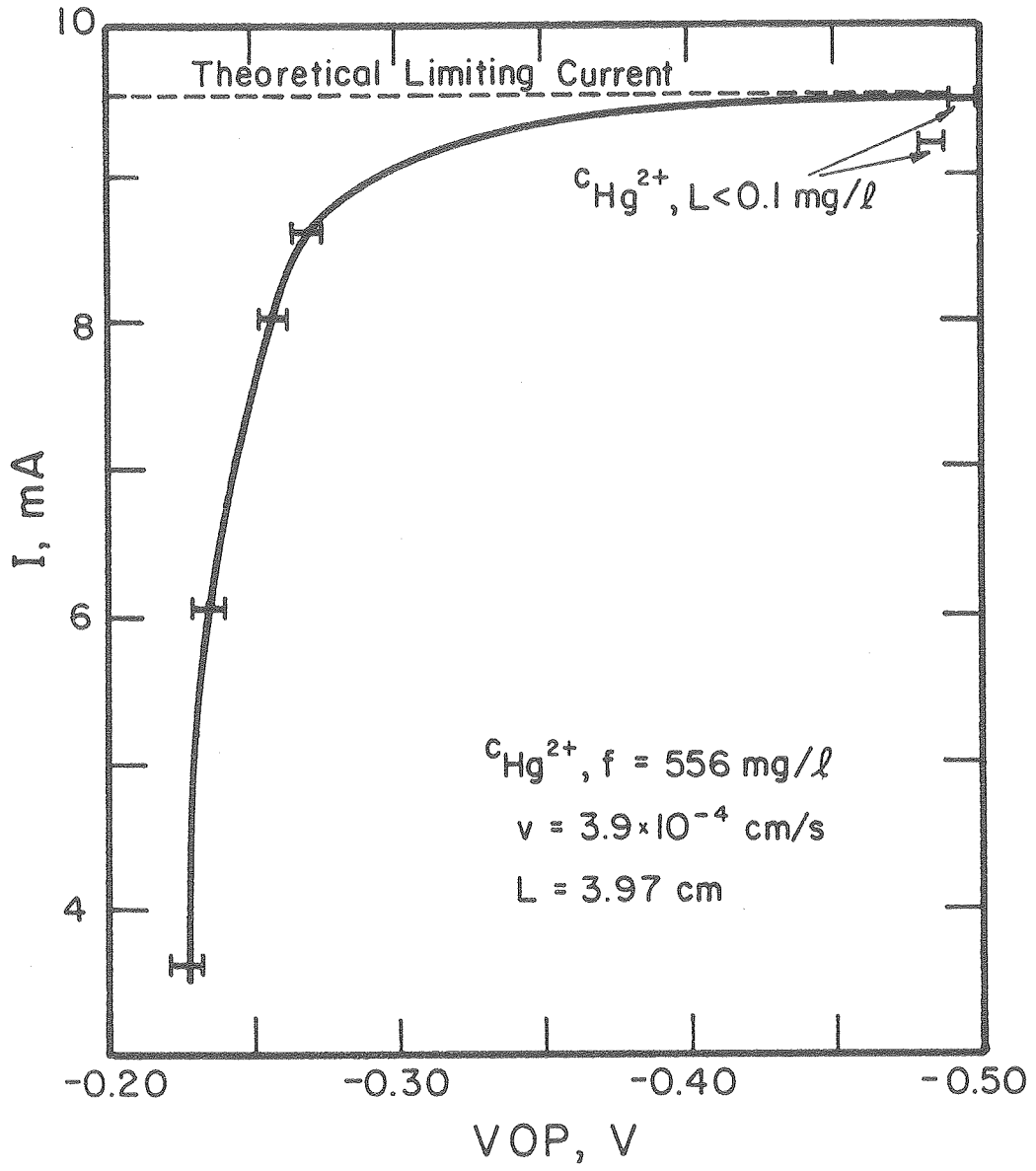

XBL 796-6393

Figure 5-1. Current-potential behavior for an electrode 7.62 cm diameter, packed with carbon flakes and chips. H are experimental data points, where the solid line drawn through these points has not been calculated. Effluent concentrations (which are not reported) were analyzed with normal AA and are not reliable. The electrode was operated in the galvanostatic mode.

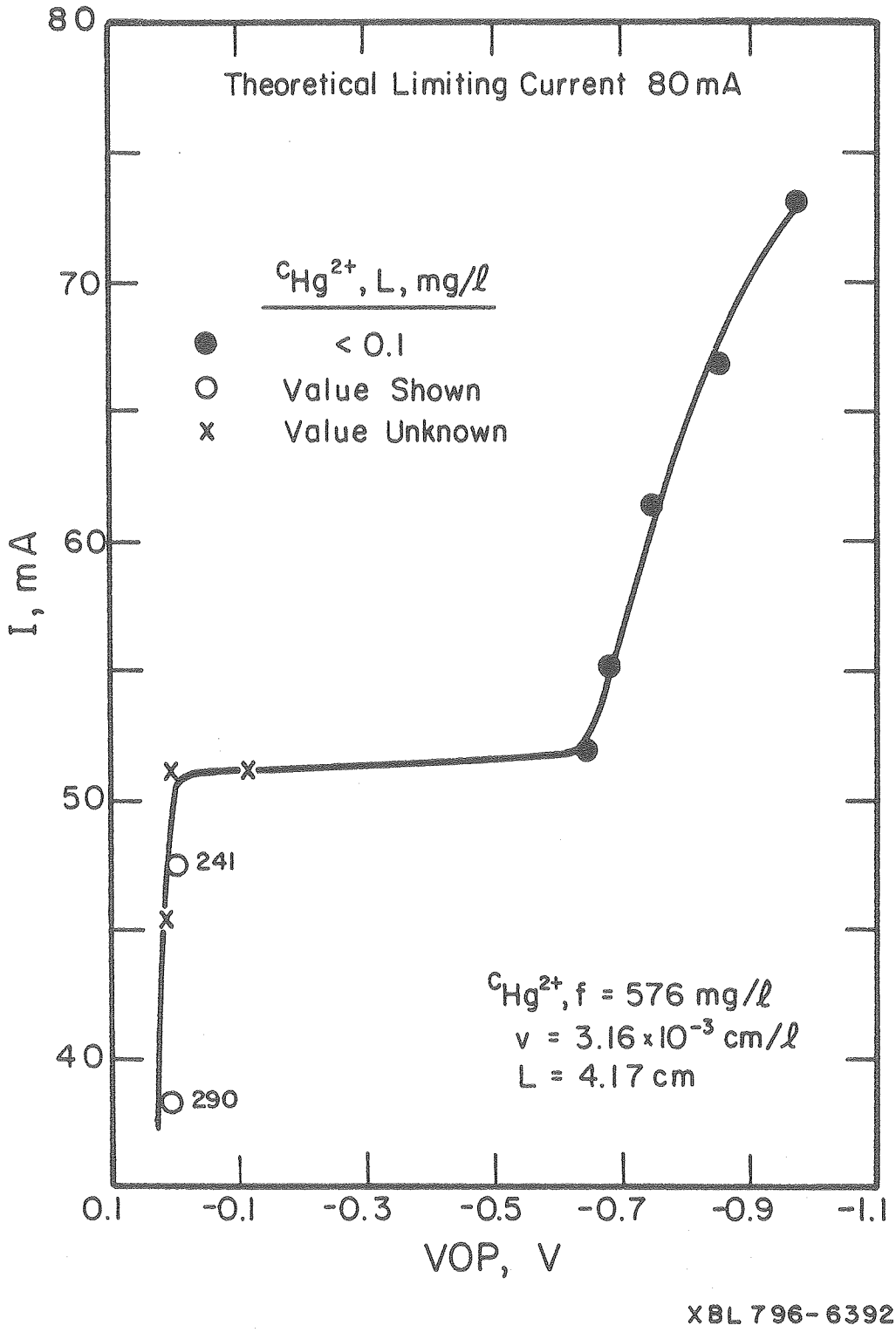

Figure 5-2. Current-potential behavior for an electrode 7.62 cm diameter, packed with carbon flakes and chips. Effluent concentrations were analyzed with an IZAA spectrometer (Hadeishi and McLaughlin (1971) and Hadeishi (1972)). The cell was operated in the constant voltage mode.

calomel reference electrode placed in the dilute product stream) and the dilute product concentrations for the specified feed composition, superficial velocity, and electrode length shown in each figure. The data in Figure 1 were obtained using the galvanostatic mode, and the data in Figure 2 by the constant voltage mode. Each data point required 3 to 5 hours to reach steady-state after each change in applied current (galvanostatic mode) or applied voltage (constant voltage mode).

Over 17 runs were attempted, and approximately 200 liters of feed solution were passed through the cell. Most of the runs were not completed because of the following: steady-state was not achieved, fluid system leaks, corrosion of the cathode current collector, and ground loops. All of these problems will be discussed in detail in the next section.

In Figure 1 the polarization curve shows the expected behavior. In addition, there is reasonable agreement with the theoretical limiting current for high conversion, $I = nFQc_{Rf}/s_R = 9.51$ mA. The two points on the limiting current plateau show effluent concentrations less than 0.1 mg/l. These samples were analyzed with an Isotope Zeeman Atomic Absorption Spectrometer (IZAA, Hadeishi and McLaughlin (1971) and Hadeishi (1972)). This particular instrument has a resolution of 0.1 mg-Hg/l and a sensitivity of approximately 0.04 mg-Hg/l. No detectable amount of mercury could be measured in either sample.

The effluent concentration of the other four points on the curve were analyzed by normal AA spectroscopy (approximate sensitivity 5 mg-Hg/l). Unfortunately, the high concentration of Cl^- interferes

to such an extent as to invalidate the results. In addition, the dilution of the samples to minimize the chloride interference reduced the mercury concentration below the limit of detectability. Similar problems were also encountered with the IZAA spectrometer; however, the relative increase in sensitivity of this instrument offset some of these difficulties.

In Figure 2 the polarization behavior is irregular and suggests spurious results. There is no obvious reason for the apparent plateau in the data at approximately 52 mA. The theoretical limiting current density is 28 mA above this value and there was no evidence of other trace metals present in the feed solutions.

Consider then two plausible causes:

1) Ground loops - these experimental maladies can affect the measurement of both VOP and I (only the cell voltage was set in this mode of operation). In the case of VOP, the data points denoted by • are at large cathodic potentials, and the equilibrium analysis in Chapter 2 indicates that the measured effluent concentration would be very small. This corresponds to the experimental observation of no detectable mercury in the effluents; however, these contradict the measured current, which would put the effluent concentration well above the detectable level.

2) Formation of insoluble mercurous chloride (Hg_2Cl_2) - if the mercuric species is not immediately reduced to liquid mercury and the mercurous dimer (Hg_2^{2+}) forms; precipitation of mercurous chloride will follow. The overall reactions are (see Table 2-1 for thermodynamic data):

$$2HgCl_{\varepsilon}^{2-\varepsilon} + 2e^- \rightarrow Hg_2^{2+} + 2\varepsilon Cl^-, \qquad (5\text{-}1)$$

and

$$Hg_2^{2+} + 2Cl^- \rightarrow Hg_2Cl_2 \qquad (5\text{-}2)$$

The solubility product of Hg_2Cl_2 is

$$K_{sp} = c_{Hg_2^{2+}} c^2_{Cl^-} f^3_{Hg_2Cl_2} = 2 \times 10^{-18} \frac{mole^3}{\ell^3} \qquad (5\text{-}3)$$

Equation 1 corresponds to a theoretical limiting current of 40 mA if all the mercury were being removed (half that of mercuric deposition), and 12 mA below the apparent plateau.

These explanations are not satisfactory considering the well behaved data in Figure 1. The only conclusion that can be drawn is that a flow-through porous electrode is an extremely effective device for removing mercuric ions from brine.

5.4 Recommendations for further work

The data presented in this chapter can be considered preliminary at best. However, the data show the process has promise and should be pursued further. The following discussion will be concerned with the problems encountered in obtaining the data and suggestions for obtaining data useful for design purposes.

Analytical technique. Perhaps the most difficult measurements to be made in these experiments are the accurate determination of the feed composition and the effluent composition. For concentration above 50 mg-Hg/ℓ, AA and IZAA spectroscopy can be used. As mentioned previously, the high Cl^- concentration interferes with these techniques; however, this interference can be reduced to an acceptable level by dilution with distilled water. A solvent extraction technique using

diphenylthiocarbamate (dithizone) in toluene was also tried. Again, the Cl^- interferred to an extent that the results were not realiable. Unfortunately, AA and IZAA spectroscopy, and solvent extraction with dithizone, were the only techniques available in the laboratory at the time the data were taken. At the present time, there is the capability of determining Hg^{2+} by differential pulse anodic stripping voltammetry using a Princeton Applied Research Model 174. The resolution of this technique is 1 ppb or greater. A gold electrode is required (see Princeton Applied Research Application short or Nürnberg (1977)).

Current collector corrosion. The first cathode-current collector that was used was made of 316 stainless steel. It was found that the value of VOP would drift continuously in the cathodic direction. This would occur whether or not current was being passed. Furthermore, it was not possible to pass enough current (below the limiting current for Hg deposition) to protect cathodically the collector in order to stop the potential drift. In addition, visual inspection of the current collector showed signs of pitting corrosion.

It should be understood that measurement of VOP under these circumstances is meaningless with respect to mercury removal, because the current collector was acting independently of the carbon bed.

In order to overcome this problem, a test was run on several types of metal rods. These included titanium, tantalum, aluminum, and zirconium. Each rod was placed in a separate beaker containing 4 M NaCl. The potential of these rods with respect to a saturated calomel reference electrode placed in the same beaker was measured. It was observed that the tantalum rod exhibited the most stable potential. (It is well documented that tantalum is one of the most passive metals

known.) With this data in mind, a current collector made of tantalum was fabricated as discussed in section 5.2. No further problems were encountered with current collector corrosion after the tantalum collector was installed in the cell.

There are two possible problems to be considered when using tantalum as an electrode material:

a. The passivation of tantalum is due to the formation of an oxide layer. In some applications, this film might cause a large contact resistance between the collector and the electrode bed.

b. Tantalum is very susceptible to hydrogen embrittlement. Therefore, evolution of hydrogen at the surface of the tantalum should be avoided whenever possible. In order to reduce this problem in a flow-through porous electrode, the tantalum current collector should always be placed where the electric driving force is the smallest (see Chapter 4). As an added precaution, a small piece of metal with a hydrogen overvoltage less than that of tantalum could be welded to the collector.

Electric power. There are three possible modes of operation for applying electric power to the cell. Two of these modes have been mentioned: galvanostatic control (I is set, and VOP varies until a steady-state is reached) and constant cell voltage (VOP and I both vary until a steady-state is reached). A third mode of operation is potentiostatic control (VOP is set, and the current varies until a steady-state is reached. The latter mode was used by Appel (1976) and Fedkiw (1978). Some runs were tried using potentiostatic control, but the cell current showed rapid fluctuations. Similar behavior was observed by Bennion and Newman (1972).

Fedkiw (1978) solved this problem by placing a 2 μf capacitor between the reference electrode and the anode. His reasoning was as follows: a potentiostat is a high gain proportional controller, and if the capacitance between the anode and the cathode were large enough, the potentiostat can be forced into oscillations. Appel (1976) was able to avoid this problem because the surface area of his electrode was small ($aL \sim 10$). Data in the galvanostatic mode could be gathered here because the rise time of the PAR 371 is reduced approximately three orders of magnitude when operated as a galvanostat rather than a potentiostat.

Ground Loops. Whenever current is passed between the working electrode and the counterelectrode, care must be exercised so as not to provide an alternative current path. These problems may be minimized by eliminating all conductors in the fluid flow system other than the electrodes. For example: thermocouples, thermistors, metal pipe, metal-pipe fittings, and conducting pump heads.

Ground loops can also occur between instruments. This can lead to erroneous measurement of current and potential. To avoid these problems, battery-powered instruments should be used whenever possible. When such instruments are not available, isolation transformers should be used on each instrument. This is especially true when a potentiostat is used, because most potentiostat circuits ground the working electrode. The object is to minimize the number of grounds in the system.

Flow control. In order to obtain the steady-state polarization behavior of a flow-through porous electrode, a steady flow rate must be maintained. If this is to be achieved in practice, several factors must be considered:

a. Air bubbles. The cell should be packed and assembled while submerged in distilled water. Before the cell is attached, the flow system should be completely flushed of air. The air bubbles not only plug the electrode and cause channeling, but their movement can cause rapid fluctuations in the flow rate.

b. Gas evolution. The evolution of gas in a porous electrode should always be avoided. Some comments under a are applicable. If a gas evolving anode is used, an isolated electrode compartment with separate anolyte flow is required (see Fedkiw (1978)).

c. Electrode plugging. This will only be a serious problem after the cell has run a substantial amount of time. The time for plugging can be estimated (Bennion and Newman (1972)):

$$t = \rho_M \varepsilon / 2M_M a k_m c_{Rf} \quad . \tag{5-4}$$

It should be noted that Bennion and Newman (1972) made an error of a factor of ten in their design calculations when applying equation 4 to the copper system. They calculated 49 days instead of 4.9 days. The latter value agrees very well with the experimentally determined plugging time of 5 days.

d. Pump system. A Fluid Metering Inc. piston pump was used to feed the system. This pump was chosen because of its convenient variable capacity and fine flow control. A column of N_2 can be used to damp the oscillations. It should be noted that the flow delivered by this pump depends on the fluctuations in the electric power applied to the motor. These variations can have a substantial effect on the flow delivered by the pump at low flow rates. Therefore, a power

leveling transformer should always be placed between the pump and the power company.

e. Tubing and tubing connectors. Leached 1/4" I.D. Tygon tubing was used to connect the fluid flow system. Connections were made with stainless steel hose clamps. This method worked in a mediocre manner because the clamps cut the tubing. In addition, the Tygon tubing is subject to chemical attack.

To eliminate these problems, plastic tube fittings made by JACO Manufacturing Company (Berea, Ohio) and Bev-a-line lined tubing made by Dynalab Company (Rochester, New York) should be used.

5.5. Summary and Conclusion

Preliminary data have been presented on the removal of mercuric chloride complexes ($HgCl_\varepsilon^{2-\varepsilon}$, $1 \leq \varepsilon \leq 4$) from a NaCl brine using a flow-through porous electrode. The data show that the process has promise, as the concentration of $HgCl_\varepsilon^{2-\varepsilon}$ was reduced from 576 mg/ℓ to less than 0.1 mg/ℓ.

The major problems encountered in obtaining design data: analytical technique, current collector corrosion, ground loops, and flow control, have been discussed, and suggestions for improvement made.

6. A comparison between flow-through and flow-by porous electrodes for redox energy storage

6.1 Introduction

In previous chapters the emphasis has been placed on the application of flow-through porous electrodes to metal-ion removal from dilute streams. This chapter will deal strictly with the application of flow-through porous electrodes to electrochemical-energy storage.

In the post "energy crisis" years the ability of electric utilities to meet peak power demands economically has become increasingly acute. One answer to this problem is to store off-peak power and to recover this power during high demand periods (power load-leveling). Energy storage requirements for electric utilities may be met in several ways. The numerous advantages of flow-redox batteries (Thaller (1974,1976), Beccu (1974), and Kangro (1954, 1969)) have been discussed by Yao and Birk (1975), and Warshay and Wright (1977). Some particularly attractive features are listed below:

1) Unlimited cycle life regardless of the depth of discharge because redox reactions do not affect the morphology of the electrode material.

2) Simple electrode reactions.

3) High temperatures not required.

4) Minimal environmental impact.

5) Readily available reagents and materials of construction.

Preliminary capital cost estimates and size estimates for an iron/titanium [Ti(III)|Ti(IV)||Fe(III)|Fe(II)] redox battery indicate economic viability for the system (Warshay and Wright (1977)). Many

other redox couples have been suggested (Thaller (1974,1976), Beccu (1974), Giner, Swette, and Cahill (1976), and Kangro (1954,1969)). Of these, the iron/chromium system [Cr(III)|Cr(II)||Fe(III)|Fe(II)] appears to be the most promising. Recently, the NASA-Lewis Research Center, using an iron/chromium cell, has achieved a power density of approximately 915 W per square meter of membrane separator (Gahn and Hagedorn(1978)).

Two basic electrode configurations have been proposed for flow-redox batteries. Kangro (1954,1969) has suggested an electrode configuration where the current and fluid flow are in parallel (flow-through configuration, see Figure 1a and b). Thaller (1974,1976) and Beccu (1974) have suggested a cell configuration where the current is perpendicular to the fluid flow and a separator is essential (flow-by configuration, see Figure 1c). The flow-through configuration (Figure 1a and b) has the advantage over the flow-by configuration (Figure 1c) that a separator is not required; however, a major disadvantage of this configuration can be seen in Figure 1b. Consider an iron/titanium cell. On discharge the unreacted Ti(III) and Fe(III) would be lost according to the reaction

$$Ti(III) + Fe(III) \rightarrow Ti(IV) + Fe(II) \qquad (6\text{-}1)$$

when the streams are allowed to mix after flowing through the porous electrodes (Newman (1977)).

The purpose of this chapter is to compare, on an economic basis, the performance of the

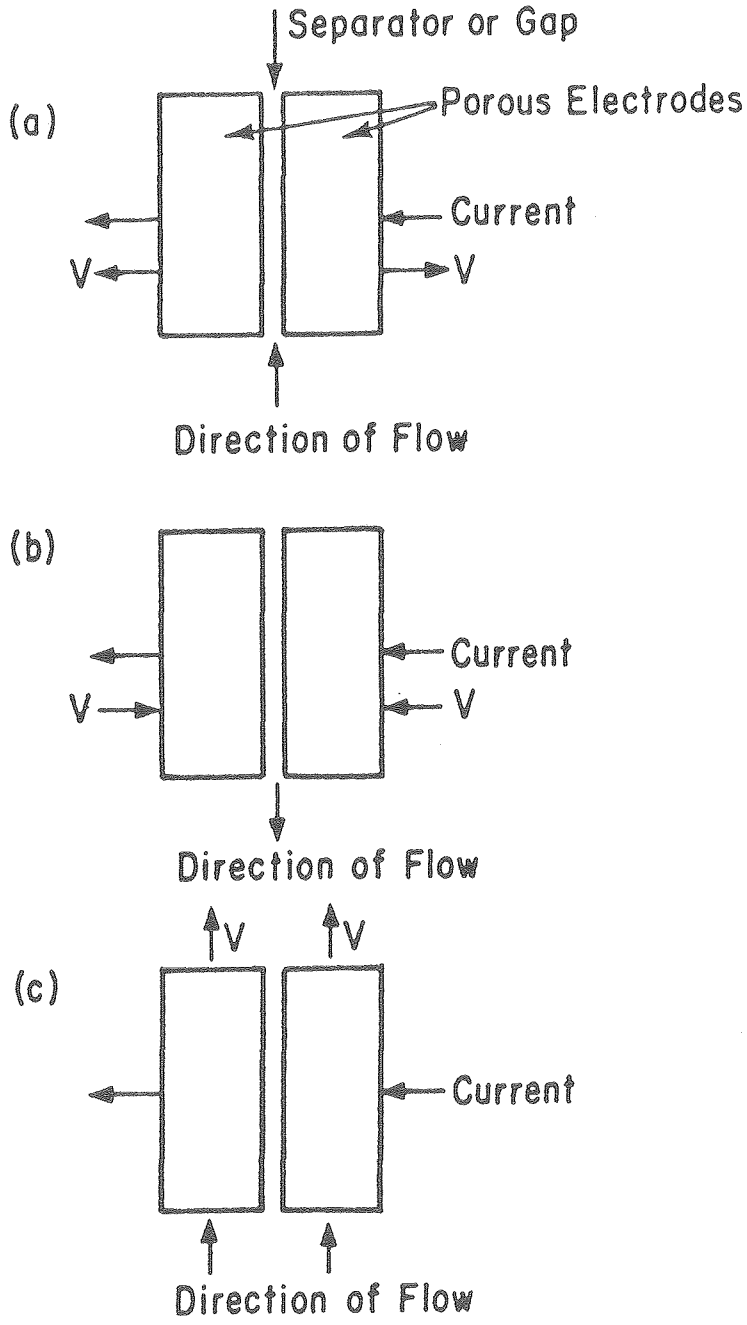

XBL 796-10074

Figure 6-1. Various configurations of electrode placement relative to the direction of fluid flow. a and b are the flow-through configuration on charge and discharge. c is the flow-by configuration.

two configurations for redox-energy storage. As mentioned above, Warshay and Wright (1977) have made preliminary capital cost estimates for the two-tank, flow by configuration. The flow-by configuration is usually considered to be either a two-tank or four-tank system. The flow-through configuration is primarily a three-tank system. The two-tank flow-by configuration can also be operated with a time varying superficial velocity, whereas, the other systems cannot due to their single-pass operation (Thaller (1974)). (By single-pass operation we mean the reactants on each half cycle pass through the electrode only once.)

The perspective here is to compare the steady-state performance of two operational redox storage systems:

1) the flow-through configuration (current parallel to the fluid flow);

2) the flow-by configuration (current perpendicular to the fluid flow). The basis for comparison is the return on investment based on operating costs.

6.2 Flow-through porous electrodes

The analysis for a redox reaction is similar to that presented for a metal-deposition reaction in section 3.3. However, if the dimensional analysis also presented in section 3.3 is to be used, separate analyses must be considered for both a cathodic limiting reactant and an anodic limiting reactant.

Cathodic reactant. From equations 3-13 through 3-17, the Butler-Volmer equation may be written as

$$i_{nR} = i_{oR,ref}\left\{\frac{c_{Pw}}{c_{Pf}}\exp\left[\frac{\alpha_{aR}F}{RT}(\Phi_1 - \Phi_2)\right] - \frac{c_{Rw}}{c_{Rf}}\exp\left[-\frac{\alpha_{cR}F}{RT}(\Phi_1 - \Phi_2)\right]\right\}, \tag{6-2}$$

where the reference electrode used in measuring Φ_2 is of the same kind as the redox reaction, and the concentration of the reactant and product species in the reference electrode compartment, c_{Rr} and c_{Pr}, and the reference concentration in equation (3-14), $c_{R,ref}$ and $c_{P,ref}$, have been set equal to c_{Rf} and c_{Pf} (the upstream feed concentration of the redox couple). It is also assumed that $s_R = -1$ and $s_P = 1$.

If axial diffusion is small compared to axial dispersion or if the diffusion coefficients of the reactant and product species are equal, the local concentration of the product species within the pores is simply related to the local reactant concentration within the pores and the feed concentration

$$c_P = c_{Rf} + c_{Pf} - c_R . \tag{6-3}$$

Also, for a redox couple, the wall fluxes of the reactant and product species are equal and opposite

$$k_{mR}(c_R - c_{Rw}) = -k_{mP}(c_P - c_{Pw}) . \tag{6-4}$$

One can now write c_{Pw} in terms of c_R and c_{Rw} with the use of equation 3 as

$$\frac{c_{Pw}}{c_{Pf}} = 1 + \frac{c_{Rf}}{c_{Pf}} - \frac{c_R}{c_{Pf}}\left(1 - \frac{k_{mR}}{k_{mP}}\right) - \frac{k_{mR}}{k_{mP}}\frac{c_{Rw}}{c_{Pf}} . \tag{6-5}$$

This equation allows the explicit dependence of the product species concentration on the local reaction rate to be removed from equation 2 with the result:

$$i_{nR} = i_{oR,ref}\left\{\left[1 + \frac{1}{c_{Pf}}\left(c_{Rf} - c_R\left(1 - \frac{k_{mR}}{k_{mP}}\right) - \frac{k_{mR}}{k_{mP}}\, c_{Rw}\right)\right] \exp\left(\frac{\alpha_{aR}F}{RT}\,\eta\right) - \frac{c_{Rw}}{c_{Rf}} \exp\left(-\frac{\alpha_{cR}F}{RT}\,\eta\right)\right\}, \qquad (6\text{-}6)$$

where $\eta = \Phi_1 - \Phi_2$, as previously defined in equation 3-20. Only one differential material balance is now required -- that for the cathodic reactant. The elimination of c_{Rw} between equations 3-11 and 6-6, results in an equation for j_{Rn} which is similar to equation 3-21. A material balance equation for the case of a cathodic limiting reactant is then obtained by substituting the above equation for j_{Rn} and equation 3-2 into equation 3-1:

$$v\frac{dc_R}{dx} = \varepsilon(D_R + D_a)\frac{d^2c_R}{dx^2} - a\,\frac{\dfrac{c_R}{c_{Rf}} - \left(1 + \dfrac{c_{Rf} - c_R}{c_{Pf}}\right)\exp\left[\dfrac{(\alpha_{aR} + \alpha_{cR})F}{RT}\,\eta\right]}{\dfrac{1}{k_{mR}c_{Rf}} - \dfrac{nF}{s_R i_{oR,ref}}\exp\left[\dfrac{\alpha_{cR}F}{RT}\,\eta\right] + \dfrac{1}{k_{mP}c_{Pf}}\exp\left[\dfrac{(\alpha_{aR}+\alpha_{cR})F}{RT}\,\eta\right]}. \qquad (6\text{-}7)$$

If the same assumptions are made about the side reaction as in chapter 3, an equation similar to equation 3-23 can be derived for the local overpotential:

$$\frac{d^2\eta}{dx^2} = \left(\frac{1}{\kappa} + \frac{1}{\sigma}\right)a \left\{ i_{oS,ref}\left[\exp\left(\frac{\alpha_{aS}F}{RT}(\eta-\Delta U)\right) - \exp\left(-\frac{\alpha_{cS}F}{RT}(\eta-\Delta U)\right)\right] \right.$$

$$\left. - \left(-\frac{nF}{s_R}\right) \frac{\frac{c_R}{c_{Rf}} - \left(1 + \frac{c_{Rf} - c_R}{c_{Pf}}\right)\exp\left[\frac{(\alpha_{aR} + \alpha_{cR})F}{RT}\eta\right]}{\frac{1}{k_{mR}c_{Rf}} - \frac{nF}{s_R i_{oR,ref}}\exp\left[\frac{\alpha_{cR}F}{RT}\eta\right] + \frac{1}{k_{mP}c_{Pf}}\exp\left[\frac{(\alpha_{aR}+\alpha_{cR})F}{RT}\eta\right]} \right\} \tag{6-8}$$

Equations 7 and 8 can be expressed in dimensionless form by introducing the dimensionless coordinate $y = ak_m x/v$, the dimensionless concentration $\theta = c_R/c_{Rf}$, and equation 3-33:

Material balance

$$\frac{d\theta}{dy} = D' \frac{d^2\theta}{dy^2} - \frac{\theta - \left(1 + \frac{1-\theta}{\theta_{Pf}}\right)P_1 \exp\left[(1 + \alpha_{aR}/\alpha_{cR})\eta'\right]}{1 + \exp(\eta') + P_1P_7/\theta_{Pf} \exp\left[(1 + \alpha_{aR}/\alpha_{cR})\eta'\right]} \tag{6-9}$$

Charge balance

$$\frac{d^2\eta'}{dy^2} = P_2\left\{P_3 \exp(-\alpha_{cS}\eta'/\alpha_{cR})\left[1 - P_4 \exp\left(\frac{\alpha_{aS} + \alpha_{cS}}{\alpha_{cR}}\eta'\right)\right]\right.$$

$$\left. + \frac{\theta - \left(1 + \frac{1-\theta}{\theta_{Pf}}\right)P_1 \exp\left[(1 + \alpha_{aR}/\alpha_{cR})\eta'\right]}{1 + \exp(\eta') + P_1P_7/\theta_{Pf} \exp\left[(1 + \alpha_{aR}/\alpha_{cR})\eta'\right]}\right\}. \tag{6-10}$$

The dimensionless parameters D', P_1, P_2, P_3, and P_4 are the same as those defined in chapter 3. The additional parameters P_7 and θ_{Pf} are given by

$$P_7 = k_{mR}/k_{mP}\ , \tag{6-11}$$

$$\theta_{Pf} = c_{Pf}/c_{Rf}\ . \tag{6-12}$$

Anodic reactant. For an anodic reactant equation 2 is expressed as

$$i_{nR} = i_{oR,ref}\left\{\frac{c_{Rw}}{c_{Rf}}\exp\left[\frac{\alpha_{aR}F}{RT}(\Phi_1-\Phi_2)\right] - \frac{c_{Pw}}{c_{Pf}}\exp\left[-\frac{\alpha_{cR}F}{RT}(\Phi_1-\Phi_2)\right]\right\}. \quad (6\text{-}13)$$

Equation 5 can then be used to eliminate c_{Pw}/c_{Pf} in equation 13. By following the same procedures used in deriving equation 7; a material balance equation for an anodic limiting reactant is obtained:

$$v\frac{dc_R}{dx} = \varepsilon(D_a + D_R)\frac{d^2c_R}{dx^2}$$

$$- a\frac{\frac{c_R}{c_{Rf}} - \left(1 + \frac{c_{Rf}-c_R}{c_{Pf}}\right)\exp\left[-\frac{(\alpha_{aR}+\alpha_{cR})F}{RT}\eta\right]}{\frac{nF}{s_R i_{oR,ref}}\exp\left[-\frac{\alpha_{aR}F}{RT}\eta\right] + \frac{1}{k_{mR}c_{Rf}} + \frac{1}{k_{mP}c_{Pf}}\exp\left[-\frac{(\alpha_{aR}+\alpha_{cR})F}{RT}\eta\right]}. \quad (6\text{-}14)$$

Consequently, the charge balance equation becomes

$$\frac{d^2\eta}{dx^2} = \left(\frac{1}{\kappa}+\frac{1}{\sigma}\right)a\left\{i_{oS,ref}\left[\exp\left(\frac{\alpha_{aS}F}{RT}(\eta-\Delta U)\right) - \exp\left(-\frac{\alpha_{cS}F}{RT}(\eta-\Delta U)\right)\right]\right.$$

$$\left. - \left(-\frac{nF}{s_R}\right)\frac{\frac{c_R}{c_{Rf}} - \left(1 + \frac{c_{Rf}-c_R}{c_{Pf}}\right)\exp\left[-\frac{(\alpha_{aR}+\alpha_{cR})F}{RT}\eta\right]}{\frac{nF}{s_R i_{oR,ref}}\exp\left[-\frac{\alpha_{aR}F}{RT}\eta\right] + \frac{1}{k_{mR}c_{Rf}} + \frac{1}{k_{mP}c_{Pf}}\exp\left[-\frac{(\alpha_{aR}+\alpha_{cR})F}{RT}\eta\right]}\right\}. \quad (6\text{-}15)$$

Equations 14 and 15 can now be put into forms identical to equations 9 and 10. This is accomplished by introducing into equations 14 and 15 a dimensionless local overpotential based on the anodic

reactant (compare with equation 3-33 for the cathodic reactant):

$$\exp(\eta^{*\prime}) = -\frac{nFk_{mR}c_{Rf}}{s_R i_{oR,ref}} \exp(-\alpha_{aR}F\eta/RT) , \qquad (6\text{-}16)$$

along with the dimensionless coordinate y and the dimensionless concentration θ to yield

Material balance

$$\frac{d\theta}{dy} = D' \frac{d^2\theta}{dy^2} - \frac{\theta - \left(1 + \frac{1-\theta}{\theta_{Pf}}\right) P_1' \exp[(1 + \alpha_{aR}/\alpha_{cR})\eta^{*\prime}]}{1 + \exp(\eta^{*\prime}) + P_1'P_7/\theta_{Pf} \exp[(1 + \alpha_{aR}/\alpha_{cR})\eta^{*\prime}]} , \qquad (6\text{-}17)$$

Charge balance

$$\frac{d^2\eta^{*\prime}}{dy^2} = P_2' \left\{ P_3' \exp(-\alpha_{cS}\eta^{*\prime}/\alpha_{aR}) \left[1 - P_4' \exp\left(\frac{\alpha_{aS} + \alpha_{cS}}{\alpha_{cR}} \eta^{*\prime} \right) \right] + \frac{\theta - \left(1 + \frac{1-\theta}{\theta_{Pf}}\right) P_1' \exp[(1 + \alpha_{cR}/\alpha_{aR})\eta^{*\prime}]}{1+\exp(\eta^{*\prime})+P_1'P_7/\theta_{Pf}\exp[(1+\alpha_{cR}/\alpha_{aR}\eta^{*\prime}]} \right\} , \qquad (6\text{-}18)$$

where the dimensionless parameters are defined as

$$P_1' = \left(\frac{s_R i_{oR,ref}}{nFk_{mR}c_{Rf}} \right)^{1+\alpha_{cR}/\alpha_{aR}} , \qquad (6\text{-}19)$$

$$P_2' = -\frac{\alpha_{aR}nF^2v^2c_{Rf}}{s_R a k_{mR} RT} \left(\frac{1}{\kappa} + \frac{1}{\sigma} \right) , \qquad (6\text{-}20)$$

$$P_3' = \frac{s_R i_{oS,ref}}{nFk_{mR}c_{Rf}} e^{-\alpha_{aS}F\Delta U/RT} \left(\frac{nFk_{mR}c_{Rf}}{s_R i_{oR,ref}} \right)^{\alpha_{aS}/\alpha_{aR}} , \qquad (6\text{-}21)$$

$$P_4' = \left(\frac{s_R i_{oR,ref}}{nFk_{mR} c_{Rf}} \right)^{\frac{\alpha_{aS}+\alpha_{cS}}{\alpha_{aR}}} \exp\left[(\alpha_{aS} + \alpha_{cS})F\Delta U/RT\right] . \qquad (6\text{-}22)$$

These parameters correspond to the dimensionless variables defined previously for the cathodic reactant in equations 3-34 through 3-37 (e.g. P_1 for the cathodic reactant corresponds to P_1' for the anodic reactant).

Boundary conditions. Before equations 9 and 10 or equations 17 and 18 can be solved simultaneously for θ and η', θ and $\eta^{*'}$, respectively, four boundary conditions are required for each electrode configuration shown in Figure 4-1. For θ, equations 4-1 are applicable. For a cathodic reactant, the conditions on η' tabulated in Table 4-1 are also applicable. For an anodic reactant, the conditions on $\eta^{*'}$ are of the same form as those given in Table 4-1 for η', except that P_5 and P_6 should be replaced by P_5' and P_6', which are defined as

$$P_5' = -\frac{\sigma P_2'}{\sigma + \kappa} , \qquad (6\text{-}23)$$

and

$$P_6' = -\frac{\kappa P_2'}{\sigma + \kappa} , \qquad (6\text{-}24)$$

so that

$$-P_2' = P_5' + P_6' . \qquad (6\text{-}25)$$

Cycling procedure. A calculational procedure is needed so that system behavior can be predicted over a complete cycle (i.e., charge and discharge). The following procedure was used for the flow-through configuration.

1. The variables listed in Table 1 were set;

2. Equations 17 and 18 were solved for the positive electrode (subject to the UD configuration boundary conditions);

3. Equations 9 and 10 were then solved for the negative electrode (subject to the UD configuration boundary conditions);

4. The cell voltage on charge was then evaluated from the results of 2 and 3, which includes the ohmic drop in the gap between the electrodes given by $\Delta\Phi_{gap} = I_c L_{gap}/\kappa_o$;

5. Equations 17 and 18 and then equations 9 and 10 were solved for the positive electrode and the negative electrode, respectively; subject to the DU configuration and the following restrictions:

   a. The feed concentrations for each electrode on charge and discharge are the same as the product concentrations on charge;

   b. The superficial velocity on discharge $v_d = v_c t_c/t_d$, where $v_{d+} = v_{d-}$ and $t_c/t_d = 1$ in the calculations which follow;

   c. The discharge current density was arbitarily set at $I_d = 0.95\ I_c$. (Note that I_d and I_c are negative for the cathode and positive for the anode);

6. The cell voltage on discharge is then calculated from the results of 5, which again includes the ohmic drop in the gap between the electrodes.

Table 6-1. Variables set on charge and conditions used in the calculations. + = positive electrode, - = negative electrode, c = charge, d = discharge

Variables set on charge		Conditions used in calculations
L_+, L_-	electrode lengths for the positive electrode and the negative electrode	$L_+ = L_-$
v_{+c}, v_{-c}	superficial velocities for the positive electrode and the negative electrode	$v_+ = v_{-c}$
I_c	current density on charge	$I_c < 0$ for cathode
c_{+c}, c_{-c}	concentration of reactants on charge in the feed tank	$c_{+c} = c_{-c}$
c_{+d}, c_{-d}	concentration of products on charge in the feed tank	$c_{+d} = c_{-d}$ at equilibrium with c_{+c} and c_{-c}

From the above results the power on charge and discharge are calculated: $P_c = I_c V_c$ and $P_D = I_D V_D$. In the optimization procedure which follows in a later section I_c, I_d, and v are optimized with respect to an objective function appropriate for this system. I_d is optimized with the condition that cell operation on discharge is at the power maximum. This choice follows from the optimization because energy is lost due to mixing in the gap between the electrodes by equation 1.

6.3 Flow-by porous electrodes

A flow-redox battery using flow-by porous electrodes (perpendicular current to fluid flow) can be modeled to include the following characteristics:

1. Each electrode exhibits linear polarization behavior; this is typical of a "practical" redox system because the exchange current densities are large.

2. The positive electrode and the negative electrode are both of length L (in the direction of fluid flow) with isotropic porosities ε_+ and ε_- and specific surface areas a_+ and a_- which remain constant in time; for a redox system no morphological changes occur in the electrode material.

3. The concentration variations in the direction of current flow are negligible.

4. The variation in potential in direction of fluid flow is negligible; this will be a good approximation except near the fluid inlet.

5. The hydrodynamics are characterized by superficial velocities v_+ and v_- and average mass transfer coefficients k_{m+} and k_{m-}.

6. Only one electrode reaction occurs at each electrode.

It should be noted that the only other modeling work completed for this configuration is that done by Alkire and Ng (1974, 1977). Their model, which was applied specifically to metal-ion removal, included two-dimensional concentration variations and complete Butler-Volmer kinetics with a side reaction.

Analysis. The emphasis is on a simplified model which includes only the pertinent features of flow-by porous redox batteries. The results obtained illustrate the important features that would be observed with a more sophisticated approach.

Figure 6.2 shows a schematic of the flow-by configuration to be modeled. The cell potential V is defined to be the difference between the positive and negative current collectors

$$V = \Phi_{l+}(d+) - \Phi_{l-}(d-) \ , \tag{6-26}$$

which may be decomposed:

$$V = U_+^\theta - U_-^\theta + \frac{RT}{n_+F} \ln \frac{c_{Ow}^+}{c_{Rw}^+} - \frac{RT}{n_-F} \ln \frac{c_{Ow}^-}{c_{Rw}^-}$$

open-circuit potential

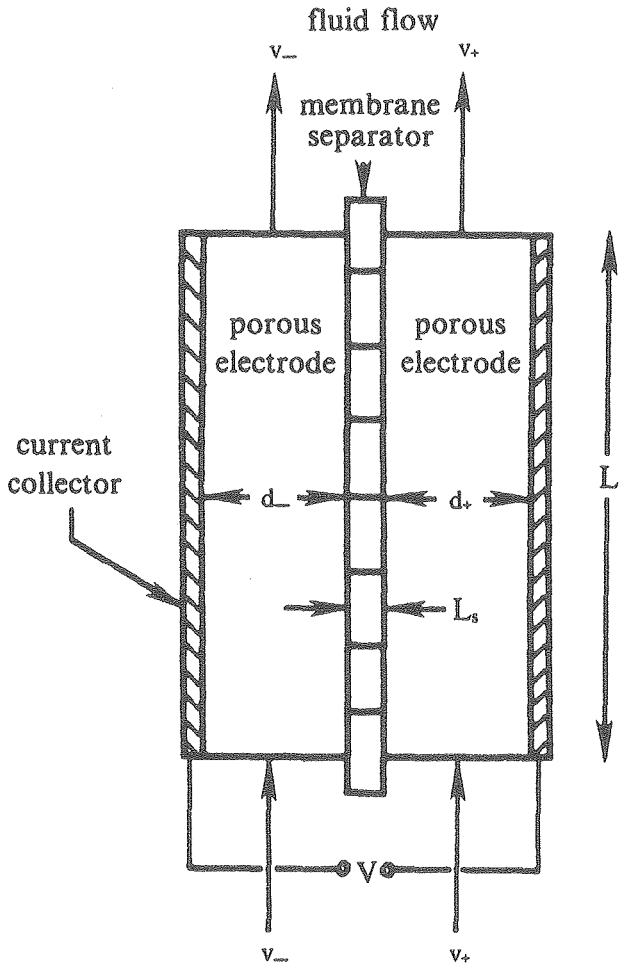

Flow-by porous electrode configuration

XBL 796-10071

Figure 6-2. Flow redox cell with current flow perpendicular to the fluid flow.

$$-i\left\{\frac{d_+}{\kappa_+ + \sigma_+}\left[1 + \frac{2 + \left(\frac{\sigma_+}{\kappa_+} + \frac{\kappa_+}{\sigma_+}\right)\cosh \nu_+}{\nu_+ \sinh \nu_+}\right]\right.$$

$$\left. + \frac{d_-}{\kappa_- + \sigma_-}\left[1 + \frac{2 + \left(\frac{\sigma_-}{\kappa_-} + \frac{\kappa_-}{\sigma_-}\right)\cosh \nu_-}{\nu_- \sinh \nu_-}\right] + \frac{L_s}{\kappa_s}\right\}, \qquad (6\text{-}27)$$

surface overpotential and ohmic-potential drop

where O and R are the oxidized and reduced species of the redox couple and subscripts + and - denote the positive and negative electrode.

Equation 27 has been written for a positive value of i on discharge and a negative value of i on charge. The first term and the second term in brackets represent the total potential loss in each electrode in the direction of current flow, a combination of surface overpotential for linear kinetics and ohmic potential drop (Newman and Tiedemann (1975)). The last term in brackets represents the ohmic potential drop across the separator.

In equation 27, ν^2 is the dimensionless exchange current density for an electrode (Newman and Tiedemann (1975))

$$\nu^2 = (\alpha_a + \alpha_c)\frac{aFd^2}{RT}\left(\frac{1}{\kappa} + \frac{1}{\sigma}\right) i_o \, . \qquad (6\text{-}28)$$

It is assumed to have a composition dependence of the form

$$i_o = i_{o,ref} \prod_i \left(\frac{c_{iw}}{c_{i,ref}}\right)^{\gamma_i}, \qquad (6\text{-}29)$$

where $i_{o,ref}$ is the value of the exchange current density at a reference composition $c_{i,ref}$. It is further assumed that the transfer coefficients α_a and α_c sum to n (in this case $n = 1$) for an electrode reaction of the form

$$\sum_i s_i M_i^{z_i} \rightarrow ne^- , \tag{6-30}$$

and that the exponents γ_i have the dependence

$$\gamma_i = q_i + \frac{\alpha_c}{n} s_i \tag{6-31}$$

such that $q_i = -s_i = 1$ for a cathodic reactant and zero otherwise. For $\alpha_a = \alpha_c = 0.5$ equation 28 becomes

$$\nu^2 = \frac{aFd^2}{RT}\left(\frac{1}{\kappa} + \frac{1}{\sigma}\right) i_{o,ref} \sqrt{\frac{c_{Ow}\, c_{Rw}}{c_{Of}\, c_{Rf}}} , \tag{6-32}$$

where the $c_{i,ref}$ have been set equal to c_{if} (the upstream feed concentration of the oxidized and reduced species of a redox couple).

Material balances. Continuity equations for reactant and product species can be used to describe the variation of concentration and current density through the porous electrode. In addition, the electrode length may be calculated for set values of the cell voltage and utilization of the reactants. From these results, the power densities on charge and discharge can be obtained.

To do this, the unknown wall concentration in equations 27 and 28 must be related to the bulk concentration of the oxidized species for the positive electrode. The wall concentrations c_{iw} and the

bulk concentrations c_i are linked through the limiting current density relationship

$$c_{iw} = c_i(1 - i/i_L) \ , \tag{6-33}$$

where

$$i_L = F\ a\ d\ k_m\ c_i \tag{6-34}$$

is the limiting current density in the direction of current flow, which follows from Faraday's law (Newman and Tiedemann (1975)):

$$aj_{in} = -\frac{s_i}{nF}\nabla\cdot\underline{i}_2 = \frac{s_i}{nF}\nabla\cdot i_1 \tag{6-35}$$

or

$$F\ a\ k_m\ c_i = \frac{\partial i_{lx}}{\partial x}^{\text{neglect}} + \frac{\partial i_{ly}}{\partial y} \tag{6-36}$$

with $i_{ly}(d) = i_L$, $i_{ly}(0) = 0$, and $s_i = -1$.

The bulk and wall concentrations of the reduced and oxidized species in each electrode can be related through the pore-wall fluxes, since these fluxes are equal and opposite for a redox reaction:

$$k_{mO}(c_O - c_{Ow}) = -\ k_{mR}(c_R - c_{Rw}) \ . \tag{6-37}$$

Equations 33 and 37 can be combined to yield the reactant-wall concentrations in terms of the bulk concentrations and the limiting current

$$c_{Rw} = c_R + \frac{k_{mO}}{k_{mR}}\frac{i}{i_{LO}}c_O \ . \tag{6-38}$$

The local bulk concentration of the reduced species is given by

$$c_R = c_{Of} + c_{Rf} - c_O \ , \tag{6-39}$$

provided that diffusion in the x-direction is neglected (or $D_R = D_O$).

Equations 37, 38, and 39 relate the wall concentrations of the reduced and oxidized species to the bulk concentration of the oxidized species in each electrode.

The differential material balance for a species i may be simplified (owing to the assumptions stated previously):

$$v\left(\frac{\partial c_i}{\partial x} + \frac{\partial c_i}{\partial y}\right) = \frac{s_i}{nF}\left(\frac{\partial i_{lx}}{\partial x} + \frac{\partial i_{ly}}{\partial y}\right) \ . \tag{6-40}$$

(neglect $\frac{\partial c_i}{\partial y}$; neglect $\frac{\partial i_{lx}}{\partial x}$)

An integration over y with $i_{ly}(d) = -i$ and $i_{ly}(0) = 0$, gives

$$vd\,\frac{dc_i}{dx} = -\frac{s_i}{nF}\,i \ . \tag{6-41}$$

It follows that for each electrode on discharge

$$d_+ v_+ F\,\frac{dc_{O+}}{dx} = -\,d_- v_- F\,\frac{dc_{R-}}{dx} = i \ , \tag{6-42}$$

or

$$c_{R-} = c_{Rf-} + \frac{d_+ v_+}{d_- v_-}\,(c_{Of+} - c_{O+}) \ . \tag{6-43}$$

With the use of equations 33, 34, 38, 39, and 43, all the unknown compositions in equations 27 and 32 can be related to the differential material balance for the oxidized species in the positive electrode

(equation 41). Either the electrode length can be calculated for a set superficial velocity and reactant utilization or the superficial velocity for a set electrode length and reactant utilization:

$$L = d_+ v_+ F \int_{c_{0+}}^{c_{0f+}} \frac{dc'_{0+}}{i} \tag{6-44}$$

or

$$v_+ = \frac{L}{d_+ F \int_{c_{0+}}^{c_{0f+}} \frac{dc'_{0+}}{i}} . \tag{6-45}$$

6.4 Cost analysis

An objective function must be specified in order to compare the performance of the flow-by and flow-through configuration on a sound economic basis. This objective function should relate the overall costs (capital, fixed, and variable costs) for an entire system to local variables, such as current density, cell voltage, and flow rate. However, for the comparison considered here, only the costs and system variables related to the net specific power of a particular configuration are important. In this case, the objective function will be based solely on the variable costs. The terminology 'net specific power' refers to the amount of power in watts per square meter recovered by storing off-peak, nighttime power. In general, the objective function should be constructed in terms of intensive variables, that is, independent of the separator or gap area (membrane area for the flow-by configuration; superficial-flow area for the

flow-through configuration).

The simplified cost analysis presented here allows a quick evaluation of the two different electrode configurations. However, it must be emphasized that construction of large scale systems should be based on more detailed cost and performance evaluations.

Capital costs and fixed costs. In this particular study, the exact functional form for these costs is not important because it is assumed that the energy storage facilities are built and are operational. However, for the sake of completeness an approximate formulation will be given (see Newman (1979)) for the case of variable, capital, and fixed costs.

The capital costs and the fixed costs in \$/ year - m^2 for each configuration are assumed to have one value:

Flow-by

$$C'_{CF} = [(C_{A+} + C_{B+}d_{+}) + (C_{A-} + C_{B-}d_{-})]r + C'_{F} , \qquad (6\text{-}46)$$

Flow-through

$$C'_{CF} = [(C_{A+} + C_{B+}L_{+}) + (C_{A-} + C_{B-}L_{-})]r + C'_{F} , \qquad (6\text{-}47)$$

where C_{Bi} and C_{Ai} are the total costs per unit volume ($\$/m^3$) and total costs per superficial-electrode area ($\$/m^2$), respectively. The factor r ($year^{-1}$) represents the effect of interest, depreciation, and taxes. This factor should reflect the average lifetime of the components in the system. If the expected lifetime of the components depends significantly on the current density or cell voltage, this simplified treatment of capital costs would have to be modified.

The term C_F' in equations 46 and 47 represent the fixed costs (i.e., labor, materials, and maintenance). This term is sometimes taken to be a fraction of the total capital investment plus the cost of labor. This assumes that the labor costs can be scaled with the superficial-electrode area.

Variable costs. The costs to be emphasized here are the power costs on charge and discharge, and the pumping costs. The variable costs also include materials makeup plus waste treatment, which may or may not be functions of the operating conditions. In any case, the relationships are not known and it will therefore be assumed that these additional costs are negligible.

The variable costs ($/year - m^2) are given by

Flow-by

$$C_V'S = \underbrace{I_c V_c t_c SC_{pN}}_{\text{charge}} - \underbrace{I_d V_d t_d SC_{pD}}_{\text{discharge}}$$

$$+ \frac{4.2\ S}{\xi_p}\left[\frac{\mu_+ d_+ a_+^2}{\varepsilon_+^3}\left(v_{+c}^2 t_c C_{pN} + v_{+d}^2 t_d C_{pD}\right)\right.$$

$$\left. + \frac{\mu_- d_- a_-^2}{\varepsilon_-^3}\left(v_{-c}^2 t_c C_{pN} + v_{-d}^2 t_d C_{pD}\right)\right], \qquad (6\text{-}48)$$

$$\text{pressure drop}$$

Flow-through

$$C_V'S = \underbrace{I_c V_c t_c SC_{pN}}_{\text{charge}} - \underbrace{I_d V_d t_d SC_{pD}}_{\text{discharge}}$$

$$+ \frac{4.2\ S}{\xi_p}\left[\frac{\mu_+ L_+ a_+^2}{\varepsilon_+^3}\left(v_{+c}^2 t_c C_{pN} + v_{+d}^2 t_d C_{pD}\right)\right.$$

$$\left. + \frac{\mu_- L_- a_-^2}{\varepsilon_-^3}\left(v_{-c}^2 t_c C_{pN} + v_{-d}^2 t_d C_{pD}\right)\right] . \qquad (6\text{-}49)$$

pressure drop

The only difference between equations 48 and 49 is that the length of electrode over which the pressure drop occurs is explicit for the flow-through configuration and implicit for the flow-by configuration.

In equation 48, the electrode thicknesses (perpendicular to the direction of fluid flow) d_+ and d_- account for the fact that the volumetric flow rate may be different for each electrode.

The factor S is the on-stream factor (either days operating per 365 days or operating cycles per year).

In equations 48 and 49, the pressure drop correlation used is for $Re = v/a\nu < 1$ (see Bird et al. (1960)). This is typical of the flow rates encountered in the cell stacks at NASA-Lewis for the flow-by configuration (Gahn and Hagedorn (1978)) and, as will be seen later, the optimum flow rates for the flow-through configuration typically give $Re < 0.001$.

As can be seen in equations 46 through 49, there is no optimum value for electrode length. An order of magnitude analysis of the terms in these equations indicates that practical systems can be built so that the pressure drop terms are small compared to the

remaining terms. In the case of the flow-by configuration, the electrode length is determined by the desired conversion and the minimum flow rate which can be easily controlled in practice. Therefore, the variable costs for either configuration can be expressed as

$$C_V'S = P_c t_c SC_{pN} - P_d t_d SC_{pD}, \tag{6-50}$$

where $P_c = V_c I_c$ and $P_d = V_d I_d$.

The total cost of a redox system can now be given by

$$\frac{\text{cost}}{\text{year}} = [C_{CF}' + P_c t_c SC_{pN} - P_d t_d SC_{pD}]A_{tot}, \tag{6-51}$$

where A_{tot} is the total superficial electrode area of the system.

For the comparison considered here, only the variable costs C_{pN} and C_{pD}, and the system variables related to these costs P_c, P_d, t_c, and t_d are important. The capital and fixed costs per unit superficial area can be optimized separately, and will not be considered further in this analysis.

Dimensional considerations indicate that only ratios of costs are needed to determine the optimum design and operating conditions. In this comparison only the ratio of the cost of daytime and nighttime power is important. Consequently, the objective function to be maximized can now be expressed as

$$NSP(W/m^2) = P_d - \frac{t_c}{t_d} CP_c, \tag{6-52}$$

where $C = C_{pN}/C_{pD}$.

6.5 Optimization procedures and results

To simplify the optimization, only the case where $v_c = v_d$ and $t_c = t_d$ will be considered. It is also convenient to equate the super-

ficial velocities in each electrode $v_{+c} = v_{-c}$. With these assumptions, equation 52 becomes

$$NSP(W/m^2) = P_d - CP_c. \qquad (6\text{-}53)$$

The method of optimization is different for each configuration. For the flow-through configuration, the net specific power is maximized over discharge current, charging current, and flow rate. For the flow-by configuration, it was only necessary to optimize the net specific power with respect to the cell voltage on discharge in order to obtain a valid comparison with the results obtained for the flow-through configuration.

It was not necessary to optimize the flow-by configuration with respect to flow rate because the pressure drop is ignored in the objective function. Furthermore, this configuration can operate at any velocity with a corresponding change in electrode length. Also, because the effluent is isolated the number of coulombs passed on charge and discharge must balance, whereas with the flow through configuration, extra charge is lost according to equation 1.

Chemical system. The results presented are for the Fe/Ti redox system. This chemical system was chosen because data on fundamental parameters, such as exchange current densities, solution conductivities, and viscosities were available (Giner et al. (1976) and Miller (1977) see Table 2). However, the values of the exchange current densities were not available on the electrode materials used in the cells at NASA-Lewis for which a power density of approximately 237 W/m^2 (Gahn and Hagedorn (1978) was achieved for the Fe/Ti system.

Table 6-2. Values of the parameters used in generating the results in Figures 3 through 10.

Parameters used in both electrode systems

$$a = 25\ cm^{-1},\ \varepsilon = 0.3\quad D_{O,Ti^{3+}} = D_{O,Ti(OH)_2^{2+}} = 5\times10^{-6}\ cm^2/s$$

$$n = 1,\ T = 298.15\ K,\ D_{O,FeCl_2} = 5.5\times10^{-6}\ cm^2/s^{(a)}$$

$$D_{O,FeCl_2^+} = 5.7\times10^{-6}\ cm^2/s^{(a)},\ \alpha_a = \alpha_c = 0.5^{(b)}$$

$$U^{\theta}_{FeCl_2/FeCl_2^+} = 0.6513\ V^{(c)},\ U^{\theta}_{Ti^{3+}/Ti(OH)_2^{2+}} = 0.1\ V^{(d)}$$

$$i_{oR} = 10\left(c_{FeCl_2,f}\ c_{FeCl_2^+,f}\right)^{1/2\ (e)},\ i_{oR} = \left(c_{Ti^{3+},f}\ c_{Ti(OH)_2^{2+},f}\right)^{1/2}$$

Flow-through configuration

$$\kappa_o = 0.25\ mho/cm,\ \sigma = 2\times10^{14}\ mho/cm,\ L = 3\ cm,\ L_{gap} = 1\ cm$$

on charge: $c_{H+} = 5\ \underline{M}$

$$c_{Ti(OH)_2^{2+},f} = c_{FeCl_2,f} = 3\ \underline{M}$$

$$c_{Ti^{3+},f} = c_{FeCl_2^+,f} = 3.2942\times10^{-4}\ \underline{M}$$

$$2Cl^- \rightarrow Cl_2(g) + 2e^- : i_{oS} = 10^{-3}c_{Cl^-},^{(f)}\quad \alpha_{aS} = 0.38,^{(f)}$$

$$\alpha_{cS} = 0.69^{(f)}$$

(Table 6-2 continued)

$$c_{Cl^-,f} = 20\ \underline{M}\ ,\quad U^{\theta}_{Cl_2/Cl^-} = 1.3595^{(g)}$$

$$H_2 \rightarrow 2H^+ + 2e^- : i_{oS} = 6.708\times10^{-13}\ A/cm^2,^{(f)}$$

$$\alpha_{aS} = \alpha_{cS} = 0.5^{(f)}$$

$$\frac{\varepsilon k_m}{aD_o} = 0.07054\left(\frac{v}{aD_o}\right)^{0.5454}\ (h)$$

Flow-by configuration

$$\kappa_{o+} = 0.176\ mho/cm^{(i)},\ \kappa_{o-} = 0.207\ mho/cm^{(i)}$$

$$d_+ = d_- = 3\ cm,\ d_+ = d_- = 0.5\ cm^{(j)},\ L_s = 0.047\ cm^{(k)}$$

$$v = 1.7\times10^{-3}\ cm/s, \qquad 1/\kappa_s = 25\ mho/cm^{(k)}$$

on discharge:

$$c_{Ti^{3+},f} = c_{FeCl_2^{2+},f} = 2.7\ M$$

$$c_{Ti(OH)_2^{2+},f} = c_{FeCl_2,f} = 0.27\ M$$

$$\frac{\varepsilon k_m}{aD_o} = 0.91\ \varepsilon\left(\frac{v}{a\nu\psi}\right)^{0.49}\ \psi^2\left(\frac{\nu}{D_o}\right)^{1/3}\ (\ell)$$

$$\psi = 0.86\ ,\ \nu = 0.0251\ cm^2/s$$

(a) Ateya and Austin (1973)
(b) All primary reactions
(c) Reid and Gahn (1977) and Wagman et al. (1968)

(Table 6-2 continued)

(d) Dean (1973) and Baes and Mesmer (1976)
(e) Miller (1977)
(f) Erdey-Gruz (1972)
(g) Newman (1973)
(h) Trainham and Newman (1978)
(i) Giner et al. (1976)
(j) Figure 10 only
(k) Alexander and Hodgdon (1978)
(ℓ) Bird et al. (1960)

The primary electrochemical reactions were assumed to be

$$FeCl_2 \rightarrow FeCl_2^+ + e^-, \qquad (6\text{-}54)$$

and

$$Ti^{3+} + 2H_2O \rightarrow Ti(OH)_2^{2+} + 2H^+ + e^-. \qquad (6\text{-}55)$$

The species assumed in these reactions are based on stability data (Baes and Mesmer (1976)), experimental measurements of open-circuit potentials (Reid and Gahn (1977)) and secondary reference state quantities (Wagman (1968)). For Ti(IV) the hydrolyzed species is expressed $Ti(OH)_2^{2+}$, as there is no strong evidence supporting the commonly written "titanyl" ion, TiO^{2+} (Baes and Mesmer (1976)).

The flow-through model has provision for side reactions, and these were assumed to be evolution of hydrogen and chlorine

$$2H^+ + 2e^- \rightarrow H_2, \qquad (6\text{-}56)$$

and

$$2Cl^- \rightarrow Cl_2(g) + 2e^-. \qquad (6\text{-}57)$$

Flow-through configuration. As mentioned previously, this configuration was optimized with respect to discharge current density, charging current density, and flow rate, with equation 53 as a criterion. To simplify this procedure, and also to reduce computer costs, the charging current density I_c was set and the value of C (cost of night-time to daytime power) was eventually calculated for which this value of I_c was an optimum. This has the advantage, first of all, that the discharge current density can be optimized separately--operation is to be at the power maximum independent of the value of C. For this reason, the search in one-dimensional rather than three-dimensional.

To be more specific, two equations result for the cost ratio C when equation 53 is differentiated with respect to v at constant I_c and then with respect to I_c at constant v, setting the results equal to zero

$$\frac{\partial P_d/\partial v}{\partial P_c/\partial v} = C, \tag{6-58}$$

$$\frac{\partial P_d/\partial I_c}{\partial P_c/\partial I_c} = C. \tag{6-59}$$

The procedure is to set I_c and guess a value for v; calculate the derivatives in equations 58 and 59; while simultaneously adjusting the current density on discharge so that cell operation is at the power maximum. The procedure is repeated at a set I_c adjusting v until a plot can be made of equations 58 and 59 versus $I_c^* = I_c/nFvc_{Rf}$ (the current density on charge made dimensionless with the limiting current density that would exist for fluid velocity v if all the reactant in the feed were completely reacted) as shown in Figure 3. I_c^* is really a dimensionless substitute for v because I_c, n, F, and c_{Rf} are set. In In Figure 3, the point of intersection of the two curves represents the value of the cost ratio for which I_c, I_d, and v are optimum. Figure 3 also shown that equation 58 is more dependent on v than equation 59.

Figure 4 shows that for an increase in optimum flow rate by a factor of 8.1, I_c increases by a factor of 20. This implies a greater utilization of the reactant species on charge at higher current densities. It should be noted that the optimum superficial velocity varied from (0.961 to 7.78) 10^{-5} cm/s over the charging range considered. However, these low velocities would probably be difficult to attain in practice.

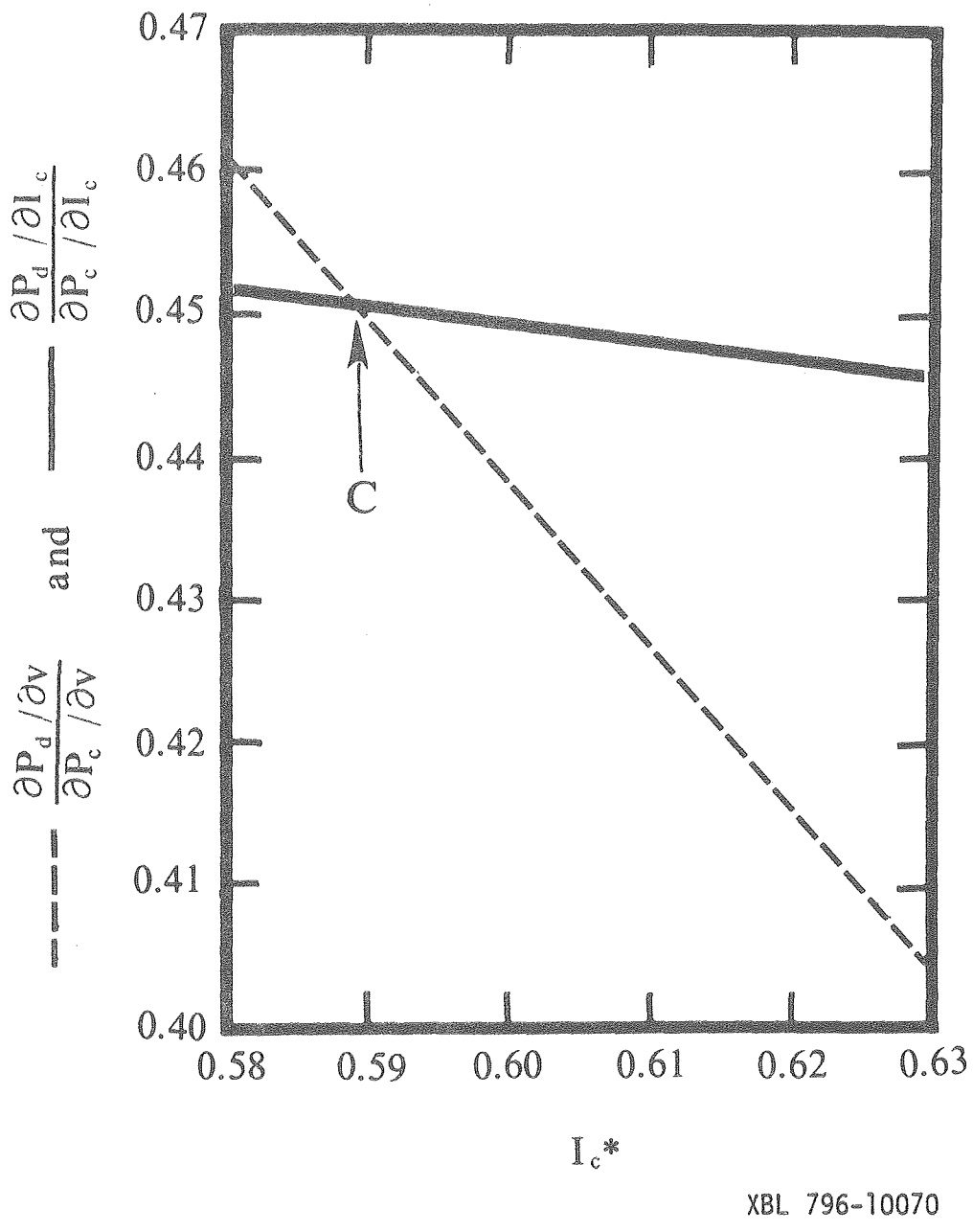

Figure 6-3. Computer-aided graphical optimization procedure.

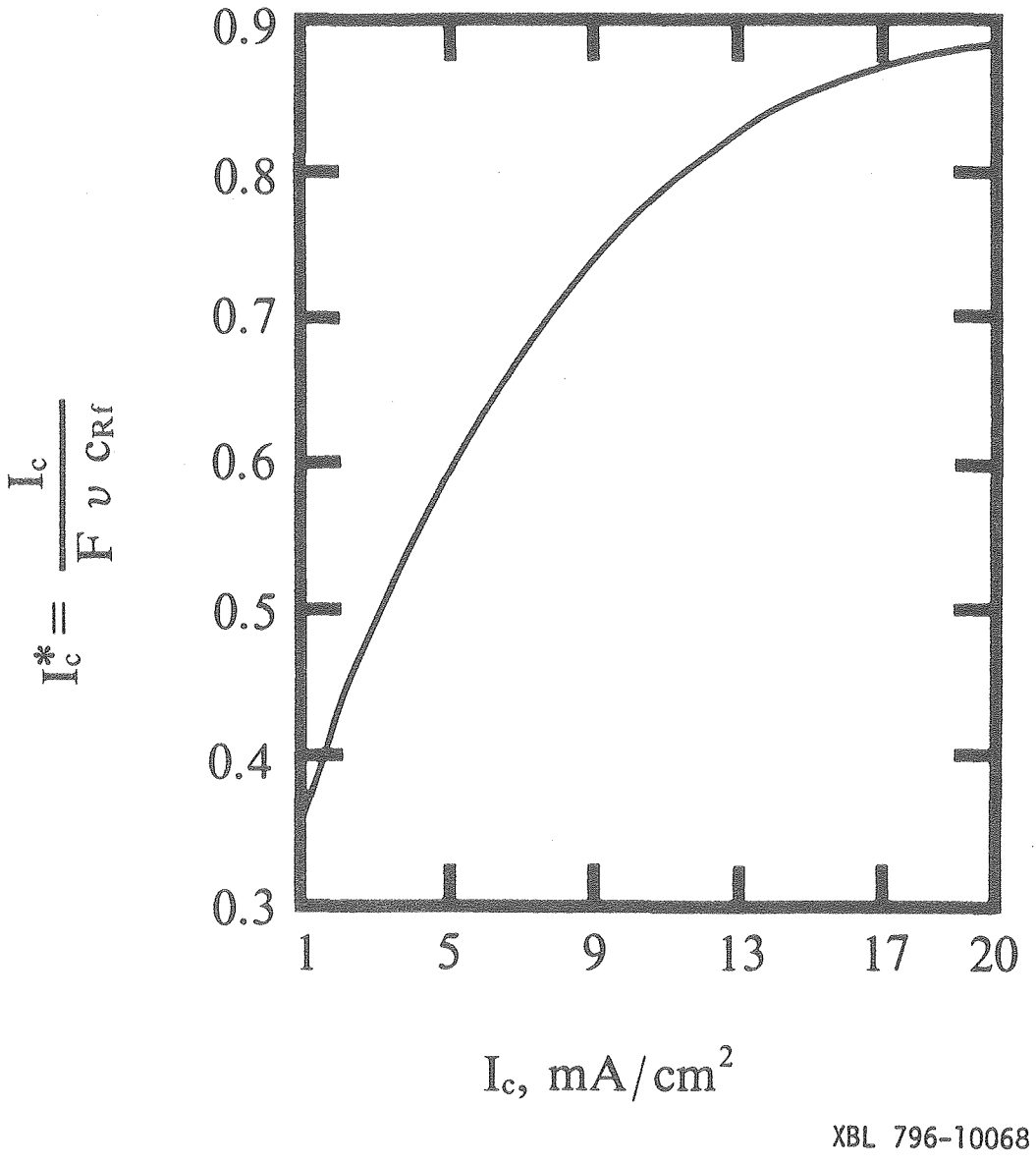

Figure 6-4. Effect of changing current density on the reciprocal of the superficial velocity.

Figure 5 shows that the cost ratio decreases with current density. Therefore, the higher the cost of daytime power relative to nighttime power, the higher the current density at which the system can be economically charged.

As might be expected from the previous graphs, Figure 6 shows that the ratio of the optimum current density recovered on discharge to that of the required charging current density, decreases with charging current density. Thus, the current efficiency is low. Also, a low value of C results in a low energy efficiency.

The decrease in the energy efficiency with current density on charge is clearly shown in Figure 7. At $I_c = 1$ mA/cm^2, P_d/P_c is 0.6, whereas at $I_c = 20$ mA/cm^2, P_d/P_c drops to 0.27.

The NSP (W/m^2) is shown in Figure 8 as a function of C. The NSP is much higher at low values of C.

Flow-by configuration. As mentioned previously, this configuration was optimized only with respect to the cell voltage on discharge. Again, optimization of the flow rate is unnecessary because the pressure drop contribution to the objective function is not included.

In order to compare the net specific power of the two systems, similar results as were obtained in Figure 8 are required. The values of V_d, v, and c_{OL} are set, and the electrode length is calculated from equations 27 and 44. Once L is known, a value of V_c that will recharge the cell to the initial concentrations can be calculated. The total current density, and consequently the power, for either charge or discharge can be obtained from

$$I_c = n_+ Fvd(c_{Rf} - c_{RL})_+/L, \qquad (6\text{-}60)$$

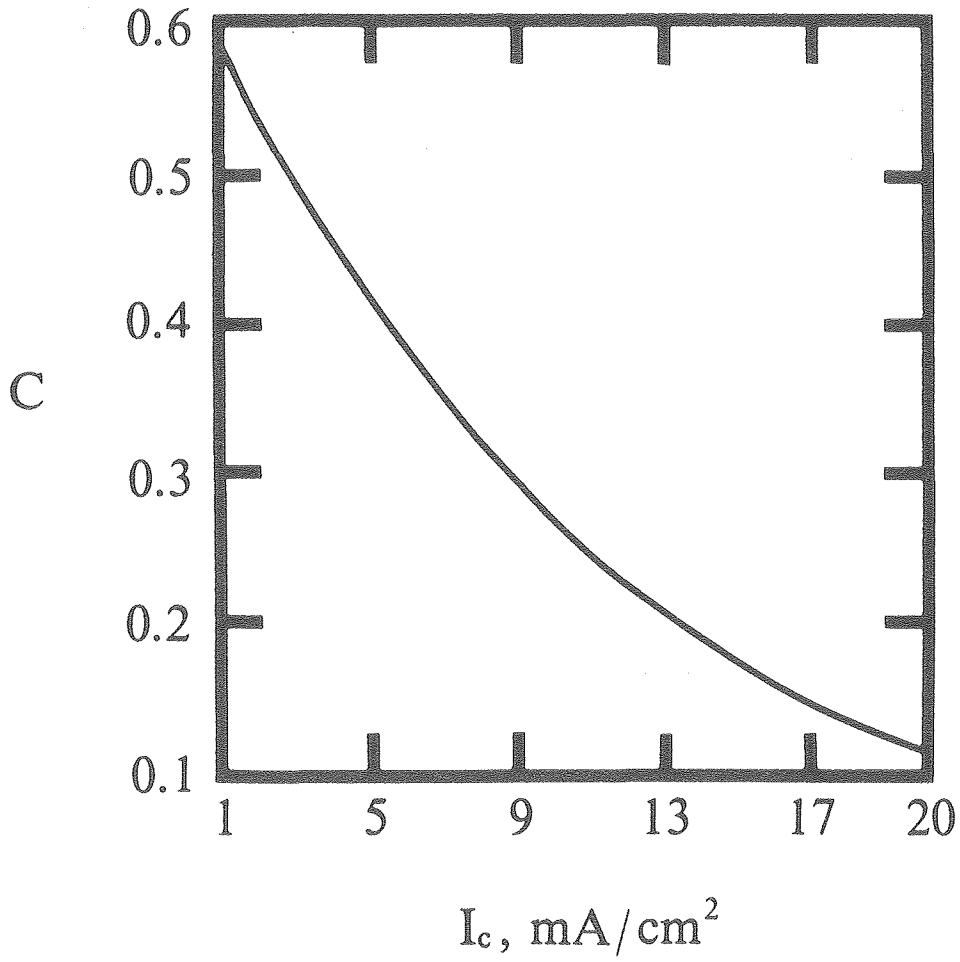

XBL 796-10069

Figure 6-5. Effect of the changing current density on the cost ratio (no nighttime to daytime power costs).

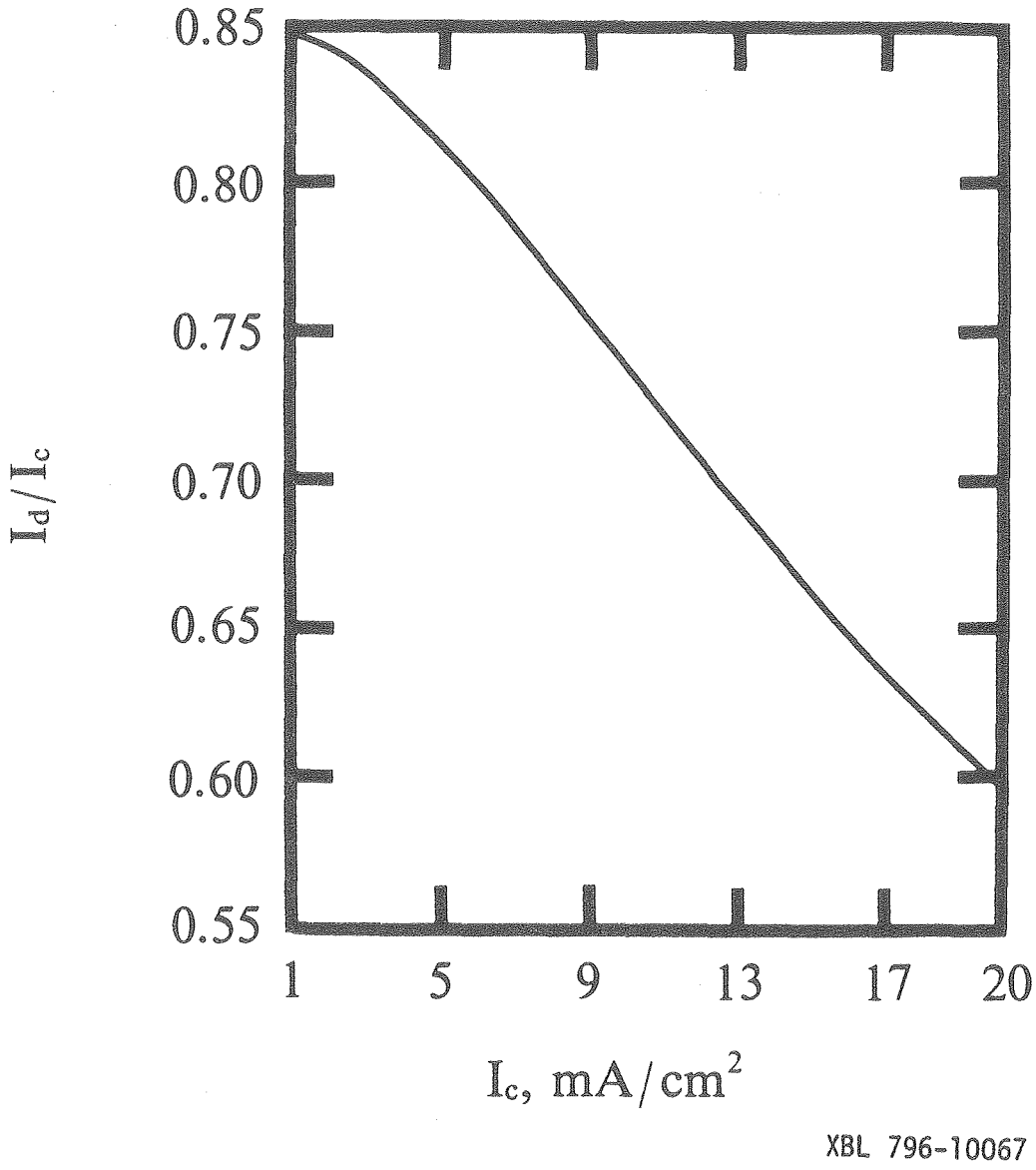

Figure 6-6. Ratio of the optimum discharge current density to the changing current density versus the the changing current density.

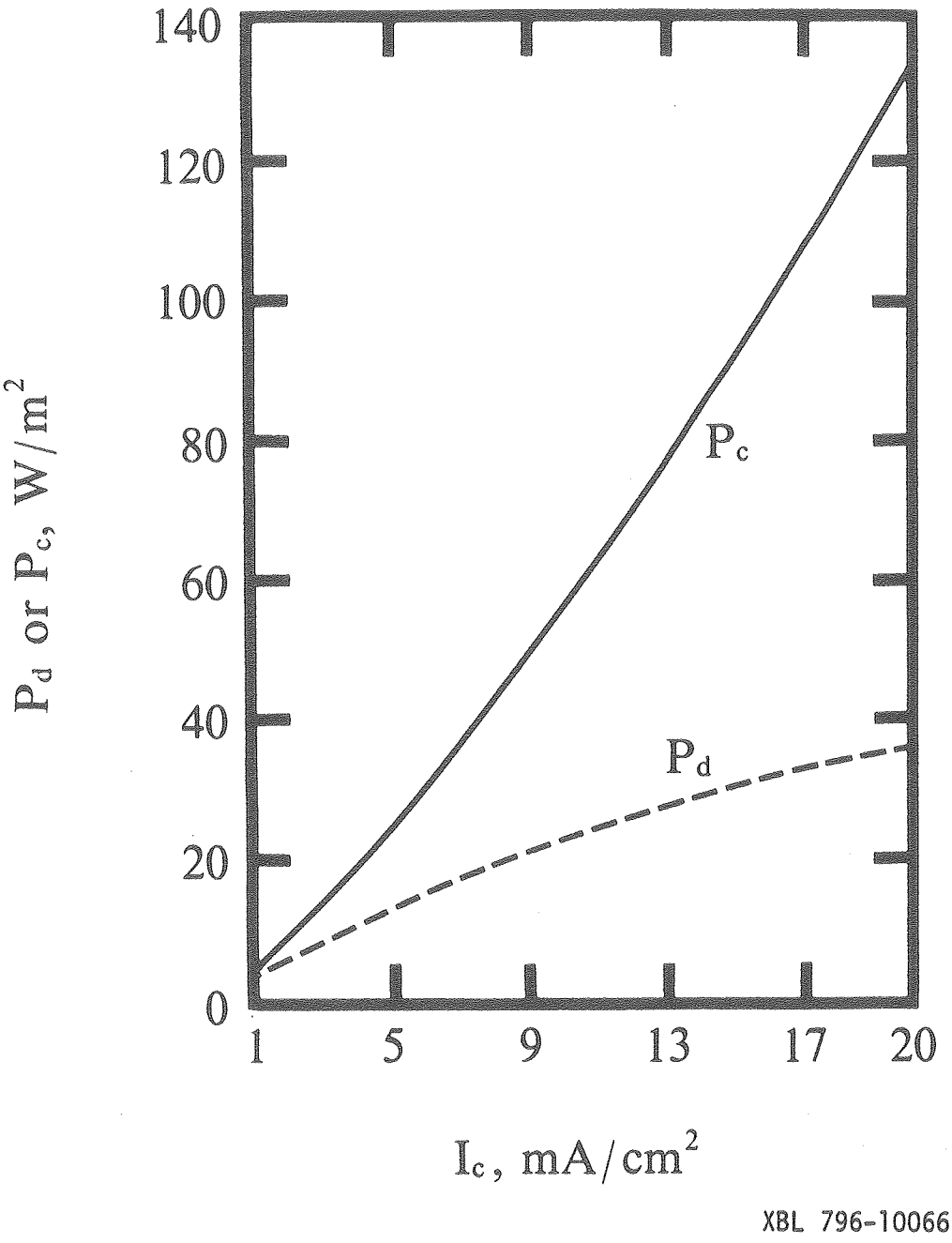

Figure 6-7. Dependence of the power required on charge and power recovered on discharge as a function of the changing current density.

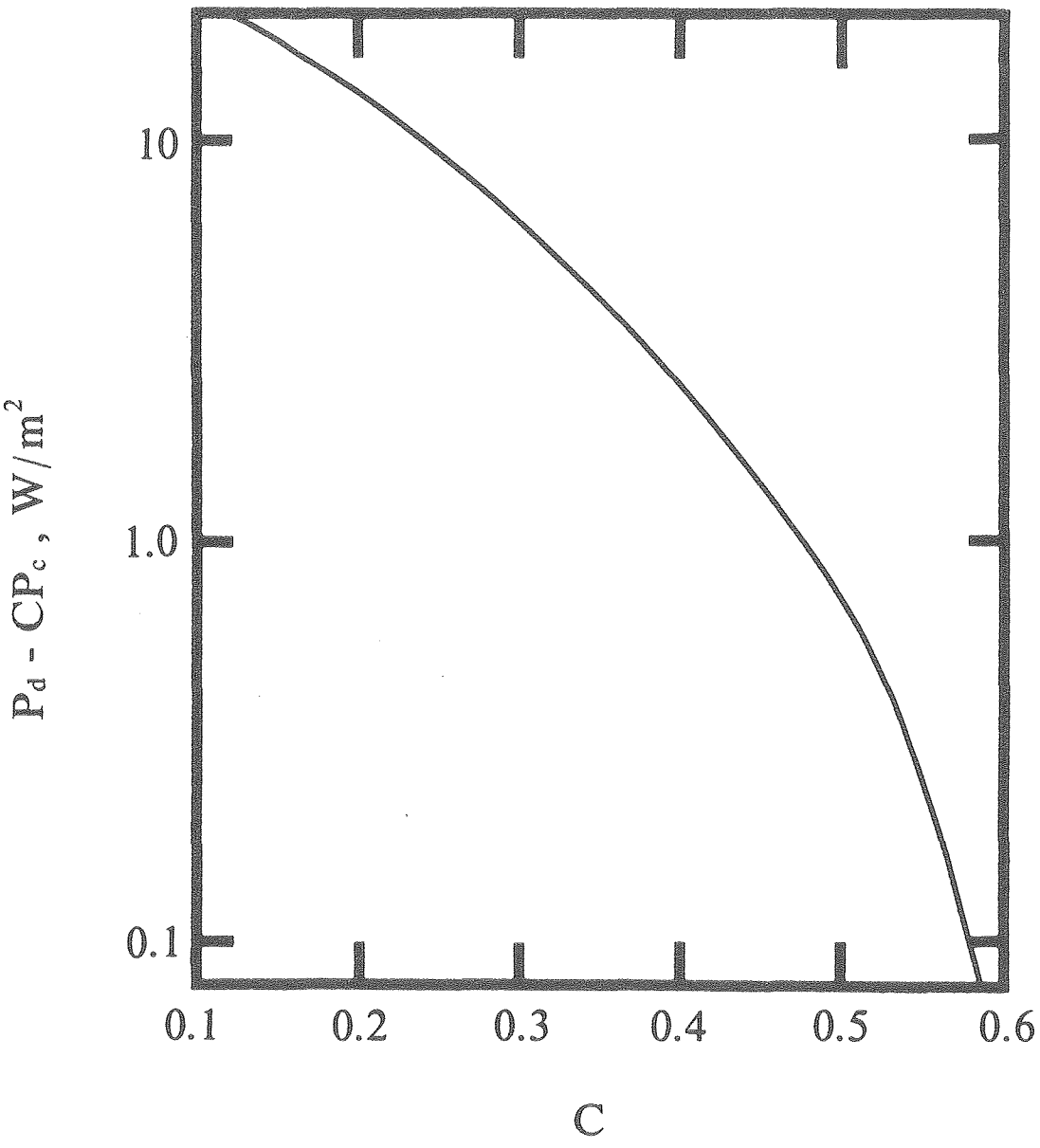

XBL 796-10065

Figure 6-8. Net specific power recovered by the flow-through configuration versus the cost ratio (nighttime to daytime power costs).

and

$$I_d = n_+ Fvd(c_{Of} - c_{OL})_+ / L. \qquad (6\text{-}61)$$

A value for C is then determined for which V_d is an optimum from the equation

$$C = \left(\partial P_d / \partial V_d\right) / \left(\partial P_c / \partial V_d\right) , \qquad (6\text{-}62)$$

and finally the net specific power is calculated with equation 53. Equation 62 is analogous to equations 58 and 59 used for optimization of the flow-through reactor.

Figure 9 shows a comparison between the flow-through and flow-by configurations. Except for very high reactant utilization on discharge (<90%), the flow-by configuration yields the greater return on investment.

In Figure 10, the effect of increasing the specific interfacial area and decreasing the electrode thickness is shown for the flow-by reactor. An increase in a by a factor of ten yields an increase in the performance by a factor of three. Similar results can be expected for the flow-through configuration.

6.6 Discussion

The results of the optimization have shown several important differences between the two configurations. However, these results have raised several pertinent questions:

1. Were the parameters used in the calculations equivalent for both systems, and if so, were values representative of actual systems?

2. Why is the performance of the flow-through configuration so much poorer?

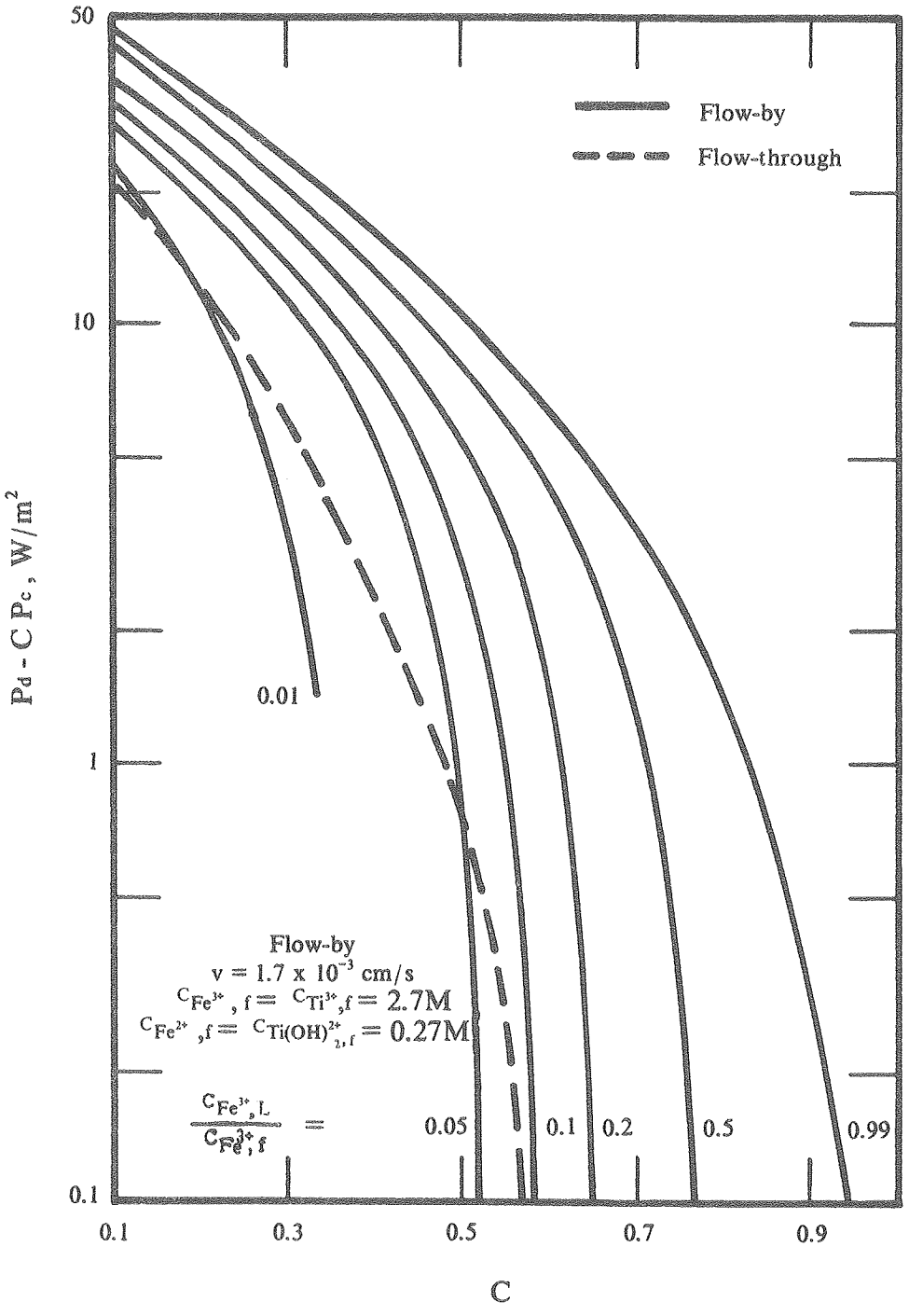

XBL 796-10073

Figure 6-9. A comparison between the flow-by configuration and the flow-through configuration based on the net specific power recovered. The curve for the flow-by configuration is the same as that shown in Figure 8. The flow-by results are for the discharge feed compositions shown at various utilizations of reactant.

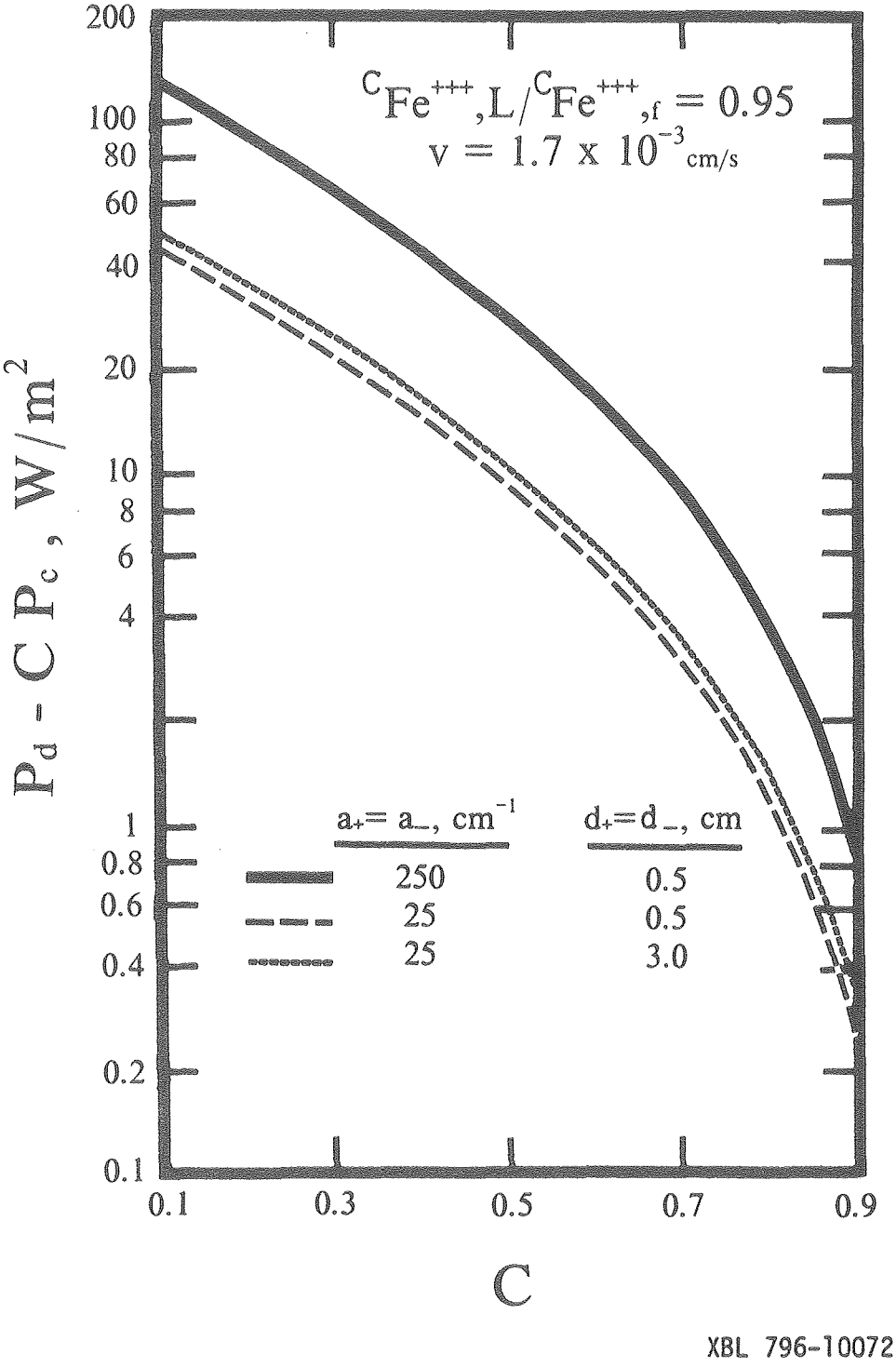

XBL 796-10072

Figure 6-10. Dependence of the net specific power on the cost ratio for the flow-by configuration with the specific interfacial area and the electrode thickness as parameters.

3. Why is the optimum flow rate for the flow-through configuration so small?

4. Is there perhaps a better configuration coupled with a different chemical system for which the flow-through electrodes would yield competitive results?

We will endeavor to answer these questions in this section.

Parameters. In order to obtain a valid comparison between the two configurations, the parameter values were shared whenever possible (see Table 2). However, the differences need some clarification. The total iron concentration and titanium concentration were each 3.00 M for the flow-through configuration and 2.97 M for the flow-by configuration.

In the flow-through case, the concentrations of Ti^{3+} and $FeCl_2^+$ in the feed (set equal to 3.2942×10^{-4} M, see Table 2) were determined from the equilibrium for the reaction which occurs in the gap between the electrodes on mixing after passing through the electrodes on discharge

$$Ti^{3+} + FeCl_2^+ + 2H_2O \rightleftharpoons Ti(OH)_2^{2+} + FeCl_2 + 2H^+ , \qquad (6\text{-}63)$$

which has an equilibrium constant

$$\frac{c_{Ti^{3+}}\, c_{FeCl_2^+}}{c_{Ti(OH)_2^{2+}}\, c_{FeCl_2}\, c_{H^+}^2} = 4.823 \times 10^{-10} \left(\frac{\ell}{\text{mole}}\right)^2 . \qquad (6\text{-}64)$$

In equation 64, the activity coefficients and the activity of water have been set equal to unity.

The results of the optimization show that the charge imbalance due to incomplete conversion of $FeCl_2^+$ on discharge is very small. In fact,

the percent of charge (stored on discharge) required to restore the system to the initial state of charge (i.e., all $FeCl_2^+$ converted to $FeCl_2$), was always less than 0.05%. Therefore, the side reactions on charge are extremely small. This is due to the optimization procedure which forces the system to operate at nearly 100% current efficiency on charge.

The correlation used in predicting the mass transfer coefficient for the flow-through configuration is the same on that determined in Chapter 3 (equation 3-51). For the flow-by configuration, a mass transfer correlation appropriate for the Reynolds numbers encountered was used (Bird et al. (1960), see quation 3-43).

Other variations in the parameters are due to the inherent differences between the two systems. For example, the superficial velocity was arbitrarily set for the flow-by system ($v = 1.7 \times 10^{-3}$cm/s), whereas, an optimum value was determined on charge for the other system. Experimental conductivity and viscosity data were available for the mixtures $FeCl_2/FeCl_2^+$ and $Ti^{3+}/Ti(OH)_2^{3+}$ encountered in typical flow-by systems (Giner et al. (1976)), but were not available for the Fe/Ti mixtures of the flow-through system. In the latter case, a value of 0.25 mho/cm was assumed (see Table 2). Experimental data for the membrane separator thickness and resistivity were also known for the flow-by system (Alexander and Hodgdon (1978)), where a 1 cm gap was assumed in the flow-through calculations.

It can be concluded from the above discussion that the differences between the parameters used in each system are minor, and therefore, will not account for the discrepancy in performance.

As mentioned previously, values for the kinetic parameters and the specific interfacial area were not available for the system at NASA-

Lewis for which a discharge power density of 237 W/m^2 (Gahn and Hagedorn (1978)) was achieved. This compares with a calculated maximum power density of 170 W/m^2 (top curve Figure 10). A value of 25 cm^{-1} for the specific interfacial area was used in most of the calculations. However, Figure 10 has shown that for a tenfold increase in the value of a, the NSP increases by factor of three. Even a value of a equal to 250 cm^{-1} could be conservative by a factor of two or three, and this would account for most of the discrepancy. In addition, the values of the exchange current densities used in the calculations (see Table 2) could easily be low by an order of magnitude. At the present time, there is no way to tell how well the models predict reality, because there are no steady-state data available.

Superficial velocity. In Figure 4, the optimum superficial velocity for the flow-through system varied from $(0.961 \text{ to } 7.78)10^{-5}$ cm/s over the charging range of 1 mA/cm^2 to 20 mA/cm^2. Again, these velocities would be extremely difficult to achieve in practice.

The optimum velocity is low for several reasons:

1. The conversion is moderate on both charge ($0.11 < c_{RL}/c_{Rf} < 0.64$) and discharge ($0.15 < c_{RL}/c_{Rf} < 0.6$) for the charging current density range of 1 mA/cm^2 to 20 mA/cm^2. A low conversion, which would allow a much higher flow rate, is not possible due to the single pass operation.

2. The feed composition of the reactants on charge is 3M. This is 300 times the feed composition of the copper removal process (Bennion and Newman (1972)) modeled in Chapter 3. This contributed substantially to the two-orders of magnitude difference in flow rate.

3. A comparison of Figure 7 with Figures 8 and 9 shows that the

system cannot be run economically a high current densities.

An estimate of the maximum allowable velocity on charge can be obtained from the limiting current design equations of Bennion and Newman (1972). The difference in the standard electrode potentials for the system is $\Delta U^{\theta} = 0.5513V$ (see Table 2). If we assume 0.0513V is lost to the separator, then there is approximately 0.2V available for ohmic losses in each electrode. If we combine equations 3-49 and 3-51 an expression for the velocity results

$$v^{1.4546} = 0.07054 \frac{s_R \kappa \Delta\Phi_2'}{\epsilon\, nF\, c_{Rf}} a^{0.5454} \nu^{0.4546}. \qquad (6\text{-}66)$$

Using the values of the parameters in Table 2 and $\Delta\Phi_2' = 0.2$, we obtain $v = 2.1 \times 10^{-5}$ cm/s. This estimate is the same order of magnitude on the velocities obtained by the optimization procedure.

As mentioned previously, the results for the flow-by configuration operating at a fixed conversion are essentially independent of velocity. For a desired conversion, the electrode length is set, and the velocity can be calculated or vice versa. This operational flexibility makes the flow-by configuration superior.

Effect of electrode thickness. For the flow-by configuration, results were obtained for electrodes of thickness 3 cm and 0.5 cm in the direction of current flow. Figure 10 shows that there is only a small improvement in the performance of the 3 cm thick electrode over the 0.5 cm thick electrode. The electrode length of the 3 cm thick varied from approximately 5.2 to 5.5 times that of the 0.5 cm thick electrode over the discharge range considered.

Other systems. It should be kept in mind that the Fe/Ti chemical system has been used for a relative comparison between two electrode configurations. Other chemical systems offer larger open-circuit potentials and reaction rates per unit volume (ai_o). However, the mathematical models and the optimization procedures developed here can be used directly or modified accordingly, so that other systems can be compared.

6.7 Summary and conclusions

Theoretical models have been developed for two electrode configurations for redox battery applications: 1) flow-through porous electrodes and 2) flow-by porous electrodes. These models were used to determine which system yields the greater return on investment. To do this, both systems were optimized with respect to an objective function appropriate for the application.

The results show that the flow-by configuration is superior. Not only does this system yield a greater return on investment, but it also offers the operational flexibility of variable flow rate and conversion. Its limitations compared to the flow-through system will be associated with the maintenance and reliability of the membrane separator.

The flow-through configuration in addition to yielding a lower return on investment, offers an impractical superficial velocity (the optimum superficial velocity was of order 10^{-5} cm/s). Its failure is due to current flow (and ohmic potential drop) in the same direction as the fluid flow.

The perspective here has been to use a simplified optimization procedure to obtain a valid comparison between two electrode systems.

Notation

a	specific interfacial area, cm^{-1}
a_i^{θ}	$= \lambda_i^{\theta}/\rho_o$ property expressing the secondary reference state, ℓ/mole
B	see equation 3-47
C	$= \ell n\ \theta$, see equation A-1, in Chapter 6 the ratio of daytime to nighttime power costs
$c_{Cl^-,sat}$	concentration of chloride in a saturated calomel reference electrode compartment, mole/ℓ
c_R	concentration of the reactant species, in the flow-by analysis of Chapter 6 it is referred to as the reduced species, mole/cm^3
c_O	concentration of the oxidized species in a redox reaction, mole/cm^3
c_P	concentration of the product species in a redox reaction, mole/cm^3
c_S	reactant species concentration in the side reaction, mole/cm^3
$c_{i,L}$	concentration at electrode exit, mole/cm^3
C_{Ai}	cost per unit volume, \$/m^3
C_{Bi}	cost per superficial-electrode area, \$/m^2
C'_{CF}	capital and fixed costs, \$/year-m^2
C'_F	fixed costs, \$/year-m^2
C'_V	variable costs, \$/year-m^2
C_{pD}	daytime power costs, \$/W
C_{pN}	nighttime power costs, \$/W

DD	downstream counterelectrode, downstream current collector
DU	downstream counterelectrode, upstream current collector
D_a	axial dispersion coefficient of the reactant species, cm^2/s
D_o	molecular diffusion coefficient of the reactant species, cm^2/s
D_R	effective diffusion coefficient of the reactant species, cm^2/s
D'	dimensionless parameter describing the relative importance of axial diffusion and dispersion, see equation 3-32
f_i	molar activity coefficient of species i
$f_{i,n}$	$= f_i/f_n^{z_i/z_n}$ molar activity coefficient of species i referred to ionic species n
F	Faraday's constant, 96487 C/equiv
h	dimensionless distance between mesh points
i	superficial current density to an electrode, A/cm^2
i_{oj}	exchange current density for reaction j , A/cm^2
$i_{oj,ref}$	exchange current density for reaction j at a reference composition $c_{i,ref}$, see equation 3-14, A/cm^2
i_1	superficial current density in the matrix, A/cm^2
i_2	superficial current density in pore-solution phase, A/cm^2
i_{nj}	transfer current for reaction j per unit interfacial area, A/cm^2
I^*	dimensionless superficial current density to an electrode, see equation 3-41
i_2^*	dimensionless current density in pore-solution phase, see equation 3-46
$i_2^*[o]$	$= -I^*$ total dimensionless current density in pore-solution phase, see equation 3-48
i_R	total current density to an electrode due to metal-deposition reaction, A/cm^2

I	total current to an electrode, A
I_c	current density on charge, A/cm^2
I_d	current density on discharge, A/cm^2
j_{in}	pore-wall flux of species i, $mole/cm^2$-s
J_R	dimensionless transfer current of metal deposition reaction, see equation A-6
J_S	dimensionless transfer current of side reaction, see equation A-9
k_m	average mass-transfer coefficient between flowing solution and electrode surface, cm/s
L	thickness of porous electrode, cm
L_s	separator thickness in flow-by porous electrode, cm
L_{gap}	gap thickness of flow-through porous electrode, cm
M_i	symbol for the chemical formula of species i
n	number of electrons transferred in an electrochemical reaction
n_j	number of electrons transferred in reaction j
N_R	superficial flux of the reactant species, $mole/cm^2$-s
p_S	hydrogen or chlorine partial pressure, atm
Pe	Péclet number, v/aD_o
P_1	dimensionless parameter describing the relative importance of the anodic term in a metal deposition reaction, and a redox reaction, see equation 3-34
P_2	dimensionless parameter describing the relative importance of the ohmic potential drop, see equation 3-35
P_3	dimensionless parameter describing the relative importance of the forward term in the side reaction, see equation 3-36
P_4	dimensionless parameter describing the relative rate of the backward term in the side reaction, see equation 3-37
P_5	dimensionless parameter which characterizes the ohmic potential drop in the pore-solution phase, see equation 3-38

P_6	dimensionless parameter which characterizes the ohmic potential drop in the matrix phase, see equation 3-39
P_7	k_{mR}/k_{mP}, ratio of mass transfer coefficients for reactant and product series in a redox reaction
P_1'	dimensionless parameter describing the relative importance of the cathodic term in a metal deposition reaction and a redox reaction, see equation 6-19
P_2'	same physical significance as P_2 only for an anodic reactant, see equation 6-20
P_3'	same physical significance as P_3, see equation 6-21
P_4'	same physical significance as P_4, see equation 6-22
P_5'	same physical significance as P_5, see equation 6-23
P_6'	same physical significance as P_6, see equation 6-24
q_{ij}	cathodic reaction order
r	the effect of interest, depreciation and taxes, yr^{-1}
R	universal gas constant, 8.3143 J/mole-K
Re	= $v/a\nu$ or $v/\psi a\nu$, Reynolds number
S	on-stream factor, days operating/365 days or operating cycles/year
s_{ij}	stoichiometric coefficient of species i in electrode reaction j
s_R	stoichiometric coefficient of reactant species
s_P	stoichiometric coefficient of product species
T	absolute temperature, K
t_c	charging time, s
t_d	discharge time, s
U	open-circuit cell potential, V
UD	upstream counterelectrode, downstream current collector
UU	upstream counterelectrode, upstream current collector

U_{jw} open-circuit potential for reaction j at local wall composition relative to a reference electrode of a given kind, V, see equation 3-17

U_j^θ standard electrode potential for reaction j, V

U_k^θ standard electrode potential for reaction k, V

U_r^θ standard electrode potential of reference electrode, V

ΔU $= U_S - U_R$ difference in open-circuit cell potentials of the side reaction and primary reaction at the reference composition, V

v superficial fluid velocity, cm/s

VOP potential of the cathode current collector relative to a saturated calomel reference electrode placed in the dilute product stream, V

$(VOP)_{max}$ maximum value of VOP at which appreciable side reaction does not occur, V

ΔV_k $VOP - U_k^\theta + V_{cal}^\theta$, V

x distance through porous electrode, cm

y $x\, ak_m/v$ dimensionless distance through porous electrode, in the flow-by analysis of Chapter 6 it is the distance in the direction of current flow, cm

z_i valance or charge number of species i

Greek Letters

α $= a\, k_m/v$, reciprocal of penertation depth at the limiting current, cm^{-1}

α_{aj} anodic transfer coefficient for reaction j

α_{cj} cathodic transfer coefficient for reaction j

β_ε overall stability constant, where ε denotes the number of ligands in the complex, (ℓ $mole^{-1}$) or (kg $mole^{-1}$)

γ_{ij}	exponent in composition dependence of exchange current density
ε	porosity or void volume, also number of ligands in a complex
Φ	quasi-electrostatic potential, V
Φ_1	electrostatic potential in matrix phase, V
Φ_2	quasi-electrostatic potential in the pore solution phase, V
$\Delta\Phi_2$	ohmic potential drop across porous electrode, V
$\Delta\Phi_2'$	estimate of ohmic potential across porous electrode at the limiting current, V see equation 3-49
$\Delta\Phi_{gap}$	$I_c L_{gap}/\kappa_o$, ohmic drop across gap in flow-through porous electrode, V
η_{sj}	$= \Phi_1 - \Phi_2 - U_{jw}$ surface overpotential for reaction j, V
η	$= \Phi_1 - \Phi_2$ local overpotential, V
η'	dimensionless local overpotential for the cathodic reactant, see equation 3-33
$\eta^{*'}$	dimensionless local overpotential for the anodic reactant, see equation 6-16
κ	effective conductivity of solution, mho/cm
κ_o	intrinsic conductivity of solution, mho/cm
κ_s	effective conductivity of the separator, mho/cm
λ_i	absolute activity of species i
λ_i^θ	property expressing secondary reference state, kg mol^{-1}
$\lambda_{i,n}^\theta$	$=\lambda_i^\theta/\lambda_n^\theta\ z_i/z_n$ property expressing secondary reference state of species i referred to ionic species n
μ	viscosity, g/cm-s
μ_i	electrochemical potential of species, i, j mol^{-1}

Superscripts

o	pure state
θ	secondary reference state at infinite dilution
*	ideal-gas secondary reference state

Subscripts

c	charge
cal	calomel
d	discharge
f	feed
L	length of electrode, exit
-	negative electrode
+	positive electrode
0	oxidized species
P	product species
r	reference electrode compartment
R	reactant species, reduced species or primary reaction
ref	reference composition
S	side reactant or side reaction
sat	saturated
w	wall or electrode surface

References

1. Adams, George B., Roger P. Hollandsworth, and Douglas N. Bennion. "Electrochemical Oxidation of Ferrous Iron in Very Dilute Solutions". Journal of the Electrochemical Society, 122, 1043 (1975).

2. Alexander, S. S., and R. B. Hodgdon. "Anion Permselective Membranes." Ionics, Inc. Watertown, Mass., CONS/010801, NASAA CR-135316 (1978).

3. Alkire, Richard, and Patrick K. Ng. "Two-Dimensional Current Distribution Within a Packed-Bed Electrochemical Flow Reactor." Journal of the Electrochemical Society, 121, 95 (1974).

4. Alkire, Richard, and Brian Gracon. "Flow-Through Porous Electrodes." Journal of the Electrochemical Society, 122, 1594 (1975).

5. Alkire, Richard, and Ronald Gould. "Analysis of Multiple Reaction Sequences in Flow-Through Porous Electrodes." Journal of the Electrochemical Society, 123, 1842 (1976).

6. Alkire, Richard, and Patrick K. Ng. "Studies on Flow-By Porous Electrodes Having Perpendicular Directions of Current and Electrolyte Flow." Journal of the Electrochemical Society, 124, 1220 (1977).

7. Appel, Peter W., and John Newman. "Applications of the Limiting-Current Method to Mass Transfer in Packed Beds at Very Low Reynolds Numbers." AIChE Journal, 22, 979 (1976).

8. Appel, Peter W., Electrochemical Systems: impedance of a rotating disk and mass transfer in packed beds, Ph.D. Dissertation, No. LBL-5132, University of California, Berkeley, May, 1976.

9. Armstrong, R. D., O. R. Brown, R. D. Giles, and J. A. Harrison. "Factors in the Design of Electrochemical Reactors." Nature, 219, 94 (1968).

10. Ateya, B. G., and L. G. Austin. "The Kinetics of $Ee^{2+}/FeCl_2^+/HCl$ (aq.) on Pyrolytic Graphite Electrodes." Journal of the Electrochemical Society, 120, 1216 (1973).

11. Ateya, B. G., and L. G. Austin. "Steady-State Polarization at Flow-Through Electrodes with Small Pore Diameter I. Reversible Kinetics." Journal of the Electrochemical Society, 124, 83 (1977).

12. Backhurst, J. R., J. M. Coulson, F. Goodridge, R. E. Plimley, and M. Fleischmann. "A Preliminary Investigation of Fluidized Bed Electrodes." Journal of the Electrochemical Society, 116, 1600 (1969).

13. Baes, C. F., Jr., and R. E. Mesmer. The Hydrolysis of Cations, John Wiley and Sons, Inc., New York (1976).

14. Beccu, Klaus D. "Zur Deckung des zunkünftigen Spitzenbedarfs elektrischer Energie mittls electrochemischer Energiespeicher." Chemie Ingenieur Technik, 46, 95 (1974).

15. Beck, Theodore R. "Final Report on Improvements in Energy Efficiency of Industrial Electrochemical Processes." ANL/OEPM-77-2 (1977).

16. Bennion, Douglas N., and John Newman. "Electrochemical removal of copper ions from very dilute solutions." Journal of Applied Electrochemistry, 2, 113 (1972).

17. Bennion, Douglas N. "Flow-Through Porous Electrodes For Removal of Ions from Dilute Solutions." Abstract 69. Zurich meeting. International Society of Electrochemistry (1976).

18. Bird, R. Byron, Warren E. Stewart, and Edwin N. Lightfoot. Transport Phenomena, Wiley, New York, pp. 411-412 (1960).

19. Chu, A. K. P., M. Fleischmann, and G. J. Hills. "Packed bed electrodes. I. The electrochemical extraction of copper ions from dilute aqueous solutions." Journal of Applied Electrochemistry, 4, 323 (1974).

20. Danckwerts, P. V. "Continuous Flow Systems. Distribution of Residence Times." Chemical Engineering Science, 2, 1 (1953).

21. Dean, John A. (editor). Lange's Handbook of Chemistry. Eleventh edition, McGraw-Hill Book Company, New York, p. 6-14 (1973).

22. Dunning, John Stephen. "Analysis of Porous Electrodes with Sparingly Soluble Reactants." Ph.D. Dissertation, University of California, Los Angeles (1971).

23. Erdey-Gruz, Tibor. Kinetics of Electrode Processes, Wiley-Interscience, New York, p. 165 (1972).

24. Euler, J., and W. Nonnenmacher. "Stromverteilung in porösen Electroden." Electrochimica Acta, 2, 268 (1960).

25. Fedkiw, Peter S., Mass Transfer Controlled Reactions In Packed Beds at Low Reynolds Numbers, Ph.D. Dissertation, No. LBL-8509, University of California, Berkeley, December, 1978.

26. Gahn, Randall, and Norman Hagedorn. Unpublished results, NASA-Lewis Research Center, Cleveland, Ohio, May, 1978.

27. Giner, J., L. Swette, and K. Cahill. "Screening of Redox Couples and Electrode Materials." (Giner Inc.; NAS 3-19760), NASA CR-134705 (1976).

28. Hadeishi, Tetsuo, and R. D. McLaughlin. "Hyperfine Zeeman Effect Atomic Absorbtion Spectrometer for Mercury." Science, 174, 404 (1971).

29. Hadeishi, Tetsuo. "Isotope-Shift Zeeman effect for trace-element detection: an application of atomic physics to environmental problems." Applied Physics Letters, 21, 438 (1972).

30. Hsueh, Limin, and John Newman. "The Approach to Limiting Current in a Stagnant Diffusion Cell." Journal of the Electrochemical Society, 117, 1242 (1970).

31. Kangro, Walther. "Verfahren zur Speicherung von elektrischer Energie." Deutsches Patentamt 914,264 (1954).

32. Kangro, Walther. "Conples redox liquides." Space Power Systems Energy Storage. Proceedings of the Sixth ESRO Summer School Noordwijk, The Netherlands, 1968: Vol. X, ESRO SP-49 (1969).

33. Kreysa, G., S. Piontech, and E. Heitz. "Comparative investigation of packed and fluidized bed electrodes with non-conducting and conducting particles." Journal of Applied Electrochemistry, 5, 305 (1975).

34. Kuhn, A. T., and R. W. Houghton. "A Comparison of the Performance of Electrochemical Reactor Designs in the Treatment of Dilute Solutions." Electrochimica Acta, 19, 733 (1974a).

35. Kuhn, A. T., and R. W. Houghton. "Antimony removal from dilute solutions using a restrained bed electrochemical reactor." Journal of Applied Electrochemistry, 4, 69 (1974b).

36. Meites, Louis (editor). Handbook of Analytical Chemistry, McGraw-Hill Book Company, New York, p. 37 (1962).

37. Miller, Riley O. "Electrochemical Behavior of 0.2 to 3 Molar Ferrous Chloride-Ferric Chloride Mixtures on Pyrolytic Graphite Rotated Disk Electrodes." ERDA/NASA-5022/77/2, NASA TM 73716 (1977).

38. Newman, John S. and Charles W. Tobias. "Theoretical Analysis of Current Distribution in Porous Electrodes." Journal of the Electrochemical Society, 109, 1183 (1962).

39. Newman, John. "Current Distribution on a Rotating Disk below the Limiting Current." Journal of the Electrochemical Society, 113, 1235 (1966).

40. Newman, John. Electrochemical Systems, Prentice-Hall, Englewood Cliffs, N. J. (1973).

41. Newman, John, and William Tiedemann. "Porous Electrode Theory with Battery Applications." AIChE Journal, 21, 25 (1975).

42. Newman, John. "Simultaneous Reactions at Disk and Porous Electrodes." Electrochimica Acta, 22, 903 (1977).

43. Newman, John and William Tiedemann. "Flow-Through Porous Electrodes." H. Gerischer and C. W. Tobias (editors). Advances in Electrochemistry and Electrochemical Engineering, 11, 353 (1978).

44. Newman, John. "Optimization of Potential and Hydrogen Utilization In An Acid Fuel Cell." Electrochimica Acta, 24, 223 (1979).

45. Parrish, W. R., and John Newman. "Current Distribution on a Plane Electrode below the Limiting Current." Journal of the Electrochemical Society, 116, 169 (1969).

46. Parrish, W. R., and John Newman. "Current Distributions on Plane, Parallel Electrodes in Channel Flow." Journal of the Electrochemical Society, 117, 43 (1970).

47. Paulin, M., D. Hutin, and F. Coeuret. "Theoretical and Experimental Study of Flow-Through Porous Electrodes." Journal of the Electrochemical Society, 124, 180 (1977).

48. Pickett, D. J. Electrochemical Reactor Design, Elsevier, Amsterdam (1977).

49. Posey, F. A. "Electrolytic Demonstration Unit for Copper Removed from Distillation Plant Blowdown." ONRL-TM-4112. Oak Ridge: Oak Ridge National Laboratory (1973).

50. Reid, Margaret A. and Randall F. Gahn. "Factors Affecting the Open-Circuit Voltage and Electrode Kinetics of Some Iron/Titanium Redox Flow Cells." ERDA-1022/77/10, NASA 7MX-73669 (1977).

51. Roe, D. K. "Electrochemical Fractionation: Potentiostatic Chromatography and Elution Voltammetry." Analytical Chemistry, 36, 2371 (1964).

52. de la Rue, R. E., and C. W. Tobias. "On the Conductivity of Dispersions." Journal of the Electrochemical Society, 106, 827 (1959).

53. Sherwood, Thomas K., Robert L. Pigford, and Charles R. Wilke. Mass Transfer, New York, McGraw-Hill Book Company, p. 136 (1975).

54. Sioda, R. E., "Current-Potential Dependence In the Flow Electrolysis on a Porous Electrode." Journal of Electroanalytical Chemistry and Interfacial Electrochemistry, 34, 399 (1972).

55. Sioda, R. E. "The ECE Mechanism in Flow Electrolysis in Porous Electrodes Under Conditions of Limiting Current." Electrochimica Acta, 20, 457 (1975).

56. Thaller, Lawrence H. "Electrically Rechargable Redox Flow Cells." NASA TMX-7154. Ninth Intersociety Energy Conversion Engineering Conference, San Francisco, California, August, 1974.

57. Thaller, Lawrence H. "Electrically Rechargable Redox Flow Cells." U.S. Patent 3,996,064 (1976).

58. Trainham, James A., and John Newman. "The Removal of Lead Ions from Very Dilute Solutions Using a Porous Flow-Through Electrode." Inorganic Materials Research Division Annual Report 1973, p. 51, LBL-2299, Berkeley, Lawrence Berkeley Laboratory, University of California, April, 1974.

59. Trainham, James A., and John Newman. Unpublished results. Berkeley: University of California (1975).

60. Trainham, James A., and John Newman. "A Thermodynamic Estimation of the Minimum Concentration Attainable in a Flow-Through Porous Electrode Reactor." Journal of Applied Electrochemistry, 7, 287 (1977a).

61. Trainham, James A., and John Newman. "A Flow-Through Porous Electrode Model: Application to Metal-Ion Removal from Dilute Streams." Journal of the Electrochemical Society, 124, 1528 (1977b).

62. Trainham, James A., and John Newman. "The Effect of Electrode Placement and Finite Matrix Conductivity on the Performance of Flow-Through Porous Electrodes." Journal of the Electrochemical Society, 125, 58 (1978).

63. Trotman, A. F., and Dickerson (executive editors). Comprehensive Inorganic Chemistry, 3, 85 (1973).

64. Van Zee, John, and John Newman. "Electrochemical Removal of Silver Ions from Photographic Fixing Solutions Using a Porous Flow-Through Electrode." Journal of the Electrochemical Society, 124, 706 (1977).

65. Wagman, D. D., W. H. Evans, V. B. Parker, I. Halow, S. M. Bailey, and R. H. Schumm. "Selected Values of Chemical Thermodynamic Properties. Tables for the First Fifty-Three Elements in Standard Order of Arrangement." NBS Technical Notes 270-3 and 270-4. Washington, D. C., National Bureau of Standards (1968).

66. Warshay, Marvin, and Lyle Wright. "Cost and Size Estimates for a Redox Bulk Energy Storage Concept." Journal of the Electrochemical Society, 124, 173 (1977).

67. Weast, Robert C. (editor). Handbook of Chemistry and Physics, 51st. Ed. Chemical Rubber Co., Cleveland, Ohio (1971).

68. Wehner, J. F., and R. H. Wilhelm. "Boundary conditions of a flow reactor." Chemical Engineering Science, 6, 89 (1956).

69. Wenger, R. S., and D. N. Bennion. "Electrochemical concentrating and purifying from dilute copper solutions." Journal of Applied Electrochemistry, 6, 385 (1976).

70. Williams, J. M., and K. B. Keating. "Extended-Surface Electrolysis Removes Metals from Waste Streams." Dupont Innovation, 6, 6 (1975).

71. Wilson, E. J., and C. J. Geankoplis. "Liquid Mass Transfer at Very Low Reynolds Numbers in Packed Beds." Industrial and Engineering Chemistry Fundamentals, 5, 9 (1966).

72. Yao, N. P., and J. R. Birk. "Battery Energy Storage for Utility Load Leveling and Electric Vehicles: A Review of Advanced Secondary Batteries." IECEC Record, p. 1107 (1975).

Appendix A. Logarithmic finite difference approximation

To obtain a more accurate representation of the derivatives in equations 3-28 to 3-31 more of the physics needed to be incorporated in their dependence. This was done by considering the concentration distribution at the limiting current, which decreases exponentially with electrode thickness (see Bennion and Newman (1972), and Newman and Tiedemann (1976)). With this in mind, a new variable was defined:

$$\theta = e^{C} \ . \tag{A-1}$$

Now apply this equation to the upstream boundary condition on the concentration (equation 3-30) to obtain

$$e^{C}\left(1 - D' \frac{dC}{dy}\right) = 1 \ . \tag{A-2}$$

Next introduce the central-difference approximations at the first real mesh point ($j = 2$, mesh point 1 is an image point):

$$\theta_2\left(1 - D' \frac{C_3 - C_1}{2h}\right) = 1 \ , \tag{A-3}$$

or

$$\theta_2\left(1 - \frac{D'}{2h} \ln \frac{\theta_3}{\theta_1}\right) = 1 \ . \tag{A-4}$$

If θ is approximately exponential in distance, then C will be approximately linear, and less error will be introduced when the derivative is approximated by a finite-difference form in the variable C .

Similarly, a central-difference approximation for the axial diffusion and axial dispersion term in equation 3-28 can be derived for any interior mesh point j

$$D' \frac{d^2\theta}{dy^2} = \frac{D'\theta_j}{h^2} \left[\frac{1}{4} \left(\ln \frac{\theta_{j+1}}{\theta_{j-1}} \right)^2 + \ln \left(\frac{\theta_{j+1}\theta_{j-1}}{\theta_j^2} \right) \right] . \qquad \text{(A-5)}$$

The resulting material balance equation at any interior mesh point j now becomes

$$\frac{\theta_j}{2h} \ln \frac{\theta_{j+1}}{\theta_{j-1}} = \frac{D'\theta_j}{h^2} \left[\frac{1}{4} \left(\ln \frac{\theta_{j+1}}{\theta_{j-1}} \right)^2 + \ln \left(\frac{\theta_{j+1}\theta_{j-1}}{\theta_j^2} \right) \right] - J_{Rj} \qquad \text{(A-6)}$$

where

$$J_{Rj} = \frac{\theta_j - P_1 e^{(\alpha_{aR}/\alpha_{cR}+1)\eta'_j}}{1 + e^{\eta'_j}} . \qquad \text{(A-7)}$$

To check a posteriori the overall application of Faraday's law, whereby the integral of the transfer current J_R for the principal reaction should be related to the difference between the inlet and outlet concentrations of the principal reactant, one should use an integration formula for J_R which also takes account of the approximately exponential dependence of J_R on distance.

So that the integrated current is also correct for the side reaction, combine equations 3-28 and 3-29 by eliminating J_R from both equations to yield

$$\frac{d}{dy}\left(\frac{1}{P_2}\frac{d\eta'}{dy} + \theta - D'\frac{d\theta}{dy}\right) = J_S \ , \qquad \text{(A-8)}$$

where

$$J_S = P_3 \exp\left(-\alpha_{cS}\eta'/\alpha_{cR}\right)\left[1 - P_4 \exp\left(\frac{\alpha_{aS} + \alpha_{cS}}{\alpha_{cR}}\eta'\right)\right] \ . \qquad \text{(A-9)}$$

Next express the outer-derivative in equation A-8 as a central-difference written between points halfway between mesh points:

$$\frac{1}{h}\left[\left(\frac{1}{P_2}\frac{d\eta'}{dy} + \theta - D'\frac{d\theta}{dy}\right)_{j+\frac{1}{2}} - \left(\frac{1}{P_2}\frac{d\eta'}{dy} + \theta - D'\frac{d\theta}{dy}\right)_{j-\frac{1}{2}}\right] = J_S \ . \qquad \text{(A-10)}$$

Now express the terms $\theta - D'd\theta/dy$ halfway between two mesh points using equation A-1 and the values of θ at the adjacent mesh points (see also equation A-2):

$$\left(\theta - D'\frac{d\theta}{dy}\right)_{j+\frac{1}{2}} = \sqrt{\theta_j\theta_{j+1}}\left(1 - \frac{D'}{h}\ln\frac{\theta_{j+1}}{\theta_j}\right) , \qquad \text{(A-11)}$$

and

$$\left(\theta - D'\frac{d\theta}{dy}\right)_{j-\frac{1}{2}} = \sqrt{\theta_j\theta_{j-1}}\left(1 - \frac{D'}{h}\ln\frac{\theta_j}{\theta_{j-1}}\right) . \qquad \text{(A-12)}$$

With these approximations and a central-difference expression for the derivative of η' , the resulting equation for the potential at any interior mesh point j becomes

$$\frac{1}{P_2}\frac{\eta'_{j+1}+\eta'_{j-1}-2\eta'_j}{h^2}+\frac{\sqrt{\theta_j\theta_{j+1}}}{h}\left(1-\frac{D'}{h}\ln\frac{\theta_{j+1}}{\theta_j}\right)-\frac{\sqrt{\theta_j\theta_{j-1}}}{h}\left(1-\frac{D'}{h}\ln\frac{\theta_j}{\theta_{j-1}}\right)$$

$$= J_{Sj} \quad . \qquad \text{(A-13)}$$

Similarly, to treat the upstream boundary condition for the potential, integrate equation A-8 from zero to $h/2$ to yield

$$\left(\frac{1}{P_2}\frac{d\eta'}{dy}+\theta-D'\frac{d\theta}{dy}\right)_{h/2}-\left(\frac{1}{P_2}\frac{d\eta'}{dy}+\theta-D'\frac{d\theta}{dy}\right)_o=\frac{h}{2}J_{Sj} \quad . \qquad \text{(A-14)}$$

Use the same approximations as above for $y = h/2$ and use the boundary conditions in equation 3-30 to obtain (for $j = 2$)

$$\frac{2}{h}\frac{1}{P_2}\frac{\eta'_{j+1}-\eta'_j}{h}+\frac{2}{h}\sqrt{\theta_j\theta_{j+1}}\left(1-\frac{D'}{h}\ln\frac{\theta_{j+1}}{\theta_j}\right)-\frac{2}{h}\left(\frac{P_5}{P_2}I^*+1\right)=J_{Sj} \quad . \qquad \text{(A-15)}$$

With equation A-13 at the interior mesh points, this corresponds then to a trapezoidal integration of the transfer current J_S over the thickness of the porous electrode.

The governing finite-difference equations A-6 and A-13 along with the upstream boundary conditions A-4 and A-15 were then linearized about a trial solution and solved simultaneously with the downstream boundary condition for θ and η' using Newman's technique (Newman (1973), Appendix C). The new approximations to the derivatives in concentration provided accurate values for θ and η' at the mesh points without introducing anomalous values for the integrated current.

Appendix B. Macroscopic description of porous electrodes*

Flooded-porous electrodes can be modeled as a superposition of two-continua, one the matrix phase, the other the solution phase (this disregards any geometric detail of the pore). Therefore, the quantities to be defined in this appendix will be assumed to be continuous functions of time and space coordinates. In this treatment, both phases are present at any point in space.

Average quantities. Consider a small volume V somewhere within the electrode (shown schematically in Figure 1).

The porosity or void fraction ε is

$$\varepsilon = \frac{1}{V} \int^{V_{pore}} dV' = \frac{V_{pore}}{V} . \qquad (B-1)$$

Define $\langle c_i \rangle$ the solution-phase concentration of species i (simply written as c_i in chapters 2 through 6), averaged over the volume of the solution in the pores:

$$\langle c_i \rangle = \frac{1}{V_{pore}} \int^{V_{pore}} c_i dV' . \qquad (B-2)$$

The superficial concentration $\varepsilon\langle c_i \rangle$ averaged over the volume of the pores and matrix is then

---

*This derivation was done by my research director Professor John Newman. It appears only in one other reference (Dunning (1971)). The author is grateful to Professor Newman for permission to use the derivation, because it elucidates the physical meaning of the equations assumed in this thesis.

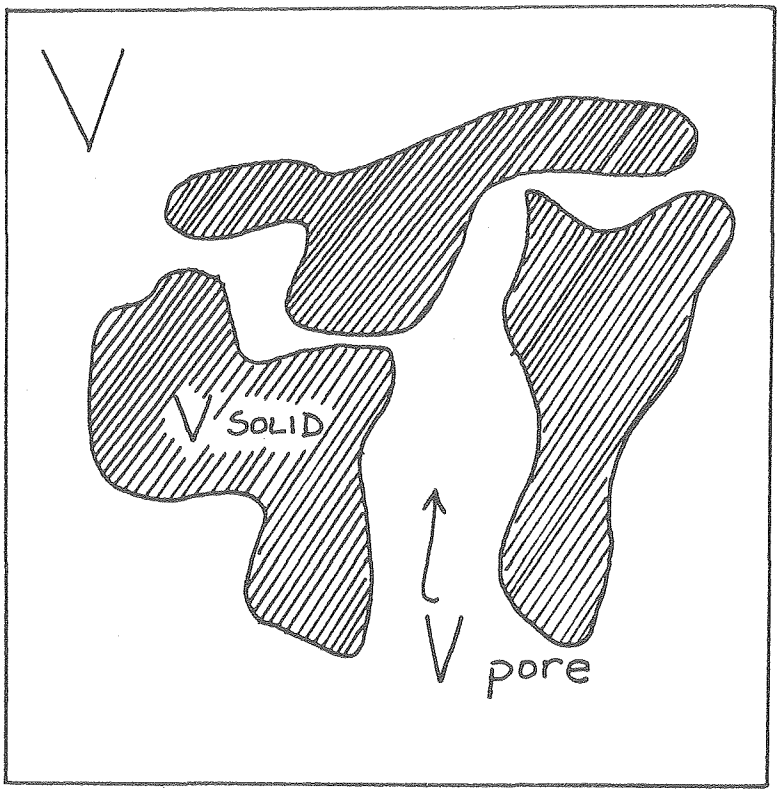

Figure B-1.

Small volume V of a porous electrode containing pore volume and solid volume.

XBL 796-10075

$$\varepsilon\langle c_i\rangle = \frac{1}{V}\int^{V_{pore}} c_i dV' = \frac{1}{V}\int^{V} c_i dV' \quad , \tag{B-3}$$

where, for flow-through porous electrodes $\langle c_i\rangle$ is the preferred concentration, because it is the cup average concentration and is continuous as the stream leaves the electrode.

Further, define j_{in} as the normal component of the flux of species i at the pore-wall interface, relative to the velocity of the pore-wall interface, pointing in the direction of the solution (shown schematically in Figure 2):

$$j_{in} = \underline{n}\cdot(\underline{N}_i - c_i\underline{v}_w) \quad , \tag{B-4}$$

where, $\underline{n}$ is a unit normal vector pointing into the solution, v_w is the velocity of the pore wall, and $\underline{N}_i$ is the total flux of species i .

The interfacial area between the solution and the matrix is then

$$A = -\int^{S_w} \underline{n}\cdot d\underline{S}' = \int^{S_w} \underline{n}\cdot\underline{n} dS' = \int^{S_w} dS' \quad , \tag{B-5}$$

where, S_w refers to the pore walls and $d\underline{S}'$ points out of the solution into the matrix.

The specific interfacial area is

$$a = A/V \quad , \tag{B-6}$$

where, again V is the total volume (shown schematically in Figure 1).

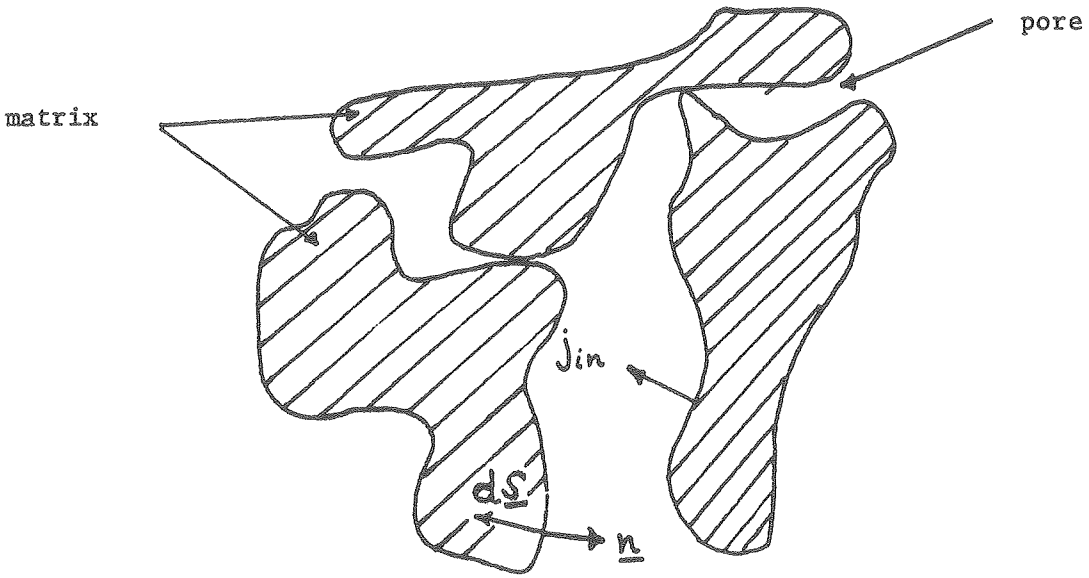

Figure B-2.

Sign conventions: unit vector $\underline{n}$ and normal component of pore-wall flux pointing into the solution and the element of interfacial area $\underline{ds}$ pointing out of the solution.

XBL 796-10076

The average value of j_{in} averaged over the interfacial area, denoted by $\langle j_{in} \rangle$ is

$$\langle j_{in} \rangle = \frac{\int_{S_w} j_{in} \underline{n} \cdot d\underline{S}'}{\int_{S_w} \underline{n} \cdot d\underline{S}'} = -\frac{1}{A} \int_{S_w} (\underline{N}_i - c_i \underline{v}_w) \cdot d\underline{S}' \ . \qquad \text{(B-7)}$$

An expression for the transfer of species i from the matrix phase to the solution phase is then obtained from equation 6 with the result

$$a\langle j_{in} \rangle = -\frac{1}{V} \int_{S_w} (\underline{N}_i - c_i \underline{v}_w) \cdot d\underline{S}' \ . \qquad \text{(B-8)}$$

[In equation 3-1 (the equation of continuity for the primary reactant R) this was written as a j_{Rn} .]

Now, define $\underline{N}_i$ as the average flux of a species i in the pore solution averaged over the cross-sectional (superficial) area.

Next, consider a plane surface cutting the porous electrode, then

$$N_i \cdot \underline{n} = \frac{\int_S \underline{n} \cdot \underline{N}_i dS'}{\int_S dS'} = \frac{\int_{S_{pores}} \underline{n} \cdot \underline{N}_i dS'}{\int_S dS'} \ , \qquad \text{(B-9)}$$

where, $\underline{n}$ is perpendicular to the plane of area S and S_{pore} is the part of the plane cutting the pore volume rather than the solid matrix.

Thus, $\langle N_i \rangle$ is the average superficial flux of species i in the solution (pore) phase, but referred to the projected area of the entire plane rather than to the area of an individual phase. [In equation 3-1 for the primary reactant R, $\langle \underline{N}_i \rangle$ was written as N_R.]

Current. In the solid matrix phase, the movement of electrons is governed by Ohm's law

$$\underline{i}_1 = -\sigma \nabla \Phi_1 \quad , \tag{B-10}$$

where, Φ_1 and $\underline{i}_1$ are the potential and current density in the matrix phase, referred to the superficial area (not to the area of an individual phase).

In the pore phase the superficial current density is denoted by $\underline{i}_2$ and is due to the movement of charged solutes

$$\underline{i}_2 = F \sum_i z_i \langle \underline{N}_i \rangle \quad . \tag{B-11}$$

Material balance. The differential material balance for a species i within the solution, in the absence of homogeneous chemical reaction is

$$\frac{\partial c_i}{\partial t} = -\nabla \cdot \underline{N}_i \quad , \tag{B-12}$$

where c_i and $\underline{N}_i$ are the concentration and total flux of a species i at any point within the pore. Next, integrate equation 12 over the volume of the pores to get

$$\int_{V_{pore}} \frac{\partial c_i}{\partial t} \, dV' = - \int_{V_{pore}} \nabla \cdot \underline{N}_i \, dV' \ . \qquad \text{(B-13)}$$

Then, apply the Gauss-Ostrogradskii (divergence) theorem

$$\oint \underline{F} \cdot d\underline{S}' = \int dV \ \nabla \cdot \underline{F} \ , \qquad \text{(B-14)}$$

to obtain

$$\int_{V_{pore}} \frac{\partial c_i}{\partial t} \, dV' = - \oint \underline{N}_i \cdot d\underline{S}' = - \int_{S_{pore}} \underline{N}_i \cdot d\underline{S}' - \int_{S_w} \underline{N}_i \cdot d\underline{S}' \ , \qquad \text{(B-15)}$$

where the integral over the surface of the pore volume is comprised of the pore cross-sectional area S_{pore} and the area S_w with the matrix. The integral over the pore cross section can also include the total superficial area S of the volume element V because $\underline{N}_i$ can be taken to be zero within the matrix phase. This allows the average flux $\langle \underline{N}_i \rangle$ in equation 9 to be introduced into first term on the right-hand side of equation 15:

$$\int_{S_{pore}} \underline{N}_i \cdot d\underline{S}' = \oint_S \underline{N}_i \cdot d\underline{S}' = \oint_S \langle \underline{N}_i \rangle \cdot d\underline{S}' \ . \qquad \text{(B-16)}$$

Again, apply the divergence theorem to obtain

$$\oint_S \langle \underline{N}_i \rangle \cdot d\underline{S}' = \int_V \nabla \cdot \langle \underline{N}_i \rangle dV' = V \ \nabla \cdot \langle \underline{N}_i \rangle \ . \qquad \text{(B-17)}$$

It should be born in mind that the average quantities are based on a volume V (shown schematically in Figure 1) which is large compared to the pore structure and small compared to the regions over which considerable macroscopic variation occur.

The equation of continuity for a species i is obtained by differentiating equation 3 with respect to time

$$\frac{\partial \varepsilon \langle c_i \rangle}{\partial t} = \frac{1}{V} \int^{V_{pore}} \frac{\partial c_i}{\partial t} \, dV' + \frac{1}{V} \int^{S_w} c_i \underline{v}_w \cdot d\underline{S}' \ . \qquad \text{(B-18)}$$

The last term expresses the fact that the pore volume may be changing with time. Next, substitute equation 15 for the first term on the right-hand side of equation 18

$$\frac{\partial \varepsilon \langle c_i \rangle}{\partial t} = - \frac{1}{V} \left[\int^{S_{pore}} \underline{N}_i \cdot d\underline{S}' + \int^{S_w} \underline{N}_i \cdot d\underline{S}' \right] + \frac{1}{V} \int^{S_w} c_i \underline{v}_w \cdot d\underline{S}' \ . \qquad \text{(B-19)}$$

It then follows from equations 16 and 17 that

$$\frac{\partial \varepsilon \langle c_i \rangle}{\partial t} = - \nabla \cdot \langle \underline{N}_i \rangle - \frac{1}{V} \int^{S_w} (\underline{N}_i - c_i \underline{v}_w) \cdot d\underline{S}' \ , \qquad \text{(B-20)}$$

and finally from equation 8 we get the material balance for species i (including the solvent):

$$\frac{\partial \varepsilon \langle c_i \rangle}{\partial t} = a \langle j_{in} \rangle - \nabla \cdot \langle \underline{N}_i \rangle \ . \qquad \text{(B-21)}$$

This equation states that the increase in concentration with time at any point within the porous electrode is due to transfer of a species from the matrix phases to the solution phase ($a\, j_{in}$) because the species is involved in electrode processes (faradaic electrochemical reactions or double-layer charging) and because the species moves toward the point (the negative of the divergence of the flux $\langle \underline{N}_i \rangle$). The term, $a\langle j_{in} \rangle$, resembles the term which would describe the bulk production of a species by homogeneous chemical reaction, this occurs because of the averaging process.

Faraday's law. An electrode reaction j can be expressed in abstract form as follows

$$\sum_i s_{ij} M_i^{z_i} \rightarrow n_j e^- \,, \tag{B-22}$$

where i refers to the species that participate in reaction j. Faraday's law is then expressed as

$$j_{in} = -\sum \frac{s_{ij}}{n_j F} i_{nj} \,, \tag{B-23}$$

where i_{nj} is the average transfer current density (from the matrix phase to the solution phase) due to reaction j. This may be related to the superficial transfer current per unit volume of the electrode $\nabla \cdot \underline{i}_2$ as follows

$$\nabla \cdot \underline{i}_2 = a \sum i_{nj} \,. \tag{B-24}$$

Appendix C. Linearization of the governing equations

The purpose of this appendix is to provide the linearized form of the governing differential equations, which are used in the computer programs found in Appendix D.

The equations are linearized by approximating the non-linear terms with a Taylor expansion around a trial solution neglecting terms higher than first order:

$$f(x_1,x_2,x_3, \ldots, x_n) \sim f(x_1,x_2,x_3, \ldots, x_n)\Big|_0 + \sum_{i=1}^{n} \left(x_i - x_i^o\right)\left(\frac{\partial f}{\partial x_i}\right)\Big|_0 , \tag{C-1}$$

where the known trial values are denoted by a naught 0 .

Material balance. In Appendix A the material balance equation for a metal deposition reaction written in logarithmic finite difference form was given by equations A-6 and A-7:

$$D' \frac{\theta_j}{h^2}\left[\frac{1}{4}\left(\ln \frac{\theta_{j+1}}{\theta_{j-1}}\right)^2 + \ln\left(\frac{\theta_{j+1}\theta_{j-1}}{\theta_j^2}\right)\right] - \frac{\theta_j}{2h} \ln \frac{\theta_{j+1}}{\theta_{j-1}} - \frac{\theta_j - P_1 e^{(\alpha_{aR}/\alpha_{cR}+1)\eta'_j}}{1 + e^{\eta'_j}} = 0 . \tag{C-2}$$

The linear form of each term is given by

Term 1.

$$D' \frac{\theta_j}{h^2}\left[\frac{1}{4}\left(\ln\frac{\theta_{j+1}}{\theta_{j-1}}\right)^2 + \ln\left(\frac{\theta_{j+1}\theta_{j-1}}{\theta_j^2}\right)\right] \approx$$

$$\frac{D'}{h^2}\left\{\left[\frac{1}{4}\left(\ln\frac{\theta^o_{j+1}}{\theta^o_{j-1}}\right)^2 + \ln\left(\frac{\theta^o_{j+1}\theta^o_{j-1}}{\theta^{o\,2}_j}\right) - 2\right]\theta_j\right.$$

$$\left. + \left[\frac{\theta^o_j}{2\theta^o_{j+1}}\ln\left(\frac{\theta^o_{j+1}}{\theta^o_{j-1}}\right) + \frac{\theta^o_j}{\theta^o_{j+1}}\right]\theta_{j+1} + \left[-\frac{\theta^o_j}{2\theta^o_{j-1}}\ln\left(\frac{\theta^o_{j+1}}{\theta^o_{j-1}}\right) + \frac{\theta^o_j}{\theta^o_{j-1}}\right]\theta_{j-1}\right\} . \quad (C\text{-}3)$$

Term 2.

$$\frac{\theta_j}{2h}\ln\frac{\theta_{j+1}}{\theta_{j-1}} \approx \frac{1}{2h}\left\{\left[\ln\frac{\theta^o_{j+1}}{\theta^o_{j-1}}\right]\theta_j + \left[\frac{\theta^o_j}{\theta^o_{j+1}}\right]\theta_{j+1} + \left[-\frac{\theta^o_j}{\theta^o_{j-1}}\right]\theta_{j-1}\right\} . \quad (C\text{-}4)$$

Term 3.

$$\frac{\theta_j - P_1 e^{(\alpha_{aR}/\alpha_{cR}+1)\eta'_j}}{1 + e^{\eta'_j}} \approx \left[1/\left(1 + e^{\eta'^o_j}\right)\right]\theta_j$$

$$- \left\{e^{\eta'^o_j}\theta^o_j + P_1 e^{(\alpha_{aR}/\alpha_{cR}+1)\eta'^o_j}\left[1 + \left(1 + e^{\eta'^o_j}\right)\alpha_{aR}/\alpha_{cR}\right]\right\}\eta'_j/\left(1 + e^{\eta'^o_j}\right)^2$$

$$+ \left\{e^{\eta'^o_j}\theta^o_j + P_1 e^{(\alpha_{aR}/\alpha_{cR}+1)\eta'^o_j}\left[1 + \left(1 + e^{\eta'^o_j}\right)\alpha_{aR}/\alpha_{cR}\right]\right\}\eta'_j/\left(1 + e^{\eta'^o_j}\right)^2$$

$$- P_1 e^{(\alpha_{aR}/\alpha_{cR}+1)\eta'^o_j}/\left(1 + e^{\eta'^o_j}\right) . \quad (C\text{-}5)$$

For a redox reaction with a cathodic reactant the third term in equation 2 becomes

$$\frac{\theta_j - [1 + (1 - \theta_j)/\theta_{Pf}]P_1 e^{(1+\alpha_{aR}/\alpha_{cR})\eta'_j}}{1 + e^{\eta'_j} + P_1 P_7/\theta_{Pf} e^{(1+\alpha_{aR}/\alpha_{cR})\eta'_j}} , \qquad (C\text{-}6)$$

which has the following linear form

$$\left[1 + \frac{P_1 e^{(1+\alpha_{aR}/\alpha_{cR})\eta'^{o}_j}}{\theta_{Pf}}\right]\theta_j/D^o + [-B^o]\eta'_j$$

$$+ B^o\eta'^{o}_j - (1 + 1/\theta_{Pf})P_1 e^{(1+\alpha_{aR}/\alpha_{cR})\eta'^{o}_j}/D^o , \qquad (C\text{-}7)$$

where

$$D^o = 1 + e^{\eta'^{o}_j} + \frac{P_1 P_7}{\theta_{Pf}} e^{(1+\alpha_{aR}/\alpha_{cR})\eta'^{o}_j}$$

$$B^o = \text{THET}\ (1 + \alpha_{aR}/\alpha_{cR})/D^o + \left[e^{\eta'^{o}_j} + \frac{P_1 P_7}{\theta_{Pf}}(1 + \alpha_{aR}/\alpha_{cR})e^{(1+\alpha_{aR}/\alpha_{cR})\eta'^{o}_j}\right]$$

$$\times (\theta^o_j - \text{THET})/D^{o^2}$$

$$\text{THET} = \left[1 + 1/\theta_{Pf}(1 - \theta^o_j)\right]P_1 e^{(1+\alpha_{aR}/\alpha_{cR})\eta'^{o}_j} . \qquad (C\text{-}8)$$

Charge balance equation. For a cathodic reactant the potential distribution was given by either equation 3-29 or 5- :

$$\left(\frac{1}{P_2}\frac{d^2\eta'_j}{dy^2} - J_{Rj}\right) - P_3 \exp(-\alpha_{cS}\eta'_j/\alpha_{cR})\left[1 - P_4 \exp\left(\frac{\alpha_{aS} + \alpha_{cS}}{\alpha_{cR}}\eta'_j\right)\right] = 0 , \qquad (C\text{-}9)$$

where J_{Rj} is given by either equation 5 or equation 6, which depends on whether a metal deposition reaction or a redox reaction is being considered. Only the last term in equation 9 remains to be linearized and is given by

$$P_3 e^{-\alpha_{cS}\eta_j'/\alpha_{cR}} - P_3P_4 e^{\alpha_{aS}\eta_j'/\alpha_{cR}} \approx P_3\left[-\frac{\alpha_{cS}}{\alpha_{cR}} e^{-\alpha_{cS}\eta_j'^{o}/\alpha_{cR}}\eta_j'\right.$$

$$\left. + e^{-\alpha_{cS}\eta_j'^{o}/\alpha_{cR}}\left(1 + \frac{\alpha_{cS}}{\alpha_{cR}}\eta_j'^{o}\right)\right] - P_3P_4\left[\frac{\alpha_{aS}}{\alpha_{cR}} e^{\alpha_{aS}\eta_j'^{o}/\alpha_{cR}}\eta_j'\right.$$

$$\left. + e^{\alpha_{aS}\eta_j'^{o}/\alpha_{cR}}\left(1 - \frac{\alpha_{aS}}{\alpha_{cR}}\eta_j'^{o}\right)\right] . \qquad \text{(C-10)}$$

For the case of a redox reaction with an anodic reactant P_1, P_2, P_3, and P_4 become P_1', P_2', P_3', and P_4', and α_{cR} is set equal to α_{aR} and <u>vice versa</u>, as discussed in chapter 6.

Appendix D. Listing of Computer Programs

This appendix contains the computer programs used to calculate the results in Chapters 3, 4, and 6. Also provided, is a key to the pertinent computer notation.

Program FRACI calculates for a cathodic metal-ion reactant distributions of concentration, current density and potential for a flow-through porous electrode (current parallel to the fluid flow). Two different listings of this program are given. The first listing is for either an upstream counterelectrode, downstream current collector (UD) or vice versa (DU). The second listing is for either an upstream counterelectrode, upstream current collector (UU) or a downstream counterelectrode, downstream current collector (DD). To run any one of these cases see notation for program FRACI and program REDOX under NCELEC. The two listings for program FRACI can be easily identified by the comment cards at the top of the programs.

Program REDOX optimizes the behavior of a flow redox cell (current parallel to the fluid flow) with respect to I_d, I_c and v_c using equation 6-53 as a criteria. The notation is similar to that found in program FRACI.

Both program FRACI and program REDOX require subroutines BAND(J) and MATINV (see Newman (1973), Appendix C for a discussion of these routines). A listing of each of these subroutines is provided, they are listed once where they first appear.

Program REDOX2 optimizes the behavior of a flow redox cell (current perpendicular to the fluid flow) with respect to V_d using equation 6-53 as a criteria.

Notation for program FRACI and program REDOX

ALPHA	α_{aR}
ALPHAL	$\alpha L = (a\ k_m/v)L$
ALPHA2	α_{aS}
ALPHC	α_{cR}
ALPHC2	α_{cS}
CCL	chloride ion concentration in the feed, M
CFC	feed concentrations on charge, mole/cm^3
CFD	feed concentrations on discharge, mole/cm^3
CH	hydrogen ion concentration in the feed, M
COLD	previous value of unknown
CPC	product concentrations after charge, mole/cm^3
CPD	product concentrations after discharge before mixing, mole/cm^3
CPDM	product concentrations after discharge and after mixing, mole/cm^3
CPF	c_{Pf}
CPW	c_{Pw}
CRF	c_{Rf}
CRFN	feed concentration of the limiting reactant to the negative electrode on discharge, mole/cm^3
CRFP	feed concentration of the limiting reactant to the positive electrode on discharge, mole/cm^3
CRPN	feed concentration of the product species to the negative electrode on discharge, mole/cm^3
CRPP	feed concentration of the product species to the positive electrode on discharge, mole/cm^3

CRW	c_{Rw}
CVC	cell voltage on charge, V
CVD	cell voltage on discharge, V
DA	D_a
DI	D_i
DP	D'
DPHI2	potential drop in the solution across the electrode, V
DPOT	damping constant for η'
DR	D_R
EFF	current efficiency
EPSIL	ϵ
ETA	η
ETAP	η'
F	F
FAC	damping factor for θ
H	mesh size
JCOUNT	number of iterations
JT	mesh point number at which logarithmic finite difference approximations change to linear finite difference approximations
NCELEC	flag for counterelectrode and current collector placement, NCELEC $\geq$ 1 → UD or UU; NCELEC < 1 → DU or DD
NJ	total number of mesh points
NM	NJ-1

OCUEFC	overall current efficiency on charge
OCUEFD	overall current efficiency on discharge
PCl2	partial pressure of Cl_2, atm
PHI1	Φ_1
PHI2	Φ_2
PIH2	partial pressure of H_2, atm
PWC	power density on charge, W/cm^2
PWD	power density on discharge, W/cm^2
P1	P_1
P2	P_2
P3	P_3
P4	P_4
P5	P_5
P6	P_6
P7	P_7
QI	i
QISTAR	I*
QIO1	$i_{oR,ref}$
QIO2	$i_{oS,ref}$
QJISTR	1/I*
QKAPAO	κ_o
QKAPPA	κ
QKM	k_m
QKR	k_{mR}
QL	L

QLS	thickness of the separator, cm
QN	n
R	R
S	a
SIGMA	σ
SR	s_R
SUA	superficial area of the electrode
T	T
TAU	τ
THETAP	c_{Pf}/c_{Rf}
THETAW	θ_w
THETA2	θ_p
TI	total current, A
TRAN1	di^*_{2R}/dy
TRAN2	di^*_{2S}/dy
UCAL	open circuit potential of the main reaction at the upstream feed conditions relative to a saturated calomel reference electrode, V
U1	U_R
U2	$U_S - U_R$
V	v
Y1	x/L

Input parameters for program REDOX2

QLS	L_s	separator thickness, cm
RS	R_s	separator resistivity, ohm-cm
DIF (I)	D_{O+}, D_{R+}, D_{R-}, D_{O-}	

Each of the following parameters are required for first the positive electrode and then the negative electrode.

A	a	
D	d	
UTH	U^{θ}	
QN	n	
S	s	
QKAPAO	κ	
SIGMA	σ	
EPSIL	ε	
RHO	ρ	
QMU	μ	
DATIO	$i_{o,ref}$	
CF	c_{Of}	concentration of reactant species on discharge
CPF	c_{Pf}	concentration of product species on discharge

```
      PROGRAM FRACI(INPUT,OUTPUT)

C     CALCULATES DISTRIBUTIONS OF CURRENT,POTENTIAL,AND CONCENTRATION
C     FOR JO AND OU CONFIGURATIONS

      DIMENSION A(2,2),B(2,2),C(2,1003),D(2,5),G(2),X(2,2),Y(2,2)
      DIMENSION ETA(1003),TRAN1(1003),TRAN2(1003),TRANT(1003),EFF(1003),
     1COLD(2,1003),PH2(1003),PH2CAL(1003),THETAW(1003),CURR1(1003),Y1(10
     103),PHI1(1003),PHI2(1003)
      COMMON A,B,C,D,G,X,Y,N,NJ,JCOUNT
  101 FORMAT(F15.0)
  102 FORMAT(I1,I3,I2)
  103 FORMAT(1H0,*S = *,F7.3,2X,*(CM-1)*,2X,*EPSILON = *,F3.2,2X,*V = *,
     1E09.4,2X,*(CM/SEC)*/1H0,*OR = *,E09.4,2X,*(CM**2/SEC)*,2X,*KAPAO =
     1*,E09.4,2X,*(MHO/CM)*,2X,*SIGMA = *,E09.4,2X,*(MHO/CM)*/1H0,*SR =
     1*,F4.1,2X,*N = *,F3.1,2X,*F = *,F6.0,2X,*(C/EQ)*,2X,*R = *,F7.5,2X
     1,*(J/MOLE-DEG K)*,2X,*T = *,F8.4,2X,*(DEG K)*/1H0,*I01 = *,E09.4,2
     1X,*(AMPS/CM**2)*,2X,*I02 = *,E09.4,2X,*(AMPS/CM**2)*,2X,*SA =*,F11.6
     1,2X,*(CM**2)*/1H0,*ALPHA-A =*,F4.2,2X,*ALPHA-C = *,F4.2,2X,*ALPHA-A
     12 = *,F4.2,2X,*ALPHA-C2 = *,F4.2,2X,*DELTA U = *,F5.3,2X,*(VOLTS)*
     1)
  104 FORMAT(1H0,05X,*CRF = *,E09.4,2X,*(MOLES/CM**3)*,2X,*I = *,E10.4,2X
     1,*(AMPS/CM**2)*)
  105 FORMAT(1H0,*P1 = *,E15.8/1H0,*P2 = *,E15.8/1H0,*P3 = *,E15.8/1H0,*
     1P4 = *,E15.8/1H0,*P5 = *,E15.8/1H0,*P6 = *,E15.8/1H0,*DP = *,E15.8
     1)
  106 FORMAT(1H0,05X,*ISTAR = *,E10.4,2X,*KM = *,E09.4,2X,*(CM/SEC)*,2X,
     1*DA = *,E09.4,2X,*(CM**2/SEC)*/)
  107 FORMAT(1H0,*L = *,E09.4,2X,*(CM)*,2X,*NJ = *,I3,2),*H = *,E09.4,2X
     1,*ALPHAL = *,E9.4,2X,*KAPPA/SIGMA = *,E10.4/)
  108 FORMAT(1H0,*THE NEXT RUN DID NOT CONVERGE*)
  109 FORMAT(1H0,15X,*THETA*,13X,*ETAPRIME*)
  110 FORMAT(10X,E15.8,5X,E15.8)
  111 FORMAT(1H0,I5)
  112 FORMAT(5X,*X/L*,09X,*THETA*,07X,*ETAPRIME*,07X,*ETA*,06X,*TRANS CU
     1RR 1*,1X,*TRANS CURR 2*,3X,*TOT CURR*,5X,*CURR EFF*,6X,*THETAW*/)
  113 FORMAT(09(E12.6,1X))
  114 FORMAT(1H0,3(E15.8,2X))
  115 FORMAT(1X,*VOP = *,F7.4,2X,*(V)*,2X,*(PHI2L-PHI20) = *,F7.4,1X,*(
     1V)*,2X,*CRWL = *,E9.4,2X,*(MOLES/CM**3)*,2X,*ITOT = *,F7.4,1X,*(AMP
     1S)*,2X,*NO. ITERATIONS*,I3/)
  116 FORMAT(1H1)
  117 FORMAT(F15.0,I2)
  118 FORMAT(1H1,4X,*X/L*,05X,*CURR1*/)
  119 FORMAT(2F10.7)
  120 FORMAT(1H0,50X,*DOWNSTREAM  COUNTER ELECTRODE*/1H0,50X,*UPSTREAM C
     1URRENT COLLECTOR*/)
  121 FORMAT(1H0,4X,*X/L*,09X,*PHI1*,09X,*PHI2*,10X,*PH2*,09X,*PH2CAL*/)
  122 FORMAT(5(E12.6,1X))
  123 FORMAT(1H0,50X,*UPSTREAM COUNTER ELECTRODE*/1H0,50X,*DOWNSTREAM CU
     1RRENT COLLECTOR*/)
      PRINT 116
      JDIST=-1
C     IF JDIST .GE. ONE NORMALIZED DEPOSIT DISTRIBUTION IS PRINTED
      READ 101,S,EPSIL,V,DR,QKAPAO,SIGMA,SR,QN,F,R,T ,ALPHA,ALPHC,ALPHA2
     1,ALPHC2,SUA
```

```
      READ 101,CRF  $  READ 102,N,NJ,NCELEC $ NJ0=NJ $ QL0=0.1
      QKM=4.369E-03*V**0.5475
      QKM=1.09/EPSIL*(S*DR/(6.*(1.-EPSIL)))**(2./3.)*V**(1./3.)
      QKM=0.0001922
      ETAP=-6.0
      GAM=0.75 $ PIH2=1.0E-24 $ CH=2.82E-03
      DATI0=0.38E-04  $  DATI02=0.70E-05
      QI01=DATI0*(CRF*1000./0.1)**GAM
      QI02=DATI02*PIH2**(0.5*ALPHC2)*CH**(1.0-ALPHC2)
      U1 = 0.337 - SR*R*T/QN/F*ALOG(CRF*1000./0.99707)
      U2 = 0.0 - 0.5*R*T/F*ALOG(PIH2/CH**2)-U1
      UCUCAL = 0.337-.2676+0.5*R*T/F*ALOG(CRF*1001.*4.17**2/.99707**3)
      PRINT 103,S,EPSIL,V,DR,QKAPA0,SIGMA,SR,QN,F,R,T,QI01,QI02,SUA,ALPH
     1A,ALPHC,ALPHA2,ALPHC2,U2
      QKAPPA = QKAPA0*EPSIL**1.5
      DA = 3.*(1. - EPSIL)*V/S/EPSIL
      P1=1. $ P2=1. $ P3=1. $ P4=1. $ P5=1. $ P6=1.
      QSIGMA=0.155
      IF(NCELEC .GE. 1)  GO TO 902
  901 P5P=P6 $ P6P=P5 $ PRINT 120 $  P5= P5P  $  P6= P6P $ GO TO 99
  902 PRINT 123
   99 READ 117,QI,JSTAR $ IF(JSTAR .LT. 0)  STOP
      READ 101,QL $ IF(QL .LE. QL0)  GO TO 97
      QSIGMA=QSIGMA+0.005  $ SIGMA=QKAPPA/QSIGMA
      SIGMA=10000.
      DELTA=QKAPPA/SIGMA
      P1 = (-SR*QI01/(QN*F*QKM*CRF))**(1.+ALPHA/ALPHC)
      P2 = CRF*QN*F/SR*V**2 /S/QKM*ALPHC*F/R/T*(1./QKAPPA + 1./SIGMA)
      P3 = -SR*QI02/QN/F/QKM/CRF*(-QN*F*QKM*CRF/SR/QIC1)**(ALPHC2/ALPHC)
     1*EXP(ALPHC2*F*U2/R/T)
      P4 = (-SR*QI01/(QN*F*QKM*CRF))**((ALPHA2 + ALPHC2)/ALPHC)*
     1EXP(-(ALPHA2 + ALPHC2)*F*U2/R/T)
      P5 = -P2/(1./QKAPPA + 1./SIGMA)*(1./QKAPPA)
      P6 = -P2/(SIGMA/QKAPPA + 1.0)
      TAU = 3.**(1./3.)
      DP=EPSIL*(DR/TAU**2+DA)*S*QKM/V**2
      PRINT 105,P1,P2,P3,P4,P5,P6,DP
      NJ=QL*NJ0/QL0+3 $ JT=(NJ-3)*7/8+2 $ JLIM=2
   97 H = QL*QKM*S/(V*FLOAT(NJ-3))$ NM=NJ-1
      ALPHAL = S*QKM*QL/V
      PRINT 107,QL,NJ,H,ALPHAL,DELTA
      PRINT 104,CRF,QI
      QISTAR = QI*SR/(QN*F*V*CRF)
      PRINT 106,QISTAR,QKM,DA
      BB = 0.5 + 0.5*SQRT(1.0 + 4.0*DP)
      ITHETA = 1  $  IETAP = 2
      IF(JSTAR .GT. 0)  GO TO 98
      DO 200 J=1,NJ $ BBEXP=EXP(-H*FLOAT(J-2)/BB)/BB
      C(ITHETA,J)=(1.0-QISTAR)*(1.0-BBEXP)+BBEXP  $  IF(QISTAR .GE. 0.99
     1)  C(ITHETA,J)=BBEXP+DP/BB**3*EXP(BB/DP*H*FLOAT(J-NJ+1)-ALPHAL/BB)
  200 C(IETAP,J) = ETAP
   98 JCOUNT = 0
    1 JCOUNT = JCOUNT + 1
      CRAL0=C(IETAP,2)
      J = 0
      DO 2 I=1,N
      DO 2 K=1,N
      Y(I,K) = 0.0
    2 X(I,K) = 0.0
    3 J = J + 1
      DO 4 I=1,N
      CCLD(I,J)=C(I,J)
```

```
      G(I) = 0.0
      DO 4 K=1,N
      A(I,K) = 0.0
      B(I,K) = 0.0
    4 D(I,K) = 0.0
      IF(J.EQ.NJ) GO TO 8 $ IF(J.GT.1) GO TO 7
      D(ITHETA,ITHETA)=1.0-DP/2.0/H*ALOG(C(ITHETA,J+2)/C(ITHETA,J))
      X(ITHETA,ITHETA) = -DP*C(ITHETA,J+1)/2.0/H/C(ITHETA,J+2)
      B(ITHETA,ITHETA)= DP*C(ITHETA,J+1)/2.0/H/C(ITHETA,J)
      G(ITHETA)=1.0
      B(IETAP,IETAP) = -1.0
      GO TO 25
    7 EP = EXP(C(IETAP,J))  $  EPA = EXP(ALPHA*C(IETAP,J)/ALPHC)*EP
      B(ITHETA,IETAP) = (EP*C(ITHETA,J) + P1*EPA*(1. + ALPHA/ALPHC*
     1(1. + EP)))/(1. + EP)**2
      G(ITHETA) = B(ITHETA,IETAP)*C(IETAP,J) - P1*EPA/(1. + EP)
      EPA2 = EXP(ALPHA2*C(IETAP,J)/ALPHC)
      EPC2 = EXP(-ALPHC2*C(IETAP,J)/ALPHC)
      B(IETAP,IETAP) = -2./H**2/P2+P3*(ALPHC2*EPC2+P4*ALPHA2*EPA2)/ALPHC
      G(IETAP) = P3*((1.+ALPHC2*C(IETAP,J)/ALPHC)*EPC2+P4*(ALPHA2*
     1C(IETAP,J)/ALPHC - 1.)*EPA2)
      B(ITHETA,ITHETA) = -2.*DP/H**2 - 1./(1. + EP)
      IF(J.GT.JT) GO TO 21
      CP = 0.5*ALOG(C(ITHETA,J+1)/C(ITHETA,J-1))/H
      COTH = -CP*(1.0 - DP*CP) + DP*ALOG(C(ITHETA,J+1)*C(ITHETA,J-1)/
     1C(ITHETA,J)**2)/H**2
      B(ITHETA,ITHETA)=B(ITHETA,ITHETA)+COTH
      A(ITHETA,ITHETA) = C(ITHETA,J)/H*(0.5 - CP*CP +DP/H)/C(ITHETA,J-1)
      D(ITHETA,ITHETA) = C(ITHETA,J)/H*(-0.5+DP*CP+DP/H)/C(ITHETA,J+1)
      RAT2=C(ITHETA,J+1)/C(ITHETA,J) $ CP2=DP*ALOG(RAT2)/H/2.
      B(IETAP,ITHETA)=(0.5-CP2+DP/H)/H*SQRT(RAT2)*2.0
      D(IETAP,ITHETA)=(0.5-CP2-DP/H)/H/SQRT(RAT2)*2.0
      IF(J .GT. 2)  GO TO 6
      G(IETAP)=G(IETAP)+2.0/H*(P5*QISTAR/P2+1.0)
      D(IETAP,IETAP)=2.0/P2/H**2
      GO TO 25
    6 RAT1=C(ITHETA,J)/C(ITHETA,J-1) $ CP1=DP*ALOG(RAT1)/H/2.
      D(IETAP,ITHETA)=0.5*D(IETAP,ITHETA)
      B(IETAP,ITHETA)=0.5*B(IETAP,ITHETA)+(CP1-.5+DP/H)/H/SQRT(RAT1)
      A(IETAP,ITHETA)=(-0.5+CP1-DP/H)/H*SQRT(RAT1)
      GO TO 24
   21 A(ITHETA,ITHETA) = (DP/H + 0.5)/H
      D(ITHETA,ITHETA) = (DP/H - 0.5)/H
      A(IETAP,ITHETA)=(-0.5-DP/H)/H $ C(IETAP,ITHETA)=(0.5-DP/H)/H
      B(IETAP,ITHETA)=2.0*DP/H**2
   24 A(IETAP,IETAP) = 1./H**2/P2
      D(IETAP,IETAP) = 1./H**2/P2
   25 CONTINUE
      IF(JCOUNT .GT. JLIM)  GO TO 14
      B(ITHETA,ITHETA) = 1.0  $  G(ITHETA) = C(ITHETA,J)
      A(ITHETA,ITHETA) = 0.0  $  C(ITHETA,ITHETA) = 0.0
      X(ITHETA,ITHETA)=0.0  $  B(ITHETA,IETAP) = 0.0
      D(ITHETA,IETAP) = 0.0
   14 CALL BAND(J)
      GO TO 3
    8 B(ITHETA,ITHETA) = 1.0
      Y(ITHETA,ITHETA) = -1.0
      B(IETAP,IETAP) = 1.0
      Y(IETAP,IETAP) = -1.0
      G(IETAP) = -2.*H*P6*QISTAR
   15 CALL BAND(J)
      FAC=10.0  $  DPOT=1.5
```

```
      DO 20 J=1,NJ $ IF(C(ITHETA,J).LT.COLD(ITHETA,J)/FAC) C(ITHETA,J)=
     1COLD(ITHETA,J)/FAC $ IF(C(ITHETA,J).GT.COLD(ITHETA,J)*FAC)
     1C(ITHETA,J)=COLD(ITHETA,J)*FAC
      IF(C(IETAP,J).GT.COLD(IETAP,J)+DPOT) C(IETAP,J)=CCLD(IETAP,J)+DPOT
   20 IF(C(IETAP,J).LT.COLD(IETAP,J)-DPOT) C(IETAP,J)=CCLD(IETAP,J)-DPOT
      IF(JCOUNT .LE. JLIM)  GO TO 1
      CRAL=C(IETAP,2)
      IF(ABS(CRAL - CRAL0).LE.1.E-06*ABS(CRAL)) GO TO 11
      IF(JCOUNT.LE.15) GO TO 1  $ PRINT 108
   11 ETA(NM)=R*T/ALPHC/F*(C(IETAP,NM)-ALOG(-QN*F*QKM*CRF/SR/QI01))
      DO 12 J=2,NM
      ETA(J) = R*T/ALPHC/F*(C(IETAP,J) - ALOG(-QN*F*QKM*CRF/SR/QI01))
      TRAN1(J) = (C(ITHETA,J) - P1*EXP((ALPHA/ALPHC + 1.)*C(IETAP,J)))/
     1(1. + EXP(C(IETAP,J)))
      QNI01=QI01*SR/QN/F/CRF/QKM $THETAW(J)=(C(ITHETA,J)-QNI01*EXP(ALPHA
     1*F/R/T*ETA(J)))/(1.0-QNI01*EXP(-ALPHC*F/R/T*ETA(J)))
      TRAN2(J) = P3*(1. - P4*EXP((ALPHA2 + ALPHC2)/ALPH(*C(IETAP,J)))*
     1EXP(-ALPHC2*C(IETAP,J)/ALPHC)
      TRANT(J) = TRAN1(J) + TRAN2(J)
      EFF(J) = TRAN1(J)/TRANT(J)
      Y1(J)=FLOAT(J-2)/FLOAT(NM-2) $ PHI1(J)=QKAPPA/(QKAPPA+SIGMA)*(ETA(
     1J)-ETA(NM)+QI*QL/QKAPPA*(Y1(J)-1.)) $ PHI2(J)=PHI1(J)-ETA(J)
      PH2(J)=ETA(NM)+PHI2(J)  $  PH2CAL(J)=PHI2(J)-UCUCAL
      IF(NCELEC .GE. 1)  GO TO 12 $ PHI1(J)=QKAPPA/(QKAPPA+SIGMA)*(ETA(J
     1)-ETA(2)-QI/QKAPPA*(1.-Y1)        $ PHI2(J)=PHI1(J)-ETA(J)
      PH2(J)=ETA(NM)+PHI2(J)  $  PH2CAL(J)=PHI2(J)-UCUCAL
   12 CONTINUE $ TI=QI*SUA
      DPHI2=PHI2(NM)-PHI2(2) $ CRW=THETAW(NM)*CRF $ PRINT 115,PH2CAL(NP)
     1,DPHI2,CRW,TI,JCOUNT $ PRINT 112
      PRINT 113,(Y1(J),C(ITHETA,J),C(IETAP,J),ETA(J),TRAN1(J),TRAN2(J),
     1TRANT(J),EFF(J),THETAW(J),J=2,NM,05)
      PRINT 121 $ PRINT 122,(Y1(J),PHI1(J),PHI2(J),PH2(J),PH2CAL(J),J=2,
     1NM,05)
      TRAN1T = 0.0  $  TRAN2T = 0.0  $ TRAP1T = 0.0  $  TRAP2T = 0.0
      IF(QI02 .LE. 1.0E-30)  GO TO 27
      DO 16 J=3,NM
      TRAP1T = TRAP1T + H*(TRAN1(J) + TRAN1(J-1))/2.0
      TRAP2T = TRAP2T + H*(TRAN2(J) + TRAN2(J-1))/2.0
      IF(TRAN1(J)/TRAN1(J-1) .LE. 0.0)  GO TO 17
      IF(TRAN1(J) .EQ. TRAN1(J-1))  GO TO 17
      TRAN1T = H*(TRAN1(J) - TRAN1(J-1))/ALOG(TRAN1(J)/TRAN1(J-1)) +
     1TRAN1T
      GO TO 18
   17 TRAN1T = H*(TRAN1(J) + TRAN1(J-1))/2.0 + TRAN1T
   18 IF(TRAN2(J)/TRAN2(J-1) .LE. 0.0)  GO TO 19
      IF(TRAN2(J) .EQ. TRAN2(J-1))  GO TO 19
      TRAN2T = H*(TRAN2(J) - TRAN2(J-1))/ALOG(TRAN2(J)/TRAN2(J-1)) +
     1TRAN2T
      GO TO 16
   19 TRAN2T = H*(TRAN2(J) + TRAN2(J-1))/2.0 + TRAN2T
   16 CONTINUE
      TRANTT = TRAN1T + TRAN2T
      TRAPTT = TRAP1T + TRAP2T
      PRINT 114,TRAN1T,TRAN2T,TRANTT
      PRINT 114,TRAP1T,TRAP2T,TRAPTT $  GO TO 28
   27 DO 30 J=3,NM
      TRAP1T = TRAP1T + H*(TRAN1(J) + TRAN1(J-1))/2.0
      IF(TRAN1(J) .EQ. TRAN1(J-1))  GO TO 29
      IF(TRAN1(J)/TRAN1(J-1) .LE. 0.0)  GO TO 29
      TRAN1T = H*(TRAN1(J) - TRAN1(J-1))/ALOG(TRAN1(J)/TRAN1(J-1)) +
     1TRAN1T
      GO TO 30
```

```
29 TRAN1T = H*(TRAN1(J) + TRAN1(J-1))/2.0 + TRAN1T
30 CONTINUE
   PRINT 114,TRAN1T,TRAP1T $ QL0=QL $ NJ0=NJ-3
28 IF(JOIST .GE. 1)  GO TO 31  $  GO TO 99
31 DO 26 J=2,NM $ CURR1(J)=TRAN1(J)*ALPHAL/TRAN1T
26 Y1(J)=FLOAT(J-2)/FLOAT(NM-2) $ PRINT 118 $ PRINT 119,(Y1(J),CURR1(
  1J),J=2,NM,05) $ GO TO 99 $ END
```

```
      SUBROUTINE BAND(J)

      DIMENSION A(2,2),B(2,2),C(2,1003),D(2,5),G(2),X(2,2),Y(2,2),
     1E(2,3,1003)
      COMMON A,B,C,D,G,X,Y,N,NJ,JCOUNT
  101 FORMAT (15HODETERM=0 AT J=,I4,*ITERATION =*,I4)
      IF (J-2)  1,6,8
    1 NP1= N + 1
      DO 2 I=1,N
      C(I,2*N+1)= G(I)
      DO 2 L=1,N
      LPN= L + N
    2 D(I,LPN)= X(I,L)
      CALL MATINV (N,2*N+1,DETERM)
      IF (DETERM)  4,3,4
    3 PRINT 101,J,JCOUNT
    4 DO 5 K=1,N
      E(K,NP1,1)= D(K,2*N+1)
      DO 5 L=1,N
      E(K,L,1)= - D(K,L)
      LPN= L + N
    5 X(K,L)= - D(K,LPN)
      RETURN
    6 DO 7 I=1,N
      DO 7 K=1,N
      DO 7 L=1,N
    7 D(I,K)= D(I,K) + A(I,L)*X(L,K)
    8 IF (J-NJ)  11,9,9
    9 DO 10 I=1,N
      DO 10 L=1,N
      G(I)= G(I) - Y(I,L)*E(L,NP1,J-2)
      DO 10 M=1,N
   10 A(I,L)= A(I,L) + Y(I,M)*E(M,L,J-2)
   11 DO 12 I=1,N
      D(I,NP1)= - G(I)
      DO 12 L=1,N
      C(I,NP1)= D(I,NP1) + A(I,L)*E(L,NP1,J-1)
      DO 12 K=1,N
   12 B(I,K)= B(I,K) + A(I,L)*E(L,K,J-1)
      CALL MATINV (N,NP1  ,DETERM)
      IF (DETERM)  14,13,14
   13 PRINT 101,J,JCOUNT
   14 DO 15 K=1,N
      DO 15 M=1,NP1
   15 E(K,M,J)= - D(K,M)
      IF (J-NJ)  20,16,15
   16 DO 17 K=1,N
   17 C(K,J)= E(K,NP1,J)
      DO 18 JJ=2,NJ
      M= NJ - JJ + 1
      DO 18 K=1,N
      C(K,M)= E(K,NP1,M)
      DO 18 L=1,N
   18 C(K,M)= C(K,M) + E(K,L,M)*C(L,M+1)
      DO 19 L=1,N
      DO 19 K=1,N
   19 C(K,1)= C(K,1) + X(K,L)*C(L,3)
   20 RETURN
      END
```

```
      SUBROUTINE MATINV (N,M,DETERM) $COMMON A,B,C,D

      DIMENSION A(2,2),B(2,2),C(2,100),D(2,5),JCOL(2),X(2,5)
      NM1=N-1 $ DETERM=1.0 $ DO 1 I=1,N $ JCOL(I)=I $ DO 1 K=1,M
    1 X(I,K)=D(I,K) $ DO 6 II=1,NM1 $ IP1=II+1 $ BMAX=ABS(B(II,II))
      JC=II $ DO 2 J=IP1,N $ IF(ABS(B(II,J)).LE.BMAX) GO TO 2 $ JC=J
      BMAX=ABS(B(II,J))
    2 CONTINUE $ DETERM=DETERM*B(II,JC) $ IF(DETERM.EQ.0.0) RETURN
      IF(JC.EQ.II) GO TO 4 $ JS=JCOL(JC) $ JCOL(JC)=JCOL(II)
      JCOL(II)=JS $ DO 3 I=1,N $ SAVE=B(I,JC) $ B(I,JC)=B(I,II)
    3 B(I,II)=SAVE $ DETERM=-DETERM
    4 DO 6 I=IP1,N $ F=B(I,II)/B(II,II) $ DO 5 J=IP1,N
    5 B(I,J)=B(I,J)-F*B(II,J) $ DO 6 K=1,M
    6 X(I,K)=X(I,K)-F*X(II,K) $ DETERM=DETERM*B(N,N)
      IF(DETERM.EQ.0.0) RETURN $ DO 7 II=2,N $ IR=N-II+2 $ IM1=IR-1
      JC=JCOL(IR) $ DO 7 K=1,M $ F=X(IR,K)/B(IR,IR) $ C(JC,K)=F
      DO 7 I=1,IM1
    7 X(I,K)=X(I,K)-B(I,IR)*F $ JC=JCOL(1) $ DO 8 K=1,M
    8 D(JC,K)=X(1,K)/B(1,1) $ RETURN $ END
```

```
      PROGRAM FRACI(INPUT,OUTPUT)

C     CALCULATES DISTRIBUTIONS OF CURRENT,POTENTIAL,AND CONCENTRATION
C     FOR UU AND DD CONFIGURATIONS

      DIMENSION A(2,2),B(2,2),C(2,1003),D(2,5),G(2),X(2,2),Y(2,2)
      DIMENSION ETA(1003),TRAN1(1003),TRAN2(1003),TRANT(1003),EFF(1003),
     1COLC(2,1003),PH2(1003),PH2CAL(1003),THETAW(1003),CURR1(1003),Y1(10
     103),PHI1(1003),PHI2(1003)
      COMMON A,B,C,D,G,X,Y,N,NJ,JCOLNT
  101 FORMAT(F15.0)
  102 FORMAT(I1,I3,I2)
  103 FORMAT(1H0,*S = *,F7.3,2X,*(CM-1)*,2X,*EPSILON = *,F3.2,2X,*V = *,
     1F09.4,2X,*(CM/SEC)*/1H0,*DI = *,E09.4,2X,*(CM+2/SEC)*,2X,*KAPA 0 =
     1*,E09.4,2X,*(MHO/CM)*,2X,*SIGMA = *,E09.4,2X,*(MHO/CM)*/1H0,*SR =
     1*,F4.1,2X,*N = *,F3.1,2X,*F = *,F5.0,2X,*(C/EQ)*,2X,*R = *,F7.5,2X
     1,*(J/MOLE-DEG K)*,2X,*T = *,F8.4,2X,*(DEG K)*/1H0,*I01 = *,E09.4,2
     1X,*(AMPS/CM+2)*,2X,*I02 = *,E09.4,2X,*(AMPS/CM+2)*,2X,*SA =*,F11.6
     1,2X,*(CM+2)*/1H0,*ALPHA-A =*,F4.2,2X,*ALPHA-C = *,F4.2,2X,*ALPHA-A
     12 = *,F4.2,2X,*ALPHA-C2 = *,F4.2,2X,*DELTA U = *,F5.3,2X,*(VOLTS)*
     1)
  104 FORMAT(1H0,05X,*CRF = *,E09.4,2X,*(MOLES/CM+3)*,2X,*I = *,E10.4,2X
     1,*(AMPS/CM+2)*)
  105 FORMAT(1H0,*P1 = *,E15.8/1H0,*P2 = *,E15.8/1H0,*P3 = *,E15.8/1H0,*
     1P4 = *,E15.8/1H0,*P5 = *,E15.8/1H0,*P6 = *,E15.8/1H0,*DP = *,E15.8
     1)
  106 FORMAT(1H0,05X,*ISTAR = *,E10.4,2X,*KM = *,E09.4,2X,*(CM/SEC)*,2X,
     1*DA = *,E09.4,2X,*(CM+2/SEC)*/)
  107 FORMAT(1H0,*L = *,E09.4,2X,*(CM)*,2X,*NJ = *,I3,2X,*H = *,E09.4,2X
     1,*ALPHAL = *,E9.4,2X,*KAPPA/SIGMA = *,E10.4/)
  108 FORMAT(1H0,*THE NEXT RUN DID NOT CONVERGE*)
  109 FORMAT(1H0,15X,*THETA*,13X,*ETAPRIME*)
  110 FORMAT(10X,E15.8,5X,E15.8)
  111 FORMAT(1H0,I5)
  112 FORMAT(5X,*X/L*,09X,*THETA*,07X,*ETAPRIME*,07X,*ETA*,06X,*TRANS CU
     1RR 1*,1X,*TRANS CURR 2*,3X,*TOT CURR*,5X,*CURR EFF*,6X,*THETAW*/)
  113 FORMAT(09(E12.6,1X))
  114 FORMAT(1H0,3(E15.8,2X))
  115 FORMAT(1X,*VOP = *,F7.4,2X,*(V)*,2X,*(PHI2L-PHI20) = *,F7.4,1X, *(
     1V)*,2X,*CRWL = *,F9.4,2X,*(MOLES/CM+3)*,2X,*ITOT = *,F7.4,1X,*(AMP
     1S)*,2X,*NO. ITERATIONS*,I3/)
  116 FORMAT(1H1)
  117 FORMAT(F15.6,I2)
  118 FORMAT(1H1,4X,*X/L*,05X,*CURR1*/)
  119 FORMAT(2F10.7)
  120 FORMAT(1H0,50X,*DOWNSTREAM  COUNTER ELECTRODE*/1H0,50X,*DOWNSTREAM
     1 CURRENT COLLECTOR*/)
  121 FORMAT(1H0,4X,*X/L*,09X,*PHI1*,09X,*PHI2*,10X,*PH2*,09X,*PH2CAL*/)
  122 FORMAT(5(E12.6,1X))
  123 FORMAT(1H0,50X,*UPSTREAM COUNTER ELECTRODE*/1H0,50X,*UPSTREAM CURR
     1ENT COLLECTOR*/)
      PRINT 116
      JDIST=-1
C     IF JOIST .GE. ONE NORMALIZED DEPOSIT DISTRIBUTION IS PRINTED
      READ 101,S,EPSIL,V,DR,QKAPA0,SIGMA,SR,ON,F,R,T ,ALPHA,ALPHC,ALPHA2
     1,ALPHC2,SUA
      READ 101,CRF  $  READ 102,N,NJ,NCELEC $ NJ0=NJ $ QL0=0.1
      CKM=(0.95/EPSIL*(S*DR/(5.*(1.-EPSIL))))**(2./3.)*V**(1./3.)
      CKM=4.369E-03*V**0.5475
```

```
      QKM=C.00C1922
      GKM=3.6705+*V**0.5454*(S*DF)**0.4346/EPSIL
      ETAP=-4.0
      GAM=0.75 $ PIH2=1.0E-24 $ CH=2.82E-03
      DATI0=1.38E-04   $  DATI02=0.70E-05
      QI01=DATI0*(CRF*1000./0.1)**GAM
      QI02=DATI02*PIH2**(0.5*ALPHC2)*CH**(1.(-ALPHC2)
      U1 = 0.337 - SR*R*T/QN/F*ALOG(CRF*10(0./(.99707)
      U2 = 0.0 - 0.5*R*T/F*ALOG(PIH2/CH**2)-U1
      UCUCAL = 0.337-.2676+0.5*R*T/F*ALOG(CRF*1000.*4.17**2/.997 07**3)
      PRINT 103,S,EPSIL,V,DR,QKAPA0,SIGMA,SR,QN,F,R,T,QI01,QI02,SUA,ALPH
     1A,ALPHC,ALPHA2,ALPHC2,U2
      QKAPPA = QKAPA0*EPSIL**1.5
      SIGMA=QKAPPA
      DELTA=QKAPPA/SIGMA
      DA = 3.*(1. - EPSIL)*V/S/EPSIL
      P1 = (-SR*QI01/(QN*F*QKM*CRF))**(1.+ALPHA/ALPHC)
      P2 = CRF*QN*F/SR*V**2 /S/QKM*ALPHC*F/R/T*(1./QKAPPA + 1./SIGMA)
      P3 = -SR*QI02/QN/F/QKM/CRF*(-QN*F*QKM*CRF/SR/QI01)**(ALPHC2/ALPHC)
     1*EXP(ALPHC2*F*U2/R/T)
      P4 = (-SR*QI01/(QN*F*QKM*CRF))**((ALPHA2 + ALPHC2)/ALPHC)*
     1EXP(-(ALPHA2 + ALPHC2)*F*U2/R/T)
      P5 = -P2/(1./QKAPPA + 1./SIGMA)*(1./QKAPPA)
      P6 = -P2/(SIGMA/QKAPPA + 1.0)
      TAU = 3.**(1./3.)
      DP=EPSIL*(DR/TAU**2+DA)*S*QKM/V**2
      PRINT 105,P1,P2,P3,P4,P5,P6,DP
      IF(NCELEC .GE. 1)  GO TO 902
  901 P5P=P6 $ P6P=P5 $ PRINT 120 $  P5= P5P  $  P6= P6P $ GO TO 99
  902 PRINT 123
   99 READ 117,QI,JSTAR $ IF(JSTAR .LT. 0)  STOP
      READ 101,QL $ IF(QL .LE. QL0)  GO TO 97
      NJ=QL*NJ0/QL0+3 $ JT=(NJ-3)*7/8+2 $ JLIM=2
   97 H = QL*QKM*S/(V*FLOAT(NJ-3)) $ NM=NJ-1
      ALPHAL = S*QKM*QL/V
      PRINT 107,QL,NJ,H,ALPHAL,DELTA
      PRINT 104,CRF,QI
      CISTAR = QI*SR/(QN*F*V*CRF)
      PRINT 106,QISTAR,QKM,DA
      BB = 0.5 + 0.5*SQRT(1.0 + 4.0*DP)
      ITHETA = 1  $  IETAP = 2
      IF(JSTAR .GT. 0)  GO TO 98
      DO 200 J=1,NJ $ BBEXP=EXP(-H*FLOAT(J-2)/BB)/BB
      C(ITHETA,J)=(1.0-QISTAR)*(1.0-BBEXP)+BBEXP  $  IF(QISTAR .GE. 0.99
     1)  C(ITHETA,J)=BBEXP+DP/BB**3*EXP(BB/DF*H*FLOAT(J-NJ+1)-ALPHAL/BB)
  200 C(IETAP,J) = ETAP
   98 JCOUNT = 0
    1 JCOUNT = JCOUNT + 1
      CRAL0=C(IETAP,2)
      J = 0
      DO 2 I=1,N
      DO 2 K=1,N
      Y(I,K) = 0.0
    2 X(I,K) = 0.0
    3 J = J + 1
      DO 4 I=1,N
      COLD(I,J)=C(I,J)
      G(I) = 0.0
      DO 4 K=1,N
      A(I,K) = 0.0
      B(I,K) = 0.0
    4 D(I,K) = 0.0
```

```
      IF(J.EQ.NJ) GO TO 3 $ IF(J.GT.1) GO TO 7
      C(ITHETA,ITHETA)=1.0-DP/2.(/H*ALOG(C(ITHETA,J+2)/C(ITHETA,J))
      X(ITHETA,ITHETA) = -DP*C(ITHETA,J+1)/2.0/H/C(ITHETA,J+2)
      B(ITHETA,ITHETA)= DP*C(ITHETA,J+1)/2.0/H/C(ITHETA,J)
      G(ITHETA)=1.0
      B(IETAP,IETAP) = -1.0
      GO TO 25
    7 EP = EXP(C(IETAP,J))  $  EPA = EXP(ALPHA*C(IETAP,J)/ALPHC)*EP
      B(ITHETA,IETAP) = (EP*C(ITHETA,J) + P1*EPA*(1. + ALPHA/ALPHC*
     1(1. + EP)))/(1. + EP)**2
      G(ITHETA) = B(ITHETA,IETAP)*C(IETAP,J) - P1*EPA/(1. + EP)
      EPA2 = EXP(ALPHA2*C(IETAP,J)/ALPHC)
      EPC2 = EXP(-ALPHC2*C(IETAP,J)/ALPHC)
      B(IETAP,IETAP) = -2./H**2/P2+P3*(ALPHC2*EPC2+P4*ALPHA2*EPA2)/ALPHC
      G(IETAP) = P3*((1.+ALPHC2*C(IETAP,J)/ALPHC)*EPC2+P4*(ALPHA2*
     1C(IETAP,J)/ALPHC - 1.)*EPA2)
      B(ITHETA,ITHETA) = -2.*DP/H**2 - 1./(1. + EP)
      IF(J.GT.JT) GO TO 21
      CP = 0.5*ALOG(C(ITHETA,J+1)/C(ITHETA,J-1))/H
      COTH = -CP*(1.0 - DP*CP) + DP*ALOG(C(ITHETA,J+1)*C(ITHETA,J-1)/
     1C(ITHETA,J)**2)/H**2
      B(ITHETA,ITHETA)=B(ITHETA,ITHETA)+COTH
      A(ITHETA,ITHETA) = C(ITHETA,J)/H*(0.5 - DP*CP +DP/H)/C(ITHETA,J-1)
      D(ITHETA,ITHETA) = C(ITHETA,J)/H*(-0.5+DP*CP+DP/H)/C(ITHETA,J+1)
      RAT2=C(ITHETA,J+1)/C(ITHETA,J) $ CP2=DP*ALOG(RAT2)/H/2.
      B(IETAP,ITHETA)=(0.5-CP2+DP/H)/H*SQRT(RAT2)*2.0
      D(IETAP,ITHETA)=(0.5-CP2-DP/H)/H/SQRT(RAT2)*2.0
      IF(J .GT. 2)  GO TO 6
      IF(NOELEC .GE. 1)  G(IETAP)=G(IETAP)+2.0/H*(1.0-GISTAR)
      IF(NOELEC .LT. 1)  G(IETAP)=G(IETAP)+2.0/H
      C(IETAP,IETAP)=2.0/P2/H**2
      GO TO 25
    6 RAT1=C(ITHETA,J)/C(ITHETA,J-1) $ CP1=DP*ALOG(RAT1)/H/2.
      C(IETAP,ITHETA)=0.5*D(IETAP,ITHETA)
      B(IETAP,ITHETA)=0.5*B(IETAP,ITHETA)+(CP1-.5+DP/H)/H/SQRT(RAT1)
      A(IETAP,ITHETA)=(-0.5+CP1-DP/H)/H*SQRT(RAT1)
      GO TO 24
   21 A(ITHETA,ITHETA) = (DP/H + 0.5)/H
      D(ITHETA,ITHETA) = (DP/H - 0.5)/H
      A(IETAP,ITHETA)=(-0.5-DP/H)/H $ D(IETAP,ITHETA)=(0.5-DP/H)/H
      B(IETAP,ITHETA)=2.0*DP/H**2
   24 A(IETAP,IETAP) = 1./H**2/P2
      C(IETAP,IETAP) = 1./H**2/P2
   25 CONTINUE
      IF(JCOUNT .GT. JLIM)  GO TO 14
      B(ITHETA,ITHETA) = 1.0  $  G(ITHETA) = C(ITHETA,J)
      A(ITHETA,ITHETA) = 0.0  $  D(ITHETA,ITHETA) = 0.0
      X(ITHETA,ITHETA)=0.0  $  B(ITHETA,IETAP) = 0.0
      C(ITHETA,IETAP) = 0.0
   14 CALL BANC(J)
      GO TO 3
    8 B(ITHETA,ITHETA) = 1.0
      Y(ITHETA,ITHETA) = -1.0
      B(IETAP,IETAP) = 1.0
      Y(IETAP,IETAP) = -1.0
      IF(NOELEC .GE. 1)  GO TO 15
      G(IETAP)=2.*H*P2*GISTAR
   15 CALL BANC(J)
      FAC=10.0  $  DPOT=1.5
      DO 20 J=1,NJ $ IF(C(ITHETA,J).LT.COLD(ITHETA,J)/FAC) C(ITHETA,J)=
     1COLD(ITHETA,J)/FAC $ IF(C(ITHETA,J).GT.COLD(ITHETA,J)*FAC)
     1C(ITHETA,J)=COLD(ITHETA,J)*FAC
```

```
      IF(C(IETAP,J).GT.COLD(IETAP,J)+DPOT) C(IETAP,J)=COLD(IETAP,J)+DPOT
   20 IF(C(IETAP,J).LT.COLD(IETAP,J)-DPOT) C(IETAP,J)=COLD(IETAP,J)-DPOT
      IF(JCOUNT .LE. JLIM)  GO TO 1
      CRAL=C(IETAP,2)
      IF(ABS(CRAL - CRAL0).LE.1.E-06*ABS(CRAL)) GO TO 11
      IF(JCOUNT.LE.15) GO TO 1  $ PRINT 108
   11 ETA(NM)=R*T/ALPH(/F*(C(IETAP,NM)-ALOG(-QN*F*QKM*CRF/SR/QI01))
      DO 12 J=2,NM
      ETA(J) = R*T/ALPHC/F*(C(IETAP,J) - ALOG(-QN*F*QKM*CRF/SR/QI01))
      TRAN1(J) = (C(ITHETA,J) - P1*EXP((ALPHA/ALPHC + 1.)*C(IETAP,J)))/
     1(1. + EXP(C(IETAP,J)))
      QNI01=QI01*SR/N/F/CRF/QKM $ THETAW(J)=(C(ITHETA,J)-QNI01*EXP(ALPHA
     1*F/R/T*ETA(J)))/(1.0-QNI01*EXP(-ALPHC*F/R/T*ETA(J)))
      TRAN2(J) = P3*(1. - P4*EXP((ALPHA2 + ALPHC2)/ALPHC*C(IETAP,J)))*
     1EXP(-ALPHC2*C(IETAP,J)/ALPHC)
      TRANT(J) = TRAN1(J) + TRAN2(J)
      EFF(J) = TRAN1(J)/TRANT(J)
      Y1(J)=FLOAT(J-2)/FLOAT(NM-2) $ PHI1(J)=QKAPPA/(QKAPPA+SIGMA)*(ETA(
     1J)-ETA(NM)) $ PHI2(J)=PHI1(J)-ETA(J)
      PH2(J)=ETA(NM)+PHI2(J)   $  PH2CAL(J)=PHI2(J)-UCUCAL
      IF(NCELEC .LT. 1)  GO TO 12 $ PHI1(J)=QKAPPA/(QKAPPA+SIGMA)*(ETA(J
     1)-ETA(2)) $ PHI2(J)=PHI1(J)-ETA(J)
      PH2(J)=ETA(NM)+PHI2(J)   $  PH2CAL(J)=PHI2(J)-UCUCAL
   12 CONTINUE $ TI=QI*SUA
      DPHI2=PHI2(NM)-PHI2(2) $ CRW=THETAW(NM)*CRF $ PRINT 115,PH2CAL(NM)
     1,DPHI2,CRW,TI,JCOUNT $ PRINT 112
      PRINT 113,(Y1(J),C(ITHETA,J),C(IETAP,J),ETA(J),TRAN1(J),TRAN2(J),
     1TRANT(J),EFF(J),THETAW(J),J=2,NM,05)
      PRINT 121 $ PRINT 122,(Y1(J),PHI1(J),PHI2(J),PH2(J),PH2CAL(J),J=2,
     1NM,05)
      TRAN1T = 0.0   $  TRAN2T = 0.0   $ TRAP1T = 0.0   $  TRAP2T = 0.0
      IF(QI02 .LE. 1.0E-30)  GO TO 27
      DO 16 J=3,NM
      TRAP1T = TRAP1T + H*(TRAN1(J) + TRAN1(J-1))/2.0
      TRAP2T = TRAP2T + H*(TRAN2(J) + TRAN2(J-1))/2.0
      IF(TRAN1(J)/TRAN1(J-1) .LE. 0.0)  GO TO 17
      IF(TRAN1(J) .EQ. TRAN1(J-1))  GO TO 17
      TRAN1T = H*(TRAN1(J) - TRAN1(J-1))/ALOG(TRAN1(J)/TRAN1(J-1)) +
     1TRAN1T
      GO TO 18
   17 TRAN1T = H*(TRAN1(J) + TRAN1(J-1))/2.0 + TRAN1T
   18 IF(TRAN2(J)/TRAN2(J-1) .LE. 0.0)  GO TO 19
      IF(TRAN2(J) .EQ. TRAN2(J-1))  GO TO 19
      TRAN2T = H*(TRAN2(J) - TRAN2(J-1))/ALOG(TRAN2(J)/TRAN2(J-1)) +
     1TRAN2T
      GO TO 16
   19 TRAN2T = H*(TRAN2(J) + TRAN2(J-1))/2.0 + TRAN2T
   16 CONTINUE
      TRANTT = TRAN1T + TRAN2T
      TRAPTT = TRAP1T + TRAP2T
      PRINT 114,TRAN1T,TRAN2T,TRANTT
      PRINT 114,TRAP1T,TRAP2T,TRAPTT $  GO TO 28
   27 DO 30 J=3,NM
      TRAP1T = TRAP1T + H*(TRAN1(J) + TRAN1(J-1))/2.0
      IF(TRAN1(J) .EQ. TRAN1(J-1))  GO TO 29
      IF(TRAN1(J)/TRAN1(J-1) .LE. 0.0)  GO TO 29
      TRAN1T = H*(TRAN1(J) - TRAN1(J-1))/ALOG(TRAN1(J)/TRAN1(J-1)) +
     1TRAN1T
      GO TO 30
   29 TRAN1T = H*(TRAN1(J) + TRAN1(J-1))/2.0 + TRAN1T
   30 CONTINUE
      PRINT 114,TRAN1T,TRAP1T $ QL0=QL $ NJ0=NJ-3
```

```
28 IF(JOIST .GE. 1)  GO TO 31  $  GO TO 99
31 DO 26 J=2,NM $ CURR1(J)=TRAN1(J)*ALPHAL/TRAN1T
26 Y1(J)=FLOAT(J-2)/FLOAT(NM-2) $ PRINT 118 $ PRINT 119,(Y1(J),CURR1(
  1J),J=2,NM,05) $ GO TO 99 $ END
```

```
      PROGRAM REDOX(INPUT,OUTPUT)

C     CALCULATES THE BEHAVIOR OF A FLOW REDOX CELL ON CHARGE AND
C     DISCHARGE WHEN THE CURRENT AND FLUID FLOW ARE IN PARALLEL

      DIMENSION A(2,2),B(2,2),C(2,1003),D(2,5),G(2),X(2,2),Y(2,2),
     1ETA(1003),TRAN1(1003),TRAN2(1003),TRANT(1003),EFF(1003),
     1CELD(2,1003),PH1(1003),PH2CAL(1003),THETAW(2,1003),CURR1(1003),Y1(
     11003),PHI1(1003),PHI2(1003),THETA2(1003),QKM(4),DI(4),U(4),CFC(4),
     1CPC(4),CFD(4),CPD(4),VEL(4),RVEL(2),R1VEL(2),CPDM(4),PC(5),PDS(5)
      COMMON A,B,C,D,G,X,Y,N,NJ,JCOUNT
  101 FORMAT(F15.0)
  102 FORMAT(I1,I3)
  103 FORMAT(1HO,*S = *,F7.3,2X,*(CM-1)*,2X,*EPSILON = *,F3.2,2X,*V = *,
     1E10.4,2X,*(CM/S)*,2X,*DR = *,E10.4,2X,*(CM**2/S)*/1HO,*DP = *,E10.4
     1,2X,*(CM**2/S)*,2X,*KAPPA0 = *,E10.4,2X,*(MHO/CM)*,2X,*SIGMA = *,E1
     10.4,2X,*(MHO/CM)*/1HO,*SR = *,F4.1,2X,*N = *,F3.1,2X,*F = *,E10.4,
     12X,*(C/EQ)*,2X,*R = *,F7.5,2X,*(J/MOLE-DEG K)*,2X,*T = *,F8.4,2X,*
     1(DEG K)*/1HO,*IOR = *,E10.4,2X,*(AMP/CM**2)*,2X,*IOS = *,E10.4,2X,*
     1(AMP/CM**2)*,2X,*SA = *,F11.6,2X,*(CM**2)*/1HO,*ALPHA-AR = *,F4.2,2X
     1,*ALPHA-CR = *,F4.2,2X,*ALPHA-AS = *,F4.2,2X,*ALPHA-CS = *,F4.2,2X
     1,*DELTA U = *,F5.3,2X,*(VOLTS)*)
  104 FORMAT(1HO,*CRF = *,E12.6,2X,*(MOLE/CM**3)*,2X,*CPF = *,E12.6,2X,*(
     1MOLE/CM**3)*,2X,*KMR = *,E12.6,2X,*(CM/S)*)
  105 FORMAT(1HO,*P1 = *,E15.8/1HO,*P2 = *,E15.8/1HO,*P3 = *,E15.8/1HO,*
     1P4 = *,E15.8/1HO,*P5 = *,E15.8/1HO,*P6 = *,E15.8/1HO,*P7 = *,E15.8
     1/1HO,*DP = *,E15.8/1HO,*CPF/CRF = *,E15.8/)
  106 FORMAT(1HO,*KMP = *,E10.4,2X,*(CM/S)*,2X,*DA = *,E10.4,2X,*(CM**2/S
     11)*,2X,*KAPPA/SIGMA = *,E10.4)
  107 FORMAT(1HO,*I = *,E10.4,2X,*(AMP/CM**2)*,2X,*ISTAR = *,E10.4,2X,*IT
     1OT = *,E10.4,2X,*(AMP)*/1HO,*L = *,E10.4,2X,*(CM)*,2X,*NJ = *,I4,
     12X,*H = *,E10.4,2X,*ALPHAL = *,E10.4,2X,*LS = *,F5.3,2X,*(CM)*/)
  108 FORMAT(1HO,*THE NEXT RUN DID NOT CONVERGE*)
  109 FORMAT(1HO,15X,*THETA*,13X,*ETAPRIME*)
  110 FORMAT(10X,E15.8,5X,E15.8)
  111 FORMAT(1HO,I5)
  112 FORMAT(5X,*X/L*,09X,*THETA*,07X,*ETAPRIME*,07X,*ETA*,06X,*TRANS CU
     1RR 1*,1X,*TRANS CURR 2*,3X,*TOT CURR*,5X,*CURR EFF*,6X,*THETAW*/)
  113 FORMAT (1X,1P9E13.6)
  114 FORMAT(1HO,3(E15.8,2X))
  115 FORMAT(1HO,*(PHI2L-PHI20) = *,F8.4,1X,*(V)*,2X,*CRWL = *,E10.4,2X,
     1*(MOLE/CM**3)*,2X,*CPWL = *,E10.4,2X,*(MOLE/CM**3)*,2X,*NO. ITERATIO
     1NS = *,I3/)
  116 FORMAT(1H1)
  117 FORMAT(F15.0,I2)
  118 FORMAT(1H1,4X,*X/L*,05X,*CURR1*/)
  119 FORMAT(2F10.7)
  120 FORMAT(1HO,50X,*DOWNSTREAM  COUNTER ELECTRODE*/1HO,50X,*UPSTREAM C
     1URRENT COLLECTOR*/)
  121 FORMAT(1HO,4X,*X/L*,09X,*PHI1*,09X,*PHI2*,10X,*PH1*,09X,*PH2CAL*,7
     1X,*THETAP*,7X,*THETAPW*/)
  122 FORMAT(7(E12.6,1X))
  123 FORMAT(1HO,50X,*UPSTREAM COUNTER ELECTRODE*/1HO,50X,*DOWNSTREAM CU
     1RRENT COLLECTOR*/)
  124 FORMAT(2F15.0)
  125 FORMAT(//,50X,*TI(IV)  +  E-  =  TI(III)*/)
```

```
126 FORMAT(//,50X,*FE(II)  =  FE(III) + E-*/)
127 FORMAT(//,50X,*TI(III)  =  TI(IV)  +  E-*/)
128 FORMAT(//,50X,*FE(III)  +  E-  =  FE(II)*/)
129 FORMAT(///62X,*SUMMARY OF RESULTS*///35X,*CHARGE*,57X,*DISCHARGE*)
130 FORMAT(//15X,*FEED CONCENTRATION*,10X,*PRODUCT CONCENTRATION*,15X,
   1*FEED CONCENTRATION*,10X,*PRODUCT CONCENTRATION*/18X,*(MOLE/CM+3)*
   1,19X,*(MOLE/CM+3)*,23X,*(MOLE/CM+3)*,19X,*(MOLE/CM+3)*/101X,*BEFOR
   1E MIXING*,6X,*AFTER MIXING*)
131 FORMAT(1X,*FE(II)*,8X,E15.8,15X,E15.8,19X,E15.8,5X,E15.8,3X,E15.8)
132 FORMAT(1X,*FE(III)*,07X,E15.8,15X,E15.8,19X,E15.8,05X,E15.8,03X,
   1E15.8)
133 FORMAT(1X,*TI(IV)*,8X,E15.8,15X,E15.8,19X,E15.8,5X,E15.8,3X,E15.8)
134 FORMAT(1X,*TI(III)*,07X,E15.8,15X,E15.8,19X,E15.8,05X,E15.8,03X,
   1E15.8)
135 FORMAT(//,2X,*- ELECTRODE VEL.*,3X,*+ ELECTRODE VEL.*,3X,*RATIO*,3
   1X,*1/RATIO*,20X,*- ELECTRODE VEL.*,3X,*+ ELECTRODE VEL.*,3X,*RATIO
   1*,3X,*1/RATIO*)
136 FORMAT(7X,*(CM/S)*,13X,*(CM/S)*,48X,*(CM/S)*,13X,*(CM/S)*/)
137 FORMAT(2X,E14.8,5X,E14.8,3X,F7.4,3X,F7.4,21X,E14.8,05X,E14.8,2X,
   1F7.4,3X,F7.4//)
138 FORMAT(2X,*CURRENT DENSITY*,5X,*CELL VOLTAGE*,5X,*CURRENT EFFICIEN
   1CY*,17X,*CURRENT DENSITY*,05X,*CELL VOLTAGE*,05X,*CURRENT EFFICIEN
   1CY*/5X,*(AMP/CM+2)*,11X,*(V)*,07X,*- ELECTRODE*,2X,*+ ELECTRODE*,
   117X,*(AMP/CM+2)*,11X,*(V)*,8X,*-ELECTRODE*,2X,*+ ELECTRODE*/)
139 FORMAT(2X,E14.8,06X,F11.8,4X,F9.6,4X,F9.6,15X,E14.8,06X,F11.8,4X,
   1F9.6,4X,F9.6)
140 FORMAT(/45X,*OVERALL*,66X,*OVERALL*//43X,F9.6,64X,F9.6)
141 FORMAT(//2X,*OHMIC POTENTIAL DROP ACROSS SEPARATOR *,F11.8,2X,*(V)
   1*,20X,*OHMIC POTENTIAL DROP ACROSS SEPARATOR *,F11.8,2X,*(V)*)
142 FORMAT(//06X,*PERCENT OF CHARGE REQUIRED TO RESTORE SYSTEM TO INTI
   1TIAL STATE DUE TO INCOMPLETE CONVERSION OF TI(III) *,F11.8,2X,*(0/
   10)*)
143 FORMAT(//06X,*PERCENT OF CHARGE REQUIRED TO RESTORE SYSTEM TO INTI
   1TIAL STATE DUE TO INCOMPLETE CONVERSION OF FE(III) *,F11.8,2X,*(0/
   10)*)
144 FORMAT(///35X,4E16.8)
145 FORMAT(1P6E20.5)
    PRINT 116
    GLS=1.0
    CRFN=0.0 $ CRPN=0.0 $ CRFP=0.0 $ CRPP=0.0
    READ 101,S,EPSIL,GKAPA0,SIGMA,F,R,T,SUA
    READ 102,N,NJ $ NJ0=NJ $ QL0=0.1
    READ 101,QL
 97 READ 101, QICHAR,QISTAR $ IF(QICHAR.EQ.0.0) STOP $ JCY=1 $ IP=1
    SR=-1.0 $ QN=1.0 $ CRF=0.003
    GI=-GICHAR $ V=QI*SR/QN/F/CRF/QISTAR $ JSTAR=0 $ VSAVE=V
    GISTAV=QISTAR
 99 NJ=GL*NJ0/QL0+3 $ JT=(NJ-3)*7/8+2 $ JLIM=0
    IF(JCY .GT. 1)  GO TO 40 $ IF(IP.EQ.1) JDC=0
    NOELEC=1
    ETAF=-3.5
    CRF=0.003 $ CPF=3.2941994E-07
    VEL(1)=V $ CFC(3)=CRF $ CFC(4)=CPF
    DI(3)=0.00000500 $ DI(4)=0.000005000 $ DR=DI(3)
    DO 34 I=3,4
    GKM(I)=1.09/EPSIL*(S*DI(I)/(6.*(1.-EPSIL)))**(2./3.)*V**(1./3.)
    GKM(1)=4.369E-03*V**0.5454
 34 CONTINUE $ QKR=QKM(3)
    P7=GKM(3)/QKM(4)
    SR=-1 $ QN=1.0 $ ALPHA=0.5 $ ALPHC=0.5
    ALPHA2=0.5 $ ALPHC2=0.5 $ PIH2=1.0E-24 $ CH=5.00
    GIC1=(CRF*CPF)**0.5
```

```
      DATIO2=3.00E-08 $ QIO2=DATIO2*PIH2**(0.5*ALPHC2)*CH**(1.0-ALPHC2)
      U1=0.1*R*T/F*ALOG(CRF*CH**2/CPF) $ U(JCY)=U1-0.2415
      U2=-0.5*R*T/F*ALOG(PIH2/CH**2)-U1
      JKMR=3 $ JKMP=4 $ IF(JDC.EQ.0) PRINT 125
      GO TO 31
   40 IF(JCY .GT. 2)  GO TO 50      $ QI=-QI $ IF(IP.EQ.1) JDC=0
      ETAP=-7.00
      CRF=0.003 $ CPF=3.2941994E-07
      VEL(2)=V $ CFC(1)=CRF $ CFC(2)=CPF
      DI(1)=0.0000055 $ DI(2)=0.0000057 $ DR=DI(1)
      DO 33 I=1,2
      QKM(I)=1.09/EPSIL*(S*DI(I)/(6.*(1.-EPSIL)))**(2./3.)*V**(1./3.)
      QKM(I)=4.369E-03*V**0.5454
   33 CONTINUE $ QKR=QKM(1)
      P7=QKM(1)/QKM(2)
      SR=1.0 $ QN=1.0 $ ALPHA=0.5 $ ALPHC=0.5
      ALPHA2=0.38 $ ALPHC2=0.69 $ PCL2=1.0E-27 $ CCL=20.
      QIO1=10.*(CRF*CPF)**0.5
      QIO2=1.0E-03*CCL**0.38*PCL2**0.655
      U1=.6513-SR*R*T/QN/F*ALOG(CRF/CPF) $ U(JCY)=U1-0.2415
      U2=1.3595-R*T/F/2.*ALOG(CCL**2/PCL2)-U1
      JKMR=1 $ JKMP=2 $ IF(JDC.EQ.0) PRINT 126
      GO TO 31
   50 IF(JCY .GT. 3)  GO TO 60 $ JDC=JDC+IP-1
      JT=NJ
      ETAP=-1.5
      NCELEC=-1
      CRF=CRFN  $  CPF=CRPN
      VEL(3)=V $ CFD(3)=CPF $ CFD(4)=CRF
      DIP3=DI(3) $ DIP4=DI(4) $ DI(3)=DIP4 $ DI(4)=DIP3 $ DR=DI(3)
      DO 37 I=3,4
      QKM(I)=1.09/EPSIL*(S*DI(I)/(6.*(1.-EPSIL)))**(2./3.)*V**(1./3.)
      QKM(I)=4.369E-03*V**0.5454
   37 CONTINUE $ QKR=QKM(3)
      P7=QKM(3)/QKM(4)
      SR=1.0 $ QN=1.0 $ ALPHA=0.5 $ ALPHC=0.5
      ALPHA2=0.38 $ ALPHC2=0.69 $ PCL2=1.0E-27 $ CCL=20.
      QIO1=(CRF*CPF)**0.5
      QIO2=1.0E-03*CCL**0.38*PCL2**0.655
      U1=0.1*R*T/F*ALOG(CPF*CH**2/CRF) $ U(JCY)=U1-0.2415
      U2=1.3595-R*T/F/2.*ALOG(CCL**2/PCL2)-U1
      JKMR=3 $ JKMP=4 $ IF(JDC.EQ.0) PRINT 127 $ GO TO 31
   60 CONTINUE
      JT=NJ
      ETAP=-3.0
      CRF=CRFP $ CPF=CRPP
      VEL(4)=V $ CFD(1)=CPF $ CFD(2)=CRF
      DIP1=DI(1) $ DIP2=DI(2) $ DI(1)=DIP2 $ DI(2)=DIP1 $ DR=DI(1)
      DO 38 I=1,2
      QKM(I)=1.09/EPSIL*(S*DI(I)/(6.*(1.-EPSIL)))**(2./3.)*V**(1./3.)
      QKM(I)=4.369E-03*V**0.5454
   38 CONTINUE $ QKR=QKM(1)
      P7=QKM(1)/QKM(2)
      SR=-1.0 $ QN=1.0 $ ALPHA=0.5 $ ALPHC=0.5
      ALPHA2=0.5 $ ALPHC2=0.5 $ PIH2=1.0E-24 $ CH=5.00
      QIO1=10.*(CRF*CPF)**0.5
      DATIO2=3.00E-08 $ QIO2=DATIO2*PIH2**(0.5*ALPHC2)*CH**(1.0-ALPHC2)
      U1=.6513-SR*R*T/QN/F*ALOG(CRF/CPF) $ U(JCY)=U1-0.2415
      U2=-0.5*R*T/F*ALOG(PIH2/CH**2)-U1
      JKMR=1 $ JKMP=2 $ IF(JDC.EQ.0) PRINT 128
   31 IF(JDC.EQ.0)
     1PRINT 103,S,EPSIL,V,DI(JKMR),DI(JKMP),QKAPAO,SIGMA,SR,QN,F,R,T,QIO
```

```
   11,QI02,SUA,ALPHA,ALPHC,ALPHA2,ALPHC2,U2
    QKAPPA = QKAPA0*EPSIL**1.5
    DA = 3.*(1. - EPSIL)*V/S/EPSIL
    QSIGMA=0.0
    QSIGMA=QSIGMA+0.0001
    DELTA=QKAPPA/SIGMA
    IF(QI .LT. 0.0)  GO TO 35
    P1=(SR*QI01/(QN*F*QKR*CRF))**(1.+ALPHC/ALPHA)
    P2=-ALPHA*QN*F*F*V*V*CRF/(SR*S*QKR*R*T)*(1./QKAPPA+1./SIGMA)
    P3=SR*QI02/(QN*F*QKR*CRF)*EXP(-ALPHA2*F*U2/R/T)*(QN*F*QKR*CRF/SR/
   1QI01)**(ALPHA2/ALPHA)
    P4=(SR*QI01/QN/F/QKR/CRF)**((ALPHA2+ALPHC2)/ALPHA)*EXP((ALPHA2+
   1ALPHC2)*F*U2/R/T)
    ALP1=ALPHA $ ALP2=ALPHC $ ALPHA=ALP2 $ ALPHC=ALP1
    GO TO 36
 35 P1 = (-SR*QI01/(QN*F*QKR*CRF))**(1.+ALPHA/ALPHC)
    P2 = CRF*QN*F/SR*V**2 /S/QKR*ALPHC*F/R/T*(1./QKAPPA + 1./SIGMA)
    P3 = -SR*QI02/QN/F/QKR/CRF*(-QN*F*QKR*CRF/SR/QI01)**(ALPHC2/ALPHC)
   1*EXP(ALPHC2*F*U2/R/T)
    P4 = (-SR*QI01/(QN*F*QKR*CRF))**((ALPHA2 + ALPHC2)/ALPHC)*
   1EXP(-(ALPHA2 + ALPHC2)*F*U2/R/T)
 36 P5 = -P2/(1./QKAPPA + 1./SIGMA)*(1./QKAPPA)
    P6 = -P2/(SIGMA/QKAPPA + 1.0)
    TAU = 3.**(1./3.)
    DR=EPSIL*(DR/TAU**2+DA)*S*QKR/V**2
    THETAP=CPF/CRF
    H = QL*QKR*S/(V*FLOAT(NJ-3))$ NM=NJ-1
    ALPHAL = S*QKR*QL/V
    QISTAR = QI*SR/(QN*F*V*CRF) $ TI=QI*SUA
    IF(JDC.NE.0) GO TO 96
    PRINT 104,CRF,CPF,QKM(JKMR)
    PRINT 106,QKM(JKMP),DA,DELTA
    PRINT 107,QI,QISTAR,TI,QL,NJ,H,ALPHAL,QLS
    PRINT 105,P1,P2,P3,P4,P5,P6,P7,DP,THETAP
 96 IF(NCELEC .GE. 1)  GO TO 902
901 P5P=P6 $ P6P=P5 $ IF(JDC.EQ.0) PRINT 120 $ P5=P5P $ P6=P6P
    GO TO 903
902 IF(JDC.EQ.0) PRINT 123
903 CONTINUE
    BB = 0.5 + 0.5*SQRT(1.0 + 4.0*DP)
    ITHETA = 1  $  IETAP = 2
    IF(JSTAR .GT. 0)  GO TO 98
    DO 200 J=1,NJ $ BBEXP=EXP(-H*FLOAT(J-2)/BB)/BB
    C(ITHETA,J)=(1.0-QISTAR)*(1.0-BBEXP)+BBEXP  $  IF(QISTAR .GE. 0.99
   1)  C(ITHETA,J)=BBEXP+DP/BB**3*EXP(BB/DP*H*FLOAT(J-NJ+1)-ALPHAL/BB)
200 C(IETAP,J) = ETAP
 98 JCOUNT = 0
  1 JCOUNT = JCOUNT + 1
    J = 0
    DO 4 I=1,N
    DO 2 K=1,N
    V(I,K) = 0.0
  2 X(I,K) = 0.0
  3 J = J + 1
    DO 4 I=1,N
    COLD(I,J)=C(I,J)
    G(I) = 0.0
    DO 4 K=1,N
    A(I,K) = 0.0
    B(I,K) = 0.0
  4 D(I,K) = 0.0
    IF(J.EQ.NJ) GO TO 8 $ IF(J.GT.1) GO TO 7
```

```
      D(ITHETA,ITHETA)=1.0-DP/2.0/H*ALOG(C(ITHETA,J+2)/C(ITHETA,J))
      X(ITHETA,ITHETA) = -DP*C(ITHETA,J+1)/2.0/H/C(ITHETA,J+2)
      B(ITHETA,ITHETA)= DP*C(ITHETA,J+1)/2.0/H/C(ITHETA,J)
      G(ITHETA)=1.0
      B(IETAP,IETAP) = -1.0
      GO TO 25
    7 EP = EXP(C(IETAP,J))   $  EPA = EXP(ALPHA*C(IETAP,J)/ALPHC)*EP
      ALP=(1.+ALPHA/ALPHC) $ DX1=1.+EP+P1*P7*EPA/THETAP
      DTHET=(1.+1./THETAP*(1.-C(ITHETA,J)))*P1*EPA
      B(ITHETA,IETAP)=DTHET*ALP/DX1+(EP+P1*P7*ALP*EPA/THETAP)*(C(ITHETA,
     1J)-DTHET)/DX1**2
      G(ITHETA)=B(ITHETA,IETAP)*C(IETAP,J)-P1*EPA*(1.+1./THETAP)/DX1
      EPA2 = EXP(ALPHA2*C(IETAP,J)/ALPHC)
      EPC2 = EXP(-ALPHC2*C(IETAP,J)/ALPHC)
      B(IETAP,IETAP) = -2./H**2/P2+P3*(ALPHC2*EPC2+P4*ALPHA2*EPA2)/ALPHC
      G(IETAP) = P3*((1.+ALPHC2*C(IETAP,J)/ALPHC)*EPC2+P4*(ALPHA2*
     1C(IETAP,J)/ALPHC - 1.)*EPA2)
      B(ITHETA,ITHETA)=-2.*DP/H**2-(1.+P1/THETAP*EPA)/DX1
      IF(J.GT.JT) GO TO 21
      CP = 0.5*ALOG(C(ITHETA,J+1)/C(ITHETA,J-1))/H
      COTH = -CP*(1.0 - DP*CP) + DP*ALOG(C(ITHETA,J+1)*C(ITHETA,J-1)/
     1C(ITHETA,J)**2)/H**2
      B(ITHETA,ITHETA)=B(ITHETA,ITHETA)+COTH
      A(ITHETA,ITHETA) = C(ITHETA,J)/H*(0.5 - DP*CP +DP/H)/C(ITHETA,J-1)
      D(ITHETA,ITHETA) = C(ITHETA,J)/H*(-0.5+DP*CP+DP/H)/C(ITHETA,J+1)
      RAT2=C(ITHETA,J+1)/C(ITHETA,J) $ CP2=DP*ALOG(RAT2)/H/2.
      B(IETAP,ITHETA)=(0.5-CP2+DP/H)/H*SQRT(RAT2)*2.0
      D(IETAP,ITHETA)=(0.5-CP2-DP/H)/H/SQRT(RAT2)*2.0
      IF(J .GT. 2)  GO TO 6
      G(IETAP)=G(IETAP)+2.0/H*(P5*QISTAR/P2+1.0)
      D(IETAP,IETAP)=2.0/P2/H**2
      GO TO 25
    6 RAT1=C(ITHETA,J)/C(ITHETA,J-1) $ CP1=DP*ALOG(RAT1)/H/2.
      D(IETAP,ITHETA)=0.5*D(IETAP,ITHETA)
      B(IETAP,ITHETA)=0.5*B(IETAP,ITHETA)+(CP1-.5+DP/H)/H/SQRT(RAT1)
      A(IETAP,ITHETA)=(-0.5+CP1-DP/H)/H*SQRT(RAT1)
      GO TO 24
   21 A(ITHETA,ITHETA) = (DP/H + 0.5)/H
      D(ITHETA,ITHETA) = (DP/H - 0.5)/H
      A(IETAP,ITHETA)=(-0.5-DP/H)/H $ D(IETAP,ITHETA)=(0.5-DP/H)/H
      B(IETAP,ITHETA)=2.0*DP/H**2
   24 A(IETAP,IETAP) = 1./H**2/P2
      D(IETAP,IETAP) = 1./H**2/P2
   25 CONTINUE
      IF(JCOUNT .GT. JLIM)  GO TO 14
      B(ITHETA,ITHETA) = 1.0   $  G(ITHETA) = C(ITHETA,J)
      A(ITHETA,ITHETA) = 0.0   $  D(ITHETA,ITHETA) = 0.0
      X(ITHETA,ITHETA)=0.0   $  B(ITHETA,IETAP) = 0.0
      D(ITHETA,IETAP) = 0.0
   14 CALL BAND(J)
      GO TO 3
    8 B(ITHETA,ITHETA) = 1.0
      Y(ITHETA,ITHETA) = -1.0
      B(IETAP,IETAP) = 1.0
      Y(IETAP,IETAP) = -1.0
      G(IETAP) = -2.*H*P6*QISTAR
      CALL BAND(J)
      FAC=5.0 $ DPOT=2.0
      DO 20 J=1,NJ $ IF(C(ITHETA,J).LT.COLD(ITHETA,J)/FAC) C(ITHETA,J)=
     1COLD(ITHETA,J)/FAC $ IF(C(ITHETA,J).GT.COLD(ITHETA,J)*FAC)
     1C(ITHETA,J)=COLD(ITHETA,J)*FAC
      IF(C(IETAP,J).GT.COLD(IETAP,J)+DPOT) C(IETAP,J)=COLD(IETAP,J)+DPOT
```

```
 20 IF(C(IETAP,J).LT.COLD(IETAP,J)-DPOT) C(IETAP,J)=COLD(IETAP,J)-DPOT
    IF(JCOUNT .LE. JLIM)  GO TO 1
    DO 998 I=1,N $ DO 998 J=1,NJ,5
998 IF(ABS(C(I,J)-COLD(I,J)) .GT. 1.E-08*ABS(C(I,J))) GO TO 999
    GO TO 11
999 IF(JCOUNT.LE.20) GO TO 1  $ PRINT 108
 11 IF(GI .GT. 0.0)  GO TO 57
    ETA(NM)=R*T/ALPHC/F*(C(IETAP,NM)-ALOG(-QN*F*QKR*CRF/SR/QIO1))
    GO TO 58
 57 ALPHA=ALP1
    ETA(NM)=R*T/ALPHA/F*(ALOG(QN*F*QKR*CRF/SR/QIO1)-C(IETAP,NM))
 58 DO 12 J=2,NM
    IF(GI .GT. 0.0)  GO TO 67
    ETA(J) = R*T/ALPHC/F*(C(IETAP,J) - ALOG(-QN*F*QKR*CRF/SR/QIO1))
    GO TO 68
 67 ETA(J)=R*T/ALPHA/F*(ALOG(QN*F*QKR*CRF/SR/QIO1)-C(IETAP,J))
    ALPHA=ALP2
 68 TRAN1(J)=(C(ITHETA,J)-P1*EXP((ALPHA/ALPHC+1.)*C(IETAP,J)))*(1.+1./T
   1HETAP*(1.-C(ITHETA,J))))/(1.+EXP(C(IETAP,J))+P1*P7*EXP((ALPHA/ALPH
   1C+1.)*C(IETAP,J))/THETAP)
    THETAW(1,J)=C(ITHETA,J)-TRAN1(J)
    TRAN2(J) = P3*(1. - P4*EXP((ALPHA2 + ALPHC2)/ALPHC*C(IETAP,J)))*
   1EXP(-ALPHC2*C(IETAP,J)/ALPHC)
    TRANT(J) = TRAN1(J) + TRAN2(J)
    EFF(J) = TRAN1(J)/TRANT(J)
    Y1(J)=FLOAT(J-2)/FLOAT(NM-2) $ PHI1(J)=QKAPPA/(QKAPPA+SIGMA)*(ETA(
   1J)-ETA(NM)+QI*QL/QKAPPA*(Y1(J)-1.)) $ PHI2(J)=PHI1(J)-ETA(J)
    PH1(J)=ETA(NM)+PHI2(J)  $  PH2CAL(J)=PHI2(J)-U(JCY)
    THETA2(J)=1.+THETAP-C(ITHETA,J)
    THETAW(2,J)=THETA2(J)+P7*(C(ITHETA,J)-THETAW(1,J))
    IF(NELEC .GE. 1)  GO TO 12 $ PHI1(J)=QKAPPA/(QKAPPA+SIGMA)*(ETA(J
   1)-ETA(2)-QI/QKAPPA*(1.-Y1)       $ PHI2(J)=PHI1(J)-ETA(J)
    PH1(J)=PHI2(J)+ETA(2) $ PH2CAL(J)=PHI2(J)-U(JCY)
 12 CONTINUE $ TI=QI*SUA
    IF(JCY .GT. 1) GO TO 55
    CRFN=THETA2(NM)*CRF $ CRPN=C(ITHETA,NM)*CRF
 55 IF(JCY .GT. 2) GO TO 56
    CRFP=THETA2(NM)*CRF $ CRPP=C(ITHETA,NM)*CRF
 56 CONTINUE
    DPHI2=PHI2(NM)-PHI2(2) $ CRW=THETAW(1,NM)*CRF $ CPW=THETAW(2,NM)*
   1CRF $ IF(JDC.NE.0) GO TO 62 $ PRINT 115,DPHI2,CRW,CPW,JCOUNT
    PRINT 112
    PRINT 113,(Y1(J),C(ITHETA,J),C(IETAP,J),ETA(J),TRAN1(J),TRAN2(J),
   1TRANT(J),EFF(J),THETAW(1,J),J=2,NM,90)
    PRINT 121 $ PRINT 122,(Y1(J),PHI1(J),PHI2(J),PH1(J),PH2CAL(J),THET
   1A2(J),THETAW(2,J),J=2,NM,90)
 62 TRAN1T = 0.0  $  TRAN2T = 0.0  $ TRAP1T = 0.0  $  TRAP2T = 0.0
    IF(GI02 .LE. 1.0E-30)  GO TO 27
    DO 16 J=3,NM
    TRAP1T = TRAP1T + H*(TRAN1(J) + TRAN1(J-1))/2.0
    TRAP2T = TRAP2T + H*(TRAN2(J) + TRAN2(J-1))/2.0
    IF(TRAN1(J)/TRAN1(J-1) .LE. 0.0)  GO TO 17
    IF(TRAN1(J) .EQ. TRAN1(J-1))  GO TO 17
    TRAN1T = H*(TRAN1(J) - TRAN1(J-1))/ALOG(TRAN1(J)/TRAN1(J-1)) +
   1TRAN1T
    GO TO 18
 17 TRAN1T = H*(TRAN1(J) + TRAN1(J-1))/2.0 + TRAN1T
 18 IF(TRAN2(J)/TRAN2(J-1) .LE. 0.0)  GO TO 19
    IF(TRAN2(J) .EQ. TRAN2(J-1))  GO TO 19
    TRAN2T = H*(TRAN2(J) - TRAN2(J-1))/ALOG(TRAN2(J)/TRAN2(J-1)) +
   1TRAN2T
    GO TO 16
```

```
19 TRAN2T = H*(TRAN2(J) + TRAN2(J-1))/2.0 + TRAN2T
16 CONTINUE
   TRANTT = TRAN1T + TRAN2T
   TRAPTT = TRAP1T + TRAP2T
   IF(JDC.NE.0) GO TO 69
   PRINT 114,TRAN1T,TRAN2T,TRANTT
   PRINT 114,TRAP1T,TRAP2T,TRAPTT $  GO TO 69
27 DO 30 J=3,NM
   TRAP1T = TRAP1T + H*(TRAN1(J) + TRAN1(J-1))/2.0
   IF(TRAN1(J) .EQ. TRAN1(J-1))  GO TO 29
   IF(TRAN1(J)/TRAN1(J-1) .LE. 0.0)  GO TO 29
   TRAN1T = H*(TRAN1(J) - TRAN1(J-1))/ALOG(TRAN1(J)/TRAN1(J-1)) +
  1TRAN1T
   GO TO 30
29 TRAN1T = H*(TRAN1(J) + TRAN1(J-1))/2.0 + TRAN1T
30 CONTINUE
   IF(JDC.EQ.0) PRINT 114,TRAN1T,TRAP1T $ QLO=QL $ NJO=NJ-3
69 IF(JCY .GT. 1) GO TO 70
   QJISTR=1./QISTAR
   QUEFNC=TRAP1T/TRAPTT $ QI1NC=TRAP1T $ QITNC=TRAPTT
   CPC(3)=CRPN $ CPC(4)=CRFN $ QI1=QI
   PH1NSC=PHI1(2) $ PH1NCC=PHI1(NM) $ PH2NSC=PH2CAL(2)
   VNC=PH1NSC-PH1NCC+PH2NSC-PH1NSC $ JCY=2 $ GO TO 99
70 IF(JCY .GT. 2) GO TO 71 $ JDC=1
   RVEL(1)=VEL(1)/VEL(2) $ R1VEL(1)=1./RVEL(1)
   QUEFPC=TRAP1T/TRAPTT
   Q11PC=TRAP1T $ QITPC=TRAPTT
   QQUEFC=(QI1NC+QI1PC)/(QITNC+QITPC)
   CPC(1)=CRPP $ CPC(2)=CRFP
   PH1PCC=PHI1(NM) $ PH1PSC=PHI1(2) $ PH2PSC=PH2CAL(2)
   VPC=PH1PCC-PH1PSC+PH1PSC-PH2PSC
   VSEPC=-QI1*QLS/QKAPA0 $ CVC=VPC+VSEPC+VNC
   PC(IP)=CVC*QI
   QI= C.985*QI $ JCY=3 $ GO TO 99
71 IF(JCY .GT. 3) GO TO 72
   QUEFND=TRAP1T/TRAPTT $. QI1ND=TRAP1T $ QITND=TRAPTT
   CPD(3)=THETA2(NM)*CRF $ CPD(4)=C(ITHETA,NM)*CRF
   PH1NSD=PHI1(NM) $ PH1NCD=PHI1(2) $ PH2NSD=PH2CAL(NM)
   VND=PH1NSD-PH1NCD+PH2NSD-PH1NSD
   QI=-QI $ JCY=4 $ GO TO 99
72 CONTINUE
   RVEL(2)=VEL(3)/VEL(4) $ R1VEL(2)=1./RVEL(2)
   QUEFPD=TRAP1T/TRAPTT $ QI1PD=TRAP1T $ QITPD=TRAPTT $ QI2=QI
   CPD(1)=THETA2(NM)*CRF $ CPD(2)=C(ITHETA,NM)*CRF
   QQUEFD=(QI1ND+QI1PD)/(QITND+QITPD) $ FE3TI3=CPD(2)-CPD(4)
   PH1PCD=PHI1(2) $ PH1PSD=PHI1(NM) $ PH2PSD=PH2CAL(NM)
   VPD=PH1PCD-PH1PSD+PH1PSD-PH2PSD $ VSEPD=QI2*QLS/QKAPA0
   CVD=VPD+VSEPD+VND
   PD=-CVD*QI $ IF(JDC.LE.1) GO TO 49 $ IF(PD.GT.PDSAVE) GO TO 51
   IF(QI.GT.QIS) QIMIN=QI  $ IF(QI.LT.QIS) QIMAX=QI  $ GO TO 52
51 IF(QI.GT.QIS) QIMAX=QIS$ IF(QI.LT.QIS) QIMIN=QIS
49 PDSAV=PDSAVE $ PDSAVE=PD $ QIS=QI
52 CONTINUE
   PRINT 145, PD,QI
   JDC=JDC-IP+1 $ IF(JDC.EQ.0) GO TO 64
   IF(JDC.GT.1) GO TO 65 $ QIO=QI $ CVDO=CVD $ QI=-0.820*QI$QIMIN=0.0
   QIMAX=QIO $ JCY=3 $ JDC=2 $ GO TO 99
65 IF(JDC.GE.9) JDC=-1   $ QINEW=0.5*(QI-CVD *(QI-QIO)/(CVD-CVDO))
   IF(JDC.EQ.2) GO TO 53 $ BQUAD=(QI-QIO)/(CVD-CVDO)
   CQUAD=(BQUAD-(QIO-QIOO)/(CVDO-CVDOO))/(CVD-CVDOO)
   BQUAD=BQUAD-CQUAD*(CVD+CVDO) $ AQUAD=QI-(BQUAD+CQUAD*CVD)*CVD
   IF(BQUAD**2.LT.3.0*AQUAD*CQUAD) GO TO 53
```

```
      CVDNEW=-AQUAD/(SQRT(BQUAD**2-3.0*AQUAD*CQUAD)+BQUAD)
      QINEW=AQUAD+CVDNEW*(BQUAD+CQUAD*CVDNEW)
   53 IF(QINEW.LT.QIMAX) QINEW=0.5*(QIMAX+QIS)
      IF(QINEW.GT.QIMIN) QINEW=0.5*(QIMIN+QIS)
      QIGG=QI $ CVDOO=CVD
      IF(ABS(QI*CVD).LT.ABS(QIO*CVDO)) GO TO 63 $ QIOO=QIO
      CVDOO=CVDO $ QIO=QI $ CVDO=CVD
   63 QI=-QINEW $ JCY=3 $ JDC=JDC+1
      IF(ABS(QINEW-QI).LT.1.E-4*ABS(QINEW)) JDC=0
      IF(JDC.EQ.1) GO TO 99 $ IF(ABS(PD-PDSAV).LT.1.E-5*PD) JDC=0
      GO TO 99
   64 PDS(IP)=PD
      IF(FE3TI3 .LT. 0.0)  GO TO 73
      CPDM(3)=CPD(3)+CPD(4) $ CPDM(4)=0.0
      CPDM(1)=CPD(1)+CPD(2)-FE3TI3*0.5 $ CPDM(2)=FE3TI3*0.5
      CHIS=FE3TI3/CFD(2)*100. $ NCHIS=1 $ GO TO 74
   73 CPDM(1)=CPD(1)+CPD(2) $ CPDM(2)=0.0
      CPDM(3)=CPD(3)+CPD(4)+FE3TI3*0.5 $ CPDM(4)=-FE3TI3*0.5
      CHIS=-FE3TI3/CFD(4)*100. $ NCHIS=-1
   74 IF(IP.NE.1) GO TO 47
      PRINT 129 $ PRINT 130
      PRINT 131,CFC(1),CPC(1),CFD(1),CPD(1),CPDM(1)
      PRINT 132,CFC(2),CPC(2),CFD(2),CPD(2),CPDM(2)
      PRINT 133,CFC(3),CPC(3),CFD(3),CPD(3),CPDM(3)
      PRINT 134,CFC(4),CPC(4),CFD(4),CPD(4),CPDM(4)
      PRINT 135 $ PRINT 136
      PRINT 137,VEL(1),VEL(2),RVEL(1),RIVEL(1),VEL(3),VEL(4),RVEL(2),RIV
     1EL(2) $ PRINT 138
      PRINT 139,QI1,CVC,CUEFNC,CUEFPC,QI2,CVD,CUEFND,CUEFPD
      PRINT 140,QCUEFC,QCUEFD $ PRINT 141,VSEPC,VSEPD
      IF(NCHIS .GT. 0) PRINT 142,CHIS $ IF(NCHIS .LT. 0) PRINT 143,CHIS
   47 PWC=-QI2*CVD $ PWC=-QI1*CVC $ EEFF=PWC/PWD
      PW1=PWD-0.4*PWC $ PW2=PWD-PWC/3.0 $ PW3=PWD-0.25*PWC $ PW4=PWD-0.2
     1*PWC $ PRINT 144,PW1,PW2,PW3,PW4
      PRINT 144,PWD,PWC,QJISTR,EEFF $ JCY=1 $ IP=IP+1 $ JDC=1
      GO TO (97,66,61,59,48,54),IP
   66 QI=-1.02*QICHAR $ V=1.02*VSAVE $ GO TO 99
   61 QI=-0.98*QICHAR $ V=0.98*VSAVE $ GO TO 99
   59 QI=-QICHAR $ V=1.02*VSAVE $ GO TO 99
   48 QI=-QICHAR $ V=0.98*VSAVE $ GO TO 99
   54 COST=(PDS(2)-PDS(3))/(PC(2)-PC(3))
      TRY=(PDS(4)-PDS(5))/(PC(4)-PC(5)) $ QISTAR=QISTAV
      PRINT 145, QICHAR,QISTAR,COST,TRY,(PDS(I),PC(I),I=1,5)
      GO TO 97 $ END
```

```
      PROGRAM REDOX2

C     CALCULATES THE BEHAVIOR OF A FLOW REDOX CELL ON CHARGE AND
C     DISCHARGE WHEN THE CURRENT IS PERPENDICULAR TO THE FLUID FLOW

      DIMENSION CF(2),CPF(2),QKM(4),DIF(4),RQKM(2),A(2),D(2),UTH(2),QN(2
     1),S(2),QKAPA0(2),QKAPA(2),SIGMA(2),EPSIL(2),RHO(2),QMU(2),QI0(2),
     1QIL(2),V(2),QNU(2),ONU(2),DATIO(2),Q(2),Z(2,6),THETA(2),THETAP(2)
     1,THETPF(2),COND(2),SINH(2),COSH(2),RI(2),P(2),QJI(1000),THETAJ(100
     10),XL(1000),QILP(1000),QILN(1000),THETAN(1000),THEPP(1000),THEPN(1
     1000),THETWP(1000),THETWN(1000),THEPWP(1000),THEPWN(1000),VOPCIR(10
     100),PWC(3),PWD(3),QID(3),QIC(3)
  100 FORMAT(F15.0)
  200 FORMAT(//50X,*THIS RUN DID NOT CONVERGE*)
  201 FORMAT(40X,E16.8,5X,E16.8,5X,I3,5X,E16.8,5X,E16.8)
  202 FORMAT(/14X,*A (CM-1)*,04X,*THICKNESS  (CM)*,05X,*UTHETA  (V)*,10X
     1,*N*,10X,*S*)
  203 FORMAT(/10X,*QNU = *,E15.8,2X,*I= *,I2)
  204 FORMAT(//10X,*X (CM)*,11X,*THETA+*,10X,*I (A/CM+2)*,07X,*IL+ (A/CM
     1+2)*,06X,*IL- (A/CM+2)*,06X,*V(I=0)  (V)*//)
  205 FORMAT(3X,E16.8,E17.8,2X,E16.8,2X,E16.8,2X,E16.8,2X,E16.8)
  206 FORMAT(/1X,*+ ELECTRODE*,F10.6,5X,F10.6,10X,F8.6,10X,F4.2,6X,F5.2)
  207 FORMAT(/1X,*- ELECTRODE*,F10.6,5X,F10.6,10X,F8.6,10X,F4.2,6X,F5.2)
  208 FORMAT(/14X,*I0 (A/CM+2)*,05X,*KAPPA0 (MHO)*,05X,*KAPPA (MHO)*,05X
     1,*SIGMA (MHO)*,5X,*EPSILON*)
  209 FORMAT(/1X,*+ ELECTRODE*,E12.6,5X,F10.6,7X,F10.6,6X,E12.6,2X,F10.6
     1)
  210 FORMAT(/1X,*- ELECTRODE*,E12.6,5X,F10.6,7X,F10.6,6X,E12.6,2X,F10.6
     1)
  211 FORMAT(/14X,*CRF (MOLE/CM+3)*,05X,*CPF (MOLE/CM+3)*,05X,*V (CM/S)*
     1,05X,*DR (CM+2/S)*,05X,*DP (CM+2/S)*,05X,*KMR (CM/S)*,05X,*KMP (CM
     1/S)*)
  212 FORMAT(/1X,*+ ELECTRODE*,E15.6,7X,E12.6,5X,E12.6,2X,E12.6,4X,E12.6
     1,4X,E12.6,3X,E12.6)
  213 FORMAT(/1X,*- ELECTRODE*,E15.6,7X,E12.6,5X,E12.6,2X,E12.6,4X,E12.6
     1,4X,E12.6,3X,E12.6)
  214 FORMAT(//10X,*X (CM)*,11X,*THETA+*,12X,*THETA-*,11X,*THETAP+*,11X,
     1*THETAP-*//)
  215 FORMAT(3X,E16.8,E17.8,2X,E16.8,2X,E16.8,2X,E16.8)
  216 FORMAT(//10X,*X (CM)*,10X,*THETAW+*,11X,*THETAW-*,11X,*THETAPW+*,
     110X,*THETAPW-*//)
  217 FORMAT(3X,E16.8,1X,E16.8,2X,E16.8,2X,E16.8,2X,E16.8)
  218 FORMAT(///44X,*DISCHARGE*///)
  219 FORMAT(///45X,*CHARGE*///)
  220 FORMAT(20X,*CELL VOLTAGE*,F9.6,2X,*(V)*,2X,*ELECTRODE LENGTH*,
     1E12.6,2X,*(CM)*,2X,E12.6,2X,E12.6)
  221 FORMAT(3X,E16.8,E17.8,2X,E16.8,2X,E16.8,2X,E16.8,2X,E16.8,2X,I3)
  222 FORMAT(//20X,*MEMBRANE THICKNESS*,F9.6,2X,*(CM)*,2X,*MEMBRANE RESI
     1TIVITY*,F11.6,2X,*(OHM-CM)*)
  223 FORMAT(//20X,*THE ELECTRODE LENGTHS ON CHARGE AND DISCHARGE ARE NO
     1T EQUAL*)
  224 FORMAT(8E16.8)
      VQ=0.00001
      THEOUT=0.3 $ NJMAX=141 $ H=(1.0-THEOUT)/FLOAT(NJMAX-1)
      F=96487. $ R=8.3143 $ T=298.15 $ IP=1 $ IN=2
      PRINT 202
      READ 100,QLS,RS
      READ 100,(DIF(I),I=1,4) $ READ 100,(A(I),D(I),UTH(I),QN(I),S(I),
     1QKAPA0(I),SIGMA(I),EPSIL(I),RHO(I),QMU(I),DATIO(I),CF(I),CPF(I),I=
     11,2) $ PSI=0.86 $ RTF=R*T/F
```

```
      V(IP)=VQ $ V(IN)=VQ
      DO 2 I=1,4 $ IF(I .GT. 2) GO TO 1
      QKM(I)=0.91*A(IP)*DIF(I)*(RHO(IP)*V(IP)/A(IP)/QMU(IP)/PSI)**0.49*
     1PSI**2*(QMU(IP)/RHO(IP)/DIF(I))**(1./3.) $ GO TO 2
    1 QKM(I)=0.91*A(IN)*DIF(I)*(RHO(IN)*V(IN)/A(IN)/QMU(IN)/PSI)**0.49*
     1PSI**2*(QMU(IN)/RHO(IN)/DIF(I))**(1./3.)
    2 CONTINUE $ RQKM(IP)=QKM(1)/QKM(2) $ RQKM(IN)=QKM(3)/QKM(4)
      PRINT 206,A(1),D(1),UTH(1),QN(1),S(1) $ PRINT 207,A(2),D(2),UTH(2)
     1,QN(2),S(2) $ PRINT 208
      CH=6.00 $ UTH(IN)=UTH(IN)+R*T/F*ALOG(CH**2)
      DELTAU=UTH(IP)-UTH(IN)
      DO 3 I=1,2 $ THETPF(I)=CPF(I)/CF(I) $ QKAPA(I)=QKAPA0(I)*EPSIL(I)*
     1*1.5 $ QI0(I)=DATI0(I)*(CF(I)*CPF(I))**0.5
      Q(I)=SQRT(A(I)*D(I)**2*F*QI0(I)/2./R/T/SQRT(THETPF(I))*(1./QKAPA(I
     1)+1./SIGMA(I)))$ COND(I)=SIGMA(I)/QKAPA(I)+QKAPA(I)/SIGMA(I)
    3 P(I)=D(I)/(QKAPA(I)+SIGMA(I))
      PRINT 209,QI0(1),QKAPA0(1),QKAPA(1),SIGMA(1),EPSIL(1)
      PRINT 210,QI0(2),QKAPA0(2),QKAPA(2),SIGMA(2),EPSIL(2) $ PRINT 211
      PRINT 212,CF(1),CPF(1),V(1),DIF(1),DIF(2),QKM(1),QKM(2)
      PRINT 213,CF(2),CPF(2),V(2),DIF(3),DIF(4),QKM(3),QKM(4)
      PRINT 222,QLS,RS
      DTSAVE=0.99
      THETA(IP)=THEOUT
      THETAP(IP)=1.+THETPF(IP)-THETA(IP)
      THETA(IN)=1.+S(IN)*D(IP)*QN(IP)*V(IP)*CF(IP)/S(IP)/D(IN)/QN(IN)/
     1V(IN)/CF(IN)*(1.-THETA(IP))
      THETAP(IN)=1.+THETPF(IN)-THETA(IN)
      UDSAVE    =DELTAU+RTF/QN(IP)*ALOG(THETA(IP)/THETAP(IP))+RTF/QN(IN)*
     1ALOG(THETA(IN)/THETAP(IN))
  904 READ 100,DELV
      IF(DELV.EQ.0.0)STOP $ CV=UDSAVE-DELV $ CVSAVE=CV $ PRINT 218
      JCHAR=1
      V(IP)=VQ $ V(IN)=VQ
  900 GO TO (903,901,902),JCHAR
  901 CV=UDSAVE-1.02*DELV $ GO TO 903
  902 CV=UDSAVE-0.98*DELV
  903 ICHARG=0 $ QJI(1)=0.01 $ J=1 $ DTHETA=0.0
   98 IF(ICHARG .GT. 0) DTHETA=DTSAVE $ IF(JCHAR.NE.1) GO TO 99
      IF(ICHARG .GT. 1)GO TO 99 $ IF(ICHARG.EQ.1)PRINT 219
   99 QI=QJI(J) $ THETA(IP)=1.-DTHETA
      THETAP(IP)=1.+THETPF(IP)-THETA(IP)
      THETA(IN)=1.+S(IN)*D(IP)*QN(IP)*V(IP)*CF(IP)/S(IP)/D(IN)/QN(IN)/
     1V(IN)/CF(IN)*(1.-THETA(IP))
      THETAP(IN)=1.+THETPF(IN)-THETA(IN)
      VOPCIR(J)=DELTAU+RTF/QN(IP)*ALOG(THETA(IP)/THETAP(IP))+RTF/QN(IN)*
     1ALOG(THETA(IN)/THETAP(IN))
      IF(ICHARG.EQ.0) USAVE=VOPCIR(1)
      IF(THETA(IP) .GT. 1.0+1.0E-08) GO TO 999
      IF(THETA(IP).LT.THEOUT)GO TO 999$IF(THETA(IN).LT.1.E-08) GO TO 999
      IF(THETAP(IP) .LT. 1.0E-08) GO TO 999
      IF(THETAP(IN) .LT. 1.0E-08) GO TO 999
      QIL(IP)=-QN(IP)*F*D(IP)*A(IP)*QKM(IP)*THETA(IP)*CF(IP)/S(IP)
      QIL(IN)=QN(IN)*F*D(IN)*A(IN)*QKM(IN+1)*THETA(IN)*CF(IN)/S(IN)
      JCOUNT=0
    4 QIOLD=QI $ JCOUNT=JCOUNT+1
      DO 5 I=1,2
      QNU(I)=Q(I)*(THETAP(I)*THETA(I)+(RQKM(I)*THETA(I)-THETAP(I))*
     1THETA(I)*QI/QIL(I)-RQKM(I)*THETA(I)**2*QI**2/QIL(I)**2)**0.25
      DNU(I)=(Q(I)/QNU(I))**3*Q(I)/4.*((RQKM(I)*THETA(I)-THETAP(I))*
     1THETA(I)/QIL(I)-2.*RQKM(I)*(THETA(I)/QIL(I))**2*QI)
      SINH(I)=(EXP(QNU(I))-EXP(-QNU(I)))/2.
      COSH(I)=(EXP(QNU(I))+EXP(-QNU(I)))/2.
```

```
      Z(I,1)=(2.+COND(I)*COSH(I))/(QNU(I)*SINH(I))
      Z(I,2)=(COND(I)*QNU(I)*SINH(I)**2*DNU(I)-(2.+COND(I)*COSH(I))*
     1(SINH(I)+QNU(I)*COSH(I))*DNU(I))/(QNU(I)*SINH(I))**2
      RI(I)=QI/QIL(I)
      Z(I,3)=ALOG(THETA(I)*(1.-RI(I)))+RI(I)/(1.-RI(I))
      Z(I,4)=1./QIL(I)/(1.-RI(I))
      Z(I,5)=ALOG(THETAP(I)+THETA(I)*RI(I)*RQKM(I))-1./(1.+THETAP(I)/
     1THETA(I)/RI(I)/RQKM(I))
    5 Z(I,6)=1./(QI+THETAP(I)*QIL(I)/THETA(I)/RQKM(I))
      QINEW=(UTH(IP)-UTH(IN)-CV+QI**2*(Z(IP,2)*P(IP)+Z(IN,2)*P(IN))+R*T/
     1F*((Z(IP,3)-Z(IP,5))/QN(IP) +(Z(IN,3)-Z(IN,5))/QN(IN)))/(P(IP)*(1.
     1+QI*Z(IP,2)+Z(IP,1))+P(IN)*(1.+QI*Z(IN,2)+Z(IN,1))+QLS*RS+RTF*((
     1Z(IP,4)+Z(IP,6))/QN(IP)+(Z(IN,4)+Z(IN,6))/QN(IN)))
      DO 30 I=1,2 $ IF(QINEW .GT. QIL(I)) QINEW=0.5*(QIOLD+QIL(I))
      CURLIM=-THETAP(I)/THETA(I)/RQKM(I)*QIL(I)
   30 IF(QINEW .LT. CURLIM) QINEW=0.5*(QIOLD+CURLIM)
      QI=QINEW $ IF(ABS(QI-QIOLD) .LE. 1.E-06*ABS(QI))  GO TO 6
      IF(JCOUNT .LE. 15)  GO TO 4 $ PRINT 200
    6 QJI(J)=QI $ THETAJ(J)=THETA(IP) $ JMAX=J $ QILP(J)=QIL(IP)
      THETAN(J)=THETA(IN) $ THEPP(J)=1.+THETPF(IP)-THETA(IP)
      THEPN(J)=1.+THETPF(IN)-THETA(IN)
      THETWP(J)=THETA(IP)*(1.-QI/QIL(IP))
      THETWN(J)=THETA(IN)*(1.-QI/QIL(IN))
      THEPWP(J)=THEPP(J)+RQKM(IP)*THETA(IP)*QI/QIL(IP)
      THEPWN(J)=THEPN(J)+RQKM(IN)*THETA(IN)*QI/QIL(IN)
      QILN(J)=QIL(IN) $ DO 7 I=1,2
      QNU(I)=Q(I)*(THETAP(I)*THETA(I)+(RQKM(I)*THETA(I)-THETAP(I))*
     1THETA(I)*QI/QIL(I)-RQKM(I)*THETA(I)**2*QI**2/QIL(I)**2)**0.25
      SINH(I)=(EXP(QNU(I))-EXP(-QNU(I)))/2.
      COSH(I)=(EXP(QNU(I))+EXP(-QNU(I)))/2.
    7 Z(I,1)=(2.+COND(I)*COSH(I))/(QNU(I)*SINH(I))
      AP=P(IP)*(1.+Z(IP,1)) $ AN=P(IN)*(1.+Z(IN,1)) $ QOHM=QLS*RS
      BLNTHP=ALOG(THETA(IP)*(1.-QI/QIL(IP))) $ BLNTHN=ALOG(THETA(IN)*
     1(1.-QI/QIL(IN))) $ CLNTHP=ALOG(THETAP(IP)+THETA(IP)*RQKM(IP)*QI/
     1QIL(IP)) $ CLNTHN=ALOG(THETAP(IN)+THETA(IN)*RQKM(IN)*QI/QIL(IN))
      ETA=-QI*(AP+AN+QOHM) $ ETACP=R*T/F/QN(IP)*(BLNTHP-CLNTHP)
      ETACN=R*T/F/QN(IN)*(BLNTHN-CLNTHN)
      IF(J.EQ.1)GO TO 10 $ IF(QJI(J)*QJI(J-1).LE.0.0)GO TO 998
   10 CV1=DELTAU+ETA+ETACP+ETACN $ IF(ABS(CV-CV1) .LT. 1.0E-06)  GO TO 8
      PRINT 201,CV,CV1,J,THETAJ(J),QJI(J) $ STOP
    8 J=J+1 $ QJI(J)=QJI(J-1) $ DTHETA=DTHETA+H
      IF(ICHARG .GE. 1) DTHETA=DTHETA-2.0*H $ GO TO 99
  998 JMAX=JMAX-1
  999 XL(1)=0.0
      QY=-QN(IP)*F*V(IP)*CF(IP)*D(IP)/S(IP) $ DO 9 M=2,JMAX
    9 XL(M)=XL(M-1)+QY/(QJI(M)-QJI(M-1))*(THETAJ(M-1)-THETAJ(M))*ALOG(QJ
     1I(M)/QJI(M-1))
      IF(ICHARG.GT.0)GO TO 14
      QID(JCHAR)=QN(IP)*F*V(IP)/S(IN)*D(IP)/XL(JMAX)*CF(IP)*(1.-THETAJ(J
     1MAX)) $ PWD(JCHAR)=QID(JCHAR)*CV
      IF(JCHAR.NE.1) GO TO 14
      PRINT 220,CV,XL(JMAX),QID(JCHAR),PWD(JCHAR)
      PRINT 204 $ PRINT 205,(XL(I),THETAJ(I),QJI(I),QILP(I),QILN(I),VOPC
     1IR(I),I=1,JMAX,10) $PRINT 221,XL(JMAX),THETAJ(JMAX),QJI(JMAX),QILP
     1(JMAX),QILN(JMAX),VOPCIR(JMAX),JMAX $ PRINT 214
      PRINT 215,(XL(I),THETAJ(I),THETAN(I),THEPP(I),THEPN(I),I=1,JMAX,10
     1) $ PRINT 216
      PRINT 217,(XL(I),THETWP(I),THETWN(I),THEPWP(I),THEPWN(I),I=1,JMAX,
     110)
   14 ICHARG=ICHARG+1 $ J=1
      IF(ICHARG.NE.1)GO TO 11
      CV=USAVE+0.00010 $ QJI(1)=-0.025 $ XLDIS=XL(JMAX)
```

```
   DTSAVE=DTHETA-H $ GO TO 98
11 IF(ICHARG.NE.2)GO TO 12
   CVOLD=CV $ XLOLD=XL(JMAX) $ CV=0.5*(CV+USAVE)
   IF(XLOLD.GT.XLDIS)CV=CVOLD+0.05 $ GO TO 98
12 DCV=(XLDIS-XL(JMAX))*(CV-CVOLD)/(XL(JMAX)-XLOLD)
   IF(DCV.LT.0.0)DCV=(CV-USAVE)*(EXP((XLDIS-XL(JMA))/(XL(JMAX)-XLOLD
  1)*ALOG((CV-USAVE)/(CVOLD-USAVE)))-1.0) $ CVOLD=CV $ XLOLD=XL(JMAX)
   IF(ABS(DCV).GT.1.0E-08)GO TO 13
   QIC(JCHAR)=QN(IP)*F*V(IP)/S(IN)*D(IP)/XL(JMAX)*CF(IP)*(THEPP(1)-
  1THEPP(JMAX)) $ PWC(JCHAR)=CV*QIC(JCHAR)
   IF(JCHAR.NE.1) GO TO 15
   PRINT 220,CV,XL(JMAX),QIC(JCHAR),PWC(JCHAR)
   PRINT 204 $ PRINT 205,(XL(I),THETAJ(I),QJI(I),QILF(I),QILN(I),VOPC
  1IR(I),I=1,JMAX,10) $PRINT 221,XL(JMAX),THETAJ(JMA)),GJI(JMAX),QILP
  1(JMAX),QILN(JMAX),VOPCIR(JMAX),JMAX $ PRINT 214
   PRINT 215,(XL(I),THETAJ(I),THETAN(I),THEPP(I),THEPN(I),I=1,JMAX,10
  1) $ PRINT 216
   PRINT 217,(XL(I),THETWP(I),THETWN(I),THEPWP(I),THEPWN(I),I=1,JMAX,
  110)
15 JCHAR=JCHAR+1 $ IF(JCHAR.LT.4)GO TO 900
   COST=(PWO(3)-PWO(2))/(PWC(3)-PWC(2))
   PROFIT=PWO(1)-COST*PWC(1)
   PRINT 224,PWO(1),PWC(1),COST,PROFIT,QIC(1),QID(1),CVSAVE
   PRINT 224, (PWO(I),PWC(I),I=2,3)
   GO TO 904
13 CV=CV+DCV $ IF(CV.LE.USAVE)CV=0.5*(CVOLD+USAVE) $ IF(ICHARG.LT.10)
  1GO TO 98 $ PRINT 223
   STOP $ END
```

Acknowledgement

Words cannot express the debt I owe Professor Newman. His "simple minded" approach to highly complex problems will forever serve as a paragon for me. Like few teachers, Professor Newman has the ability to transfer a clear perspective of physics to his students.

I am also indebted to Professor Hanson. He not only encouraged me to work with Professor Newman, but he inspires us all to be as good a person as he.

My colleagues: Tom Edwards, Peter Fedkiw, Clarence Law, Peter Pierini, Richard Pollard, and Ralph White deserve recognition because they contributed greatly to my education and spirit.

Special thanks go to Lon Newman for all the moral support and wonderful meals.

Thanks also to Professor Israel Cornet of the Mechanical Engineering Department and to Professor Pier Filippo Marconi of the University of Pisa who read this work.

I'd like to thank Nancy Charpentier, Marie Devlin, Ann Harrington, and Linda McGuire for typing this dissertation. Their patience with me over the years has been remarkable. I owe Clarence Law a special thanks for doing all the footwork in getting this dissertation filed. Most of the figures which appear in this dissertation were beautifully traced by Gloria Pelatowski.

This work was supported by the Division of Solar, Geothermal, Electric and Storage Systems, Office of the Assistant Secretary for Energy Technology, U.S. Department of Energy under Contract No. W-7405-Eng-48.

TECHNICAL INFORMATION DEPARTMENT
LAWRENCE BERKELEY LABORATORY
UNIVERSITY OF CALIFORNIA
BERKELEY, CALIFORNIA 94720